Theoretical Investigations of Electron States
in Small-Scale Semiconductor Structures

Thesis by
Christian Mailhiot

In Partial Fulfillment of the Requirements
for the Degree of
Doctor of Philosophy

California Institute of Technology
Pasadena, California

1984

(Submitted September 13, 1983)

To Claire

ACKNOWLEDGEMENTS

I would like to thank Dr. T. C. McGill for his support and assistance during the course of this work. Dr. T. C. McGill has provided me with an excellent and unmatched research environment that made my graduate work a very fruitful and enjoyable experience. Throughout my stay within his research group, he has shown great care and contributed tremendously to the original ideas contained in this work. I owe him a lot. It is a pleasure for me to acknowledge the careful and precise secretarial work of V. Snell. Her competence in coordinating the administrative actions within Dr. McGill's research group cannot be overestimated.

I would also like to thank my fellow graduate students A. Zur, A. Prabhakar, T. E. Schlesinger, S. R. Hetzler, T. J. Jones, R. J. Hauenstein, G. Wu and M. B. Johnson for discussions. I am particularly grateful to R. T. Collins for fresh, lively and always profitable exchanges of ideas about our respective research projects. At an earlier stage of my graduate career, I profited from fruitful interactions with Dr. C. A. Swarts, Dr. M. S. Daw, Dr. R. Feenstra, Dr. G. Mitchard and Dr. R. B. James. It is always a pleasure to discuss with Dr. A. T. Hunter of Hughes Research Laboratories his current research on GaAs. I would also like to thank Dr. J. N. Schulman of the University of Hawaii whose collaboration on a part of this work has been a rich experience.

I am particularly indebted to Dr. Yia-Chung Chang of the University of Illinois for introducing me to many aspects of theoretical semiconductor physics. His guidance and advice are mostly acknowledged. It is an honor for me to have had the chance to collaborate with Dr. D. L. Smith on some aspects of the present work. My interaction with Dr. Smith will always remain one of the most rewarding and enjoyable experiences at Caltech. I am most indebted to him for his influence will be felt throughout my career. I am most thankful to my wife, Claire, for her

support, encouragement and patience throughout the realization of this work.

The financial assistance of the Natural Sciences and Engineering Research Council of Canada and the *Fonds F.C.A.C. pour l'aide et le soutien à la recherche* of Québec is gratefully acknowledged.

ABSTRACT

The work presented here is concerned with theoretical investigations of *electronic states in small-scale semiconductor structures.* This last term encompasses layered structures made up of two dissimilar, but lattice-matched, semiconductors. The semiconductors of interest here are mostly the tetrahedrally bonded zincblende semiconductors GaAs and the alloy $Ga_{1-x}Al_xAs$. The thesis is subdivided in three major chapters. The first chapter is concerned with *electrical doping* of $Ga_{1-x}Al_xAs$-GaAs-$Ga_{1-x}Al_xAs$ quantum well structures. The second chapter addresses the question of the *transport of electrons* through GaAs-$Ga_{1-x}Al_xAs$-GaAs double heterojunction structures. In the final chapter, we develop a *theory of the electronic structure* of semiconductor superlattices particularly suitable for the *study of the optical properties and the recombination mechanisms.*

In Chapter 2, we study the *energy spectrum of ground state and excited states of shallow donor states in* $Ga_{1-x}Al_xAs$-GaAs-$Ga_{1-x}Al_xAs$ *quantum well structures.* In this system, an impurity atom is located within a GaAs slab of finite thickness. The GaAs slab is, in turn, centered between two semi-infinite layers of $Ga_{1-x}Al_xAs$. We use a *variational method* to solve the *effective mass equation* for the donor envelope function. We study the variation of the binding energy as a function of

- thickness of the GaAs containing the impurity,
- alloy composition x in $Ga_{1-x}Al_xAs$, and
- position of the impurity in the GaAs slab.

Two cases are treated:

(i) In the first case we assume that the potential well is formed by *finite* conduction band offsets at the GaAs-$Ga_{1-x}Al_xAs$ interface (*imperfect confinement*).

(ii) In the second case we consider *infinite* confining potential at the GaAs-$Ga_{1-x}Al_xAs$ interface (*perfect confinement*).

The major result of this study is that *the binding energy of the donor ground state is considerably modified as the thickness of the GaAs slab containing the impurity is varied.* At *large* GaAs *slab thicknesses*, the binding energy is that of shallow donors in *bulk* GaAs. At *small* GaAs *slab thicknesses*, the binding energy is that of shallow donors in *bulk* $Ga_{1-x}Al_xAs$ for the case of *imperfect confinement*, but corresponds to the *two-dimensional* Coulomb limit in the case of *perfect confinement.* It is also found that *the binding energy depends on the position of the impurity atom within the* GaAs *slab.* Thus, we have a confinement-induced lifting of the Coulomb energy levels.

In Chapter 3, we study the *transport characteristics of electrons through* GaAs-$Ga_{1-x}Al_xAs$-GaAs *double heterojunction structures.* In this system, a $Ga_{1-x}Al_xAs$ slab of finite thickness is centered between two semi-infinite layers of GaAs. An electron is incoming from the GaAs onto the $Ga_{1-x}Al_xAs$ barrier. Transport coefficients are calculated using the formalism of the *complex-***k** *energy band structure within the empirical tight-binding method.* Transmission into states derived from different energy extrema of the GaAs lowest conduction band is obtained. We consider both the (111) and the (100) GaAs-$Ga_{1-x}Al_xAs$ interfaces. Transport coefficients are calculated as a function of

- o GaAs conduction band minimum from which the electron state is derived,
- o energy of the electron incoming on the $Ga_{1-x}Al_xAs$ barrier,
- o thickness of the $Ga_{1-x}Al_xAs$ barrier, and
- o alloy composition x in the $Ga_{1-x}Al_xAs$.

The major result of the study is that *states derived from different energy extrema of the* GaAs *lowest conduction band appear to couple weakly across*

the GaAs-$Ga_{1-x}Al_xAs$ *interface.* Thus, if we consider the (111) interface, is seems possible to *reflect the L-point component of the current* while *transmitting the Γ-point component.* There exists two regimes of transport: *tunneling transport* and *propagating transport.* In the case where the energy incoming electron is *below* the energy barrier, *transmission is small* and the transport occurs via a *tunneling process.* However, in the case where the energy incoming electron is *above* the energy barrier, *transmission is large* and the transport occurs via a *propagating process.* Depending on the $Ga_{1-x}Al_xAs$ slab thickness, it is possible to induce *resonances* whereby the *transmission coefficient is unity.*

In Chapter 4, we develop a theoretical framework to investigate the *electronic structure of semiconductor superlattices.* The theoretical formulation is based on the $\mathbf{k} \cdot \mathbf{p}$ method derived from an accurate local pseudopotential method. The formalism developed is particularly well suited for the study of the *optical properties* and the investigation of the *recombination mechanisms* in semiconductor superlattices. Here again, we make extensive use of the *complex-*$\mathbf{k}$ *energy band structure obtained via the* $\mathbf{k} \cdot \mathbf{p}$ *method.* Realistic boundary conditions are imposed on the *multi-component superlattice envelope function.* From these boundary conditions, the energy spectrum of the superlattice is deduced. For the first time, *we develop a scheme whereby the superlattice state function in both solids is expanded in terms of the same set of basis functions.* By doing so, we relax the often used approximation that assumed that the basis functions are the same for all zincblende semiconductors.

Parts of this thesis have been or will be published under the following titles:

CHAPTER 2:

Energy Spectra of Donors in GaAs-$Ga_{1-x}Al_xAs$ Quantum Well Structures,

C. Mailhiot, Yia-Chung Chang, and T. C. McGill, *Surf. Sci.* **113**, 161 (1982).

Energy Spectra of Donors in GaAs-$Ga_{1-x}Al_xAs$ Quantum Well Structures in the Effective Mass Approximation,

C. Mailhiot, Yia-Chung Chang, and T. C. McGill, *J. Vac. Sci. Technol.* **21**, 519 (1982).

Energy Spectra of Donors in GaAs-$Ga_{1-x}Al_xAs$ Quantum Well Structures in the Effective Mass Approximation,

C. Mailhiot, Yia-Chung Chang, and T. C. McGill, *Phys. Rev.* **B26**, 4449 (1982).

CHAPTER 3:

Tunneling and Propagating Transport in GaAs-$Ga_{1-x}Al_xAs$ (100) Double Heterojunctions,

C. Mailhiot, T. C. McGill, and J. N. Schulman, *J. Vac. Sci. Technol.* **B1**, April-June (1983).

Transport Characteristics of L-point and Γ-point Electrons through GaAs-$Ga_{1-x}Al_xAs$ (111) Double Heterojunctions,

C. Mailhiot, D. L. Smith, and T. C. McGill, *J. Vac. Sci. Technol.* **B1**, July-September (1983).

CHAPTER 4:

New Approach to the Theory of the Electronic Structure of Semiconductor Superlattices,

C. Mailhiot, D. L. Smith, and T. C. McGill, *to appear in Phys. Rev* **B**.

CONTENTS

• ACKNOWLEDGEMENTS iii

• ABSTRACT v

• CHAPTER 1: THEORETICAL INVESTIGATIONS OF ELECTRON STATES IN SMALL-SCALE SEMICONDUCTOR STRUCTURES 2

o 1.1 Scope and Justification of this Study 2
1.1.1 General Background 2
1.1.2 Relevance of the Study 5

o 1.2 Outline 7
1.2.1 Electronic Spectrum in Quantum Well 7
1.2.2 Electronic Transport in Double Heterojunctions 10
1.2.3 Electronic Structure of Superlattices 14

o 1.3 Summary of Major Results 16
1.3.1 Electronic Spectrum in of Donors Quantum Well 16
1.3.2 Electronic Transport in Double Heterojunction 18
1.3.3 Electronic Structure of Superlattices 20

o References 21

• CHAPTER 2: ENERGY SPECTRUM OF SHALLOW DONORS IN $Ga_{1-x}Al_xAs$-GaAs-$Ga_{1-x}Al_xAs$ QUANTUM WELL STRUCTURES 22

o 2.1 Introduction 23
2.1.1 Scope of the Study 23
2.1.2 Outline of Chapter 2 25
2.1.3 Summary of the Results of Chapter 2 27

o 2.2 Effective-Mass Theory for Donors in $Ga_{1-x}Al_xAs$-GaAs-$Ga_{1-x}Al_xAs$ Quantum Well Structures: Imperfect Confinement and Off-Center Impurity 30
2.2.1 Scope of the Study 30
2.2.2 Outline of Section 2.2 32
2.2.3 Calculational Method 34
2.2.4 Results 49
2.2.5 Summary and Conclusions 58

o 2.3 Effective-Mass Theory for Donors in $Ga_{1-x}Al_xAs$-GaAs-$Ga_{1-x}Al_xAs$ Quantum Well Structures: Perfect Confinement and On-Center Impurity 60
2.3.1 Scope of the Study 60
2.3.2 Outline of Section 2.3 61
2.3.3 Calculational Method 63
2.3.4 Results 74
2.3.5 Summary and Conclusions 85

o References 87

• CHAPTER 3: ELECTRONIC TRANSPORT THROUGH GaAs-$Ga_{1-x}Al_xAs$-GaAs DOUBLE HETEROJUNCTIONS **89**

o 3.1 Introduction 90
3.1.1 Scope of the Study 90
3.1.2 Outline of Chapter 3 93
3.1.3 Summary of the Results of Chapter 3 95

o 3.2 Transport Characteristics of L-point and Γ-point Electrons through GaAs-$Ga_{1-x}Al_xAs$-GaAs (111) Double Heterojunction Structures 97
3.2.1 Scope of the Study 97
3.2.2 Outline of Section 3.2 99
3.2.3 Calculational Method 102
3.2.4 Results 114
3.2.5 Summary and Conclusions 124

o 3.3 Transport Characteristics of X-point and Γ-point Electrons through GaAs-$Ga_{1-x}Al_xAs$-GaAs (100) Double Heterojunction Structures 126
3.3.1 Scope of the Study 126
3.3.2 Outline of Section 3.3 128
3.3.3 Results 130
3.3.4 Summary and Conclusions 143

o References 145

• CHAPTER 4: ELECTRONIC STRUCTURE OF SEMICONDUCTOR SUPERLATTICES **147**

- 4.1 Introduction 148
  - 4.1.1 Scope of the Study 148
  - 4.1.2 Outline of Chapter 4 150
  - 4.1.3 Summary of the Results of Chapter 4 152

- 4.2 Electronic Structure of Semiconductor Superlattices 153
  - 4.2.1 Outline of Section 4.2 153
  - 4.2.2 Introduction 154
  - 4.2.3 $\mathbf{k} \cdot \mathbf{p}$ Theory of Superlattices 156
  - 4.2.4 Superlattice Bandstructure 166
  - 4.2.5 Results 182
  - 4.2.6 Summary and Conclusions 188

- References 190

• APPENDICES

- Appendices: Chapter 2 191
  - A.2.1 Effective Mass Theory: Bulk Semiconductors 192
  - A.2.2 Effective Mass Theory: Quantum Well 201
  - A.2.3 Hamiltonian: Shallow Donors 210

- Appendices: Chapter 3 213
  - A.3.1 Empirical Tight-Binding Theory: Bulk Semiconductors 214
  - A.3.2 Transfer Matrix Theory 226
  - A.3.3 Complex-$\mathbf{k}$ Band Structures: Tight-Binding 236
  - A.3.4 Calculation of Transport Coefficients 244

- Appendices: Chapter 4 250
  - A.4.1 $\mathbf{k} \cdot \mathbf{p}$ Theory: Bulk Semiconductors 251
  - A.4.2 Pseudopotential Theory: Bulk Semiconductors 258
  - A.4.3 $\mathbf{k} \cdot \mathbf{p}$ and Pseudopotential Theories 265
  - A.4.4 Complex-$\mathbf{k}$ Band Structures: $\mathbf{k} \cdot \mathbf{p}$ Theory 273
  - A.4.5 Equivalent States: Pseudopotential Theory 300
  - A.4.6 Equivalent States: $\mathbf{k} \cdot \mathbf{p}$ Theory 343
  - A.4.7 Symmetry Properties of Transfer Matrix 356

- General Appendices: 360
  - A.5.1 Properties of Complex-$\mathbf{k}$ Hamiltonian 361
  - A.5.2 Energy Band Offsets 369

CHAPTER 1

THEORETICAL INVESTIGATIONS OF ELECTRON STATES IN SMALL-SCALE SEMICONDUCTOR STRUCTURES: INTRODUCTION

Section 1.1

1.1 Scope and Justification of this Study:

1.1.1 General Background:

In the past decade, tremendous progress has been made towards the fabrication of new electronic devices. In particular, thanks to the introduction of new fabrication technologies, semiconductor structures in which the physical dimension, in a given direction, is of the order of few Å can now be made. We refer generically to this category of structures as *small-scale structures.* The best example of the new generation of growth technologies is the introduction of the *molecular-beam epitaxy* as an important growth technique. It is now possible to grow *very high quality semiconductor-semiconductor interfaces.* This advance in semiconductor materials technology has provoked a large number of experimental and theoretical studies on semiconductor interfaces. As one of the consequences of these investigations, it is now fairly safe to assess that *the semiconductor-semiconductor interface is one of the best characterized interfaces.*

Another crucial aspect of the new growth techniques is the possibility of growing *small-scale semiconductor structures* of reduced physical size. With this reduction in the physical size, *new quantum mechanical phenomena* related to the the nature and the behavior electron states. These new aspects have no counterparts whatsoever with more conventional semiconductor devices exploiting the bulk properties of the solids.

Intrinsically coupled to these materials advances, is therefore *a need to understand the nature of the electron states pertaining to these small-scale devices.* The work presented here in concerned with the nature of electron states in small-scale semiconductor structures. An interface constructed from two lattice-matched

semiconductors of different nature is called an *heterojunction.* A major concept that enters the investigation of small-scale device and semiconductor heterojunction is that of *relative position of the energy bands,* or *energy band offsets.* This effect is related to the fact that when two lattice-matched semiconductors are brought in contact at an interface, *their respective conduction and valence band edges do not line up.* We must determine a relative energy scale between the two semiconductors forming the heterojunctions. A sketchy presentation of the various concepts that help to understand the value of energy band offsets is presented in Appendix (5.2) at the end of this work.

The difference in energy band gaps between the two semiconductors, ΔE_g , is split into a *conduction band offset,* ΔE_c , and a *valence band offset,* ΔE_v . Naturally, the following sum rule

$$\Delta E_g = \Delta E_v + \Delta E_c , \tag{1}$$

must hold. A lot of *electronic properties described in the present work arise from the presence of conduction band offsets.* We regard the quantities ΔE_v and ΔE_c as *inputs* of the calculations presented in this work rather than *outputs.*

Having defined an *heterojunction,* it is possible to envision more complicated structures.

(*i*) In the case where two heterojunctions are formed back to back, the energy band diagram of the structure resembles either that of a one-dimensional *quantum well,* (if a small band gap semiconductor is centered between two large band gap semiconductors), or that of a one-dimensional *barrier* (if a large band gap semiconductor is centered between two small band gap semiconductors).

(*ii*) In the case where the semiconductors are grown in an alternating way, we obtain a periodic set of heterojunctions. An energy band diagram of such a

structure resembles that of a periodic series of quantum wells separated by barriers. We call such a structure a *semiconductor superlattice.*

Let us consider the case where a small band gap semiconductor is centered between two large band gap semiconductors. As seen above, the energy band diagram of such a structure resembles that of a *one-dimensional quantum well.* The energy band edge discontinuities constitute potential energy barriers for the electronic states within these structures. A consequence of the introduction of a potential energy discontinuity at the interface is the *confinement of the electron states.* In a zeroth-order picture, the electron states in such a structure resemble that of the eigenstates of the particle in a well problem. This approach neglects the detailed electronic energy band structure of the constituent semiconductors forming the structure. Although very simplistic, a lot of physical insight can be gained by considering this approximation.

However, in some situations where the atomic character of the semiconductor-semiconductor interface plays a dominant role, we must resort to superior theoretical techniques. In those instances, it becomes necessary to include the atomic character of the interfaces and to impose realistic boundary conditions on the wavefunction. This can only be achieved by considering the detailed electronic energy band structure of each of the constituent semiconductors forming the structure.

Having now introduced the new theoretical elements (*i.e.*, energy band offsets, confinement of electron states, potential energy barriers, ...) that underlie the nature of the electrons states in small-scale structures, we now turn more specifically to the properties that make these small-scale semiconductor structures potentially interesting.

1.1.2 Relevance of the Study:

With the introduction of small-scale semiconductor structures, one has to determine whether or not it is feasible to use the small-scale structures in the practical realization of *semiconductor devices.* This, in major part, will be determined by answering the following questions:

(i) A first aspect of semiconductor devices regards the extensive control of electronic properties of semiconductor devices by the addition of electronically active impurities. This process is referred to as *doping.*

• Is it possible to dope these structures just like bulk semiconductors ?

• How does the binding energy of impurity states in small-scale structure differ from that of bulk semiconductors ?

• Is it possible to vary the binding energy of impurity states by changing the physical dimensions of the structure ?

• How does the breaking of three-dimensional periodicity affect the binding energy of impurity states ?

We will consider this aspect of small-scale semiconductor structures in Chapter 1. In this chapter, we investigate the *energy spectrum of shallow impurity states in* $Ga_{1-x}Al_xAs$-GaAs-$Ga_{1-x}Al_xAs$ *quantum well structures.*

(ii) A second aspect of major importance in the realization of semiconductor devices concerns the *transport of electronic carriers.*

• How are the transport properties of electrons modified by the special geometry of small-scale semiconductor structures ?

• Is it possible to put to profit the properties of small scale semiconductor structures to develop interesting new transport regimes ?

• How can energy band offsets be used to modify the transport of electrons ?

The aspect of transport in small-scale semiconductor structures will be the

subject of Chapter 2. In this Chapter, we study the *transport characteristics of* GaAs-$Ga_{1-x}Al_xAs$-GaAs *double heterojunctions structures.*

(iii) A third facet that influences the performance of semiconductor devices is related to *optical properties* and *recombination mechanisms.* Optical phenomena in semiconductor superlattices have become the center of much experimental investigations since the fabrications of *quantum well lasers.* A satisfying theoretical study has yet not been given.

- What are the optical properties of the small-scale structures (*i.e.*, optical absorption, ...) and how do they differ from those of bulk semiconductors ?

- How different are the *radiative recombination mechanisms* in small-scale semiconductor structures compared to those of bulk semiconductors ?

- How different are the *non-radiative recombination mechanisms* in small-scale semiconductor structures compared to those of bulk semiconductors ?

- Can some of these recombination mechanisms be modified by the geometry of these structures ?

- Due to the recent development of *quantum well lasers*, is it possible to understand the optical efficiency of these structures within a more complete theoretical description ?

In Chapter 3, we develop a new and efficient formalism for the calculation of *electronic properties of semiconductor superlattices.* This new formalism is especially well-suited for the treatment of *optical properties* and *recombination mechanisms* in semiconductor superlattices.

Section 1.2

1.2 Outline of thesis:

In this section, we give a general outline of the thesis. In addition, some aspects of the theoretical techniques are briefly discussed.

1.2.1 Chapter 2:

Electronic Spectrum of Shallow Donor States

in $Ga_{1-x}Al_xAs$ -GaAs-$Ga_{1-x}Al_xAs$ Quantum Well Structures

As mentioned above, the understanding of electrical doping of small-scale semiconductor structures is an all important step towards the fabrication of electronic devices.

In Chapter 1, we consider the *variation of the binding energy for shallow donors in* $Ga_{1-x}Al_xAs$-GaAs-$Ga_{1-x}Al_xAs$ *quantum well structures.* In these structures, a finite slab of GaAs is located between two semi-infinite layers of $Ga_{1-x}Al_xAs$. In this case a *small band gap* semiconductor (GaAs) is located between two *large band gap* semiconductors ($Ga_{1-x}Al_xAs$), thereby forming a confining potential energy well for the electrons located within the central GaAs slab. The donor atom is located within the central GaAs slab.

To understand the nature of the electron states in quantum well structures, it is most instructive to consider the following oversimplified picture. In a quantum well semiconductor structure, a small band gap semiconductor is located between two large band gap semiconductors and the *electronic states closely resemble eigenstates of a particle confined within a one-dimensional quantum well.* We refer to this approximation as the *well model.* Thus, the conduction band offset ΔE_c confines the electrons and the valence band offset ΔE_v confines the holes. In this approach, a series of quantized subbands arise due to the confinement of

the motion of the electron along the quantum well axis. For example, due to this quantization of the energy levels associated with the motion of the electron along the quantum well axis, the zero of energy does not correspond to the minimum of the conduction band but rather to the first subband.

In essence, the well model only considers the nature of the semiconductors forming the structure through bulk parameters like effective masses and bulk dielectric constant and uses a description of the electron states valid only for **k** near the center of the Brillouin zone. Approximate as this approach may be, it nevertheless gives a certain degree of guidance as to how to describe the electron states when the quantum well is large and a microscopic description of the solids is not crucial. When a Coulomb center is located within the quantum well structure, we can view this new potential as a perturbation on the quantum well eigenstates. Thus the Coulomb potential mixes the states belonging to the different subbands.

We specifically study the *binding energy of the donor ground state and the low-lying excited states with respect to the first conduction subband of the quantum well.* Two separate cases are treated.

(1) In the first case, we take into account the finite value of the electron potential barrier ΔE_c at the GaAs-$Ga_{1-x}Al_xAs$ interface. In this *finite barrier* model, the donor wavefunction is imperfectly confined by the electron potential barrier and is now allowed to penetrate in the $Ga_{1-x}Al_xAs$. We refer to this as the *imperfect confinement* case.

(2) In the second case we consider that the electron potential barrier created by ΔE_c at the interface can be assumed to be *infinite* with respect to the energy scale of the binding energy. In this *infinite barrier* model, the donor state is not allowed to leak out in the adjacent $Ga_{1-x}Al_xAs$ layers and is perfectly confined to the GaAs slab. We refer to this as the *perfect confinement* case.

Variations of binding energies with respect to the first conduction subband are examined as a function of

- the thickness of the GaAs slab containing the impurity,
- the alloy composition x in the alloy $Ga_{1-x}Al_xAs$, and
- the position of the impurity atom within the GaAs slab.

We treat shallow donors within the *effective mass approximation*. This approximation essentially treats the physics at $\mathbf{k} = \mathbf{0}$. All the electronic features of the solid containing the impurity atom are lumped into an electron effective mass and a bulk dielectric constant. A variational method is used to solve the effective mass equation for the donor wavefunction. In this scheme, the donor envelope function is expanded onto a physically reasonable *variational basis set*. The Hamiltonian matrix is written in this variational representation. Direct diagonalization of the Hamiltonian matrix yields the energy eigenvalues and the energy eigenstates.

Chapter 3:

Theory of Electronic Transport through

in GaAs-$Ga_{1-x}Al_xAs$ -GaAs Double Heterojunction Structures

Another aspect of the fabrication of small-scale electronic devices lies in understanding the *transport of charge carriers.*

In Chapter 2, we analyse the *transport of electrons through* GaAs-$Ga_{1-x}Al_xAs$-GaAs *double heterojunction structures.* In these structures, a finite slab of $Ga_{1-x}Al_xAs$ is located between two semi-infinite layers of GaAs. In this case, a *large band gap* semiconductor ($Ga_{1-x}Al_xAs$) is located between two *small band gap* semiconductors (GaAs), thereby forming a potential energy barrier for the electrons on each side of the central $Ga_{1-x}Al_xAs$ slab. Transport coefficients are calculated for electrons incoming from the GaAs onto the central $Ga_{1-x}Al_xAs$ barrier. We are specifically interested in the cases where the *incoming electron is derived from different extrema* of the GaAs conduction band. We must therefore include a description of the electronic states that is not confined to that region of the Brillouin zone near $\mathbf{k} = \mathbf{0}$. To do so, we provide a description of the electronic energy spectrum of the two semiconductors forming the double heterojunction structure. Such a description is obtained via a realistic band structure calculation.

There are many schemes to calculate band structures of semiconductors. These vary in rigor and accuracy. A simple approach uses a *description of the solutions of the crystal Hamiltonian in terms of atomic orbitals.* The matrix elements of the Hamiltonian between these local atomic orbitals are then treated as disposable parameters chosen to fit the band structure obtained by more accurate methods at high symmetry $\mathbf{k}$ points in the Brillouin zone. The band structure at other $\mathbf{k}$ points is then obtained via an *interpolation* scheme first introduced by Slater

and Koster[1]. Such a band calculation scheme is referred to as the *empirical tight-binding method*. It describes accurately enough valence bands and low-lying conduction bands for the purposes of the present study.

Since the three-dimensional periodicity of the bulk semiconductor is now disrupted by the presence of an interface, the use of the *real* quantum number **k** to label the irreducible representations of the crystal translation group is no longer permitted. Simply put, the component of the wavevector **k** normal to the interface plane cannot be used to label the solutions of the interface Hamiltonian. This component is now allowed to take on complex values. An electronic energy spectrum where **k** can be complex is referred to as a *complex-**k** band structure*. In that case, the solutions associated with complex-**k** are not running wave solutions. The imaginary part of the complex wavevector **k** is directly related to the decay length of the solution in **x**-space.

In the $Ga_{1-x}Al_xAs$ barrier, the wavefunction exists in regions of energy where free propagation is forbidden. This region is called a *flat barrier region*, since the potential resembles locally that of bulk $Ga_{1-x}Al_xAs$. The complex-**k** band structure is thus an indispensable ingredient for an accurate description of the wavefunction in these barrier regions. Such a band structure is calculated within the empirical tight-binding method.

Apart from flat barrier regions, there exist *interfacial regions* in which the potential varies from one lattice site to the next. In order to describe the electronic wavefunction in these regions, we use a *transfer matrix method* to express the tight-binding wavefunction on one side in terms of the tight-binding wavefunction on the other side of the interface. A full description of this method is given in Appendix (2.2).

In the foregoing study we treat the cases of the GaAs-$Ga_{1-x}Al_xAs$-GaAs

double heterojunction structures along the (111) and (100) interfaces. The purpose of this study is to analyse how an electron, incoming from a given energy minimum of the GaAs conduction band on one side of the $Ga_{1-x}Al_xAs$ barrier, transmits into different energy extrema of the GaAs conduction band on the other side of the $Ga_{1-x}Al_xAs$ barrier.

(1) For the (111) interface, we consider the cases of incoming electrons derived from near the Γ-point GaAs conduction band minimun, and from near the L-point conduction band valley. The regions of interest in the Brillouin zone are therefore the Γ-point,

$$\mathbf{k}(\Gamma) = \left[\frac{2\pi}{a}\right](0, 0, 0), \tag{2.a}$$

and the L-point

$$\mathbf{k}(L) = \left[\frac{2\pi}{a}\right]\left(\frac{1}{2}, \frac{1}{2}, \frac{1}{2}\right). \tag{2.b}$$

(2) In the case of the (100) interface, we analyse the transport pertaining to electrons in the Γ-point conduction band minimum and in the X-point conduction band valley. The regions of interest in the Brillouin zone are therefore the Γ-point,

$$\mathbf{k}(\Gamma) = \left[\frac{2\pi}{a}\right](0, 0, 0), \tag{2.c}$$

and the X-point

$$\mathbf{k}(X) = \left[\frac{2\pi}{a}\right](1, 0, 0). \tag{2.d}$$

Transport coefficients are studied for electrons associated with different extrema of the GaAs conduction band. The theoretical apparatus uses complex-$\mathbf{k}$ energy band structures and transfer matrices within the empirical tight-binding formulation. We analyse transport coefficients of electrons incoming from the GaAs side of the double heterojunction structure as a function of

- the GaAs conduction band minimum from which they are derived,

- the energy of the incoming electrons,
- the thickness of the $Ga_{1-x}Al_xAs$ barrier, and
- the alloy composition x in the $Ga_{1-x}Al_xAs$ barrier.

1.2.3 Chapter 4:

Theory of Electronic Structure

of Semiconductor Superlattices: $\mathbf{k} \cdot \mathbf{p}$ Theory

In this Chapter, we develop a new formalism to calculate the electronic properties of semiconductor superlattice. The formalism uses the $\mathbf{k} \cdot \mathbf{p}$ perturbation theory derived from an accurate *local pseudopotential calculation.* In this approach, the bulk solutions of the crystal Hamiltonian at a general point $\mathbf{k}$, are expanded in terms of a set of basis functions that are *solutions of the crystal Hamiltonian at a given point* $\mathbf{k}_0$. This theoretical technique has the advantage that the *expansion set is exact for a certain point* $\mathbf{k}_0$ *in the Brillouin zone.* This is not the case of the tight-binding approach described above. Furthermore, the *expansion set is the same for both semiconductors forming the superlattice structure.*

The superlattice wavefunction is expanded in terms of this common basis set. The corresponding expansion coefficients are referred to as the *multi-component envelope function.* The use of the $\mathbf{k} \cdot \mathbf{p}$ formalism allows a description of the superlattice state which is particularly well suited for the study of the optical properties. This is due to the fact that, in the $\mathbf{k} \cdot \mathbf{p}$ method used here, the input to the calculation are the matrix elements of the momentum operator, $\mathbf{p}$, between two basis functions at $\mathbf{k}_0$.

A suitable set of boundary conditions on the superlattice wavefunction allows us to obtain the complex-$\mathbf{q}$ energy spectrum of the superlattice, where $\mathbf{q}$ is the superlattice wavevector that classifies the superlattice solutions. We thus obtain the *complex-*$\mathbf{q}$ *energy band structure of the superlattice.*

- We would like to stress two very attractive features of the above formalism:

(i) The only empirical input parameters are the *local pseudopotential form*

factor and *the energy band offsets.*

(ii) The superlattice state function in each solid is expressed in terms of a *set of basis functions associated with the same reference solid.* We therefore relax the often used approximation that the $\mathbf{k}_0$ functions for all semiconductor of the group III-V are the same[2—4], which is clearly a convenient approximation when matching the superlattice state function onto the interface plane.

(iii) The formalism is well suited for the study of superlattices with large primitive cells.

Section 1.3

1.3 Summary of Major Results:

In this section, we present a summary of the major results.

1.3.1 Chapter 2:

Electronic Spectrum of Shallow Donor States

in $Ga_{1-x}Al_xAs$-GaAs-$Ga_{1-x}Al_xAs$ Quantum Well Structures

The major result concerning the binding energy of shallow donors in semiconductor quantum well structures is that, *the binding energy is considerably modified when the GaAs quantum well thickness is reduced from a large value to few monolayers.*

(1) We discuss first the case of a donor atom at the *center* of the GaAs slab.

(i) In the case of *finite barrier*, the binding energy varies from the bulk GaAs limit to the bulk $Ga_{1-x}Al_xAs$ limit when the dimensions of the quantum well are reduced. At large GaAs thicknesses, the donor wavefunction has a large amplitude in the GaAs slab, and the binding energy is close to that of bulk GaAs. At small GaAs thicknesses, the donor wavefunction leaks out appreciably in the $Ga_{1-x}Al_xAs$ alloy and the binding energy corresponds to that of bulk $Ga_{1-x}Al_xAs$. Between these two limits, the binding energy measured from the first conduction subband as a function of the thickness of the GaAs slab forming the quantum well, shows a maximum corresponding to a maximum confinement of the wavefunction.

(ii) In the case of *infinite barrier*, the binding energy increases from the three-dimensional limit at large well thicknesses to the two-dimesional limit at small well thicknesses. Thus the *reduction in dimensionality is accompanied by an increase in the binding.* For example, a two-dimensional Coulomb ground state is *four* times as tightly bound as a three-dimensional one.

(2) We discuss now the case of a donor atom *displaced from the center* of the GaAs slab.

It is found that a displacement of the impurity atom from the *center* of the GaAs slab towards the *edge* of the quantum well has the effect of reducing the binding. For a donor state at the edge of the GaAs quantum well, *i.e.*, at the GaAs-$Ga_{1-x}Al_xAs$ interface, the effect of the repulsive barrier, ΔE_c , is more important and reduces the binding effect of the attractive Coulomb potential produced by the ionized impurity. We thus have a confinement-induced lifting of the ground states degeneracy of the Coulomb spectrum.

(3) We discuss now the effect of the alloy composition x in $Ga_{1-x}Al_xAs$ on the binding energy.

In the model used for the $Ga_{1-x}Al_xAs$-GaAs-$Ga_{1-x}Al_xAs$ quantum well structures, the electron potential barrier, ΔE_c increases linearly with the Al fraction x in the $Ga_{1-x}Al_xAs$ alloy. It is found that an increase of the Al content in $Ga_{1-x}Al_xAs$ increases the binding of the donor state as a larger electron potential barrier is more effective at confining the wavefunction within the GaAs quantum well.

1.3.2 Chapter 3:

Theory of Electronic Transport through in GaAs-$Ga_{1-x}Al_xAs$-GaAs Double Heterojunction Structures

The major result of the transport study is that *transmission seems to be large for states corresponding to states derived from equivalent extrema of the conduction band.* We now discuss the (111) and (100) interfaces separately.

(1) Let us consider the case of the (111) interface. A state incoming in GaAs from the Γ-point on one side of the $Ga_{1-x}Al_xAs$ barrier transmits largely to the Γ-point minimum in GaAs on the other side of the $Ga_{1-x}Al_xAs$ barrier. Transmission into other GaAs conduction band extrema seems to be much smaller. The same is true for states originating from the GaAs L-point valley in GaAs and transmitting strongly into the L-point valley and weakly into the Γ-point minimum.

(2) Let us now consider the case of the (100) interface. For a state incoming in GaAs from the Γ-point on one side of the $Ga_{1-x}Al_xAs$ barrier, transmission into other GaAs conduction band extrema seems to be much smaller. The same is true for states orginating from the GaAs X-point valley in GaAs and transmitting strongly into the X-point valley and weakly into the Γ-point minimum.

Another interesting result is related to the *energy dependence of the transport coefficients.* Depending on the energy of the incoming state, transmission could occur *below* or *above* the $Ga_{1-x}Al_xAs$ barrier.

(1) When the energy of an incoming state derived from a given conduction band extremum is *below* the $Ga_{1-x}Al_xAs$ barrier corresponding to the same extremum, transport is characteristic of *tunneling.* In that case *transmission is small* and the wavefunction is damped in the $Ga_{1-x}Al_xAs$ barrier. In the *tunneling regime,* transport within the $Ga_{1-x}Al_xAs$ barrier occurs via *evanescent Bloch states with complex values of* $\mathbf{k}$.

(2) On the other hand, when the energy of a incoming state derived from a given conduction band extremum is *above* the $Ga_{1-x}Al_xAs$ barrier corresponding to the same extremum, transport is *propagating* . In that case *transmission shows a resonant behavior* whenever the thickness of the $Ga_{1-x}Al_xAs$ barrier is an integer multiple of a half-wavelength of the wavefunction inside that region. In the *propagating regime*, transport within the $Ga_{1-x}Al_xAs$ barrier occurs via *propagating Bloch states with real values of* $\mathbf{k}$. In the case of the (100) interface, it seems possible to induce *very sharp resonance* whereby an incoming state at $\mathbf{k}(\Gamma)$ in GaAs couples *very weakly* to a propagating state at $\mathbf{k}(X)$ in $Ga_{1-x}Al_xAs$.

1.3.3 Chapter 4:

Theory of Electronic Structure

of Semiconductor Superlattices: $\mathbf{k} \cdot \mathbf{p}$ Theory

We have applied the above formalism to the case of the GaAs-Alas superlattice.

The complex-$\mathbf{k}$ energy band structure is accurately described by this truncated $\mathbf{k} \cdot \mathbf{p}$ Hamiltonian derived from a more complete local pseudopotential calculation. In the present scheme, the complex-$\mathbf{k}$ energy band structure of each constituent semiconductor forming the superlattice is obtained such that the bulk Bloch solutions are expanded in terms of the *same set of* $\mathbf{k}_0 = \mathbf{0}$ *basis functions.* This approach has the advantage that the boundary conditions on the superlattice state function are *exact* without the approximation that the $\mathbf{k}_0 = \mathbf{0}$ of all III-V solids are the same.

We also present results for complex-$\mathbf{q}$ energy band structure for GaAs-AlAs superlattices of different periods. The method is shown to provide an accurate means of determining the electronic structure of semiconductor superlattices without relying on trial-and-error techniques as is presently done within the tight-binding formalism[5].

The formalism presented in Chapter 4 serves as a basis for future studies concerning the optical properties of superlattices. As mentioned earlier, optical phenomena in quantum well structures and semiconductor superlattices have generated a lot of experimental effort since the fabrication of *quantum well lasers.* It is the purpose of Chapter 4 to present a general theory that will serve as a basis for future investigations of the optical properties of semiconductor superlattices.

References

1. J. C. Slater and G. F. Koster, *Phys. Rev.* **94**, 1498 (1954).

2. S. R. White and L. J. Sham, *Phys. Rev. Lett.* **47**, 879 (1981).

3. G. Bastard, *Phys. Rev.* **B25**, 7584 (1982).

4. M. Altarelli, *Phys. Rev.* **B28**, 842 (1983).

4. J. N. Schulman and Yia-Chung Chang, *Phys. Rev.* **B24**, 4454 (1981).

CHAPTER 2

ENERGY SPECTRUM OF SHALLOW DONORS IN $Ga_{1-x}Al_xAs$-GaAs-$Ga_{1-x}Al_xAs$ QUANTUM WELL STRUCTURES

Section 2.1

INTRODUCTION

2.1.1 Scope of the study

Most electronic properties of semiconductor devices are largely determined by the addition of electronically active doping species within a bulk crystal. Semiconductor superlattices, when employed as active electronic devices, can also have their electronic properties modified by the introduction of dopant impurities. Furthermore, impurities are inevitably introduced during the growth of the semiconductor superlattice, whereas it is possible to grow highly pure bulk semiconductor. *It is therefore crucial to have an understanding of the effect of doping on the electronic properties of semiconductor superlattices.* Superlattices open a new avenue as far as the *control of electronic parameters* such as energy band gap, effective masses, ... In a superlattice or a quantum well (*i.e.*, a single-period superlattice) these *parameters that determine the overall electronic properties of the semiconductor structure can be adjusted independently by varying the superlattice period* or other quantities easily controllable during the growth.

This chapter is concerned with the energy spectrum of shallow donors in $Ga_{1-x}Al_xAs$-GaAs-$Ga_{1-x}Al_xAs$ quantum well structures. The unique nature of electronic states associated with semiconductor superlattices has been the subject of a great deal of interest[1—3]. In view of the potential applications of these structures[4—7], the understanding of impurity states found within these systems is an issue of technical as well as scientific importance. The conduction and valence band offsets arising at the interface between the two semiconductors forming the superlattice produce a series of rectangular potential wells confining the electronic states in the smaller band gap material. It has been shown analytically[1] and verified

experimentally[8] that both the electronic transport[9,10] and the optical properties[11] are largely determined by the nature of the electronic states confined within these potential wells.

2.1.2 Outline of Chapter 2

We now present an outline of the chapter. This chapter addresses the question of the calculation of the binding energy for shallow donors in $Ga_{1-x}Al_xAs$-GaAs-$Ga_{1-x}Al_xAs$ quantum well structures. In these structures, a finite slab of GaAs is located between two semi-infinite layers of $Ga_{1-x}Al_xAs$. In this case, a small band gap semiconductor (GaAs) is located between two large band gap semiconductors ($Ga_{1-x}Al_xAs$), thereby forming a *confining potential energy well for the electrons located within the central* GaAs *slab.* Variations of binding energies are examined as a function of the thickness of the GaAs slab, the alloy composition x in the alloy $Ga_{1-x}Al_xAs$, and the position of the impurity atom within the GaAs slab. Two specific cases are treated.

(*i*) In the first case, we take into account the *finite value* of the electron potential barrier, which has its origin in the conduction band offset ΔE_c , at the GaAs-$Ga_{1-x}Al_xAs$ interface. In this *finite barrier* model, the donor wavefunction is imperfectly confined by the electron potential barrier and is allowed to penetrate in the $Ga_{1-x}Al_xAs$. In bulk GaAs, the binding energy is independent of the position of the impurity ion within the crystal. This is *not* the case in the case of quantum well structure where the motion of the electron is confined in the direction normal to the pair of interfaces. We also study the *lifting of the degeneracy due to the spatial distribution of the donors.* In order to do so, the effect of the position of the impurity ion within the central GaAs slab is studied.

(*ii*) In the second case, we consider an idealized case in which the electron potential barrier created by the conduction band offset ΔE_c at the interface is assumed to be *infinite* with respect to the energy scale of the binding energy. In this *infinite barrier* model, the donor state is not allowed to leak out in the adjacent $Ga_{1-x}Al_xAs$ layers and is perfectly confined to the GaAs slab. The purpose of this

exercise is to study the behavior of the *donor excited states* as the thickness of the central GaAs slab is varied.

The GaAs-$Ga_{1-x}Al_xAs$ system was chosen since the EMA is known to hold to a high degree of accuracy for shallow donor states in GaAs[12]. Since we treat a single quantum well, the results discussed below should apply to superlattices in which the $Ga_{1-x}Al_xAs$ barriers are thick enough so that there is little overlap between the states confined to adjacent GaAs quantum wells. In the case of thin superlattices, one should take into account the spreading of the donor envelope function into the adjacent quantum wells.

We treat shallow donors in quantum well structures along the lines of an *effective mass theory.* A variational method is used to calculate the binding energy of the shallow donors. A review of the single-valley effective mass theory for bulk solids can be found in Appendix (2.1). The variational solutions of the effective mass equation for the donor envelope function can be found in Appendix (2.2).

2.1.3 Summary of the Results of Chapter 2

This study focuses on the variation of the binding energy of a shallow donor state within a $Ga_{1-x}Al_xAs$-GaAs-$Ga_{1-x}Al_xAs$ quantum well structure as a function of

- thickness of the GaAs slab containing the donor atom,
- alloy composition in $Ga_{1-x}Al_xAs$, and
- position of the impurity ion within the GaAs slab.

The binding energy with respect to the the first conduction subband is calculated for the donor ground state and the low-lying excited states. We present now a brief summary of the results of Chapter 2. A detailed discussion of these results can be found below in Sections (2.2) and (2.3).

1. Variation of Binding Energy with GaAs Well Thickness:

Generally, it is found that *the binding energy is considerably modified when the* GaAs *quantum well thickness is reduced from a large value to few monolayers.* This effect is more important for the donor ground state than for the donor excited states. Let us first consider the case of a donor atom at the *center* of the GaAs slab.

(i) In the case of *finite barriers,* the *binding energy varies from the GaAs limit to the* $Ga_{1-x}Al_xAs$ *limit when the dimensions of the quantum well are reduced from a large value to a few monolayers.* At *large* GaAs *thicknesses,* the donor wavefunction has larger amplitude around the ionized center, in the GaAs slab, and the binding energy is close to that of *bulk* GaAs. At *small* GaAs *thicknesses,* the donor wavefunction has more amplitude in the $Ga_{1-x}Al_xAs$ alloy and the binding energy corresponds to that of *bulk* $Ga_{1-x}Al_xAs$. Between these two limits, the binding energy measured from the first conduction subband as a

function of the thickness of the GaAs slab forming the quantum well, shows a maximum corresponding to a maximum confinement of the wavefunction.

(ii) In the case of *infinite barrier*, the *binding energy increases from the three-dimensional limit at large well thicknesses* to *the two-dimesional limit at small well thicknesses.* A two-dimensional Coulomb state is *more bound* than a three-dimensional one. For example, it is found that the two-dimensional Coulomb ground state is *four times as tightly bound* as the three-dimensional Coulomb ground state. Thus the reduction in dimensionality leads to an increase in the binding of the donor state.

2. Variation of Binding Energy with Position of Impurity Atom:

It is found that a *displacement of the impurity atom from the center of the* GaAs *slab towards the edge of the quantum well has the effect of reducing the binding.* For a donor state at the edge of the GaAs quantum well, *i.e.*, at the GaAs-$Ga_{1-x}Al_xAs$ interface, the effect of the repulsive barrier, ΔE_c , is more important and reduces the binding effect of the attractive Coulomb potential produced by the ionized impurity. When the donor is located near the edge of the quantum well two opposite effects play a major role in reducing the binding:

(1) the Coulomb attraction tends to pull the wavefunction on the edge of the quantum well where the ionized donor is located, and,

(2) the repulsive potential of the barrier tends to push the wavefunction towards the center of the quantum well, away from the position of the attractive center.

This finding leads to the conclusion that, due to the *confinement of the wavefunction*, there is a *lifting of the degeneracy of the Coulomb states.* This effect is related to the breaking of the three-dimensional periodicity found in bulk solids.

3. Variation of Binding Energy with Alloy Composition:

In the model used for the $Ga_{1-x}Al_xAs$-GaAs-$Ga_{1-x}Al_xAs$ quantum well structures, the electron potential barrier, ΔE_c increases linearly with the Al fraction x in the $Ga_{1-x}Al_xAs$ alloy. Is is found that an *increase of the* Al *content in* $Ga_{1-x}Al_xAs$ *increases the binding of the donor state* as a larger electron potential barrier is more effective at confining the wavefunction within the GaAs quantum well.

Section 2.2

EFFECTIVE MASS THEORY FOR DONORS IN GaAs-$Ga_{1-x}Al_xAs$ QUANTUM WELL STRUCTURES: IMPERFECT CONFINEMENT OFF-CENTER IMPURITY

2.2.1 Scope of this Study:

In this section, we study the *energy spectrum of the ground state and the low-lying excited states for shallow donors in* $Ga_{1-x}Al_xAs$-GaAs-$Ga_{1-x}Al_xAs$ *quantum well structures.* In order to study the *confinement-induced lifting of the Coulomb degeneracies,* the effect of the position of the impurity atom within the central GaAs slab is investigated for different slab thicknesses and alloy compositions.

Two limiting cases are presented:

- one in which the impurity atom is located at the *center* of the quantum well (*on-center impurity*),
- the other in which the impurity atom is located at the *edge* of the quantum well (*on-edge impurity*).

Throughout this section, we consider a quantum well structure formed by a rectangular confining potential of finite magnitude (*imperfect confinement*). The strength of the finite potential barriers is determined by realistic conduction band offsets. We find that both the on-center and the on-edge donor ground state are bound for all values of GaAs slab thicknesses and alloy compositions. The alloy composition, x, is varied between 0.1 and 0.4. In this composition range,

$Ga_{1-x}Al_xAs$ is direct and the single-valley effective mass theory is an adequate technique for treating shallow donor states.

2.2.2 Outline of Section 2.2:

In this section, we report on a study of the energy spectrum of shallow donor states in a single GaAs-$Ga_{1-x}Al_xAs$ quantum well. The energy spectrum of a donor state located within the GaAs slab is studied as a function of the width of the rectangular potential well formed by the conduction band offset at the GaAs-$Ga_{1-x}Al_xAs$ interface. The effect of the alloy composition, x, in the barrier material as well as the position of the donor atom within the well are also investigated. To illustrate the effect of the position of the donor on the electronic spectra, two positions of the donor ion were studied:

(1) donor ion at the *center* of the quantum well (*on-center impurity*) and

(2) donor ion on the *edge* of the quantum well boundary (*on-edge impurity*).

We find that the donor energy spectrum, both for the on-center and the on-edge impurity, is considerably modified as the dimension of the quantum well is varied. Both the on-center and the on-edge donor energies with respect to the first conduction subband versus GaAs slab thickness present a maximum (in absolute value) whose magnitude depends on the alloy composition. *The on-edge impurity, produces a more shallow donor state than the on-center impurity.* This reduction of binding of the on-edge donor ground state results from the fact that the repulsive barrier potential tends to push the electronic charge distribution away from the attractive ionized center thereby leading to a reduced effective Coulomb attraction. This finding is in accord with calculations carried in the case of infinite confining potential for on-center defect and for an on-edge defect[13]. We present such calculations in the next section where we study the *infinite barrier* limit.

In Section (2.2.3), we present the calculational techniques. We describe the basis orbitals on which the donor state is expanded and we discuss the validity of

this expansion. In Section (2.2.4), the main results are presented. First we discuss the energy spectrum for the on-center impurity, then we treat the case of the on-edge impurity. A comparison is made between these two limiting cases. A summary of the results and a conclusion are presented in Section (2.2.5).

2.2.3 Calculational Method:

Calculations are based on the single valley effective-mass approximation (EMA). A detailed presentation of the EMA for shallow impurity states in bulk semiconductors is presented in Appendix (2.1). In Appendix (2.2), we present a modification of the EMA in the case of systems in which a planar defect (*i.e.*, surface, interface,...) perturbs the three-dimensional periodicity characteristic of bulk systems. Also, Appendix (2.2) gives the prescription to solve the resulting single valley effective-mass equation for the donor envelope function within a variational formalism. Most of the mathematical derivations are relegated to these two Appendices and will not be repeated here.

We are concerned with a single $Ga_{1-x}Al_xAs$-GaAs-$Ga_{1-x}Al_xAs$ quantum well, and the results discussed in this section below should apply to superlattices in which the $Ga_{1-x}Al_xAs$ barriers are thick enough so that there is little overlap between the states confined to adjacent GaAs quantum wells. In the case of very thin superlattices, the effective mass theory may be expected to give a wrong description of the impurity system. In such cases, superior theoretical techniques that take into account the atomic character of the interface should be used. In Chapters 3 and 4 we consider such techniques where realistic description of the interfaces are obtained via energy band structures.

Throughout the present investigation, the composition of the $Ga_{1-x}Al_xAs$ alloy was varied in the range where the alloy remains direct, so that the single-valley effective mass theory stills holds. Realistic conduction band offsets of finite magnitude were used, thereby *allowing the wavefunction to penetrate into the barrier material as the dimensions of the confining quantum well are reduced.* The use of finite conduction band offsets has a large effect on the binding energy of the donor state in the thin GaAs slab limit and should be compared with

approximate calculations carried out using infinitely high barrier height (quantum *box* case)[14—15]. For example, as first shown by Levine[16], hydrogenic donor states at a semiconductor surface cannot exist unless the sum of the angular and magnetic Coulomb quantum numbers, $[l + m]$, is an *odd integer* if the potential discontinuity is *assumed to be infinite at the surface.* In this case, the ground state corresponds to a $2p_z$ hydrogenic state. In particular, in the case of infinite barriers, spherically symmetric states are not allowed since the donor envelope function is required to vanish at the interface.

When finite conduction band offsets are taken into account, the condition that the wavefunction vanishes at the interface is relaxed and penetration in the barrier material is allowed. *The infinite barrier case should be viewed as a limiting case valid only for very wide quantum wells for which the penetration of the donor state into the barrier material is small.*

2.2.3.1 Effective Mass Hamiltonian:

We now describe the impurity system within an effective mass Hamiltonian formalism. The effective mass Hamiltonian corresponding to a Coulomb center located at a distance c from the center of a finite quantum well of width $2a$ along the $\hat{\mathbf{z}}$ direction (the $\hat{\mathbf{z}}$-axis is normal to the interface plane) and height V_0 (see Figure 1 for geometry) is:

$$\hat{H}(1) = \frac{-\hbar^2}{2m_1^*}\nabla_{\mathbf{x}}^2 + U_1(\mathbf{x}) \qquad \ldots\text{in region (1)},(1.a)$$

$$\hat{H}(2) = \frac{-\hbar^2}{2m_2^*}\nabla_{\mathbf{x}}^2 + U_2(\mathbf{x}) + V_0 \qquad \ldots\text{in region (2)},(1.b)$$

$$\hat{H}(3) = \frac{-\hbar^2}{2m_2^*}\nabla_{\mathbf{x}}^2 + U_3(\mathbf{x}) + V_0 \qquad \ldots\text{in region (3)},(1.c)$$

where m_1^* refers to the bulk GaAs (well material) effective mass and m_2^* refers to the interpolated effective mass in $Ga_{1-x}Al_xAs$ (barrier material). Since the bulk dielectric constants of GaAs and $Ga_{1-x}Al_xAs$, ϵ_1 and ϵ_2 respectively, differ slightly, the Hamiltonian must include terms due to electrostatic image charges[17-18]. The potentials $U_1(\mathbf{x})$, $U_2(\mathbf{x})$ and $U_3(\mathbf{x})$ represent the Coulomb interaction between the electron and the impurity ion as well as the ion image charge. The explicit form of these potentials, including the image potentials terms is given in Appendix (2.3).

A finite number of image charges was included in the donor effective mass Hamiltonian. Since the dielectric mismatch,

$$\frac{[\epsilon_1 - \epsilon_2]}{[\epsilon_1 + \epsilon_2]},$$

is at most of the order of 5% for the $x = 0.4$ alloy, the contributions due to higher order image charge terms are negligible.

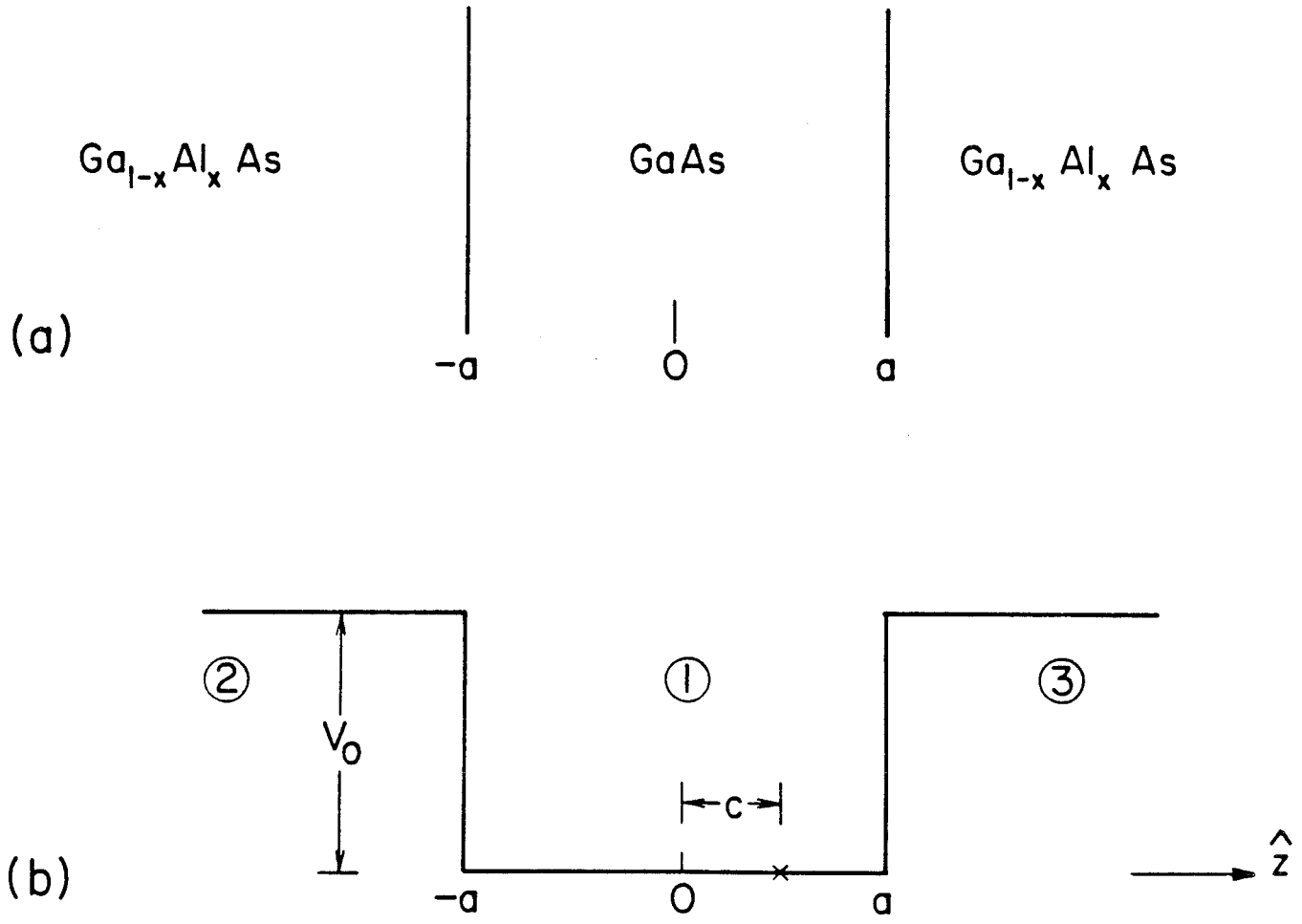

Figure 1: Geometry of a Coulomb center located at a distance c from the center of a finite quantum well of width $2a$ (along the $\hat{\mathbf{z}}$-direction) and height V_0. *(a)* Physical structure. *(b)* Quantum well potential profile along the $\hat{\mathbf{z}}$-axis normal to the interfaces.

Throughout the calculations, the conduction band offset, ΔE_c, is taken to be 85% of the difference of the Γ-point band gaps of GaAs and $Ga_{1-x}Al_xAs$, ΔE_Γ [19]. Since the alloy composition range studied was such that the alloy was direct ($x < 0.45$)[19], both the effective mass m_2^* and the conduction band offset $V_0 \equiv \Delta E_c$ were determined using the Γ-point values in $Ga_{1-x}Al_xAs$[19]:

$$m_1^* = 0.067 m_0, \tag{2.a}$$

$$m_2^* = (0.067 + 0.083x) m_0, \tag{2.b}$$

$$\epsilon_1 = 13.1 \epsilon_0, \tag{2.c}$$

$$\epsilon_2 = [13.1(1-x) + 10.1x]\, \epsilon_0, \tag{2.d}$$

$$V_0 = 1.06x \text{ eV}, \tag{2.e}$$

where m_0 and ϵ_0 are the free electron mass and the vacuum static dielectric constant, respectively.

To calculate binding energies, we must solve for the Hamiltonian defined in Eqs.(1) without the impurity potentials $U_1(\mathbf{x})$, $U_2(\mathbf{x})$ and $U_3(\mathbf{x})$. That is, we must find the *ground state of an electron in the quantum well without the impurity potential.* In this case, the Hamiltonian for the particle is given by:

$$\hat{H}_0(1) = \frac{-\hbar^2}{2m_1^*}\nabla_{\mathbf{x}}^2 \qquad \text{...in region (1),(3.}a\text{)}$$

$$\hat{H}_0(2) = \frac{-\hbar^2}{2m_2^*}\nabla_{\mathbf{x}}^2 + V_0 \qquad \text{...in region (2),(3.}b\text{)}$$

$$\hat{H}_0(3) = \frac{-\hbar^2}{2m_2^*}\nabla_{\mathbf{x}}^2 + V_0 \qquad \text{...in region (3).(3.}c\text{)}$$

The energies (E) of the Coulomb states with respect to the first conduction subband edge are given by the difference between the donor energy, $E(\hat{H})$, and the subband

energy $E(\hat{H}^0)$:

$$E = E(\hat{H}) - E(\hat{H}^0), \tag{4}$$

In the cases

- where the impurity ion is at the *center* of the GaAs quantum well and,
- where we consider the Hamiltonian without the Coulomb center, $\hat{H}^0$,

then the *Hamiltonian is even with respect to reflection through the xy-plane.* Therefore *eigenstates of these Hamiltonians must have definite parity.* Let us consider the Hamiltonian *without* the Coulomb center, $\hat{H}^0$, that gives rise to the subband structure. Eigenstates of $\hat{H}^0$ belonging to *odd-number subbands* ($n = 1, 3, 5, \ldots$) must be *even* with respect to reflection through the xy-plane. Eigenstates of $\hat{H}^0$ belonging to even-number subbands ($n = 2, 4, 6, \ldots$) must be *odd* with respect to reflection through the xy-plane.

The donor effective mass equation was solved using a *variational method.* In this technique, the donor envelope function is expanded in terms of a *variational basis set.* The Hamiltonian for the donor is then expressed as a matrix in the representation of these variational basis functions. Diagonalization of the Hamiltonian matrix yields the energy eigenvalues and the energy eigenstates. The details of the technique are presented in Appendix (2.2)

To preserve the cylindrical geometry of the system, the trial basis orbitals on which the donor state envelope function is expanded are of the form of Gaussian-type orbitals (*gto's*) defined in an *ellipsoidal coordinate system* and *shifted with respect to the ionized donor* taken to be at the origin:

$$\langle \mathbf{x}' | nlm \rangle \equiv \sum_{i=1,2,3} N_i(nl)\left[|\mathbf{x}|(\lambda, d_l)'^l\right] \exp\left[-\varsigma_i(n,l)\left[|\mathbf{x}|(\lambda, d_l)'^2\right]\right] Y_l^m(\hat{\mathbf{x}}'), \tag{5}$$

where,

$$|\mathbf{x}|(\lambda, d_l)' \equiv \sqrt{x^2 + y^2 + \lambda^2(z - d_l)^2}, \tag{6}$$

and $N_i(nl)$ is a normalization constant. The index $i = 1, 2, 3$ labels the region of space where the gto orbital is defined. The paramater λ is a *shape parameter*, and the parameter d_l is a *shift parameter.*

2.2.3.2 Variational basis set:

We pause here to justify the functional form of the variational basis functions $\langle \mathbf{x}' | nlm \rangle$. As seen by the explicit form of Eq.(4), the basis functions $\langle \mathbf{x}' | nlm \rangle$ on which the envelope function is expanded can be decomposed into a product,

$$\langle \mathbf{x}' | nlm \rangle = \xi_\mu(\mathbf{x}_\parallel) g_n(z), \tag{7}$$

where both the variational functions $\xi_\mu(\mathbf{x}_\parallel)$ and $g_n(z)$ are of the form of gto. The vector $\mathbf{x}_\parallel$ is a two-dimensional position vector in the plane of the interface,

$$\mathbf{x}_\parallel = x\hat{\mathbf{x}} + y\hat{\mathbf{y}}. \tag{8}$$

According to Appendix (2.2), the basis functions can be chosen to be of the form of a product:

$$\langle \mathbf{x} | nl; mj \rangle = \xi_l^{(m)}(\mathbf{x}_\parallel) \varphi_n^{(j)}(z), \tag{9}$$

where $\xi_l^{(m)}(\mathbf{x}_\parallel)$ can be taken to be of the same gto functional form as $\xi_\mu(\mathbf{x}_\parallel)$ in Eq.(5) but the function $\varphi_n^{(j)}(z)$ appearing in Eq.(6) is now an *eigenstate of the quantum well Hamiltonian* as defined in Appendix (2.2):

$$\hat{H}^0(z) \equiv \frac{-\hbar^2}{2m_1^*}\left[\frac{\partial^2}{\partial z^2}\right] + V(z), \tag{10}$$

where $V(z)$ is the confining quantum well potential of width $2a$. The eigenstates of $\hat{H}^0(z)$ have *definite parity* and are of the form:

$$\varphi_n^{(g)}(z) \approx \cos\left[k_n^{(g)} z\right] \qquad \ldots z < |a|, (11.a)$$

$$\varphi_n^{(u)}(z) \approx \sin\left[k_n^{(u)} z\right] \qquad \ldots z < |a|, (11.b)$$

$$\varphi_n^{(j)}(z) \approx \pm \exp\left[\pm \kappa_n^{(j)} |z|\right] \qquad \ldots z > |a|, (11.c)$$

where $j = g$ for states *even* with respect to reflection through the xy-plane, and $j = u$ for states *odd* with respect to reflection through the xy-plane.

Is is clear to see that as the GaAs quantum well thickness is reduced, $a \rightarrow 0$, then the subband energy increases and $E \rightarrow V_0$ and the *first conduction subband merges with the* $Ga_{1-x}Al_xAs$ *conduction band edge.* In that case, the eigenstates $\varphi_n^{(j)}(z)$ describe a free state and form a poor basis set for the Coulomb problem. This is due to the fact that, in the small quantum well limit, the eigenstates $\varphi_n^{(j)}(z)$ have a nearly constant amplitude throughout space and fail to describe a Coulomb state adequately. Similarly, for very large quantum well thicknesses, $a \rightarrow \infty$, the *first conduction subband merges with the* GaAs *conduction band edge.* The functions $\varphi_n^{(j)}(z)$ fail to provide an accurate description of a Coulomb state for the same reason. In the case of finite potential barrier, the variational set $\{|nlm\rangle\}$ mimics the Coulomb problem in a cylindrical geometry in both limits of large and small quantum well thicknesses. We therefore label the variational functions $|nlm\rangle$ by the usual Coulomb quantum numbers.

The boundary conditions that *both the wavefunction and the particle current are continuous across the interface*[20] determine relations between the normalization constants, $N_i(nl)$, and the orbital exponents, $\zeta_i(n,l)$, in the barrier material ($i = 2, 3$) in terms of those in the well material ($i = 1$). To produce an accurate description of the donor envelope wavefunction, a *shape parameter*, or eccentricity (λ), as well as a *shift parameter* (d_l), were incorporated in the variational basis set $\{|nlm\rangle\}$. The shape parameter λ determines the compression of the envelope function along the quantum well axis ($\hat{\mathbf{z}}$). The shift parameter d_l determines the location of the electron charge distribution when the impurity ion is moved towards the quantum well edge. In the calculation presented here we chose:

- $d_l \equiv 0$ in the case of the on-center impurity and

• $d_0 \neq 0$ for $l = 0$ and $d_l \equiv 0$ for $l \neq 0$ in the case of the on-edge impurity.

Throughout the calculations, energy is measured in units of

$$E^* \equiv \left[\frac{e^2}{\epsilon_1}\right]^2 \left[\frac{m_1^*}{2\hbar^2}\right], \tag{12}$$

(*donor rydberg*) and distance is measured in units of

$$a^* \equiv \left[\frac{\epsilon_1}{e^2}\right] \left[\frac{\hbar^2}{m_1^*}\right]. \tag{13}$$

(*donor bohr*), where the effective mass, m_1^*, and the static dielectric constant, ϵ_1, both refer to GaAs bulk values.

The gto orbital exponents $\varsigma_1(n, l)$ appearing in Eq.(4) are taken to be of the form, in atomic rydberg units:

$$\varsigma_1(n, l) = \left[\frac{\varsigma_0}{b(n)(l+1)}\right], \tag{14}$$

with

$$b(n) = \{1, 2, 4, 8, 16, 32, 1/2\} \tag{15}$$

so as to cover a physically reasonable range. The exponent at the center of the distribution, ς_0, is taken to be

$$\varsigma_0 = \left[\frac{8}{9\pi}\right] \text{bohr}^{-2}. \tag{16}$$

The choice of ς_0 is dictated by the fact that if one solves the hydrogen atom Hamiltonian for the ground state with a trial Gaussian orbital of the variational form $N \exp(-\varsigma_0 |\mathbf{x}|^2)$, then one easily finds that the variational orbital exponent ς_0 that minimizes the expectation value of the energy is $\varsigma_0 = 8/(9\pi)$ bohr^{-2}.

The boundary condition that *the particle current*

$$\left[\frac{1}{m^*}\right] \left[\nabla \langle \mathbf{x}' | nlm \rangle \cdot \hat{\mathbf{z}}\right] \tag{17}$$

must be continuous across the interface is required since the difference in effective masses was taken into account in the expression of the Hamiltonian. As shown by Ando and Mori[21], these are adequate boundary conditions in the case of GaAs-$Ga_{1-x}Al_xAs$ quantum well structures as long as $Ga_{1-x}Al_xAs$ is direct. For other electronic systems, a more careful analysis of the wavefunction at the interface should be done[20] and would not lead to as simple boundary conditions as the ones outlined above. For our purposes, these boundary conditions will turn out to be adequate.

2.2.3.3 Calculational technique:

The donor envelope function, $|\Psi\rangle$ is expanded on this set of trial orbitals:

$$|\Psi\rangle = \sum_{nlm} |nlm\rangle C(nlm), \tag{18}$$

where the set of basis orbitals $\{|nlm\rangle\}$ are the ellipsoidal gto's defined above in Eq.(4).

The problem of solving the EMA Schrödinger equation for the donor envelope function

$$\hat{H}|\Psi\rangle = E(\hat{H})|\Psi\rangle, \tag{19}$$

reduces to that of solving the generalized eigenvalue problem

$$\sum_{n'l'm'} \left[\langle nlm|\hat{H}|n'l'm'\rangle - E\langle nlm|n'l'm'\rangle\right] C(n'l'm') = 0, \tag{20}$$

for the eigenenergy $E(\hat{H})$ and the expansion coefficients $C(nlm)$ appearing in the expansion Eq.(18).

Calculations were carried out using both *s*-like ($l = 0$) and *p*-like ($l = 1$) gto's.

(1) In the case of the *on-center impurity* ($c = 0$), the Hamiltonian in Eqs.(1) mixes only orbitals whose angular momentum l differ by an even integer. For the *on-center impurity*, only *s*-like gto's were included in the expansion Eq.(18).

(2) However, for the *on-edge* impurity ($c = a$), the mixing between *s*- and *p*-like orbitals becomes appreciable and must be included to provide an accurate description of the neutral donor. For the *on-edge impurity*, 7 *s*-like gto's and 7 *p*-like gto's were included in the expansion Eq.(18).

The calculation of the subband energy, $E(\hat{H}^0)$, was carried through using 7 *s*-like gto's . As mentioned above, eigenstates of $\hat{H}^0$ belonging to the first conduction subband are even with respect to reflection through the xy-plane and thus the

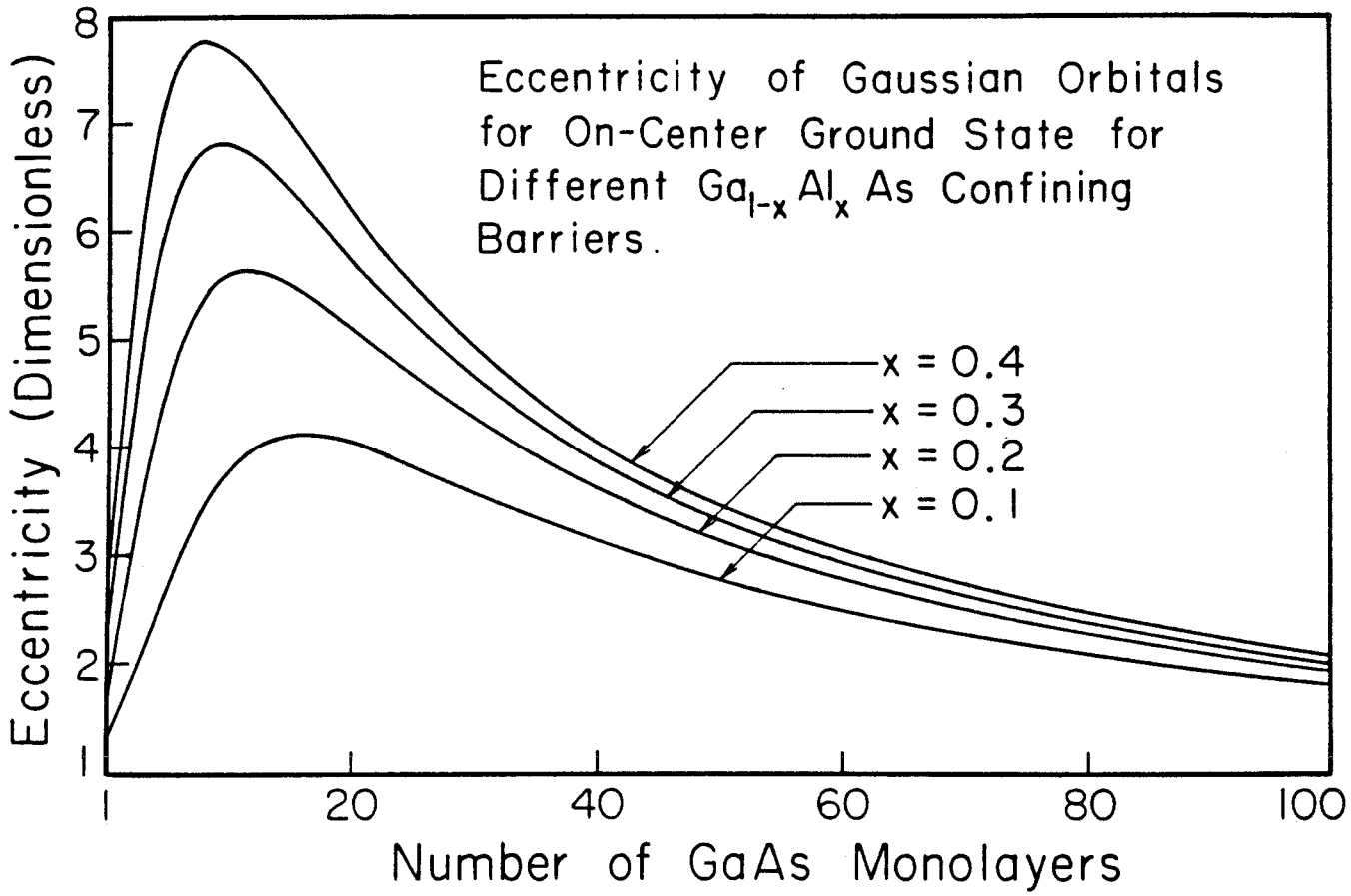

Figure 2: Eccentricity (shape parameter)λ of ellipsoidal Gaussian-type orbitals as a function of GaAs slab thickness for four alloy compositions, $x = 0.1, 0.2, 0.3, 0.4$, of $Ga_{1-x}Al_xAs$. A GaAs monolayer is 2.83 Å thick along the [100] direction.

donor envelope function can be fairly well described by s-like basis orbitals. For each value of GaAs slab thickness, $(2a)$, impurity position (c) and barrier height V_0, the shape parameter λ as well as the shift parameter d_l were determined by minimizing the energy expectation value in the ground state, $E_0(\lambda, d_l)$.

This shifted ellipsoidal Gaussian set has the advantage of reproducing reasonably well the Coulomb center at both the small $(a \rightarrow 0)$ and the large $(a \rightarrow \infty)$ slab thickness limit where the binding energy reduces, in the case of the on-center donor, to that of the barrier material or the well material bulk values, respectively. At the same time, it retains the non-spherical character of the problem and allows the basis orbitals to reshape themselves in order to minimize the total energy. *The inclusion of a shift parameter d_l in the variational basis set allows the electronic charge distribution associated with the donor ground state envelope function to be shifted away from the position of the impurity ion.* This degree of freedom appears to be most important in the case of the on-edge donor where the Coulomb potential tends to pull the charge distribution towards the ionized center whereas the repulsive barrier potential tends to push it away from the ionized center.

2.2.3.4 Shape Parameter or Eccentricity:

Figure 2 shows the *eccentricity* (shape parameter λ) for the on-center donor state as a function of the GaAs slab thickness for different alloy compositions x. As shown in the figure, greater values of x (*i.e.*, greater conduction band offset) result in larger shape parameter and therefore tighter gto's. Furthermore, *the shape parameter-versus-slab thickness curve presents a maximum corresponding to a maximum confinement of the donor envelope function around the impurity atom.* For both very large and very small slab thicknesses, the shape parameter λ reduces to unity as it should in order to describe the isotropic case corresponding

to bulk GaAs or bulk $Ga_{1-x}Al_xAs$, respectively.

2.2.4 Results

We first treat the results obtained for the on-center impurity case ($c = 0$). Then we treat the on-edge impurity case ($c = a$). Comparisons are made between these two limiting cases.

2.2.4.1 On-Center Donor Ground State Envelope Function:

Figure 3 shows the *on-center donor ground state envelope function* through the Coulomb center and normal to the interface plane for different GaAs slab thicknesses and alloy compositions. Greater Al composition produces higher conduction band offsets which, in turn, tend to localize the donor envelope function more effectively. As shown in Figure 3, for very thin GaAs slab, the envelope function leaks appreciably into the barrier material ($Ga_{1-x}Al_xAs$). *In the limit of very thin* GaAs *slab thicknesses, one should recover the binding energy corresponding to bulk* $Ga_{1-x}Al_xAs$. Conversely, *for large* GaAs *slab thicknesses, the on-center donor ground state is mostly confined within the quantum well and one should recover the binding energy for bulk* GaAs. As mentioned above, the EMA Hamiltonian for the on-center impurity mixes only orbitals whose angular momentum l differ by an even integer.

2.2.4.2 On-Center Donor Ground State Binding Energy:

Figure 4 shows the energy, with respect to the first conduction subband, for the *on-center donor ground state as a function* of GaAs slab thickness for four alloy compositions, $x = 0.1, 0.2, 0.3, 0.4$. Along the [100] direction, GaAs monolayers are measured in units of $a/2$, where $a = 5.656$ Å is the GaAs bulk lattice constant. For the on-center impurity, the energy with respect to the first conduction subband versus GaAs slab thickness presents a maximum (in absolute value) whose magnitude depends on the alloy composition of the barrier material. Greater Al

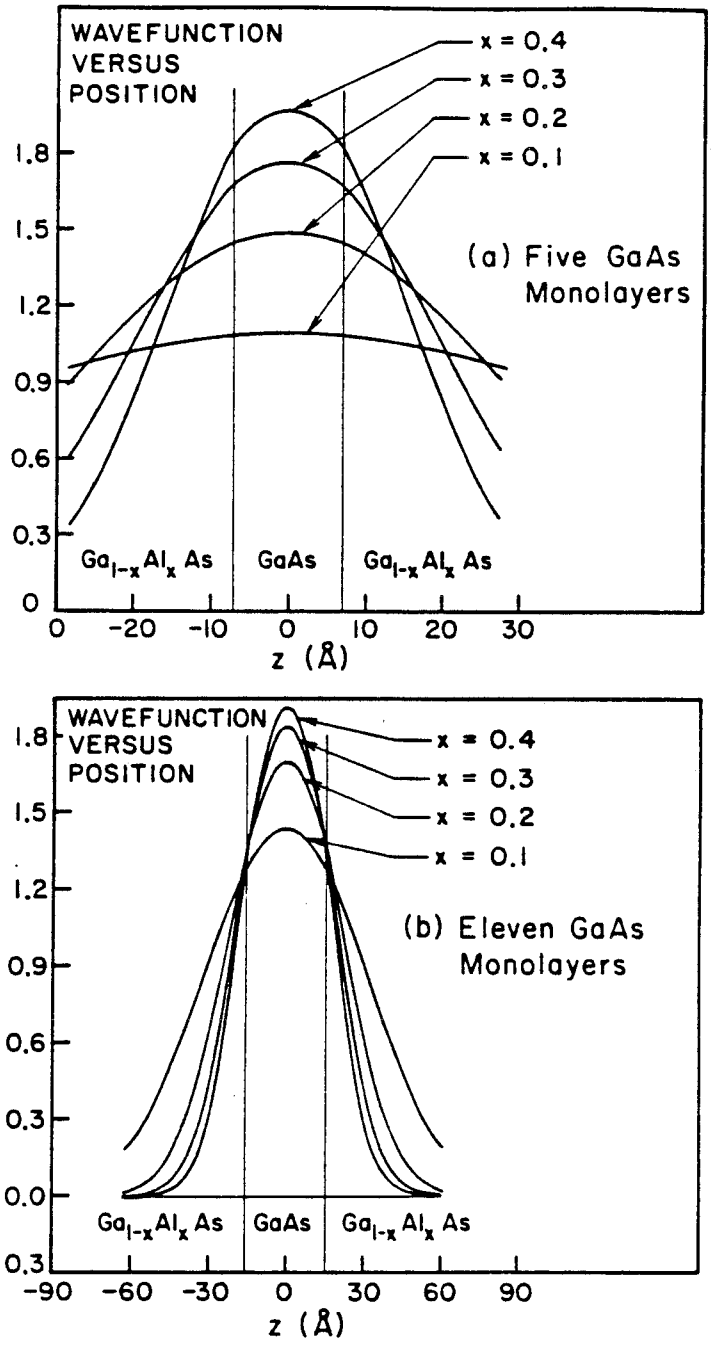

Figure 3: On-center donor ground state envelope function plotted along the axis normal to the interfaces for different GaAs slab thicknesses and four alloy compositions, $x = 0.1, 0.2, 0.3, 0.4$, of $Ga_{1-x}Al_xAs$.

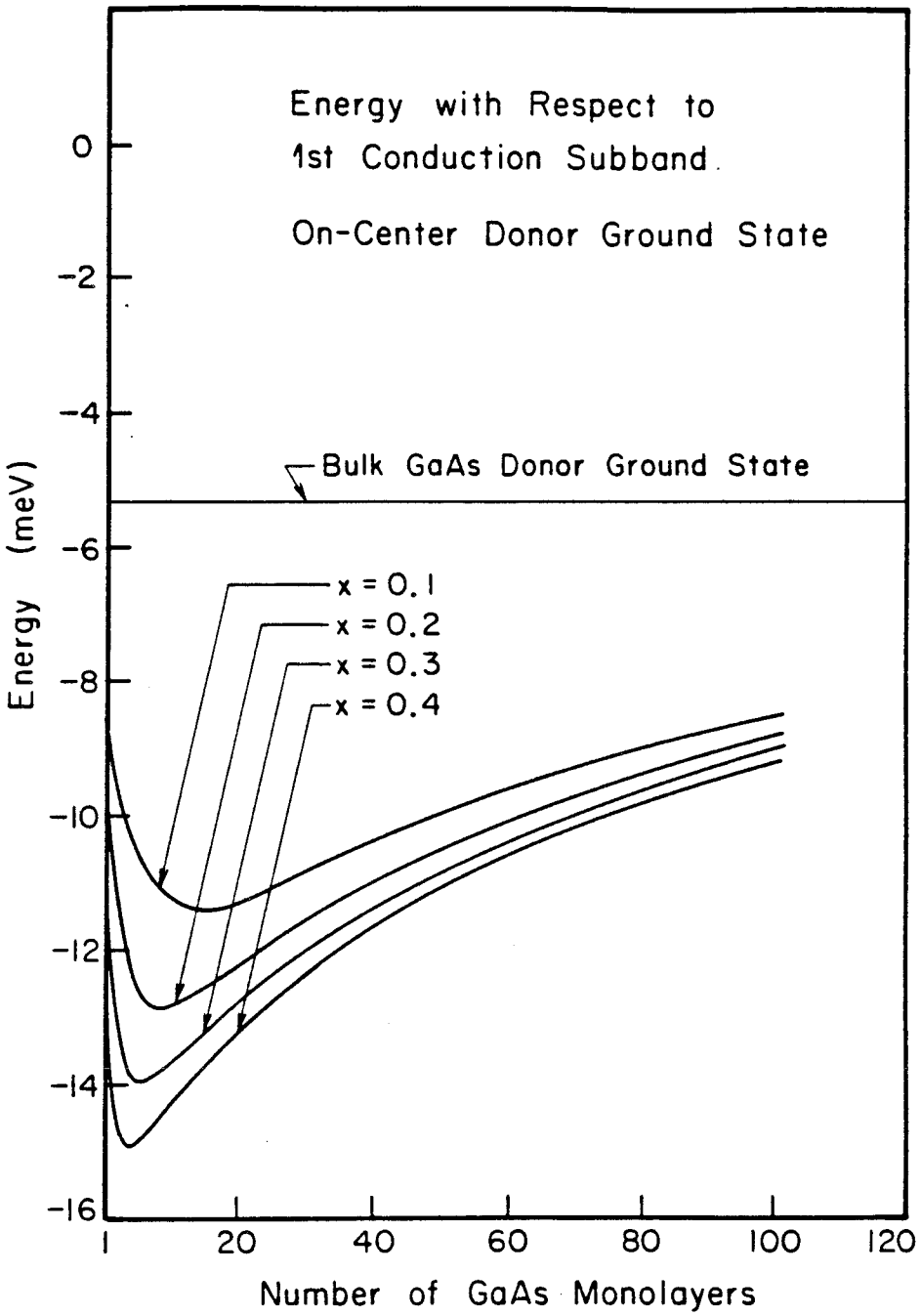

Figure 4: Energy of the on-center donor ground state with respect to the first conduction subband as a function of GaAs slab thickness for four alloy compositions, $x = 0.1, 0.2, 0.3, 0.4$, of $Ga_{1-x}Al_xAs$. Calculations are carried through using 7 s-like ellipsoidal Gaussian-type orbitals as defined in the text. A GaAs monolayer is 2.83 Å thick along the [100] direction.

composition in the barrier material leads to larger conduction band offsets and therefore more complete confinement of the donor envelope function. Since greater confinement of the donor state leads to a more sharply peaked wavefunction as the envelope function builds up amplitude around the impurity ion, the attractive Coulomb potential is more effective in binding the donor state when the Al content in the $Ga_{1-x}Al_xAs$ barrier is increased. For large GaAs slab thicknesses, the effect of the alloy composition x or, equivalently, of the barrier height V_0, on the on-center donor ground state energy and wavefunction is greatly reduced since the envelope function is strongly localized around the impurity ion in the center of the quantum well and does not feel much the repulsive barrier potential.

2.2.4.3 On-Center Donor Excited States Binding Energy:

Figure 5 shows the energy, with respect to the first conduction subband, for the *on-center low-lying excited states of even parity* as a function of GaAs slab thickness for four alloy compositions, $x = 0.1, 0.2, 0.3, 0.4$. The qualitative dependence of the GaAs slab thickness on the energy with respect to the first conduction subband of the even-parity excited states is similar, though not as important, to that of the ground state as can be seen by comparing Figures 4 and 5. The envelope functions corresponding to these excited states are even with respect to reflection through the xy-plane since these are made up from states derived from the first conduction subband. Recent calculations on hydrogenic impurity states in $Ga_{1-x}Al_xAs$-GaAs-$Ga_{1-x}Al_xAs$ quantum well structures[22] are in accord with ours and reinforce the above conclusions.

2.2.4.4 On-Edge Donor Ground State Envelope Function:

Figure 6 shows the *on-edge donor ground state envelope function* through the Coulomb center and normal to the interface plane. As mentioned above, al-

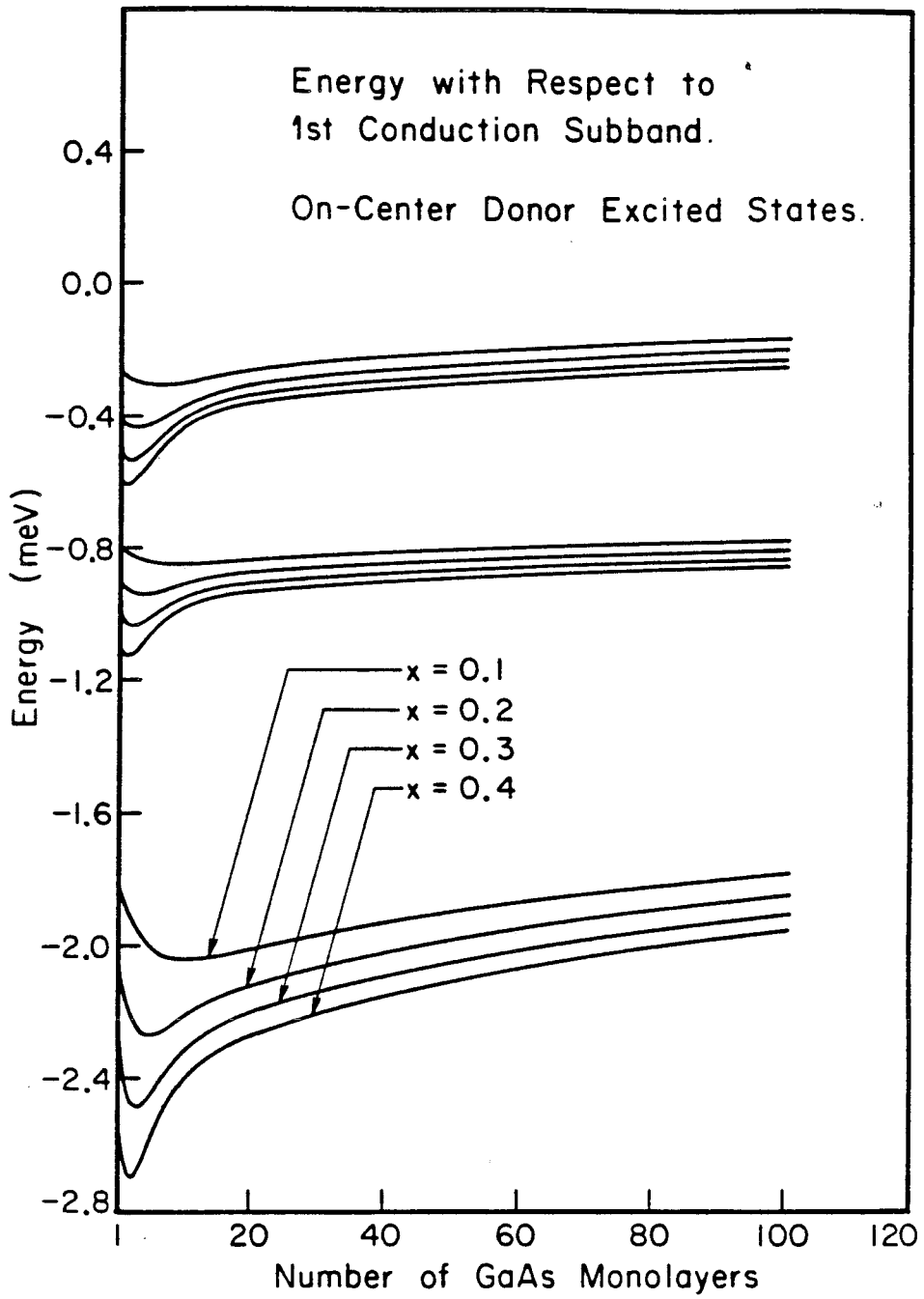

Figure 5: Energy of the on-center low-lying excited states of even parity with respect to the first conduction subband as a function of GaAs slab thickness for four alloy compositions, $x = 0.1, 0.2, 0.3, 0.4$, of $Ga_{1-x}Al_xAs$. Calculations are carried through using 7 s-like ellipsoidal Gaussian-type orbitals as defined in the text. A GaAs monolayer is 2.83 Å thick along the [100] direction.

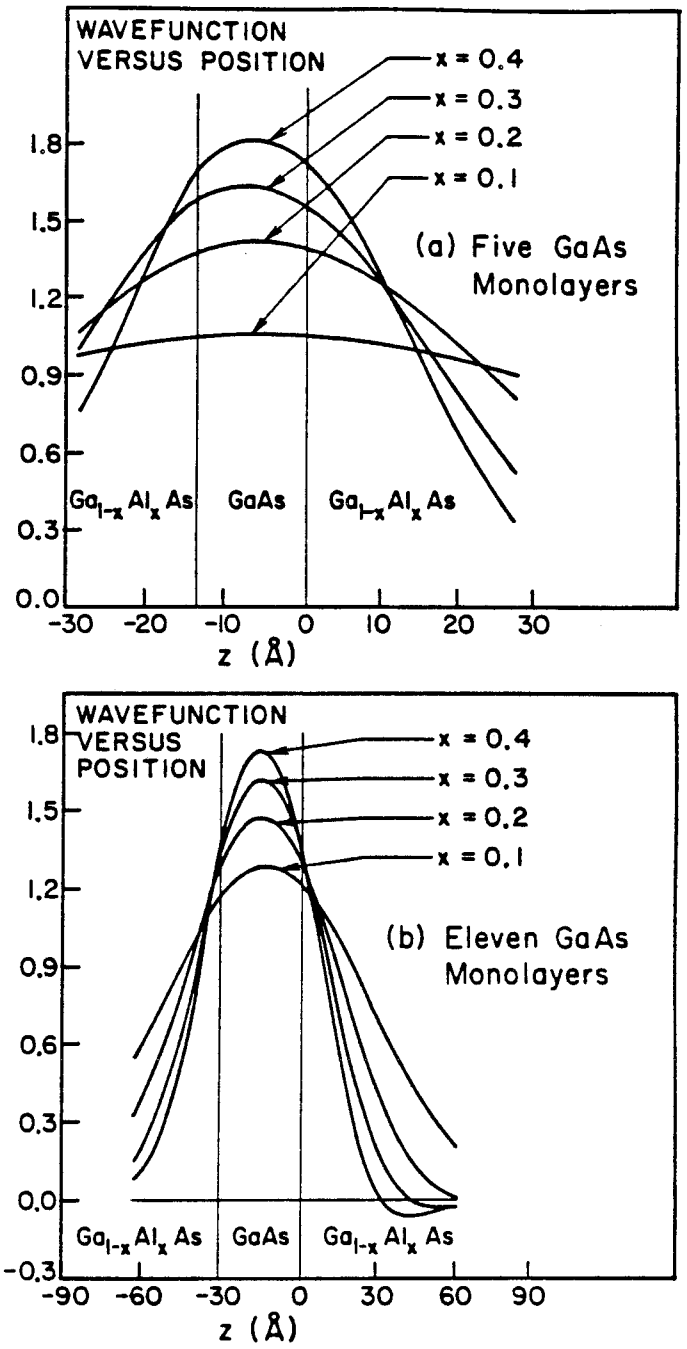

Figure 6: On-edge donor ground state envelope function plotted along the axis normal to the interfaces for different GaAs slab thicknesses and four alloy compositions, $x = 0.1, 0.2, 0.3, 0.4$, of $Ga_{1-x}Al_xAs$. A GaAs monolayer is 2.83 Å thick along the [100] direction.

though the on-center donor wavefunction is entirely s-like, the on-edge wavefunction develops a strong p-like character. The p-like character of the on-edge wavefunction increases as the height of the conduction band offset, V_0, increases.

2.2.4.5 On-Edge Donor Ground State Binding Energy:

Figure 7 shows the energy, with respect to the first conduction subband, of the *on-edge donor ground state* as a function of the GaAs slab thickness for four alloy compositions, $x = 0.1, 0.2, 0.3, 0.4$. The on-edge donor energy curve presents qualitatively the same features as the on-center donor energy curve. In the thin GaAs slab limit, the energy curves for the on-center and the on-edge donor are very similar. In the thick GaAs slab limit, the on-edge donor is less tightly bound than the on-center donor. This is mainly due to the fact that, as the impurity ion approaches the quantum well edge, the donor ground state envelope function should be constructed more and more from Bloch states derived from the $Ga_{1-x}Al_xAs$ conduction band edge. These states lie above the GaAs conduction band edge by an energy equal to the conduction band offset between GaAs and $Ga_{1-x}Al_xAs$. As the on-edge donor ground state envelope function includes more of these higher energy states, the on-edge donor ground state becomes more shallow than the on-center donor ground state.

In the case of the on-edge center, *the repulsive barrier potential tends to push the electronic charge distribution away from the ionized donor* , leading to a *reduced Coulomb attraction.* For the on-edge impurity, the results presented here using finite conduction band offsets are qualitatively similar to the case where infinite conduction band offsets are assumed[13], thereby preventing the donor envelope function from leaking out of the quantum well. The dashed line in Figure 7 indicates the binding energy in the limit of large GaAs slab. The boundary condi-

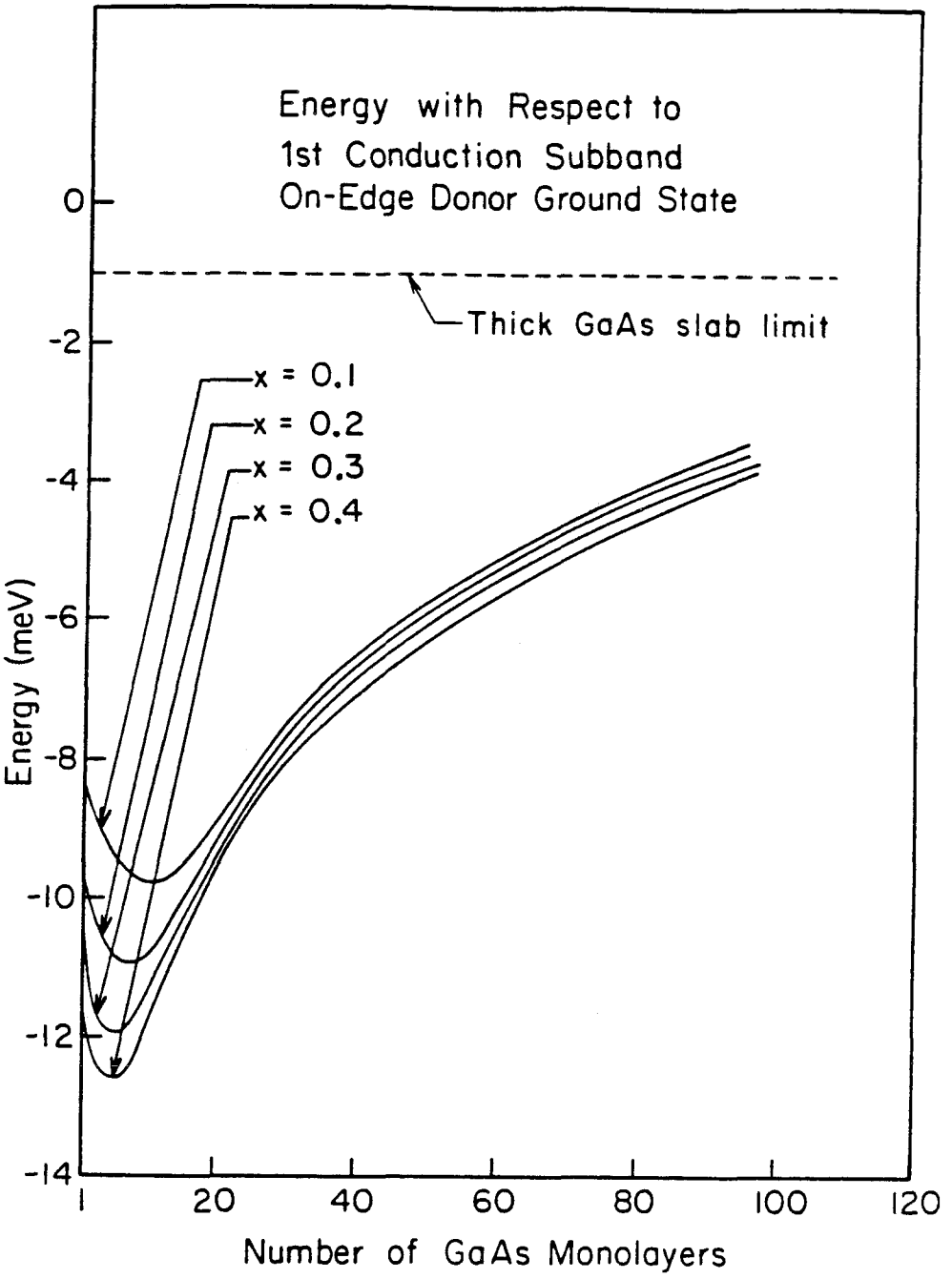

Figure 7: Energy of the on-edge donor ground state with respect to the first conduction subband as a function of GaAs slab thickness for four alloy compositions, $x = 0.1, 0.2, 0.3, 0.4$, of $Ga_{1-x}Al_xAs$. Calculations are carried through using 7 *s*-like and 7 *p*-like ellipsoidal Gaussian-type orbitals as defined in the text. The dashed line indicates the energy with respect to the first conduction subband in the large GaAs slab thickness limit. A GaAs monolayer is 2.83 Å thick along the [100] direction.

tions on the wavefunction at the interface in the finite conduction band offset case gives the donor envelope function a *d*-like character as the slope of the wavefunction is vanishingly small on the donor center. In the large slab limit, the *p*-like character of the donor envelope function is less important for the finite conduction band offset case and the donor ground state mostly consists of shifted *s*-like orbitals.

2.2.5 Summary and Conclusion

We have calculated the energy spectrum of shallow donor states in $Ga_{1-x}Al_xAs$-GaAs-$Ga_{1-x}Al_xAs$ quantum well structures using the effective mass approximation scheme. The variation in energy with respect to the first conduction subband of the donor ground state and the low-lying excited states was studied as a function of

- the central GaAs slab thickness,
- the position of the impurity atom within the GaAs slab,
- the alloy composition x of $Ga_{1-x}Al_xAs$.

Calculations were done for four alloy compositions of $Ga_{1-x}Al_xAs$ in a range in which the alloy remains direct ($x < 0.45$). Realistic values for conduction band offsets of finite magnitude were used. The effect of the impurity position on the binding energy of the donor state was investigated in the two limit cases where the impurity ion was

- at the center of the quantum well (*on-center impurity*) and
- at the edge of the quantum well (*on-edge impurity*).

In the case of both the on-center and the on-edge impurities, *the energy with respect to the first conduction subband versus slab thickness presents a maximum (in absolute value) corresponding to a maximum confinement of the donor state envelope wavefunction.* In the case of the on-edge impurity, the donor ground state is not as tightly bound as the on-center ground state. *The reduction in the binding for the on-edge impurity is a direct consequence of the repulsive interface potential which tends to push the electronic charge distribution away from the Coulomb center.*

For both the on-center and the on-edge impurity, it was found that the energy spectrum of the donor ground state and the low-lying excited states are considerably modified as the thickness of the GaAs slab containing the impurity was varied.

This variation in binding energy should be easily observed experimentally since molecular-beam epitaxy (MBE) techniques[23] now allow for the fabrication of superlattices consisting of alternating slabs of few monolayers of GaAs-$Ga_{1-x}Al_xAs$. It seems possible to adjust the binding of a Coulomb center in a superlattice by varying the thickness of the slab containing the impurity center.

Section 2.3

EFFECTIVE MASS THEORY FOR DONORS IN GaAs-$Ga_{1-x}Al_xAs$ QUANTUM WELL STRUCTURES: PERFECT AND IMPERFECT CONFINEMENT ON-CENTER IMPURITY

2.3.1 Scope of this Study:

In this section, we study the *energy spectrum of the ground state and the low-lying excited states for shallow donors centrally located within quantum well structures (on-center impurity)* consisting of a single slab of GaAs sandwiched between two semi-infinite layers of $Ga_{1-x}Al_xAs$. The binding energy of the donor with respect to the first conduction subband is investigated for different slab thicknesses and alloy compositions. In the work presented here, the *impurity atom is located at the center of the quantum well.* The on-center donor ground state is bound for all values of GaAs slab thicknesses and alloy compositions. The alloy composition, x, is varied between 0.1 and 0.4. In this composition range, $Ga_{1-x}Al_xAs$ is direct and the single-valley effective mass theory as presented in Appendices (1.1) and (1.2) is a valid technique for treating shallow donor states. Calculations are carried out in the two following cases:

- infinite confining potential that does not allow the donor wavefunction to penetrate the adjacent $Ga_{1-x}Al_xAs$ regions, (*perfect confinement*),
- finite confining potential that allows the donor wavefunction to penetrate the adjacent $Ga_{1-x}Al_xAs$ regions, (*imperfect confinement*).

2.3.2 Outline of Section (2.3):

In this section, we report on a study of the energy spectrum of shallow donor states in a single GaAs-$Ga_{1-x}Al_xAs$ quantum well, *i.e.*, a structure formed by a central GaAs slab (*well material*) flanked by two semi-infinite $Ga_{1-x}Al_xAs$ layers (*barrier material*). The energy spectrum of a donor state centered the GaAs slab is studied as a function of the width of the rectangular potential well formed by the conduction band offset at the GaAs-$Ga_{1-x}Al_xAs$ interface. The effect of the alloy composition, x, in the barrier material is also investigated in the case of imperfect confinement. We find that *the donor energy spectrum is considerably modified as the dimension of the quantum well is varied.*

• In the case of *perfect confinement* of the defect wavefunction, the binding energy increases from its value in bulk GaAs up to four times that value as the width of the quantum well is reduced from infinity down to zero. This increase in binding energy for a perfectly confined donor state as the well width is reduced is in accord with the two-dimensional limit of the Coulomb problem[24].

• On the other hand, in the case of *imperfect confinement* of the defect wavefunction, the binding energy with respect to the first conduction subband versus GaAs slab thickness present a maximum (in absolute value) whose magnitude depends on the alloy composition. For *large* GaAs slab thickness, the binding energy reduces to that of *bulk* GaAs. For *small* GaAs slab thickness, the binding energy reduces to that of *bulk* $Ga_{1-x}Al_xAs$.

In Section (2.3.3), we present the calculational techniques. We discuss first the effective mass Hamiltonian used for treating the shallow states and its validity, then we describe the basis orbitals on which the donor state is expanded. Comparisons are made for the infinite potential and the finite potential cases. In Section (2.3.4), the main results are presented. First we discuss the energy spectrum for the per-

fectly confined impurity (infinite barrier), then we treat the case of the imperfectly confined impurity (finite barrier). A summary of the results and a conclusion are presented in Section (2.3.5)

2.3.3 Calculational Method:

Calculations are based on the single-valley effective-mass approximation (EMA) as presented in Appendices (2.2) for quantum well systems. The GaAs-$Ga_{1-x}Al_xAs$ system was chosen since the EMA is known to hold to a high degree of accuracy for shallow donor states in GaAs[12]. Since we treat a single quantum well, the results discussed below should apply to superlattices in which the $Ga_{1-x}Al_xAs$ barriers are thick enough so that there is little overlap between the states confined to adjacent GaAs quantum wells. In the case of thin superlattices, one should take into account the spreading of the donor envelope function into the adjacent quantum wells.

• In the case of *perfect confinement* of the defect wavefunction, the electronic structure of the semiconductor of the barrier material is unimportant since the wavefunction is not allowed to leak out of the quantum well into the barrier material.

• However, in the case of *imperfect confinement* the composition of the $Ga_{1-x}Al_xAs$ alloy was varied in the range where the alloy remains direct, so that the single-valley effective mass theory stills holds. Realistic conduction band offsets of finite magnitude were used, thereby allowing the wavefunction to penetrate into the barrier material as the dimensions of the confining quantum well are reduced. As was seen in the preceding section, *the use of finite conduction band offsets has a large effect on the binding energy of the donor state in the thin GaAs slab limit.*

2.3.3.1 Effective Mass Hamiltonian

In the case where the confining potential is of *infinite strength*, the effective mass Hamiltonian corresponding to a Coulomb center located at the center of a quantum well of width $2a$ along the $\hat{\mathbf{z}}$ direction (the $\hat{\mathbf{z}}$-axis is normal to the interface plane) (see Figure 1(a) for potential profile) is:

$$\hat{H} = \frac{-\hbar^2}{2m_1^*}\nabla_{\mathbf{x}}^2 + U_1(\mathbf{x}) \qquad \ldots z < |a|, (1.a)$$

$$\hat{H} = \infty \qquad \ldots z > |a|, (1.b)$$

However, in the case where the confining potential is of *finite strength* V_0, the effective mass Hamiltonian corresponding to the same system (see Figure 1(b) for potential profile) becomes:

$$\hat{H} = \frac{-\hbar^2}{2m_1^*}\nabla_{\mathbf{x}}^2 + U_1(\mathbf{x}) \qquad \ldots z < |a|, (2.a)$$

$$\hat{H} = \frac{-\hbar^2}{2m_2^*}\nabla_{\mathbf{x}}^2 + U_2(\mathbf{x}) + V_0 \qquad \ldots z > |a|, (2.b)$$

where m_1^* refers to the bulk GaAs (well material) effective mass and m_2^* refers to the composition-dependent interpolated effective mass in $Ga_{1-x}Al_xAs$ (barrier material). As mentioned above, the bulk dielectric constants of GaAs and $Ga_{1-x}Al_xAs$, ϵ_1 and ϵ_2 respectively, differ slightly, and the Hamiltonian should include terms due to electrostatic image charges[17-18]. In the present work these image charge potentials were neglected since they go like (*cf.* Appendix (2.3)):

$$\frac{[\epsilon_1 - \epsilon_2]}{[\epsilon_1 + \epsilon_2],} \qquad (3)$$

which is at most of the order of 5% for the system treated here.

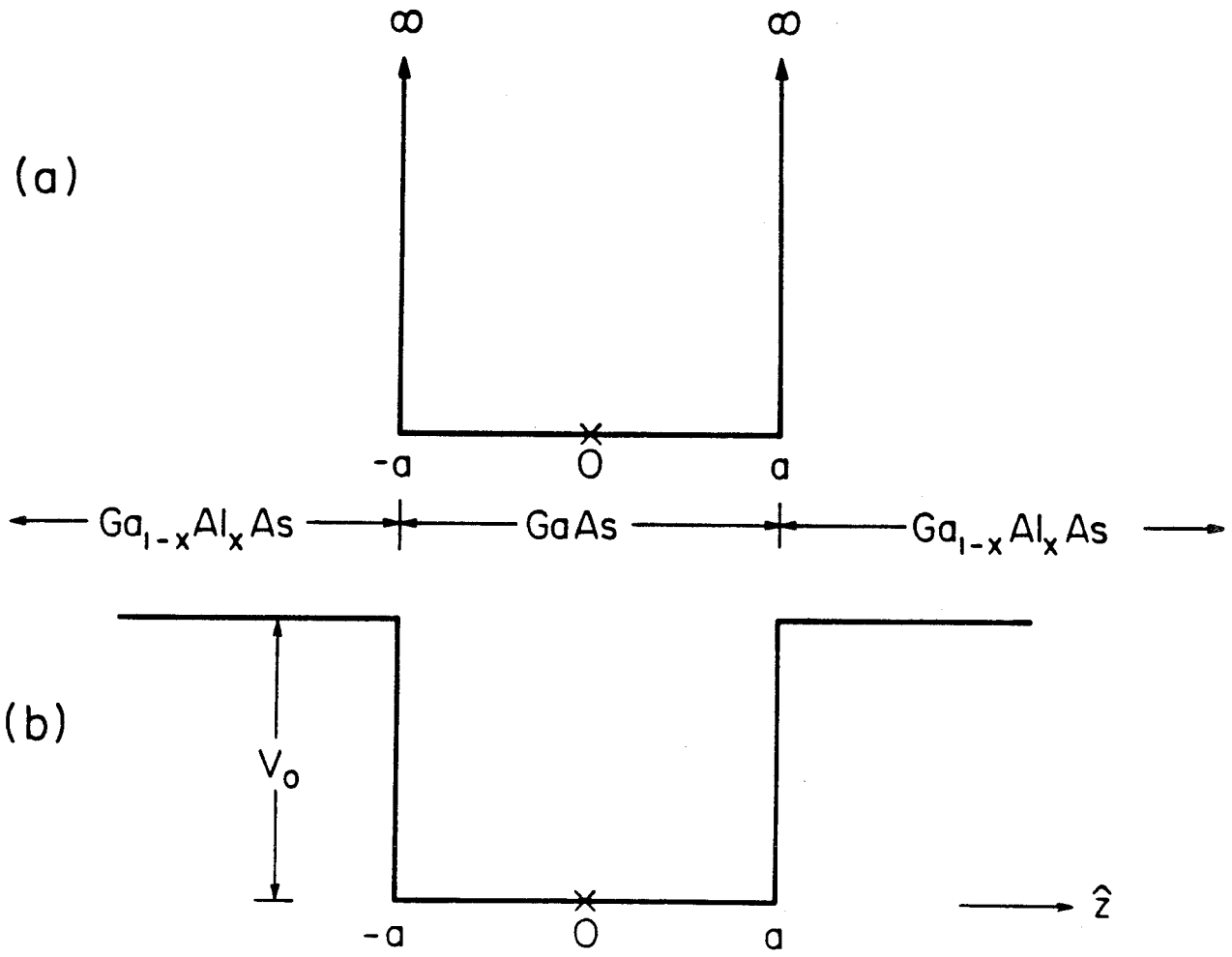

Figure 1: Quantum well potential profile along the $\hat{z}$-axis normal to the interfaces. The position of the impurity is at the center ($z = 0$) of the quantum well of width $2a$. *(a)* Infinite potential: $V(z) \equiv \infty$. *(b)* Finite potential: $V(z) \equiv V_0$.

When the origin is taken to be on the ionized donor, the left and right boundaries of the quantum well are respectively $z_0 = -[a]$ and $z_0 = [a]$. The potentials $U_1(\mathbf{x})$ and $U_2(\mathbf{x})$ appearing in Eqs.(1) and (2) represent the Coulomb interaction between the electron and the impurity ion:

$$U_1(\mathbf{x}) = -\frac{e^2}{\epsilon_1|\mathbf{x}|}, \tag{4.a}$$

and

$$U_2(\mathbf{x}) = -\frac{e^2}{\epsilon_2|\mathbf{x}|}, \tag{4.b}$$

where

$$|\mathbf{x}| = \sqrt{x^2 + y^2 + z^2} \tag{4.c}$$

is the distance from the impurity ion.

In the case of the *finite potential*, the strength of the quantum well potential, V_0, has its origin in the conduction band offset ΔE_c at the GaAs-$Ga_{1-x}Al_xAs$ interface. Throughout the calculations, the conduction band offset, ΔE_c, was taken to be 85% of the difference of the Γ-point band gaps of GaAs and $Ga_{1-x}Al_xAs$, ΔE_Γ [19]. Since the alloy composition range studied was such that the alloy was direct ($x < 0.45$)[19], both the effective mass m_2^* and the conduction band offset $V_0 \equiv \Delta E_c$ were determined using the Γ-point values in $Ga_{1-x}Al_xAs$[19]:

$$m_1^* = 0.067 m_0, \tag{5.a}$$

$$m_2^* = (0.067 + 0.083x) m_0, \tag{5.b}$$

$$\epsilon_1 = 13.1 \epsilon_0, \tag{5.c}$$

$$\epsilon_2 = [13.1(1-x) + 10.1x]\, \epsilon_0, \tag{5.d}$$

$$V_0 = 1.06x \text{ eV}, \tag{5.e}$$

where m_0 and ϵ_0 are the free electron mass and the vacuum static dielectric constant, respectively.

2.3.3.2 Variational Basis Set:

As demonstrated in Appendix (2.2) it is possible to expand the defect wavefunction in a Wannier representation and to obtain a variational formulation of the effective-mass equation. Since the Hamiltonians for the on-center impurity, with and without the Coulomb potential, $\hat{H}$ and $\hat{H}^0(z)$ are both *invariant with respect to reflection through the xy-plane and rotation about the $\hat{\mathbf{z}}$-axis, the eigenstates of $\hat{H}$ and $\hat{H}^0(z)$ must have definite parity.*

Let the variational expansion set be composed of a product of the form $\{\xi_l^{(m)}(\mathbf{x}_\parallel)\varphi_n^{(j)}(z)\}$. The vector $\mathbf{x}_\parallel$ is a position vector parallel to the interface plane,

$$\mathbf{x}_\parallel = x\hat{\mathbf{x}} + y\hat{\mathbf{y}}. \tag{6}$$

The quantum number j of the functions $\varphi_n^{(j)}(z)$ indicates the parity of the wavefunction with respect to reflection through the xy-plane. We use $j = g$ for *even*-parity states and $j = u$ for *odd*-parity states. The eigenstates of $\hat{H}^0$, $\varphi_n^{(j)}(z)$, belonging to *odd-number* subbands ($n = 1, 3, 5, \ldots$) go like $\cos\left[k_n^{(g)}z\right]$ and therefore must be *even* with respect to reflection through the xy-plane, $j = g$, and eigenstates of $\hat{H}^0$ belonging to *even-number* subbands ($n = 2, 4, 6, \ldots$) go like $\sin\left[k_n^{(u)}z\right]$ and therefore must be *odd* with respect to reflection through the xy-plane, $j = u$. The quantum number m of the functions $\xi_l^{(m)}(\mathbf{x}_\parallel)$ plays the role of a magnetic quantum number associated with rotations about the $\hat{\mathbf{z}}$ axis. Thus, *in the case of the on-center Coulomb potential, the parity index (j) and the magnetic quantum number (m) are good labels to classify the solutions of the quantum well Hamiltonian.*

The variational functions $\xi_l^{(m)}(\mathbf{x}_\parallel)$, whose explicit form will be given below, are taken to be two-dimensional Gaussian-type orbitals (*gto's*), and the functions $\varphi_n^{(j)}(z)$ are eigenstates of the one-dimensional operator $\hat{H}^0(z)$ representing the

quantum well potential

$$\hat{H}^{0}(z)\varphi_n^{(j)}(z) = \left[\frac{\hbar^2}{2m_1^*}\left[k_n^{(j)}\right]^2\right]\varphi_n^{(j)}(z), \tag{7}$$

where,

$$\hat{H}^{0}(z) \equiv \frac{-\hbar^2}{2m_1^*}\left[\frac{\partial^2}{\partial z^2}\right] + V(z), \tag{8}$$

represents the the one-dimensional Hamiltonian giving rise to the energy-subbands:

$$E_n^{(j)} = \frac{\hbar^2}{2m_1^*}\left[k_n^{(j)}\right]^2, n = 1, 2, 3, \ldots \tag{9}$$

Therefore the expansion of the defect wavefunction becomes:

$$\langle \mathbf{x}|\Psi^{(mj)}\rangle = \sum_{nl} C(nl)^{(mj)}\xi_l^{(m)}(\mathbf{x}_\parallel)\varphi_n^{(j)}(z). \tag{10.a}$$

or,

$$\langle \mathbf{x}|\Psi^{(mj)}\rangle \equiv \sum_{nl} C(nl)^{(mj)}\langle \mathbf{x}|nl;mj\rangle. \tag{10.b}$$

As a consequence of the symmetry properties of the the Hamiltonian $\hat{H}$ of Eqs.(1) and (2), we label the donor wavefunction $|\Psi^{(mj)}\rangle$ by a parity quantum number j and a magnetic quantum number m.

As in Section (2.2), we impose continuity of the wavefunction and of the velocity operator across the quantum well boundary[20]. The boundary condition that

$$\left[\frac{1}{m^*}\right]\left[\nabla\varphi_n^{(j)}(z)\cdot\hat{\mathbf{z}}\right] \tag{11}$$

must be continuous across the interface is required since the difference in effective masses was taken into account in the expression of the Hamiltonian.

2.3.3.3 Eigenstates of Quantum Well Hamiltonian:

In the case of *infinite potential* $V(z) = \infty$, it is well known from elementary quantum mechanics[25], that the eigenstates of $\hat{H}^0(z)$, *i.e.*, the functions $\varphi_n^{(j)}(z)$ entering in the expansion Eq.(10) are of the form:

$$\varphi_n^{(g)}(z) \approx \cos\left[k_n^{(g)} z\right] \qquad \ldots z < |a|, (12.a)$$

$$\varphi_n^{(u)}(z) \approx \sin\left[k_n^{(u)} z\right] \qquad \ldots z < |a|, (12.b)$$

$$\varphi_n^{(j)}(z) \equiv 0 \qquad \ldots z > |a|, (12.c)$$

where:

$$k_n^{(g)} \equiv n\left[\frac{\pi}{2a}\right], \qquad n = 1, 3, 5, \ldots (13.a)$$

$$k_n^{(u)} \equiv n\left[\frac{\pi}{2a}\right], \qquad n = 2, 4, 6, \ldots (13.b)$$

However, in the case of *finite potential* $V(z) = V_0$, that the eigenstates of $\hat{H}^0(z)$, *i.e.*, the functions $\varphi_n^{(j)}(z)$ entering in the expansion Eq.(10) are of the form:

$$\varphi_n^{(g)}(z) \approx \cos\left[k_n^{(g)} z\right] \qquad \ldots z < |a|, (14.a)$$

$$\varphi_n^{(u)}(z) \approx \sin\left[k_n^{(u)} z\right] \qquad \ldots z < |a|, (14.b)$$

$$\varphi_n^{(j)}(z) \approx \pm \exp\left[\pm \kappa_n^{(j)} |z|\right] \qquad \ldots z > |a|, (14.b)$$

where:

$$\left[k_n^{(j)}\right]^2 = \left[\frac{2m_1^*}{\hbar^2}\right] E, \qquad (15.a)$$

and,

$$\left[\kappa_n^{(j)}\right]^2 = \left[\frac{2m_2^*}{\hbar^2}\right] (V_0 - E) \qquad (15.b)$$

are determined by solving

$$k\tan(ka) = \gamma\kappa \tag{16.a}$$

for the *even-parity eigenstates*, $\varphi_n^{(g)}(z)$, and,

$$k\cot(ka) = -\gamma\kappa \tag{16.b}$$

for the *odd-parity eigenstates*, $\varphi_n^{(u)}(z)$. In Eqs.(14), we have defined

$$\gamma \equiv \left[\frac{m_1^*(\Gamma)}{m_2^*(\Gamma)}\right] \tag{17}$$

as the ratio of the Γ-point effective masses in the well and in the barrier.

The variational set of basis functions, $\{\xi_l^{(m)}(\mathbf{x}_\parallel)\}$ was taken to be of the functional form of two-dimensional Gaussian-type orbitals (*gto*). More specifically:

$$\xi_l^{(m)}(\mathbf{x}_\parallel) = N(l)^{(m)}\rho^{|m|}\exp\left[-\varsigma_l\rho^2\right]\exp(im\phi), \tag{18}$$

where $N(l)^{(m)}$ is a normalization constant and,

$$x = \rho\cos(\phi), \tag{19.a}$$

$$y = \rho\sin(\phi), \tag{19.b}$$

$$\rho = \sqrt{x^2 + y^2}, \tag{19.c}$$

in a two-dimensional cylindrical system.

The two-dimensional gto orbital exponents ς_l appearing in Eq.(17) are fixed and taken to be of the form, in atomic rydberg units:

$$\varsigma_l = \left[\frac{\varsigma_0}{b(l)}\right]. \tag{20}$$

Energy is measured in units of

$$E^* \equiv \left[\frac{e^2}{\epsilon_1}\right]^2 \left[\frac{m_1^*}{2\hbar^2}\right], \tag{21}$$

(*donor rydberg*) and distance is measured in units of

$$a^* \equiv \left[\frac{\epsilon_1}{e^2}\right]\left[\frac{\hbar^2}{m_1^*}\right]. \tag{22}$$

(*donor bohr*), where the effective mass, m_1^*, and the static dielectric constant, ϵ_1, both refer to GaAs bulk values. The coefficients $b(l)$ are chosen so as to cover a physically reasonable range. The central exponent ς_0 was taken to be

$$\varsigma_0 = \left[\frac{8}{9\pi}\right] \text{bohr}^{-2}. \tag{23}$$

The choice of ς_0 is dictated by the fact that if one solves the hydrogen atom Hamiltonian for the ground state with a trial Gaussian orbital of the form $N \exp(-\varsigma_0 |\mathbf{x}|^2)$, then one easily finds that the orbital exponent ς_0 that minimizes the expectation value of the energy is $\varsigma_0 = 8/(9\pi)$ bohr^{-2}.

2.3.3.4 Calculational Technique:

To calculate binding energies, we must solve for the Hamiltonian defined in Eqs.(1) and (2) without the impurity potentials $U_1(\mathbf{x})$ and $U_2(\mathbf{x})$. That is, we must find the *ground state of an electron in the quantum well without the impurity potential.* The energies $E^{(mj)}$ of the Coulomb states with respect to the first conduction subband edge are given by the difference between the donor energy, $E^{(mj)}(\hat{H})$, and the first subband energy $E_1^{(g)}$:

$$E^{(mj)} = E^{(mj)}(\hat{H}) - E_1^{(g)}, \tag{24}$$

The donor envelope function, $|\Psi^{(mj)}\rangle$ is expanded on this set of trial orbitals:

$$\langle \mathbf{x}|\Psi^{(mj)}\rangle = \sum_{nl} C(nl)^{(mj)} \xi_l^{(m)}(\mathbf{x}_\parallel)\varphi_n^{(j)}(z), \tag{25.a}$$

or,

$$\langle \mathbf{x}|\Psi^{(mj)}\rangle \equiv \sum_{nl} C(nl)^{(mj)} \langle \mathbf{x}|nl;mj\rangle, \tag{25.b}$$

where the set of basis orbitals $\{\xi_l^{(m)}(\mathbf{x}_\parallel)\varphi_n^{(j)}(z)\}$ is defined above. The problem of solving the EMA Schrödinger equation for the donor envelope function

$$\hat{H}|\Psi^{(mj)}\rangle = E^{(mj)}(\hat{H})|\Psi^{(mj)}\rangle, \tag{26}$$

reduces to that of solving the generalized eigenvalue problem

$$\sum_{n'l'} \Big[\langle nl;mj|\hat{H}|n'l';mj\rangle - E^{(mj)}\langle nl;mj|n'l';mj\rangle \Big] \; C(n'l')^{(mj)} = 0, \tag{27}$$

for the eigenenergy $E^{(mj)}(\hat{H})$ and the expansion coefficients $C(n'l')^{(mj)}$ appearing in the expansion Eq.(25). Since the Hamiltonian is invariant under reflection through the xy-plane and under rotation through the $\hat{\mathbf{z}}$-axis, the on-center donor

state can be labelled by $\nu\alpha^{(j)}$ where

$$\nu = 1, 2, 3, \ldots \tag{28.a}$$

is a principal quantum number that labels the states in order of increasing energy, and,

$$\alpha = \sigma, \pi, \delta, \ldots \tag{28.b}$$

corresponds to the magnetic quantum numbers,

$$m = 0, \pm 1, \pm 2, \ldots \tag{28.c}$$

Calculations were carried out using a set of 19 gto with magnetic quantum numbers $m = 0, 1, 2$ for the two-dimensional basis functions $\{\xi_l^{(m)}(\mathbf{x}_\parallel)\}$. Since the Hamiltonian of Eqs.(1) and (2) has even parity, only states of the same parity can be mixed.

• For the *infinite potential*, Eq.(1), a set of 5 states $\varphi_n^{(j)}(z)$ was included in the expansion of the defect wavefunction, Eq.(25).

• However, for the case of *finite potential*, a single basis function $\varphi_1^{(g)}(z)$ was included in the expansion since a finite one-dimensional potential well can bind only one state as the width of the well is reduced below a certain value.

2.3.4 Results:

We first discuss the results obtained for the perfectly confined impurity case, *i.e.*, $V(z) \equiv \infty$.

2.3.4.1 Infinite Potential: Binding Energy of Donor Ground State:

Figure 2 shows the energies, with respect to the first conduction subband $E_1^{(g)}$, of the lowest-lying states of $\sigma^{(g)}$ and $\sigma^{(u)}$ symmetries as a function of the number of GaAs monolayers forming the infinite quantum well. Along the [100] direction, GaAs monolayers are measured in units of $a/2$, where $a = 5.656\,\text{Å}$ is the GaAs bulk lattice constant. Since GaAs is a direct band gap semiconductor with spherical energy surface, we obtain simple hydrogen atom-like solutions in the limit of large GaAs slab thicknesses:

$$E_N(a\to\infty) = -\left[\frac{1}{N^2}\right], N = 1, 2, 3, \ldots, \tag{29}$$

where the energy, in GaAs rydberg units, is measured from the first conduction subband. The quantum number N is the principal quantum number. Each energy level is N^2-fold degenerate.

As seen in Fig.2, the donor energy eigenvalue spectrum is modified considerably as the GaAs slab thickness is reduced. It is found that the energy eigenvalue spectrum of a hypothetical two-dimensional hydrogen atom is given[24] by:

$$E_N(a\to 0) = -\left[\frac{1}{(N+\frac{1}{2})^2}\right], N = 0, 1, 2, \ldots, \tag{30}$$

with respect to the conduction subband edge. The quantum number N is the principal quantum number. In this two-dimensional limit, each level is $(2N+1)$-fold degenerate. Thus, *in the limit of infinitely thin* GaAs *slab* $(a\to 0)$, *the donor ground state* $1\sigma^{(g)}$ *should become as much as four times more tightly bound*

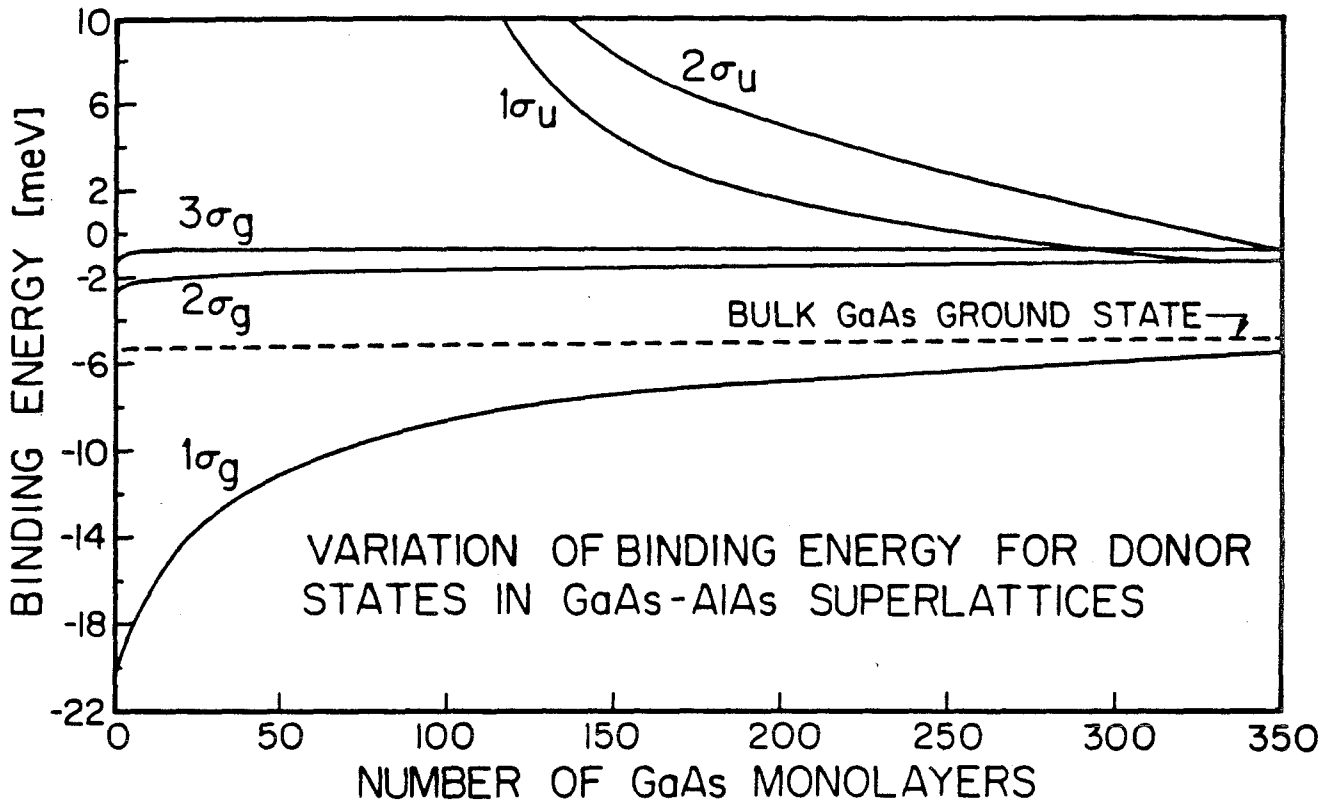

Figure 2: Binding energy of donor states of $\sigma^{(g)}$ and of $\sigma^{(u)}$ symmetries as a function of the number of GaAs monolayers forming the quantum well structure. We assume infinite potential barrier as the GaAsGa$_{1-x}$Al$_x$As interface. Binding energies are measured with respect to the first conduction subband, $E_1^{(g)}$. A GaAs monolayer is 2.83 Å thick.

than in the case of infinitely thick GaAs *slab* ($a \rightarrow \infty$). The binding energy of the excited states of *even parity* $j = g$ do not show as big an effect as that of the ground state. This is due to the fact that the Rydberg series Eqs(29) and (30) do not vary appreciably for N large.

However, the binding energy of states of *odd-parity* $j = u$ shows a very different behavior for small GaAs slab thicknesses. At small GaAs slab thicknesses, these *odd-parity states are not bound with respect to the first conduction subband,* $n = 1$, *since these states are associated with even-numbered subbands,* $n = 2, 4, 6, \ldots$.

Table 1 shows the correspondence between the Coulomb states in the two-dimensional and three-dimensional limit. Three-dimensional Coulomb states that are *odd* with respect to reflection through the xy-plane correspond to two-dimensional $j = u$ states. As mentioned above these odd-parity states are derived from even number subbands and are not bound with respect to the first conduction subband when $a \rightarrow 0$.

2.3.4.2 Infinite Potential: Binding Energy of Donor Excited States:

Figures 3 and 4 show the binding energy of donor states of $\sigma^{(g)}$, $\pi^{(g)}$, $\delta^{(g)}$, $\sigma^{(u)}$, and of $\pi^{(u)}$ symmetries as a function of the number of GaAs monolayers forming the infinite quantum well structure. In the thin GaAs slab limit,

- the *even-parity* states are bound with respect to the first conduction subband, whereas
- the *odd-parity* states are not bound with respect to the first conduction subband, whereas

2.3.4.3 Donor Ground State Envelope Function:

We now consider the case of a finite strength quantum well $V(z) \equiv V_0$ that

3D Coulomb states	2D Coulomb states
$1s$	$1\sigma^{(g)}$
$2s$	$2\sigma^{(g)}$
$2p_0$	$1\sigma^{(u)}$
$2p_{\pm 1}$	$2\pi^{(g)}$
$3s$	$3\sigma^{(g)}$
$3p_0$	$2\sigma^{(u)}$
$3p_{\pm 1}$	$3\pi^{(g)}$
$3d_0$	$4\sigma^{(g)}$
$3d_{\pm 1}$	$2\pi^{(u)}$
$3d_{\pm 2}$	$3\delta^{(g)}$

Table 1. Correspondence between three-dimensional and two-dimensional Coulomb states.

3D Coulomb states	2D Coulomb states
$4s$	$5\sigma^{(g)}$
$4p_0$	$3\sigma^{(u)}$
$4p_{\pm 1}$	$4\pi^{(g)}$
$4d_0$	$6\sigma^{(g)}$
$4d_{\pm 1}$	$3\pi^{(u)}$
$4d_{\pm 2}$	$4\delta^{(g)}$
$4f_0$	$4\sigma^{(u)}$
$4f_{\pm 1}$	$5\pi^{(g)}$
$4f_{\pm 2}$	$3\delta^{(u)}$
$4f_{\pm 3}$	$4\delta^{(g)}$

Table 2. Correspondence between three-dimensional and two-dimensional Coulomb states.

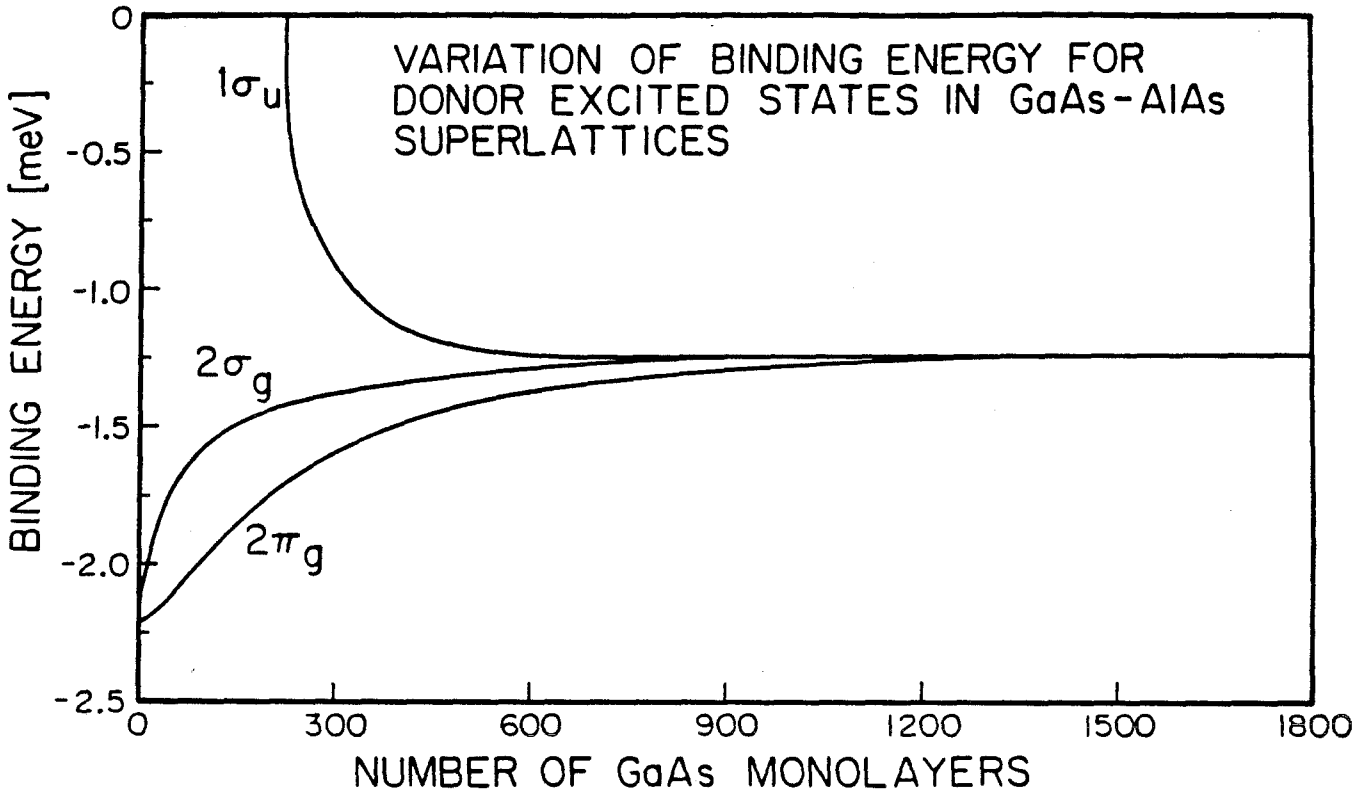

Figure 3: Binding energy of donor states of $\sigma^{(g)}$, $\pi^{(g)}$, and of $\sigma^{(u)}$ symmetries as a function of the number of GaAs monolayers forming the quantum well structure. We assume infinite potential barrier as the GaAsGa$_{1-x}$Al$_x$As interface. Binding energies are measured with respect to the first conduction subband, $E_1^{(g)}$. A GaAs monolayer is 2.83 Å thick.

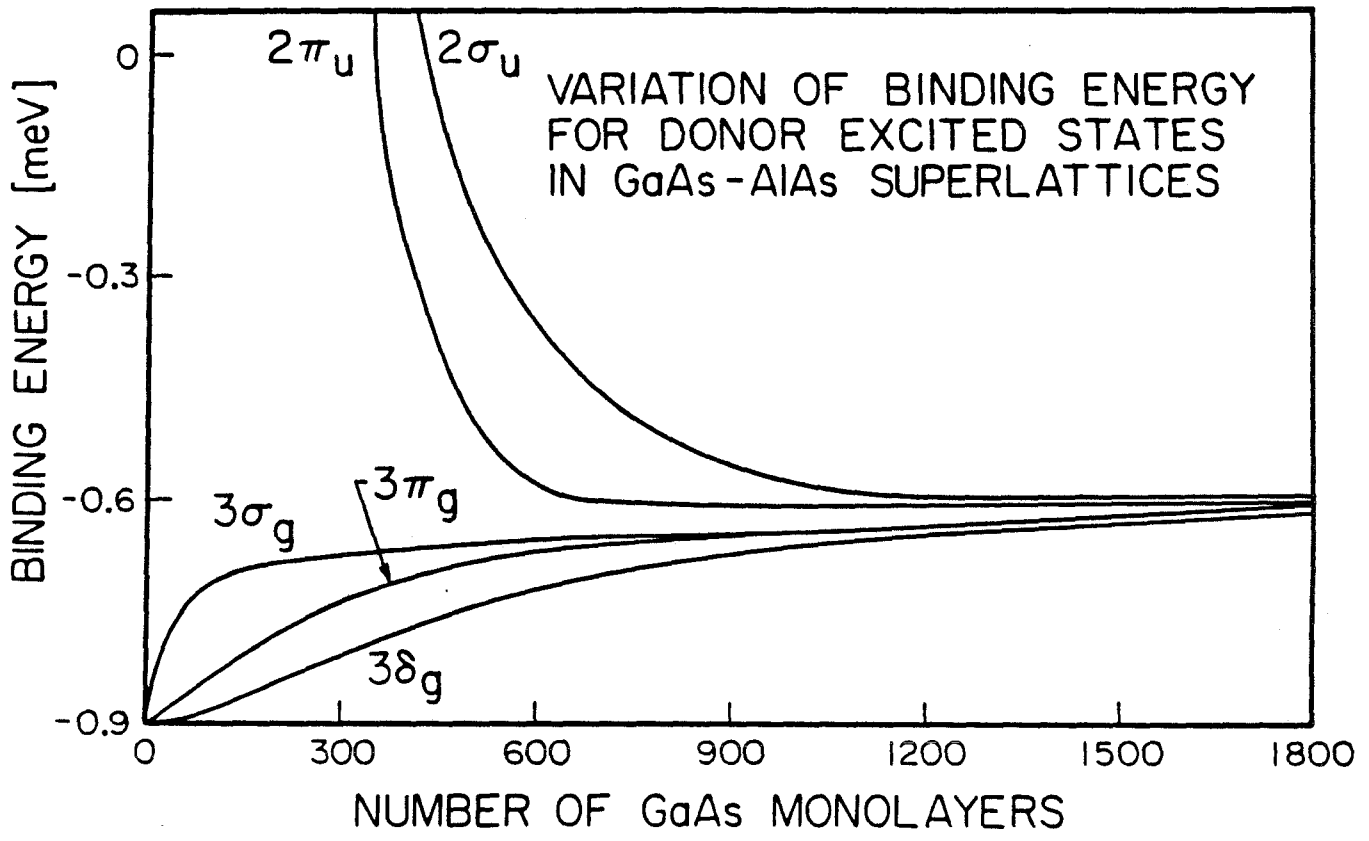

Figure 4: Binding energy of donor states of $\sigma^{(g)}, \pi^{(g)}, \delta^{(g)}, \sigma^{(u)}$, and of $\pi^{(u)}$ symmetries as a function of the number of GaAs monolayers forming the quantum well structure. We assume infinite potential barrier as the $GaAsGa_{1-x}Al_xAs$ interface. Binding energies are measured with respect to the first conduction subband, $E_1^{(g)}$. A GaAs monolayer is 2.83 Å thick.

produces an imperfect confinement of the donor state wavefunction. Figure 5 shows the on-center donor ground state envelope function through the Coulomb center and normal to the interface plane for four GaAs slab thicknesses, $a = 3$ Å, 7 Å, 10 Å and 50 Å, and an alloy compositions of $x = 0.4$. The comparison is made between the finite quantum well (solid line) and the infinite quantum well (dotted line). Greater Al composition produces higher conduction band offsets which, in turn, tend to localize the donor envelope function more effectively. As shown in Figure 5, for very thin GaAs slabs, the envelope function leaks appreciably into the barrier material ($Ga_{1-x}Al_xAs$). In the limit of very thin GaAs slab thicknesses, one should recover the binding energy corresponding to bulk $Ga_{1-x}Al_xAs$. Conversely, for large GaAs slab thicknesses, the on-center donor ground state is mostly confined within the quantum well. As Figure 5 shows, the wavefunctions in the infinite barrier and the finite barrier cases are quite similar and one should recover the binding energy for bulk GaAs.

2.3.4.4 Finite Potential: Binding Energy of Donor Ground State:

Figure 6 shows the energy, with respect to the first conduction subband, for the on-center donor ground state $1\sigma^{(g)}$ as a function of GaAs slab thickness for four alloy compositions, $x = 0.1, 0.2, 0.3, 0.4$. For the on-center impurity, the energy with respect to the first conduction subband versus GaAs slab thickness presents a maximum (in absolute value) whose magnitude depends on the alloy composition of the barrier material. Greater Al composition in the barrier material leads to larger conduction band offsets and therefore more complete confinement of the donor envelope function. Since greater confinement of the donor state leads to a more sharply peaked wavefunction as the envelope function builds up amplitude around the impurity ion, the attractive Coulomb potential is more effective in binding the

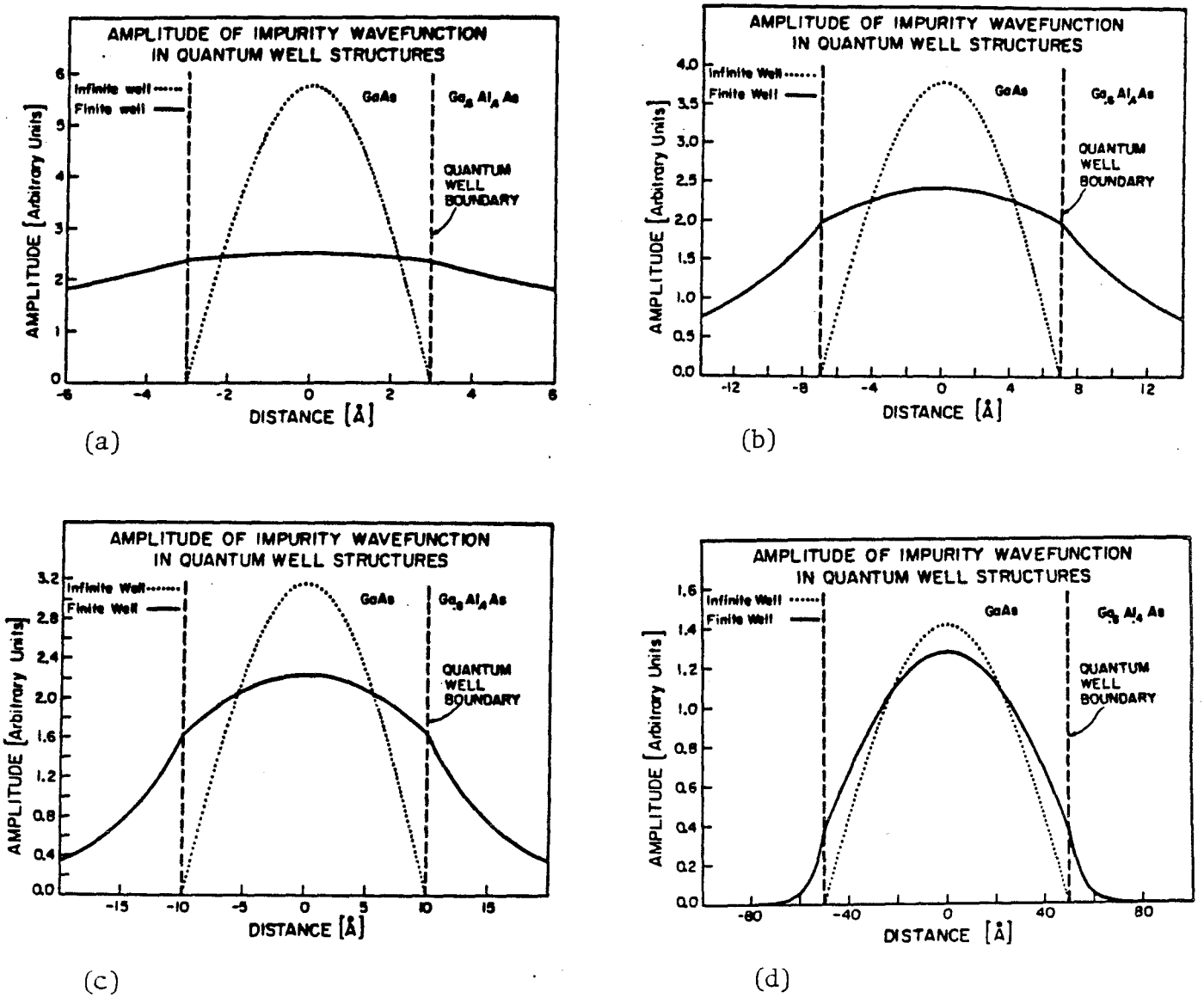

Figure 5: On-center donor ground state envelope function plotted along the axis normal to the interfaces for four GaAs slab thicknesses $a = 3$ Å, 7 Å, 10 Å and 50 Å, and an alloy compositions of $x = 0.4$. Solid line: Finite potential barrier: $V(z) = V_0$. Dotted line: Infinite potential barrier: $V(z) = \infty$.

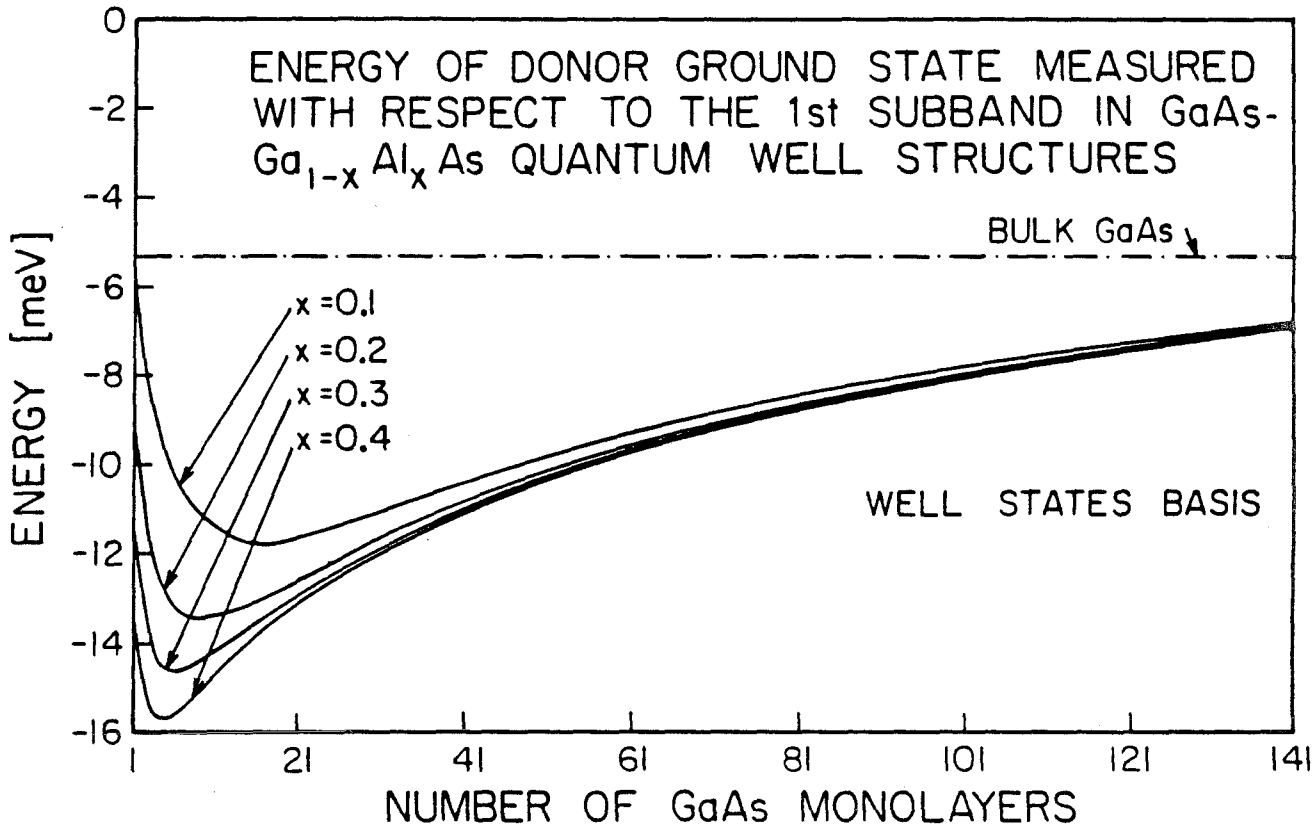

Figure 6: Energy of the on-center donor ground state $1\sigma^{(g)}$ with respect to the first conduction subband as a function of GaAs slab thickness for four alloy compositions, $x = 0.1, 0.2, 0.3, 0.4$, of $Ga_{1-x}Al_xAs$. A GaAs monolayer is 2.83 Å thick.

donor state when the Al content in the $Ga_{1-x}Al_xAs$ barrier is increased. For large GaAs slab thicknesses, the effect of the alloy composition x or, equivalently, of the barrier height V_0, on the on-center donor ground state energy and wavefunction is greatly reduced since the envelope function is strongly localized around the impurity ion in the center of the quantum well and does not feel much the repulsive barrier potential.

By comparing the binding energy spectrum of the donor ground state $1\sigma^{(g)}$ in the case of perfect confinement (Figure 2) and in the case of imperfect confinement (Figure 6), it is clear that the differences in qualitative behavior appear at small GaAs slab thicknesses. In the thin GaAs slab region, the envelope function of the donor ground state for $V(z) = \infty$ and for $V(z) = V_0$ are qualitatively very different: *As the* GaAs *slab thickness decreases, the infinite-barrier wavefunction becomes two-dimensional in character, whereas the finite-barrier wavefunction penetrates the* $Ga_{1-x}Al_xAs$ *region more substantially.* We conclude that *the perfect confinement case should only be regarded as an approximation valid only for thick* GaAs *slab thicknesses when the leaking of the on-center donor ground state wavefunction in* $Ga_{1-x}Al_xAs$ *is negligible.* In the thick GaAs slab limit, the binding energies for the infinite-barrier and the finite-barrier show similar behavior since the finite-barrier wavefunction leaks considerably less as the thickness a of the quantum well is increased.

2.3.5 Summary and Conclusion:

We have calculated the energy spectrum of shallow donor states in $Ga_{1-x}Al_xAs$-GaAs-$Ga_{1-x}Al_xAs$ quantum well structures using the effective mass approximation scheme. The donor atom is located at the *center* of the GaAs slab. Two cases were treated,

- infinite potential discontinuity at the GaAs-$Ga_{1-x}Al_xAs$ interface, (*perfect confinement*),
- finite potential discontinuity at the GaAs-$Ga_{1-x}Al_xAs$ interface, (*imperfect confinement*).

The variation in energy with respect to the first conduction subband of the donor ground state and the low-lying excited states was studied as a function of

- the central GaAs slab thickness, and
- the alloy composition x of $Ga_{1-x}Al_xAs$ in the case of imperfect confinement.

Calculations were done for four alloy compositions of $Ga_{1-x}Al_xAs$ in a range in which the alloy remains direct ($x < 0.45$).

- For the infinite potential case, it is found that, for states of *even-parity* the binding energy spectrum *evolves continuously from a three-dimensional limit to a two-dimensional limit as the width of the quantum well is reduced.* In particular, *in the limit of infinitely thin* GaAs *slab* ($a \rightarrow 0$), *the donor ground state* $1\sigma^{(g)}$ *should become as much as four times more tightly bound than in the case of infinitely thick* GaAs *slab* ($a \rightarrow \infty$).

However, the binding energy of states of *odd-parity* show a very different behavior for small GaAs slab thicknesses. At small GaAs slab thicknesses, these *odd-parity states are not bound with respect to the first conduction subband,* $n = 1$, *since these states are associated with even-numbered subbands,* $n = 2, 4, 6, \ldots$.

• In the finite potential case, the energy with respect to the first conduction subband versus GaAs slab thickness presents a maximum (in absolute value) whose magnitude depends on the alloy composition of the barrier material. The binding energy varies from the bulk value in $Ga_{1-x}Al_xAs$ for the thick slab limit, to the bulk value in GaAs for the thin slab limit. Increasing the alloy composition x results in a greater binding as the height of the potential barrier is increased.

We conclude that *the perfect confinement case should only be regarded as an approximation valid only for thick* GaAs *slab thicknesses when the leaking of the on-center donor ground state wavefunction in* $Ga_{1-x}Al_xAs$ *is negligible.* The use of finite conduction band offsets has a large effect on the binding energy of the donor state in the thin GaAs slab limit.

References

1. J. N. Schulman and T. C. McGill, *Phys. Rev. Lett.* **39**, 1680 (1977).
2. R. N. Nucho and A. Madhukar, *J. Vac. Sci. Technol.* **15**, 1530 (1978).
3. J. N. Schulman and T. C. McGill, *Phys. Rev.* **B19**, 6341 (1979).
4. D. Mukherji and B. R. Nag, *Phys. Rev.* **B12**, 4338 (1975).
5. G. A. Sai-Halasz. L. Esaki, and W. A. Harrison, *Phys. Rev.* **B18**, 2812 (1978).
6. S. Satpathy and M. Altarelli, *Phys. Rev.* **B23**, 2977 (1981).
7. R. Dingle, W. Wiegmann, and C. Henry, *Phys. Rev. Lett.* **33**, 827 (1974).
8. R. Tsu, A. Koma, and L. Esaki, *J. Appl. Phys.* **46**, 842 (1975).
9. L. L. Chang, H. Sakaki, C. A. Chang, and L. Esaki, *Phys. Rev. Lett.* **38**, 1489 (1977).
10. P. Manuel, G. A. Sai-Halasz, L. L. Chang, C. A. Chang, and L. Esaki, *Phys. Rev. Lett.* **37**, 1701 (1976).
11. J. P. van der Ziel, R. Dingle, R. C. Miller, W. Wiegmann, and W. A. Nordland Jr., *Appl. Phys. Lett.* **26**, 463 (1975).
12. G. E. Stilman, D. M. Larsen, C. M. Wolfe, and R. C. Brandt, *Solid State Commun.* **9**, 2245 (1971).
13. G. Bastard, Proceeding of the *Fourth International Conference on Electronic Properties of Two-Dimensional Systems*, August 24-28 1981, New Hampshire, *Surface Sci.* **113**, 165 (1982).
14. P. Voisin, G. Bastard, C. E. T. Gonçalves da Silva, M. Voos, L. L. Chang, and L. Esaki, *Solid State Commun.* **39**, 79 (1981).
15. R. C. Miller, D. A. Kleinman, W. T. Tsang, and A. C. Gossard, *Phys. Rev.* **B24**, 1134 (1981).

16. J. D. Levine, *Phys. Rev.* **140**, A586 (1965).

17. B. V. Pethukov, V. L. Pokrovskii, and A. V. Shaplik, *Soviet Phys. Solid State* **9**, 51 (1967).

18. N. O. Lipari, *J. Vac. Sci. Technol.* **15**, 1412 (1978).

19. H. C. Casey and M. B. Panish, *Heterostructure Lasers* (Academic Press, New York, 1978), Part A, Chapter 4.

20. W. A. Harrison, *Phys. Rev.* **123**, 85 (1961).

21. T. Ando and S. Mori, Proceeding of the *Fourth International Conference on Electronic Properties of Two-Dimensional Systems*, August 24-28 1981, New Hampshire, *Surface Sci.* **113**, 124 (1982).

22. R. L. Greene, and K. K. Bajaj, *Solid State Commun.* **45**, 825 (1983).

23. A. C. Gossard, P. M. Petroff, W. Wiegmann, R. Dingle, and A. Savage, *Appl. Phys. Lett.* **29**, 323 (1976).

24. M. Shinada and S. Sugano, *J. Phys. Soc. Japan* **20**, 1275 (1965).

25. L. I. Schiff, *Quantum Mechanics, 3rd Edition* (McGraw-Hill Book Company, 1968), pp. 102-104.

CHAPTER 3

ELECTRONIC TRANSPORT THROUGH SEMICONDUCTOR DOUBLE HETEROJUNCTION STRUCTURES

Section 3.1

INTRODUCTION

3.1.1 Scope of this Study:

The process of making new semiconductor structures rest, in major part, in providing answers to the two following questions:

(i) Is it possible to modify the electronic properties of the semiconductor structure by addition of electrically active dopants ? How do the binding energy of the impurity states vary with growth parameters ?

(ii) What are the transport properties of electrons within such a structure ? How can the transport properties be modified so as to improve the performance of the device ?

In Chapter 2, we partly addressed the first question. We analysed the doping of $Ga_{1-x}Al_xAs$-GaAs-$Ga_{1-x}Al_xAs$ quantum well structures and found that it was possible to *vary the binding energy of a shallow donor state appreciably by changing the thickness of the* GaAs *slab in which the donor center was located.*

In Chapter 3, we are concerned with the second question. We study the *transport properties* of electrons through double heterojunction structures (DHS) formed by a finite slab of $Ga_{1-x}Al_xAs$ located between two semi-infinite layers of GaAs.

In this case, a large band gap semiconductor ($Ga_{1-x}Al_xAs$) is located between two small band gap semiconductors (GaAs), thereby forming a *potential energy barrier for the electrons on each side of the central* $Ga_{1-x}Al_xAs$ *slab.* Transport coefficients were calculated for electrons incoming from the GaAs onto the central $Ga_{1-x}Al_xAs$ barrier. Since we are specifically interested in the cases where the incoming electron is derived from different extrema of the GaAs conduction band,

we must include a description of the electronic states that is not confined to that region of the Brillouin zone near $\mathbf{k} = \mathbf{0}$. To do so, we provide a description of the electronic energy spectrum of the two semiconductors forming the DHS.

As mentioned in Section (1.1), the electronic band structure of each of the constituent semiconductors is obtained by means of the *empirical tight-binding method* (ETBM) as developed by Slater and Koster[1]. The tight-binding theory uses a *description of the solutions of the crystal Hamiltonian in terms of atomic orbitals.* The matrix elements of the Hamiltonian between these local atomic orbitals are then treated as disposable parameters chosen to fit the band structure obtained by more accurate methods at high symmetry **k** points in the Brillouin zone. The band structure at other **k** points is then obtained via an *interpolation* scheme. A review of the ETBM for bulk solids is given in Appendix (3.1), along with an application for zincblende semiconductors and a list of empirical tight-binding interactions for GaAs and AlAs.

Since the three-dimensional periodicity of the bulk semiconductor is now disrupted by the presence of an interface, the use of the real quantum number **k** to label the irreducible representations of the crystal translation group is not permitted anymore. Simply put, the component of the wavevector **k** *normal to the interface plane* cannot be used to label the solutions of the interface Hamiltonian. This component is now allowed to take on complex values. An electronic energy spectrum where **k** can be complex is referred to as a *complex-***k** *band structure.* Bulk solutions associated with complex values of **k** are not running wave solutions. The imaginary part of the complex wavevector **k** is directly related to the evanescent character of the solution in **x**-space.

3.1.1.1 Flat Barrier Regions:

In the $Ga_{1-x}Al_xAs$ barrier, the wavefunction exists in regions of energy where

free propagation is forbidden. This region is called a *flat barrier region*, since the potential resembles locally that of bulk $Ga_{1-x}Al_xAs$. The *complex-***k** *band structure* is thus an indispensable ingredient for an accurate description of the wavefunction in these barrier regions. The energy eigenvalue spectrum for complex values of the wavevector **k** provides a description of the wavefunvtion in terms of *evanescent solutions*. Within the formalism of Chapter 3, the complex-**k** energy band structure is calculated within the empirical tight-binding method.

3.1.1.2 Disrupted Interfacial Regions:

Apart from flat barrier regions, there exist *interfacial regions* in which the potential varies one lattice site to the next. In order to describe the electronic wavefunction in these regions, we use a *transfer matrix method* to express the tight-binding wavefunction on one side in terms of the tight-binding wavefunction on the other side of the interface.

A detailed treatment of the transfer matrix method, as derived in the ETBM formalism, is given in Appendix (3.2) Appendix (3.3) gives the prescription to obtain the complex-**k** energy band structure of a solid within the ETBM given a knowlodge of the transfer matrix. As in Chapter 2, mathematical derivations will be relegated to Appendices and not repeated within the main course of the discussion.

3.1.2 Outline of Chapter 3:

In the foregoing study we treat the cases of the GaAs-$Ga_{1-x}Al_xAs$-GaAs double heterojunction structures

- along the (111) interface in Section (3.2), and
- along the (100) interface in Section (3.3).

As mentioned above, transmission and reflection coefficients are calculated for an electron incoming from the GaAs and derived from a given extremum of the conduction band.

- For the (111) interface, we consider the cases of incoming electrons derived from near the Γ-point GaAs conduction band minimum,

$$\mathbf{k}(\Gamma) = \left[\frac{2\pi}{a}\right](0, 0, 0), \tag{1.a}$$

and from near the L-point conduction band valley such that,

$$\mathbf{k}(L) = \left[\frac{2\pi}{a}\right]\left(\frac{1}{2}, \frac{1}{2}, \frac{1}{2}\right). \tag{1.b}$$

- In the case of the (100) interface, we analyse the transport pertaining to electrons in the Γ-point conduction band minimum and in the X-point conduction band valley,

$$\mathbf{k}(X) = \left[\frac{2\pi}{a}\right](1, 0, 0). \tag{1.c}$$

Transmission coefficients are calculated as a function of

- GaAs conduction band minimum from which the incoming electron is derived,
- energy of the incoming electron,
- thickness of the $Ga_{1-x}Al_xAs$ barrier, and
- alloy composition x in the $Ga_{1-x}Al_xAs$ barrier.

Transport coefficients are calculated for different extrema of the GaAs lowest conduction band. Applications of these ideas to the physics of semiconductor devices is discussed.

3.1.3 Summary of the Results of Chapter 3

This chapter focuses on the transport coefficients of electronic carriers through GaAs-$Ga_{1-x}Al_xAs$-GaAs DHS. We consider both the (111) and the (100) zincblende interface. We present now a brief summary of the results of Chapter 3.

3.1.3.1 Transport Through GaAs-$Ga_{1-x}Al_xAs$ -GaAs DHS (111):

It is found that *transmission seems to be large for states corresponding to states derived from equivalent extrema of the conduction band.* A state incoming in GaAs from the Γ-point on one side of the $Ga_{1-x}Al_xAs$ barrier transmits largely to the Γ-point minimum in GaAs on the other side of the $Ga_{1-x}Al_xAs$ barrier. Transmission into other GaAs conduction band extrema seems to be much smaller. The same is true for states originating from the GaAs L-point valley in GaAs and transmitting strongly into the L-point valley and weakly into the Γ-point minimum.

It is also found that, depending on the energy of the incoming state, transmission could occur *below* or *above* the $Ga_{1-x}Al_xAs$ barrier giving rise to two distinct regimes of transport.

o When the energy of an incoming state derived from a given conduction band extremum is *below* the $Ga_{1-x}Al_xAs$ barrier corresponding to the same extremum, transport is characteristic of *tunneling.* In that case *transmission is small* and the wavefunction is damped in the $Ga_{1-x}Al_xAs$ barrier. In the case of *tunneling transport* the incoming state couples mostly to evanescent Bloch states associated with complex values of $\mathbf{k}$ in the $Ga_{1-x}Al_xAs$ barrier.

o On the other hand, when the energy of a incoming state derived from a given conduction band extremum is *above* the $Ga_{1-x}Al_xAs$ barrier corresponding to the same extremum, transport is *propagating* . In that case *transmission shows a resonant behavior* whenever the thickness of the $Ga_{1-x}Al_xAs$ barrier is an integer

multiple of a half-wavelength of the wavefunction in that region. In the case of *propagating transport* the incoming state couples mostly to propagating Bloch states associated with real values of **k** in the $Ga_{1-x}Al_xAs$ barrier.

3.1.3.2 Transport Through GaAs-$Ga_{1-x}Al_xAs$-GaAs DHS (100):

In this case also, it is found that *transmission seems to be large for states corresponding to states derived from equivalent extrema of the conduction band.* A state incoming in GaAs from the Γ-point on one side of the $Ga_{1-x}Al_xAs$ barrier transmits largely to the Γ-point minimum in GaAs on the other side of the $Ga_{1-x}Al_xAs$ barrier. Transmission into other GaAs conduction band extrema seems to be much smaller. The same is true for states orginating from the GaAs X-point valley in GaAs and transmitting strongly into the X-point valley and weakly into the Γ-point minimum

In the case of the (100) interface, two regimes of transport, *propagating and tunneling*, are also found depending on the energy of the incoming electron. *Resonant transport* is also found whenever the thickness of the $Ga_{1-x}Al_xAs$ barrier is an integer multiple of a half-wavelength of the wavefunction if that region. In the case of the (100) interface, it is also possible to induce *very sharp resonance* when an incoming state is derived in GaAs from the Γ-point and couples weakly to a state derived from the X-point minimum in $Ga_{1-x}Al_xAs$. The *sharpness of the resonance is an indication of the weakness of the coupling between states derived from different extrema of the conduction band.*

Section 3.2

TRANSPORT CHARACTERISTICS OF L-POINT AND Γ-POINT ELECTRONS THROUGH GaAs-$Ga_{1-x}Al_xAs$-GaAs (111) DOUBLE HETEROJUNCTIONS

3.2.1 Scope of this Study:

In this section we present here a study on the transport characteristics of L-point and Γ-point derived electrons through abrupt GaAs-$Ga_{1-x}Al_xAs$-GaAs (111) double heterojunctions. The use of complex-**k** band structures in the tight-binding approximation and transfer matrices provide a reasonably accurate description of the wavefunction at the GaAs-$Ga_{1-x}Al_xAs$ interface.

- A representation of the wavefunction in terms of bulk complex-**k** Bloch states, $\{|\mathbf{k}_{\|}E;k_z\rangle\}$, is used in the GaAs regions where the potential is bulk-like.

- A representation of the wavefunction in terms of planar orbitals, $\{|\alpha\sigma;\mathbf{k}_{\|}\rangle\}$ is used at the GaAs-$Ga_{1-x}Al_xAs$ interface where the potential deviates from its bulk value (*i.e.*, interfacial region).

Within the theoretical framework outlined in the Appendices (3.1), (3.2), and (3.3), realistic band structure effects are taken into account and no artificial rules regarding the connection of the wavefunction across the interface are introduced. The ten-band tight-binding model includes admixture in the total wavefunction of states derived from different extrema of the GaAs conduction band.

The major result of this study is that, *states derived from the same extremum*

of the conduction band appear to couple strongly to each other, whereas *states derived from different extrema are found to couple weakly.* Transport characteristics of incoming L-point and Γ-point Bloch states are examined as a function of

- the energy of the incoming state,
- thickness of the $Ga_{1-x}Al_xAs$ barrier, and
- alloy composition, x, int the central $Ga_{1-x}Al_xAs$ barrier.

Transmission through the $Ga_{1-x}Al_xAs$ barrier is either *tunneling* or *propagating* depending on the nature of the Bloch states available for strong coupling in the alloy. Since Bloch states derived from different extrema of the conduction band appear to couple weakly to each other, it seems possible to reflect the low-velocity L-point component of the current while transmitting the high-velocity Γ-point component.

3.2.2 Outline of Section 3.2:

The introduction of new device fabrication technologies has allowed the realization of planar electronic devices in which the dimension perpendicular to the growth plane is of the order of a few lattice spacings. The understanding of the transport of electrons through semiconductor interfaces is of great importance regarding the performance of these very small-scale electronic devices. The major reason that makes GaAs a prime candidate for high-speed electronic devices is the very high velocities that can be achieved by electrons derived from the Γ-point conduction band minimum. The small value of the Γ-point effective mass is in major part responsible for the very high velocities that can be achieved by these electrons. At higher energies, electrons start to populate the low-velocity L-point and X-point GaAs conduction band valleys, therefore reducing the population of the high-velocity Γ-point minimum. This has the direct effect of setting an upper limit to the speed at which the device can operate. The study of the transport of electrons associated with the various GaAs conduction band valleys is therefore of crucial importance.

The work presented here is concerned with the transport of L-point and Γ-point derived electron states through a GaAs-$Ga_{1-x}Al_xAs$-GaAs (111) double heterojunction structure (DHS). The transport in these structures is either *tunneling* or *propagating* depending on the nature of the states with strong coupling available for transmission in the $Ga_{1-x}Al_xAs$ barrier (*i.e.*, evanescent or propagating).

- In the *tunneling regime of transport*, the Bloch states with strong coupling available for transmission in the $Ga_{1-x}Al_xAs$ barrier are *evanescent* and the wavevector **k** is complex.

- In the *propagating regime of transport*, the Bloch states with strong coupling available for transmission in the alloy are *propagating* and the wavevector **k**

takes on real values.

In the following, we examine DHS in which the perpendicular dimension of the central barrier region is of the order of a few atomic layers. Since the potential varies over distances on an atomic scale, a theoretical approach beyond the effective-mass theory is needed.

The theoretical framework used here exploits the bulk properties of the constituent semiconductors forming the DHS. The transport of electrons through a region of space in which the energy of the state is such that *free propagation is not allowed* is best described in terms of the complex-**k** bulk band structure. The breakdown of translational invariance induced by the interface implies a new set of boundary conditions that do not exclude the component of the wavevector **k** normal to the interface to take on *complex values*. The problem of calculating the transport coefficients of Bloch states at an abrupt interface using complex-**k** band structure, cast in a tight-binding band calculation scheme, has been addressed in the past[2—5].

The major result of the following theoretical study is that the mixing between L-point and Γ-point states appears to be small. Therefore, there seem to exist two distinctive energy barriers for L-point and Γ-point electrons. Given an alloy composition of the $Ga_{1-x}Al_xAs$ barrier, there is a range of energies for which the electrons incoming from the Γ-point minimum of GaAs are mostly *transmitted* whereas the electrons incoming from the L-point extremum of GaAs are mostly *reflected*. It seems then possible to *reflect back* the low-velocity L-point component of the current while allowing the high-velocity Γ-point component to be *transmitted*.

In Section (3.2.3) , the basic ingredients of the theoretical technique used to calculate the transport coefficients are presented. The major results are presented

and discussed in Section (3.2.4). A summary and conclusions are given in Section (3.2.5)

3.2.3 Calculational method:

The DHS studied consists of a region of $Ga_{1-x}Al_xAs$ located between two semi-infinite layers of GaAs. Figure 1 shows the energy band diagram and the physical configuration of the DHS. The energy band diagram of the structure indicates the relative positions of the Γ-point and the L-point conduction band edges for an alloy composition of $x \approx 0.3$ in the $Ga_{1-x}Al_xAs$ barrier.

• An electron incoming in the bulk region I (GaAs) at a total energy E above the GaAs Γ-point minimum

o is scattered at the boundaries of the barrier region II ($Ga_{1-x}Al_xAs$)

o and is finally transmitted in another bulk region III (GaAs).

The incoming electron is derived from the Γ-point or from the L-point in GaAs. The Γ-point conduction band offset,ΔE_Γ , is a fraction of the difference in the Γ-point conduction band gaps between GaAs and $Ga_{1-x}Al_xAs$. Depending on whether we describe the total wavefunction in a bulk region or an interfacial region, different representations are used accordingly. We now discuss these two representations in the light of the theoretical discussion of Appendix (3.3)

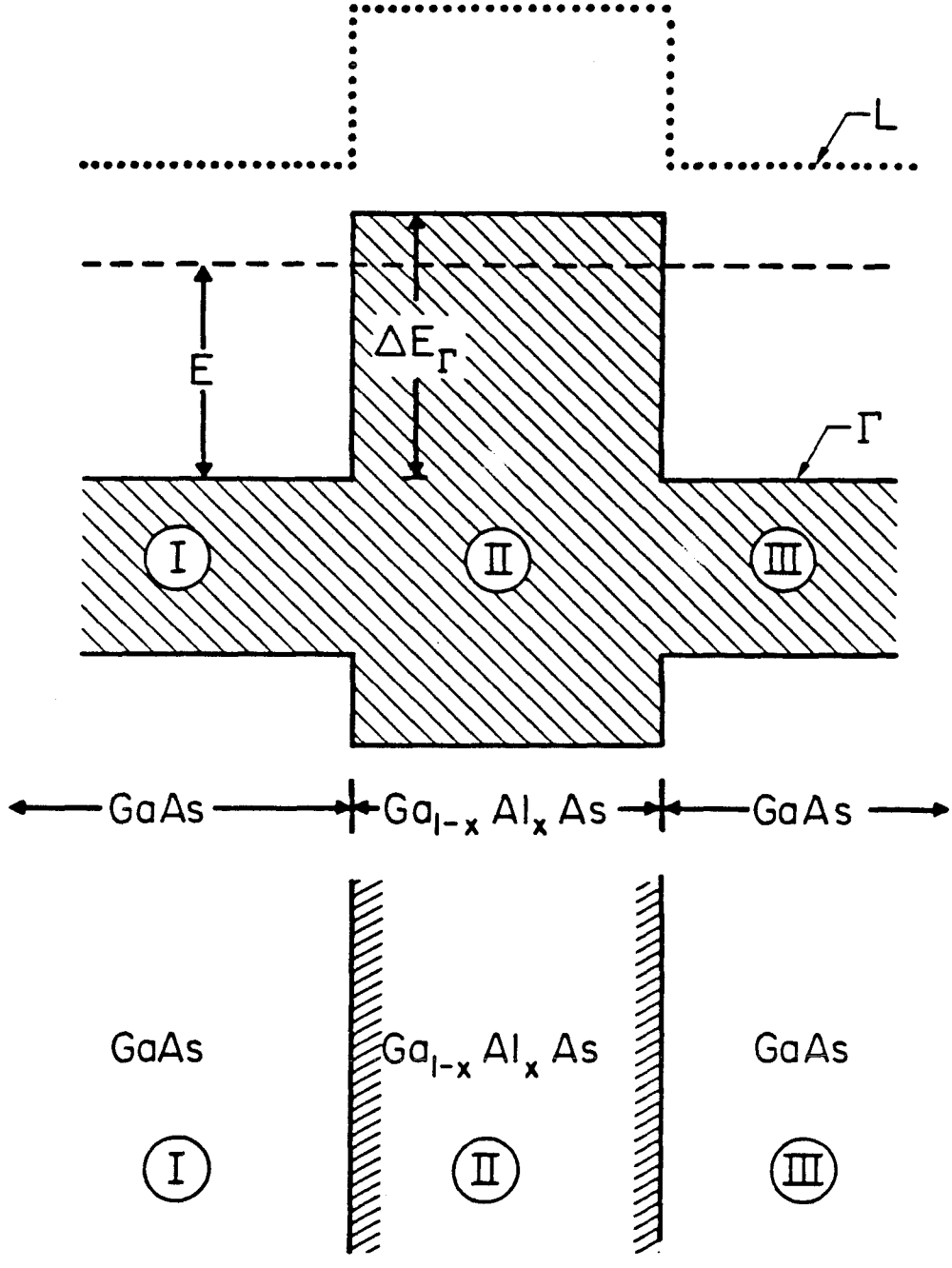

Figure 1: Energy band diagram of GaAs-$Ga_{1-x}Al_xAs$-GaAs DHS and corresponding physical structure. The electron is derived from the Γ-point or from the L-point and has a total energy E measured with respect to the GaAs Γ-point conduction band minimum. The relative positions of the Γ-point (solid line) and the L-point (dotted line) conduction band edges are also shown for an alloy composition of $x \approx 0.3$ in the $Ga_{1-x}Al_xAs$ barrier. The Γ-point conduction band offset is indicated by ΔE_Γ .

3.2.3.1 Planar Orbital Representation:

Systems which exhibit two-dimensional periodicity are best described in a planar orbital representation[6-11]. A planar orbital is a two-dimensional Bloch sum consisting of localized atomic functions as defined in Appendix (3.2). We define a planar orbital corresponding to an atomic orbital of symmetry α within the sublayer labelled by σ to be the *two-dimensional Bloch sum*

$$|\alpha\sigma;\mathbf{k}_{\|}\rangle \equiv \frac{1}{\sqrt{N_{\|}}}\sum_{\mathbf{R}_{\|}} \exp(i\mathbf{k}_{\|}\cdot\mathbf{R}_{\|})|\alpha;\mathbf{R}_{\|}\sigma\rangle, \tag{1}$$

where $\mathbf{R}_{\|}$ is a two-dimensional primitive lattice translation vector and σ labels the layer in the $\hat{\mathbf{z}}$-direction. $N_{\|}$ is the number of two-dimensional primitive cells in the crystal. In the case of the (111) interface, a sublayer can be thought of as a monoatomic plane, either anion or cation. Let $\hat{\mathbf{z}}$ be the direction normal to the interface and

$$\mathbf{k}_{\|} = \hat{\mathbf{x}}k_x + \hat{\mathbf{y}}k_y, \tag{2}$$

be the two-dimensional wavevector parallel to the interface.

We assume that space lattice matching at the interface is such that $\mathbf{k}_{\|}$ is a good quantum for the planar orbital. As seen in Appendix (3.2), the bulk Bloch states $|\mathbf{k}_{\|}E;k_\lambda\ ,\Sigma\rangle$, corresponding to the wavevector $k_z = k_\lambda$, evaluated on layer Σ, labelled by the wavector

$$\mathbf{k} = \mathbf{k}_{\|} + \hat{\mathbf{z}}k_\lambda \qquad [\lambda = 1,\ldots,2N], \tag{3}$$

can be expanded in terms of this set of planar orbitals, $\{|\alpha\sigma;\mathbf{k}_{\|}\rangle\}$,

$$|\mathbf{k}_{\|}E;k_\lambda\ ,\Sigma\rangle = \exp(ik_\lambda\ \Sigma a_0)\sum_{\sigma=1}^{2N_\sigma}\cdot$$

$$\left[\sum_{\alpha=1}^{N_\alpha} S(\alpha\sigma,k_\lambda\ ;\mathbf{k}_{\|})|\alpha\sigma;\mathbf{k}_{\|}\rangle\right] \qquad [\lambda = 1,\ldots,2N], \tag{4}$$

where the index σ labels the $2N_\sigma$ sublayers forming the layer Σ.

The total number $2N$ of Bloch states $\{|\mathbf{k}_\parallel E; k_\lambda\rangle\}$ with $k_z = k_\lambda$ corresponding to a given parallel wavevector $\mathbf{k}_\parallel$ and total energy E is equal to $[2N_\sigma \cdot N_\alpha] \equiv 2N$. The eigenvector matrix $\mathbf{S}(\mathbf{k}_\parallel)$ that diagonalizes the product of L transfer matrices, allows us to transform the description of the wavefunction from the planar orbital representation $\{|\alpha\sigma; \mathbf{k}_\parallel\rangle\}$ to the Bloch states representation $\{|\mathbf{k}_\parallel E; k_\lambda\rangle\}$.

• In the light of the discussions of the preceding sections, wherever the total Hamiltonian is bulk-like, the wavefunction is expanded in a set of bulk Bloch states, $\{|\mathbf{k}_\parallel E; k_z\rangle\}$.

At the GaAs-$Ga_{1-x}Al_xAs$ interfaces, the potential is no longer bulk-like and a description in terms of bulk Bloch states is prohibited. In the interfacial regions, the wavefunction is described in a planar orbital representation, $\{|\alpha\sigma; \mathbf{k}_\parallel\rangle\}$. The connection between the bulk Bloch states representation, $\{|\mathbf{k}_\parallel E; k_z\rangle\}$, and the planar orbital representation, $\{|\alpha\sigma; \mathbf{k}_\parallel\rangle\}$, is described in Appendix (3.2) and will not be repeated here. The matrix $\mathbf{S}(\mathbf{k}_\parallel)$ provides such a connection.

As discussed earlier, the total number $2N$ of Bloch states $\{|\mathbf{k}_\parallel E; k_\lambda\rangle\}$ with $k_z = k_\lambda$ corresponding to a given parallel wavevector $\mathbf{k}_\parallel$ and total energy E depends on the particular tight-binding model (*i.e*, the number N_α) used and on the orientation of the interface plane (*i.e*, the number $2N_\sigma$). In the sp^3s^* tight-binding representation used here[12], we have five orbitals per atom, $N_\alpha = 5$, and only first nearest-neighbor interactions were included. *Along the (111) direction, a sublayer consists of a monoatomic plane*, $N_\sigma = 1$. There are therefore *ten* Bloch states for each parallel wavevector $\mathbf{k}_\parallel$ and total energy E,

$$N_\alpha \cdot 2N_\sigma \equiv 2N = 10 \tag{5}$$

Half of the states have to be discarded because they either grow away from the

interface, if $\mathrm{Im}[k_z]$ does not have the proper sign, or are propagating in the wrong direction when k_z is real.

3.2.3.2 Theoretical Apparatus: Transfer Matrix

Let the incoming Bloch state $|\mathbf{k}_{\|}E;k_0\rangle$ with real wavevector k_0 be incident from the left in GaAs onto the GaAs-$Ga_{1-x}Al_xAs$ interface. The total wavefunction on a given layer Σ composed of the $2N_\sigma$ sublayers σ, can be written as[2]:

$$|\Psi(\mathbf{k}_{\|}E;\Sigma)\rangle = |\mathbf{k}_{\|}E;k_0\ ,\Sigma\rangle + \sum_{\lambda=1}^{2N} A^{(I)}(k_\lambda\ ;\mathbf{k}_{\|},E)|\mathbf{k}_{\|}E;k_\lambda\ ,\Sigma\rangle \quad \text{region I } (6.a)$$

$$|\Psi(\mathbf{k}_{\|}E;\Sigma)\rangle = \sum_{\alpha=1}^{N_\alpha}\sum_{\sigma=1}^{2N_\sigma} C^{(I-II)}(\alpha\sigma;\mathbf{k}_{\|},E)|\alpha\sigma;\mathbf{k}_{\|}\rangle \quad \text{interface I-II } (6.b)$$

$$|\Psi(\mathbf{k}_{\|}E;\Sigma)\rangle = \sum_{\lambda=1}^{2N} A^{(II)}(k_\lambda\ ;\mathbf{k}_{\|},E)|\mathbf{k}_{\|}E;k_\lambda\ ,\Sigma\rangle \quad \text{region II } (6.c)$$

$$|\Psi(\mathbf{k}_{\|}E;\Sigma)\rangle = \sum_{\alpha=1}^{N_\alpha}\sum_{\sigma=1}^{2N_\sigma} C^{(II-III)}(\alpha\sigma;\mathbf{k}_{\|},E)|\alpha\sigma;\mathbf{k}_{\|}\rangle \quad \text{interface II-III } (6.d)$$

$$|\Psi(\mathbf{k}_{\|}E;\Sigma)\rangle = \sum_{\lambda=1}^{2N} A^{(III)}(k_\lambda\ ;\mathbf{k}_{\|},E)|\mathbf{k}_{\|}E;k_\lambda\ ,\Sigma\rangle \quad \text{region III } (6.e)$$

• The expansion coefficients $A^{(I)}(k_\lambda;\mathbf{k}_{\|},E)$, $A^{(II)}(k_\lambda;\mathbf{k}_{\|},E)$ and $A^{(III)}(k_\lambda;\mathbf{k}_{\|},E)$ are associated with the bulk Bloch states representation, $\{|\mathbf{k}_{\|}E;k_z\rangle\}$, in regions I, II and III, respectively. The expansion coefficients $C^{(I-II)}(\alpha\sigma;\mathbf{k}_{\|},E)$ and $C^{(II-III)}(\alpha\sigma;\mathbf{k}_{\|},E)$ are associated with the planar orbital representation, $\{|\alpha\sigma;\mathbf{k}_{\|}\rangle\}$, across the interfaces.

Appendix (3.4) gives the prescription to obtain the transport coefficients with the aid of the transfer matrix. Transmission and reflection coefficients are obtained by imposing the proper *boundary conditions* on the *incoming* and *outgoing* waves. We impose the boundary conditions that there are *no growing states at* $z = +\infty$ *and at* $z = -\infty$.

3.2.3.3 Transport Coefficients:

At fixed total energy E and parallel wavevector $\mathbf{k}_{\|}$, we denote by $R_\lambda(\mathbf{k}_{\|}, E)$ and $T_\lambda(\mathbf{k}_{\|}, E)$ the k_z-resolved reflection and transmission coefficients corresponding to the Bloch states $|\mathbf{k}_{\|}E; k_\lambda\rangle$ in GaAs. The k_z-resolved transport coefficients $R_\lambda(\mathbf{k}_{\|}, E)$ and $T_\lambda(\mathbf{k}_{\|}, E)$ are related to the expansion coefficients in the bulk Bloch state representation, $A^{(I)}(k_\lambda\,; \mathbf{k}_{\|}, E)$ and $A^{(III)}(k_\lambda\,; \mathbf{k}_{\|}, E)$, respectively. Given an incoming Bloch state $|\mathbf{k}_{\|}E; k_0\rangle$ with wavevector $k_z \equiv k_0$ normal to the interface, we define the k_z-resolved transport coefficients in the following way

$$T_\lambda(\mathbf{k}_{\|}, E) \equiv |A^{(III)}(k_\lambda\,; \mathbf{k}_{\|}, E)|^2 \cdot \frac{\left|\left[\frac{\partial E(\mathbf{k})}{\partial k_z}\right]_{k_z=k_\lambda}\right|}{\left|\left[\frac{\partial E(\mathbf{k})}{\partial k_z}\right]_{k_z=k_0}\right|}, \tag{7.a}$$

and

$$R_\lambda(\mathbf{k}_{\|}, E) \equiv |A^{(I)}(k_\lambda\,; \mathbf{k}_{\|}, E)|^2 \cdot \frac{\left|\left[\frac{\partial E(\mathbf{k})}{\partial k_z}\right]_{k_z=k_\lambda}\right|}{\left|\left[\frac{\partial E(\mathbf{k})}{\partial k_z}\right]_{k_z=k_0}\right|}, \tag{7.b}$$

where the group velocity, normal to the interface, of the Bloch state $|\mathbf{k}_{\|}E; k_\lambda\rangle$ is

$$v_z(k_\lambda) \equiv \left[\frac{1}{\hbar}\right]\left[\frac{\partial E(\mathbf{k})}{\partial k_z}\right]_{k_z=k_\lambda}. \tag{8}$$

The total transport coefficients $R(\mathbf{k}_{\|}, E)$ and $T(\mathbf{k}_{\|}, E)$ are just the sum of the transport coefficients $R_\lambda(\mathbf{k}_{\|}, E)$ and $T_\lambda(\mathbf{k}_{\|}, E)$,

$$R(\mathbf{k}_{\|}, E) \equiv \sum_\lambda R_\lambda(\mathbf{k}_{\|}, E), \tag{9.a}$$

$$T(\mathbf{k}_{\|}, E) \equiv \sum_\lambda T_\lambda(\mathbf{k}_{\|}, E). \tag{9.b}$$

Flux conservation requires $R(\mathbf{k}_{\|}, E) + T(\mathbf{k}_{\|}, E) = 1$.

As shown in Ref. 1 , the transmission coefficient for the Bloch state $|\mathbf{k}_{\|} E; k_{\lambda}\rangle$ vanishes when the wavevector of the incoming Bloch state, k_0 , approaches a critical point such that

$$\left[\frac{\partial E(\mathbf{k})}{\partial k_z}\right]_{k_z = k_0} = 0. \tag{10}$$

In that case, the incoming state is identical with the reflected state. At this critical point, the incoming state $|\mathbf{k}_{\|} E; k_0\rangle$ has *no component of the group velocity perpendicular to the interface and does not couple to any Bloch states in* $Ga_{1-x}Al_xAs$. Therefore, transmission starts to occur as the incident wavevector k_0 moves away from the critical point.

3.2.3.4 Complex-k Energy Bandstructure:

The transport states originate in the complex-**k** band structure of GaAs and $Ga_{1-x}Al_xAs$. The complex-**k** band structure for GaAs and AlAs is well known[7,13]. We have used similar techniques to obtain the complex-**k** band structure for $Ga_{1-x}Al_xAs$ within the virtual crystal approximation. Within the ten-band tight-binding description used here, the GaAs Γ-point conduction band minimum is $E_\Gamma^{\rm GaAs} = 1.509$ eV above the GaAs Γ-point valence band maximum and the GaAs L-point conduction band valley is at an energy $E_L^{\rm GaAs} = 0.50$ eV above the GaAs Γ-point conduction band minimum.

Figures (2) and (3) show the complex-**k** band structure of GaAs and AlAs along the (111) direction, respectively. The complex-**k** band structure corresponds to vanishing wavevector parallel to the (111) interface plane, *i.e.*, $\mathbf{k}_{||} = \mathbf{0}$. At a given energy E, the purely real values of k_z are indicated by a solid line on the right panel of the figure and the purely imaginary values of k_z are indicated by a solid line on the left panel of the figure. Complex values of k_z are indicated by a dashed line, Re$[k_z]$ being on the right and Im$[k_z]$ being on the left of the figure respectively. As seen in Figures (2) and (3) complex band connect to real bands at points of vanishing slope, *i.e.*, where

$$\left[\frac{\partial E(\mathbf{k})}{\partial k_z}\right]_{k_z=k_0} = 0, \tag{11}$$

for a real value of the wavevector k_0. Appendix A gives a collection of the properties of the energy functions $E_n(\mathbf{k})$ in the case where the wavevector **k** is *complex*.

The *propagating* or *evanescent* nature of the Bloch states depends on the *real* or *complex* character of the wavevector k_z normal to the (111) interface plane.

- Propagating Bloch states are associated with real values of k_z, whereas
- evanescent Bloch states are associated with complex values of k_z.

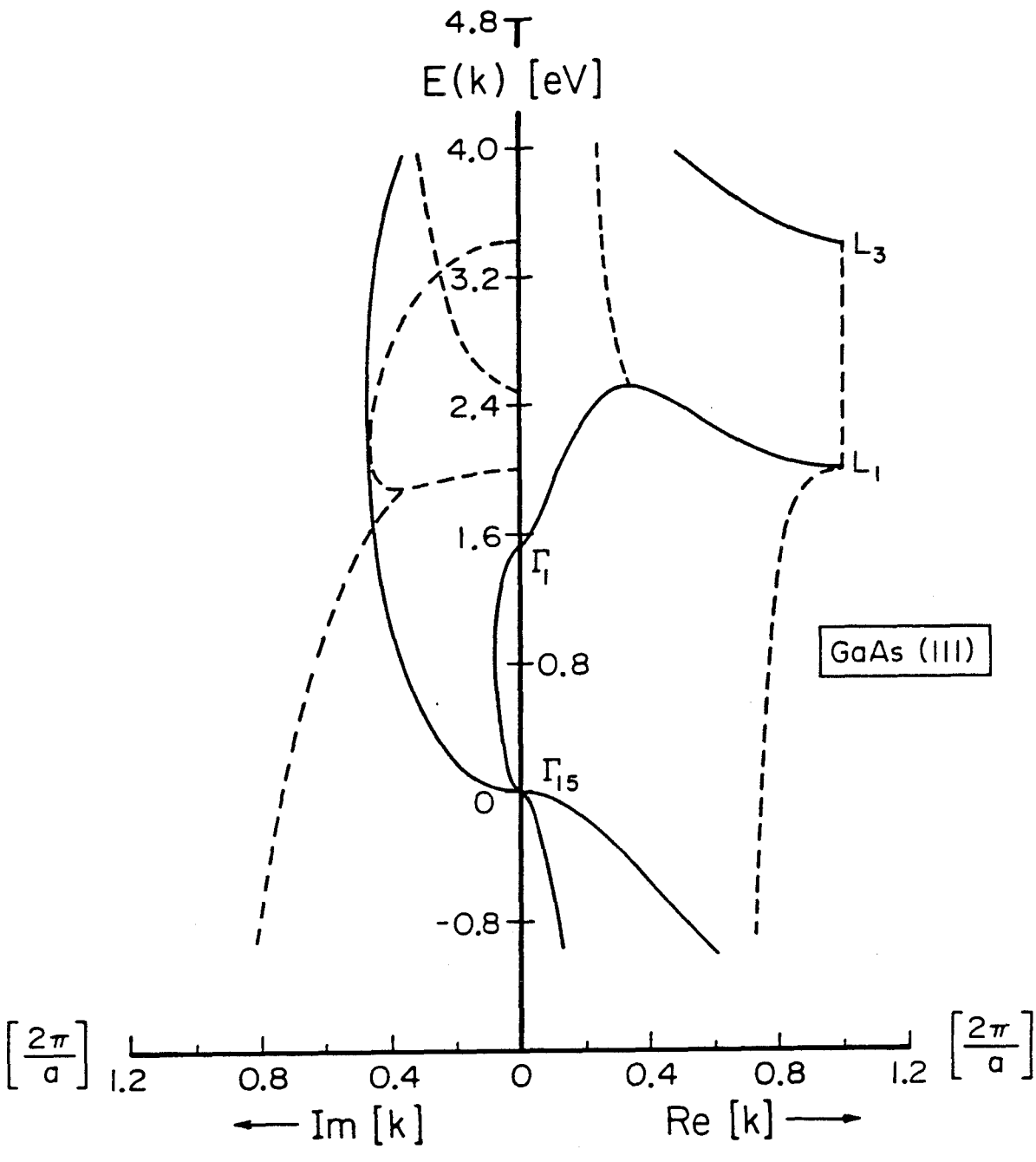

Figure 2: Complex-**k** band structure of GaAs along the (111) direction, respectively. The complex-**k** band structure corresponds to vanishing wavevector parallel to the (111) interface plane, *i.e.* $\mathbf{k}_{\parallel} = \mathbf{0}$. At a given energy E, the purely real values of k_z are indicated by a solid line on the right panel of the figure and the purely imaginary values of k_z are indicated by a solid line on the left panel of the figure. Complex values of k_z are indicated by a dashed line, $\mathrm{Re}[k_z]$ being on the right and $\mathrm{Im}[k_z]$ being on the left of the figure respectively. The zero of energy is taken at the top of the GaAs valence band maximum.

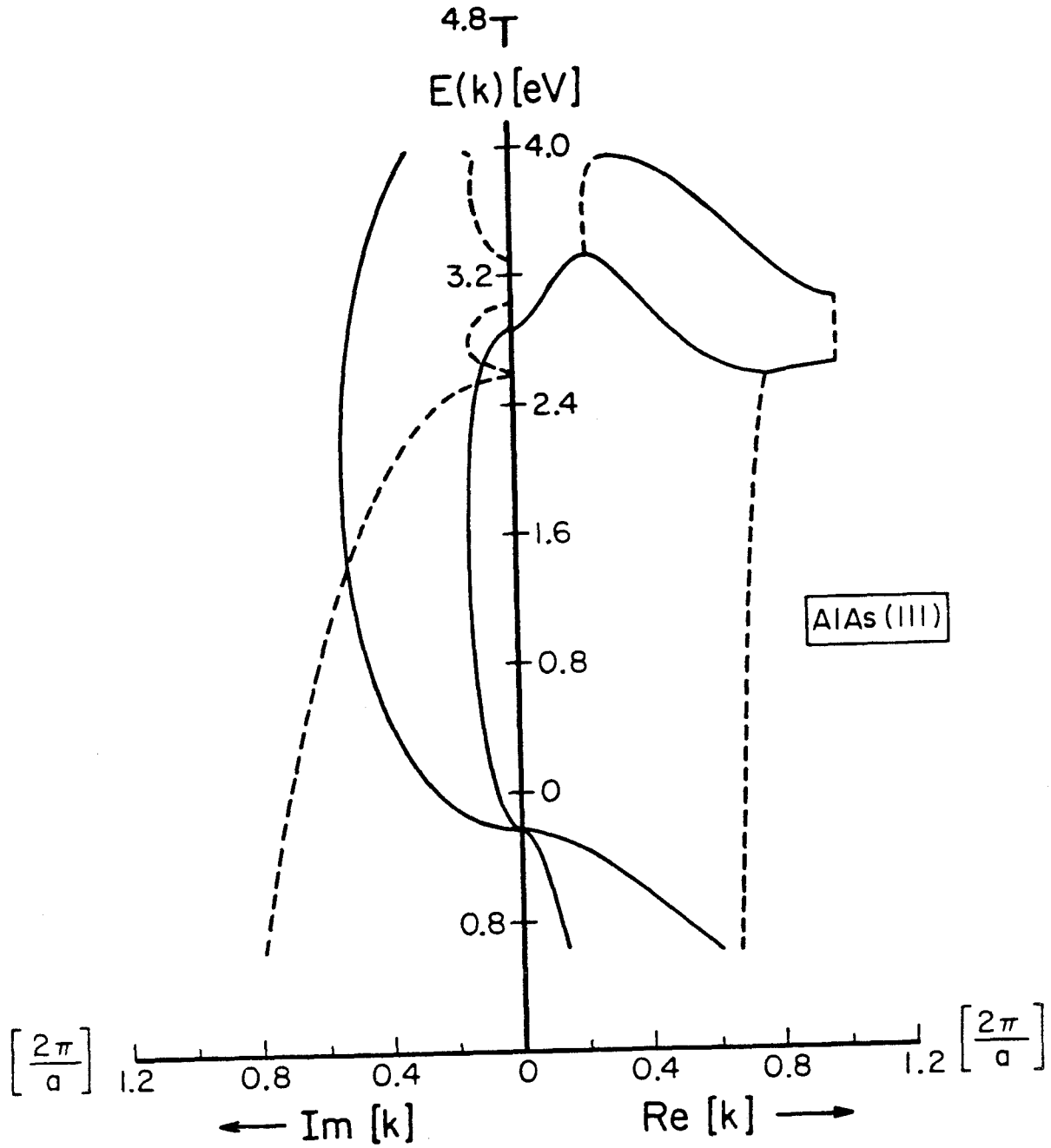

Figure 3: Complex-**k** band structure of AlAs along the (111) direction, respectively. The complex-**k** band structure corresponds to vanishing wavevector parallel to the (111) interface plane, *i.e.* $\mathbf{k}_{\parallel} = \mathbf{0}$. At a given energy E, the purely real values of k_z are indicated by a solid line on the right panel of the figure and the purely imaginary values of k_z are indicated by a solid line on the left panel of the figure. Complex values of k_z are indicated by a dashed line, $\mathrm{Re}[k_z]$ being on the right and $\mathrm{Im}[k_z]$ being on the left of the figure respectively. The zero of energy is taken at the top of the GaAs valence band maximum.

We denote the bulk states with $k_z = k_\lambda$ in spatial region μ by $|\mathbf{k}_\parallel E; k_\lambda{}^{\mu}\rangle$. In the discussion that follows, the incident Bloch state is derived either from near the GaAs conduction band L-point with real wavevector $k_0 \equiv k_L^I$, *e.g.* $|\mathbf{k}_\parallel E; k_0\rangle \equiv |\mathbf{k}_\parallel E; k_L{}^{I}\rangle$, or from the the GaAs conduction band Γ-point with real wavevector $k_0 \equiv k_\Gamma^I$, *e.g.* $|\mathbf{k}_\parallel E; k_0\rangle \equiv |\mathbf{k}_\parallel E; k_\Gamma{}^{I}\rangle$.

Throughout the calculations, the valence band offset ΔE_Γ is taken to be equal to 15% of the difference of the Γ-point band gap between GaAs and $Ga_{1-x}Al_xAs$ [14—15]. The virtual crystal approximation is used to weight the tight-binding parameters of $Ga_{1-x}Al_xAs$ according to the alloy composition, x. In the following, we consider alloy compositions in the range $x \leq 0.3$, for which $Ga_{1-x}Al_xAs$ is direct. Within this composition range, the dependence of the Γ-point and L-point conduction band energy edges in $Ga_{1-x}Al_xAs$ on the alloy composition x is, in the virtual crystal approximation: $E_\Gamma^{Ga_{1-x}Al_xAs} \approx 1.35\,x$ eV and $E_L^{Ga_{1-x}Al_xAs} \approx (0.50 + 0.65\,x)$ eV, above the GaAs Γ-point conduction band minimum.

Throughout this study, we neglect carrier scattering by the electron-phonon interaction and by the alloy disorder. Such scattering would undoubtedly occur in the structures we consider here and will have some influence on the transport in them. We point out, however, that the thickness of the barrier in the structures we discuss is less than the phonon scattering mean free path, which is of the order of 58 Å in GaAs at room temperature[16]. The scattering processes could be discussed in perturbation theory using the wavefunctions we calculate here as the unperturbed states.

3.2.4 Results:

We present the main results for the transmission coefficients of electrons derived from the L-point and Γ-point of GaAs through the GaAs-$Ga_{1-x}Al_xAs$-GaAs (111) DHS. We discuss the transport across the central $Ga_{1-x}Al_xAs$ barrier as a function of

- the total energy, E, of the incoming state,
- thickness of the $Ga_{1-x}Al_xAs$ barrier, and
- alloy composition, x.

3.2.4.1 Transmission Coefficient vs. Energy:

The different transport regimes (tunneling and propagating) can be demonstrated by studying the *transmission coefficient for fixed barrier thickness as a function of the energy of the incoming state.* Figure 4 shows the transmission coefficient, $T(\mathbf{k}_{\|}, E)$, as a function of the energy, E, of the incoming Bloch state. The incoming Bloch state is either derived from the GaAs L-point ($k_0 \equiv k_L^I$), or from the GaAs Γ-point ($k_0 \equiv k_\Gamma^I$). Energy is measured with respect to the GaAs Γ-point conduction band minimum. We consider the case of vanishing parallel wavevector $\mathbf{k}_{\|} = \mathbf{0}$. Calculations were carried out for an alloy composition of $x = 0.1$ and a barrier thickness of seven $Ga_{1-x}Al_xAs$ layers. For the $x = 0.1$ alloy, the $Ga_{1-x}Al_xAs$ Γ-point and the L-point energies are: $E_\Gamma^{Ga_{1-x}Al_xAs} = 0.135$ eV, and $E_L^{Ga_{1-x}Al_xAs} = 0.565$ eV, above the GaAs Γ-point conduction band minimum. For energies of the incoming states near a given GaAs conduction band extremum (L or Γ), transmission through the $Ga_{1-x}Al_xAs$ barrier appears to occur mostly via the coupling to states that connect to the alloy conduction band at the same extremum in the Brillouin zone (L or Γ). Since the Bloch states derived from different extrema of the conduction band appear to couple

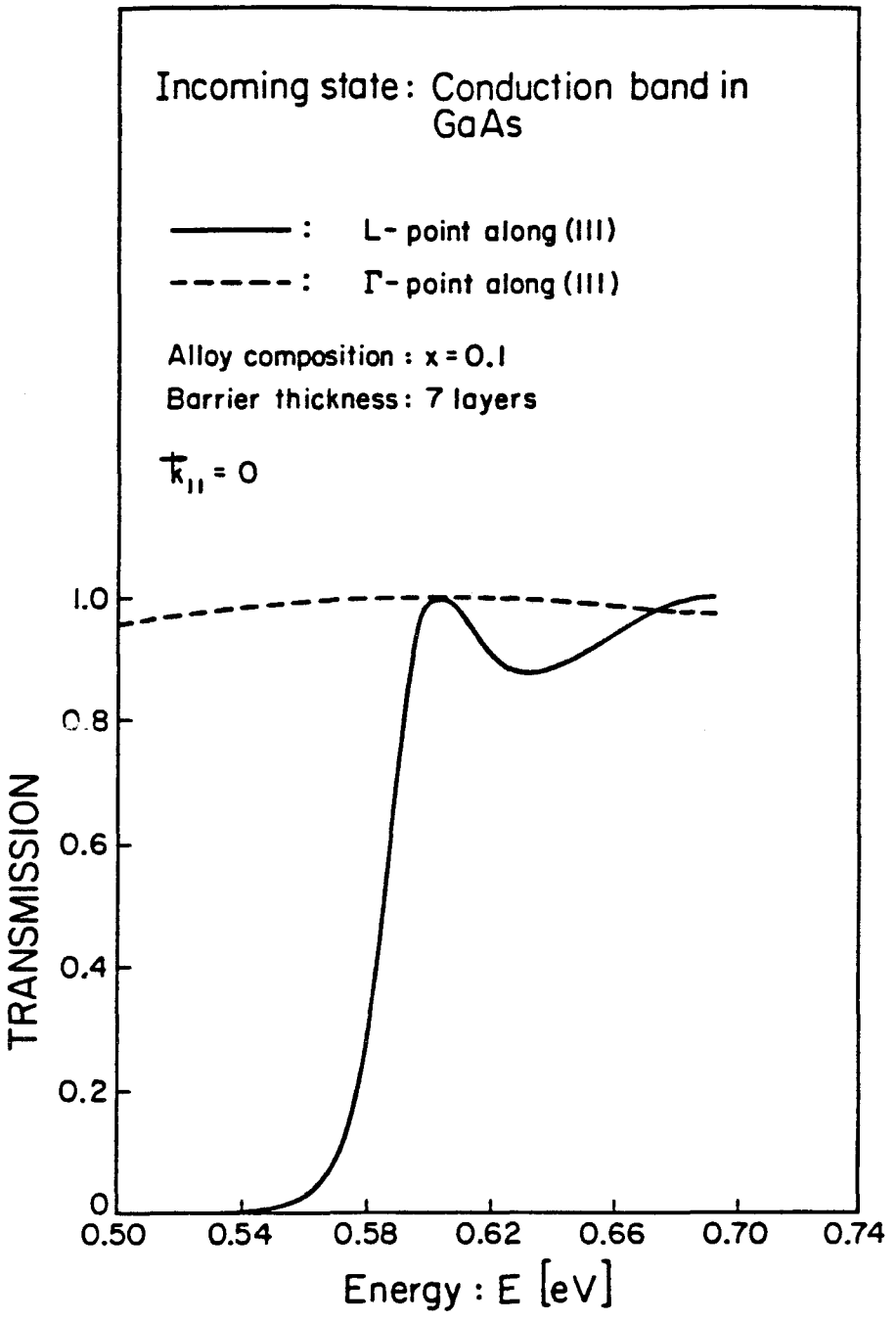

Figure 4: Transmission coefficient, $T(\mathbf{k}_{\|}, E)$, as a function of the energy, E, of incoming electron. The incoming electron is either derived from the GaAs L-point (solid line), or from the GaAs Γ-point (dashed line). The alloy composition of $x = 0.1$ and the $Ga_{1-x}Al_xAs$ barrier is seven layers thick. Energy is measured with respect to the GaAs Γ-point conduction band minimum and $\mathbf{k}_{\|} = \mathbf{0}$.

weakly to each other, the energy barrier for the states derived from the L-point is different than the energy barrier for the states derived from the Γ-point.

The figure clearly demonstrates that there seems to exist a range of energies above the GaAs *L-point valley* (E_L^{GaAs}) *and below the* $\mathrm{Ga}_{1-x}\mathrm{Al}_x\mathrm{As}$ *L-point valley* ($E_L^{\mathrm{Ga}_{1-x}\mathrm{Al}_x\mathrm{As}}$), *such that transmission is large for incoming Bloch states derived from the Γ-point and small for incoming Bloch states derived from the L-point.* In this energy range, $E_L^{\mathrm{GaAs}} < E < E_L^{\mathrm{Ga}_{1-x}\mathrm{Al}_x\mathrm{As}}$, Bloch states incoming from the Γ-point in GaAs couple mostly to *propagating* Γ-point states in the barrier (k_Γ^{II} real), and Bloch states incoming from the L-point in GaAs couple mostly to *evanescent* L-point states in the barrier (k_L^{II} complex). The energy range for which the transmission $|\mathbf{k}_\parallel E; k_\Gamma{}^{I}\rangle \rightarrow |\mathbf{k}_\parallel E; k_\Gamma{}^{III}\rangle$ is much greater than the transmission $|\mathbf{k}_\parallel E; k_L{}^{I}\rangle \rightarrow |\mathbf{k}_\parallel E; k_L{}^{III}\rangle$ roughly corresponds to the composition-dependent L-point energy barrier that the incoming L-point Bloch states have to overcome in order for them to become propagating (k_L^{II} real) in the barrier. For the $x = 0.1$ alloy, the L-point valley of the alloy lies at $E_L^{\mathrm{Ga}_{1-x}\mathrm{Al}_x\mathrm{As}} = 0.565$ eV above the GaAs conduction band minimum, and

- $|\mathbf{k}_\parallel E; k_L{}^{I}\rangle \rightarrow |\mathbf{k}_\parallel E; k_L{}^{III}\rangle$ transmission will remain small below this energy

whereas

- $|\mathbf{k}_\parallel E; k_\Gamma{}^{I}\rangle \rightarrow |\mathbf{k}_\parallel E; k_\Gamma{}^{III}\rangle$ transmission will be important.

Thus, for a given $\mathrm{Ga}_{1-x}\mathrm{Al}_x\mathrm{As}$ composition ,x, there is a range of energies, roughly $E_L^{\mathrm{GaAs}} < E < E_L^{\mathrm{Ga}_{1-x}\mathrm{Al}_x\mathrm{As}}$, for which *electrons incoming in GaAs from the Γ-point are mostly transmitted whereas electrons incoming in GaAs from the L-point are mostly reflected.*

Generally, when an incoming state in GaAs is derived from a conduction band extremum, say λ, such that $k_0 \equiv k_\lambda^I$ and $|\mathbf{k}_\parallel E; k_0\rangle \equiv |\mathbf{k}_\parallel E; k_\lambda{}^{I}\rangle$ the mode of

transport (*i.e.*, tunneling or propagating) appears to be determined by the nature of the states in $Ga_{1-x}Al_xAs$ derived from the same conduction band extremum, $|\mathbf{k}_{\|}E; k_\lambda{}^{II}\rangle$. For energies of the incoming state less than the alloy conduction band edge $E_\lambda^{Ga_{1-x}Al_xAs}$, the states that couple strongly in the alloy are gap states ($|\mathbf{k}_{\|}E; k_\lambda{}^{II}\rangle$ evanescent) and hence the wavefunction is damped in the barrier. However, for energies of the incoming state greater than the alloy conduction band edge $E_\lambda^{Ga_{1-x}Al_xAs}$, the states that couple strongly in the alloy are band states ($|\mathbf{k}_{\|}E; k_\lambda{}^{II}\rangle$ propagating) and hence the wavefunction is not damped in the barrier.

Electron derived from the *L*-point:

We now discuss the energy dependence of the transmission for incoming electrons derived from the GaAs L-point valley. As mentioned in section (3.2.3), the transmission coefficient vanishes for incoming states derived from the L-point at an energy equal to the L-point extremum of GaAs, E_L^{GaAs}. At this energy, the component of the group velocity normal to the interface vanishes, $\left[\frac{\partial E(\mathbf{k})}{\partial k_z}\right]_{k_z=k_L^I} \equiv 0$, and the incoming state $|\mathbf{k}_{\|}E; k_L{}^{I}\rangle$ does not couple to any Bloch states in $Ga_{1-x}Al_xAs$. The overall energy dependence is found to be similar to that of plane waves incident on a rectangular barrier as derived from a one-dimensional quantum-mechanical treatment[17].

For incoming states derived from the GaAs L-point with energy *below* $E_L^{Ga_{1-x}Al_xAs} = 0.565$ eV, transport through the barrier is *tunneling and the transmission is small.* However, for incoming states derived from the GaAs L-point with energy *above* $E_L^{Ga_{1-x}Al_xAs}$, transport through the barrier is *propagating and the transmission becomes important.* For a fixed barrier thickness, propagating transport exhibits maximum transmission whenever the energy of the incoming state is such that the thickness of the $Ga_{1-x}Al_xAs$ barrier contains an integral number of half-wavelengths in the barrier region. At energies $E > E_L^{Ga_{1-x}Al_xAs}$, the transmis-

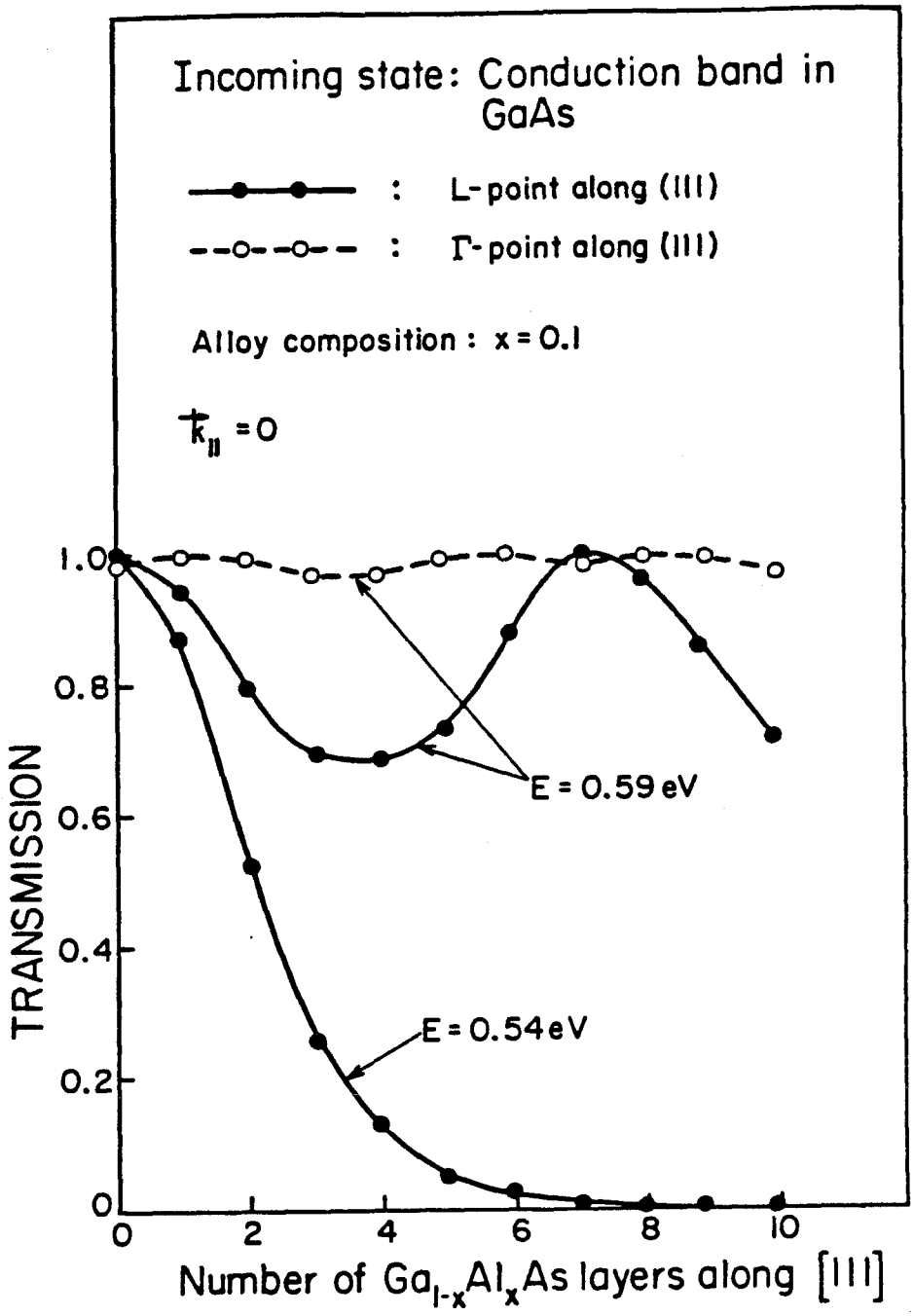

Figure 5: Transmission coefficient $T(\mathbf{k}_{\|}, E)$, as a function of the number of layers forming the central $Ga_{1-x}Al_xAs$ barrier for various energies of the incoming electron. The incoming electron is either derived from the GaAs L-point (solid line), or from the GaAs Γ-point (dashed line). The alloy composition is $x = 0.1$. Energy is measured with respect to the GaAs Γ-point conduction band minimum and $\mathbf{k}_{\|} = \mathbf{0}$. Layers are measured in units of $a/\sqrt{3}$, where a is the GaAs lattice constant.

sion oscillates as a function of energy and is maximum at resonance. The off-resonance transmission amplitude increases with increasing incoming energy.

3.2.4.2 Transmission Coefficient vs. $Ga_{1-x}Al_xAs$ Barrier Thickness:

The different transport regimes (tunneling and propagating) can also be demonstrated by studying the transmission coefficient for fixed incoming energy as a function of the barrier thickness. Figure 5 shows the transmission coefficient $T(\mathbf{k}_{\|}, E)$, as a function of the number of layers forming the central $Ga_{1-x}Al_xAs$ barrier for various energies of the incoming Bloch state. The alloy composition is $x = 0.1$ and $\mathbf{k}_{\|} = \mathbf{0}$. Layers are measured in units of $a/\sqrt{3}$, where a is the GaAs lattice constant. For the $x = 0.1$ alloy, the Γ-point and L-point conduction band energies in $Ga_{1-x}Al_xAs$ are: $E_{\Gamma}^{Ga_{1-x}Al_xAs} = 0.135$ eV and $E_{L}^{Ga_{1-x}Al_xAs} = 0.565$ eV, above the GaAs Γ-point conduction band minimum. The incoming Bloch state is either derived from the GaAs L-point ($k_0 \equiv k_L^I$), or from the GaAs Γ-point ($k_0 \equiv k_{\Gamma}^I$). For the case where the incoming Bloch state is derived from the GaAs L-point valley, the different types of transport (tunneling and propagating) are shown for an energy $E = 0.54$ eV $< E_{L}^{Ga_{1-x}Al_xAs}$, in which case the transport is tunneling and for an energy $E = 0.59$ eV $> E_{L}^{Ga_{1-x}Al_xAs}$, in which case the transport is propagating.

Electron derived from the L-point:

We discuss first the case of incoming electrons derived from the GaAs L-point valley.

• In the tunneling regime of transport ($E < E_{L}^{Ga_{1-x}Al_xAs}$), transmission occurs mostly via the coupling to *evanescent* states (k_L^{II} complex) derived from the L-point of $Ga_{1-x}Al_xAs$. As seen in Figure 5, the evanescent character of the wavefunction in $Ga_{1-x}Al_xAs$ is reflected in the fact that the transmission

coefficient $T(\mathbf{k}_{\|}, E)$ is an exponentially decaying function of the $Ga_{1-x}Al_xAs$ barrier thickness. These results are similar to those obtained from the thick-barrier WKB approximation[18-19].

• In the propagating regime of transport ($E > E_L^{Ga_{1-x}Al_xAs}$), transmission occurs mostly via the coupling to ***propagating*** states (k_L^{II} real) near the conduction band L-point of $Ga_{1-x}Al_xAs$. For energies of the L-point incoming electron greater than $E_L^{Ga_{1-x}Al_xAs}$, the transmission coefficient is a periodic function of the $Ga_{1-x}Al_xAs$ barrier thickness. The period is determined by the wavevector $q_L^{II} \equiv k_L^0 - k_L^{II}$, where k_L^0 is the L-point Brillouin zone edge.

The transmission coefficient is unity when the thickness of the $Ga_{1-x}Al_xAs$ barrier contains an integral number of half-wavelengths (determined by q_L^{II}) in the barrier region. Since the wavevector q_L^{II} increases with the energy of the incoming L-point Bloch state, the period of the transmission amplitude decreases with the energy of the incident L-point electron.

The off-resonance transmission amplitudes increase with increasing incident energy. The general qualitative behavior of the transport is similar to that exhibited by plane wave states incident on a rectangular quantum-mechanical barrier. Similar regimes of transport have also been reported for incoming states near the GaAs Γ-point for GaAs-$GaAs_{1-x}P_x$-GaAs strained (100) DHS[5].

Electron derived from the Γ-point:

Also shown in Figure 5 is a comparison between the transmission for incoming electrons derived from the GaAs Γ-point and from the GaAs L-point at the same energy, namely $E = 0.59$ eV. At this energy, k_Γ^{II} and k_L^{II} are real and, consequently, the Bloch states $|\mathbf{k}_{\|}E; k_\Gamma{}^{II}\rangle$ and $|\mathbf{k}_{\|}E; k_L{}^{II}\rangle$ are propagating. At a given layer thickness, the transmission is greater for states incoming from the GaAs Γ-point than for the states derived from the L-point. This is due to the fact that,

for a given energy of $E = 0.59$ eV, the Γ-point states lie at an energy of about 0.46 eV above the Γ-point minimum of the alloy, $E_{\Gamma}^{Ga_{1-x}Al_xAs} = 0.135$ eV. On the other hand, the L-point states lie at an energy of only 0.03 eV above the L-point valley of the alloy, $E_{L}^{Ga_{1-x}Al_xAs} = 0.565$ eV. As seen in the figure, it seems possible to tune the thickness of the $Ga_{1-x}Al_xAs$ barrier in such a way as to reduce the transmission for the incoming states derived from the GaAs L-point while the transmission for the Γ-point remains close to unity.

3.2.4.3 Transmission Coefficient vs. $Ga_{1-x}Al_xAs$ Alloy Composition:

Figure 6 shows the transmission coefficient, $T(\mathbf{k}_{\|}, E)$, as a function of alloy composition for two different $Ga_{1-x}Al_xAs$ barrier thicknesses. The incoming Bloch state is either derived from the GaAs L-point ($k_0 \equiv k_L^I$), or from the GaAs Γ-point ($k_0 \equiv k_\Gamma^I$). The incoming Bloch state has $\mathbf{k}_{\|} = \mathbf{0}$. The energy of the incoming state is $E = 0.501$ eV above the GaAs Γ-point conduction band minimum. As mentioned above, the Γ-point and L-point energy edges, $E_{\Gamma}^{Ga_{1-x}Al_xAs}$ and $E_{L}^{Ga_{1-x}Al_xAs}$, scale linearly with the alloy composition for $x \leq 0.3$. The composition x is therefore directly related to the Γ-point and L-point barrier heights at the interface. For the range of alloy compositions studied, the Γ-point and the L-point energies of $Ga_{1-x}Al_xAs$ vary in the range 0 eV$\leq E_{\Gamma}^{Ga_{1-x}Al_xAs} \leq 0.405$ eV and 0.50 eV$\leq E_{L}^{Ga_{1-x}Al_xAs} \leq 0.70$ eV, above the GaAs Γ-point conduction band minimum. For a fixed energy of $E = 0.501$ eV, the transport is propagating for Bloch states incoming from the Γ-point although it is mostly tunneling for Bloch states incoming from the L-point in the composition range $x \leq 0.3$. This is due to the fact that, in this composition range, we have $E_{\Gamma}^{Ga_{1-x}Al_xAs} < E < E_{L}^{Ga_{1-x}Al_xAs}$ so that k_Γ^{II} is real whereas k_L^{II} is mostly complex.

Electron derived from the L-point:

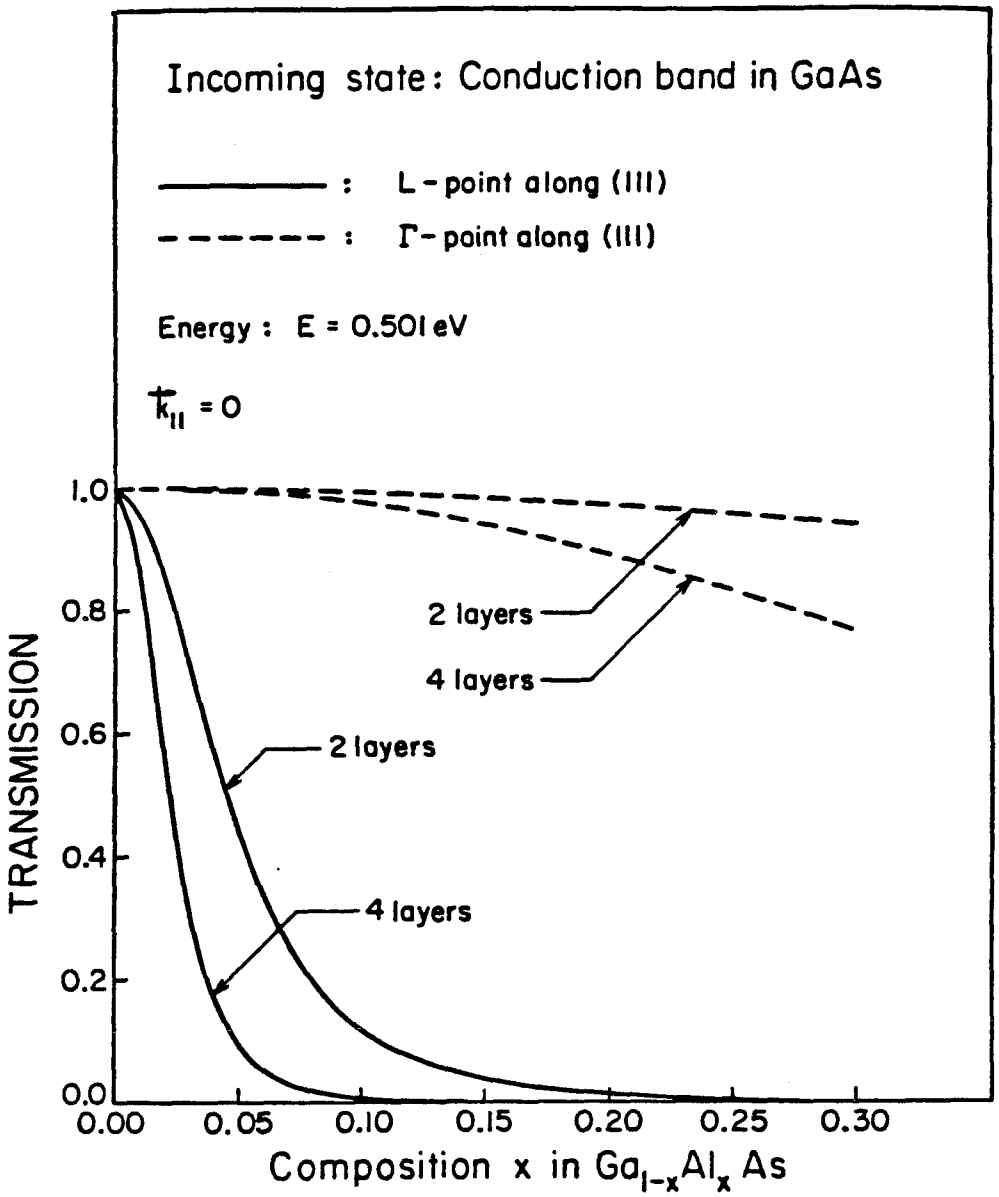

Figure 6: Transmission coefficient, $T(\mathbf{k}_{\parallel}, E)$, as a function of alloy composition for two different $Ga_{1-x}Al_xAs$ barrier thicknesses. The incoming electron is either derived from the GaAs L-point (solid line), or from the GaAs Γ-point (dashed line). The energy of the incoming state is $E = 0.501$ eV above the GaAs Γ-point conduction band minimum and $\mathbf{k}_{\parallel} = \mathbf{0}$. Layers are measured in units of $a/\sqrt{3}$, where a is the GaAs lattice constant.

We first discuss the case of incoming electrons derived from the GaAs L-point valley. As the Al concentration increases, the L-point energy edge in $Ga_{1-x}Al_xAs$, $E_L^{Ga_{1-x}Al_xAs}$, increases and so does the magnitude of $\mathrm{Im}(k_L^{II})$. Therefore, the L-point derived states have smaller decay lengths and tunnel less efficiently across the barrier. This, in turn, implies an increased reflection probability for the L-point derived states. At a given alloy composition, x, the transmission is greater for states incoming from the GaAs Γ-point than for the states derived from the L-point. This is due to the fact that the Γ-point states are transmitted in the propagating regime ($E > E_\Gamma^{Ga_{1-x}Al_xAs}$), whereas the L-point states are transmitted in the tunneling regime ($E < E_L^{Ga_{1-x}Al_xAs}$).

Since the mixing between L-point and Γ-point states appears to be small, there seem to exist two distinctive energy barriers for L-point and Γ-point electrons. In the light of the results presented above, it seems possible to create a situation (by either selecting the energy, the barrier thickness or the alloy composition) such that both the Γ-point and the L-point states were propagating in GaAs but only the Γ-point states would be propagating in $Ga_{1-x}Al_xAs$, the L-point states being evanescent in the barrier. Such a situation may have applications in GaAs high-speed low-power devices to provide a way of reflecting back the low-velocity L-point component of the current while allowing the high-velocity Γ-point component to be transmitted.

3.2.5 Summary and Conclusion:

We have calculated the transport coefficients of L-point Γ-point electrons through GaAs-$Ga_{1-x}Al_xAs$-GaAs (111) double heterojunctions within a ten-band tight-binding formalism. The model takes reasonably well into account band effects through the use of complex-**k**band structures and transfer matrix methods. Within this theoretical framework, k_z-resolved transport coefficients can be calculated. This, in turn, allows for a better understanding of the transmission coefficients of electrons derived from different extrema of the conduction band in GaAs. Calculation of transport coefficients associated with various conduction band valleys were carried out as a function of

- energy of the incoming electron,
- thickness of the central $Ga_{1-x}Al_xAs$ barrier, and
- alloy composition, x, in the central $Ga_{1-x}Al_xAs$ barrier.

It is generally found that *states originating from the same extremum of the conduction band appear to couple strongly to each other, whereas states derived from different extrema are found to couple weakly.* For energies of the incoming states near a given GaAs conduction band extremum (L or Γ), transmission through the $Ga_{1-x}Al_xAs$ barrier occurs mostly via the coupling to states (evanescent or propagating) that connect to the alloy conduction band at the same extremum (L or Γ). Transmission through the $Ga_{1-x}Al_xAs$ barrier is either *tunneling* or *propagating* depending on the *nature of the Bloch states available for strong coupling in the alloy.* Since the mixing between L-point and Γ-point states appears to be small, there seem to exist two distinctive energy barriers for L-point and Γ-point electrons. This observation may lead to interesting effects in GaAs high-speed low-power electronic devices whereby the low-velocity L-point component of the current could be blocked (*i.e.*, small transmission below the L-point barrier) while

the high-velocity Γ-point component could be transmitted (*i.e.*, large transmission above the Γ-point barrier).

Section 3.3

TRANSPORT CHARACTERISTICS OF *X*-POINT AND Γ-POINT ELECTRONS THROUGH GaAs-$Ga_{1-x}Al_xAs$-GaAs (100) DOUBLE HETEROJUNCTIONS

3.3.1 Scope of this Study:

In this section, we present a study of the transport characteristics of electrons through abrupt GaAs-$Ga_{1-x}Al_xAs$-GaAs (100) double heterojunctions. As in the preceding section, the theoretical apparatus uses complex-**k** band structures in the tight-binding approximation and transfer matrices. States on each side of the $Ga_{1-x}Al_xAs$ central barrier are expanded in terms of a complex-**k** bulk state basis so as to provide a description of the wavefunction at the GaAs-$Ga_{1-x}Al_xAs$ (100) interface. We treat the case where the incoming state in GaAs is derived from near the conduction band Γ-point . Transmission through the $Ga_{1-x}Al_xAs$ barrier is either tunneling or propagating depending on the nature of the Bloch states available for strong coupling in the alloy. *States derived from the same extremum of the conduction band appear to couple strongly to each other across the* GaAs-$Ga_{1-x}Al_xAs$ *interface.* Transport characteristics of incoming states derived from near the conduction band Γ-point are examined as a function of

- the energy of the incoming state,
- thickness of the $Ga_{1-x}Al_xAs$ barrier and
- alloy composition, x, in the $Ga_{1-x}Al_xAs$ barrier.

Transmission through the $Ga_{1-x}Al_xAs$ barrier is either *tunneling* or *propagating* depending on the nature of the Bloch states available for strong coupling in the alloy.

3.3.2 Outline of Section 3.3:

The work presented in this section is concerned with the transport of electrons through a GaAs-$Ga_{1-x}Al_xAs$-GaAs (100) double heterojunction structure (DHS). An energy band diagram of the Γ-point conduction band edge is shown in Figure 1 along with the physical structure.

The mode of transport in these structures is either *tunneling* (energy less than the potential barrier height) or *propagating* (energy greater than the potential barrier height).

o In the *tunneling regime of transport* the Bloch states available for transmission in the $Ga_{1-x}Al_xAs$ are *evanescent* and the wavevector **k** is complex.

o In the *propagating regime of transport* the Bloch states available for transmission in the alloy are *propagating* and the wavevector **k** takes on real values.

The theoretical framework exploits the bulk properties of the constituent semiconductors forming the DHS as developed in Appendices (3.2) and (3.3). The bulk Bloch states associated with complex-**k** provide a suitable basis for a full description of the wavefunction. The calculational technique has been exposed in Section (3.2) and only the results applicable to the (100) interfaces will be discussed in Section (3.3.3) A summary and conclusions are given in Section (3.3.4)

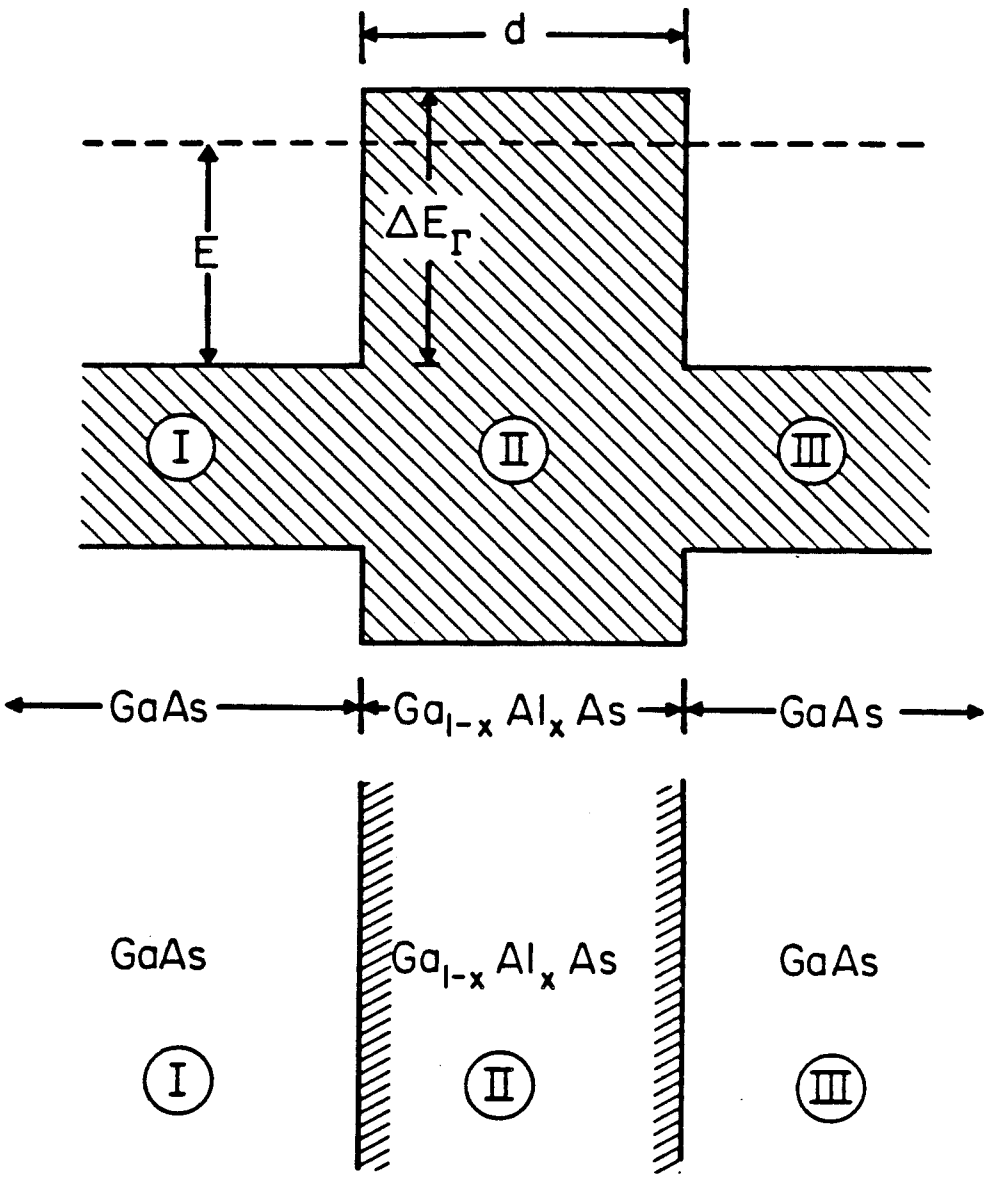

Figure 1: Energy band diagram of GaAs-$Ga_{1-x}Al_xAs$-GaAs DHS and corresponding physical structure. The electron is derived from the GaAs Γ-point and has a total energy E measured with respect to the GaAs Γ-point conduction band minimum. The Γ-point conduction band offset is indicated by ΔE_Γ. The thickness of the $Ga_{1-x}Al_xAs$ barrier is d.

3.3.3 Results:

The complex-**k** bandstructure of GaAs and $Ga_{1-x}Al_xAs$ was calculated using the ten-band tight-binding model described in the preceding section. Within the ten-band tight-binding description used here, the GaAs Γ-point conduction band minimum is at an energy $E_\Gamma^{\mathrm{GaAs}} \approx 1.51$ eV above the GaAs Γ-point valence band maximum, and the GaAs X-point conduction band valley is at an energy $E_X^{\mathrm{GaAs}} \approx 0.52$ eV above the GaAs Γ-point conduction band minimum.

We denote the bulk states with $k_z = k_\lambda$ in spatial region μ by $|\mathbf{k}_\parallel E; k_\lambda{}^{\mu}\rangle$. In the discussion that follows, the incident Bloch state is derived from near the GaAs conduction band Γ-point with real wavevector $k_0 \equiv k_\Gamma^I$, *e.g.* $|\mathbf{k}_\parallel E; k_0\rangle \equiv |\mathbf{k}_\parallel E; k_\Gamma{}^{I}\rangle$. The k_z values of interest are those near the conduction band extrema $\Gamma(k_\Gamma)$ and $X(k_X)$.

In the energy range between the bottom of the GaAs conduction band and the GaAs X-point valley, k_Γ^I is *real* and k_X^I is *complex* such that $|\mathbf{k}_\parallel E; k_\Gamma{}^{I}\rangle$ has a *travelling character* and $|\mathbf{k}_\parallel E; k_X{}^{I}\rangle$ has an *evanescent character.*

However, in the energy range above the X-point valley, both k_Γ^I and k_X^I are *real* such that $|\mathbf{k}_\parallel E; k_\Gamma{}^{I}\rangle$ and $|\mathbf{k}_\parallel E; k_X{}^{I}\rangle$ have *travelling character.*

Similar considerations apply to the Bloch states available for transport in the alloy $Ga_{1-x}Al_xAs$.

For an alloy composition $x < 0.45$[13], $Ga_{1-x}Al_xAs$ is direct and $E_\Gamma^{Ga_{1-x}Al_xAs} < E_X^{Ga_{1-x}Al_xAs}$ in this composition range. As in the preceding section, the valence band offset ΔE_Γ was taken to be equal to 15% of the difference of the Γ-point band gap between GaAs and $Ga_{1-x}Al_xAs$. The dependence on the alloy composition x of the Γ-point energy edge in $Ga_{1-x}Al_xAs$ is, in the virtual crystal approximation: $E_\Gamma^{Ga_{1-x}Al_xAs} \approx 1.35\ x$ eV , above the GaAs Γ-point conduction band minimum.

We present the main results for the transmission coefficients of electrons through a GaAs-$Ga_{1-x}Al_xAs$-GaAs (100) DHS. The incident Bloch state is derived from near the GaAs conduction band Γ-point with real wavevector $k_0 \equiv k_\Gamma^I$, *e.g.* $|\mathbf{k}_\parallel E; k_0\rangle \equiv |\mathbf{k}_\parallel E; k_\Gamma{}^I\rangle$. We discuss the transport across the central $Ga_{1-x}Al_xAs$ barrier as a function of

- energy, E, of the incoming Bloch state, $|\mathbf{k}_\parallel E; k_0\rangle$,
- thickness of the $Ga_{1-x}Al_xAs$ barrier and
- alloy composition, x, in the central $Ga_{1-x}Al_xAs$ barrier.

3.3.3.1 Complex-k Energy Band Structure:

Figures (2) and (3) show the complex-**k** band structure of GaAs and AlAs along the (100) direction, respectively. The complex-**k** band structure corresponds to vanishing wavector parallel to the (100) interface plane, *i.e.*, $\mathbf{k}_\parallel = \mathbf{0}$. At a given energy E, the purely real values of k_z are indicated by a solid line on the right panel of the figure and the purely imaginary values of k_z are indicated by a solid line on the left panel of the figure. Complex values of k_z are indicated by a dashed line, $\mathrm{Re}[k_z]$ being on the right and $\mathrm{Im}[k_z]$ being on the left of the figure respectively. As seen in Figures (2) and (3) complex bands connect to real bands at points of vanishing slope, *i.e.*, where

$$\left[\frac{\partial E(\mathbf{k})}{\partial k_z}\right]_{k_z=k_0} = 0, \tag{4.13}$$

for a real value of the wavevector k_0 . General properties of the energy function $E_n(\mathbf{k})$ in the case where the wavevector **k** is complex can be found in Appendix A.

3.3.3.2 Transport Coefficient vs. Energy:

Figure 4 shows the total transmission and reflection coefficients , $T(\mathbf{k}_\parallel, E)$ and $R(\mathbf{k}_\parallel, E)$, as a function of the energy, E, of the incoming Bloch state. Energy

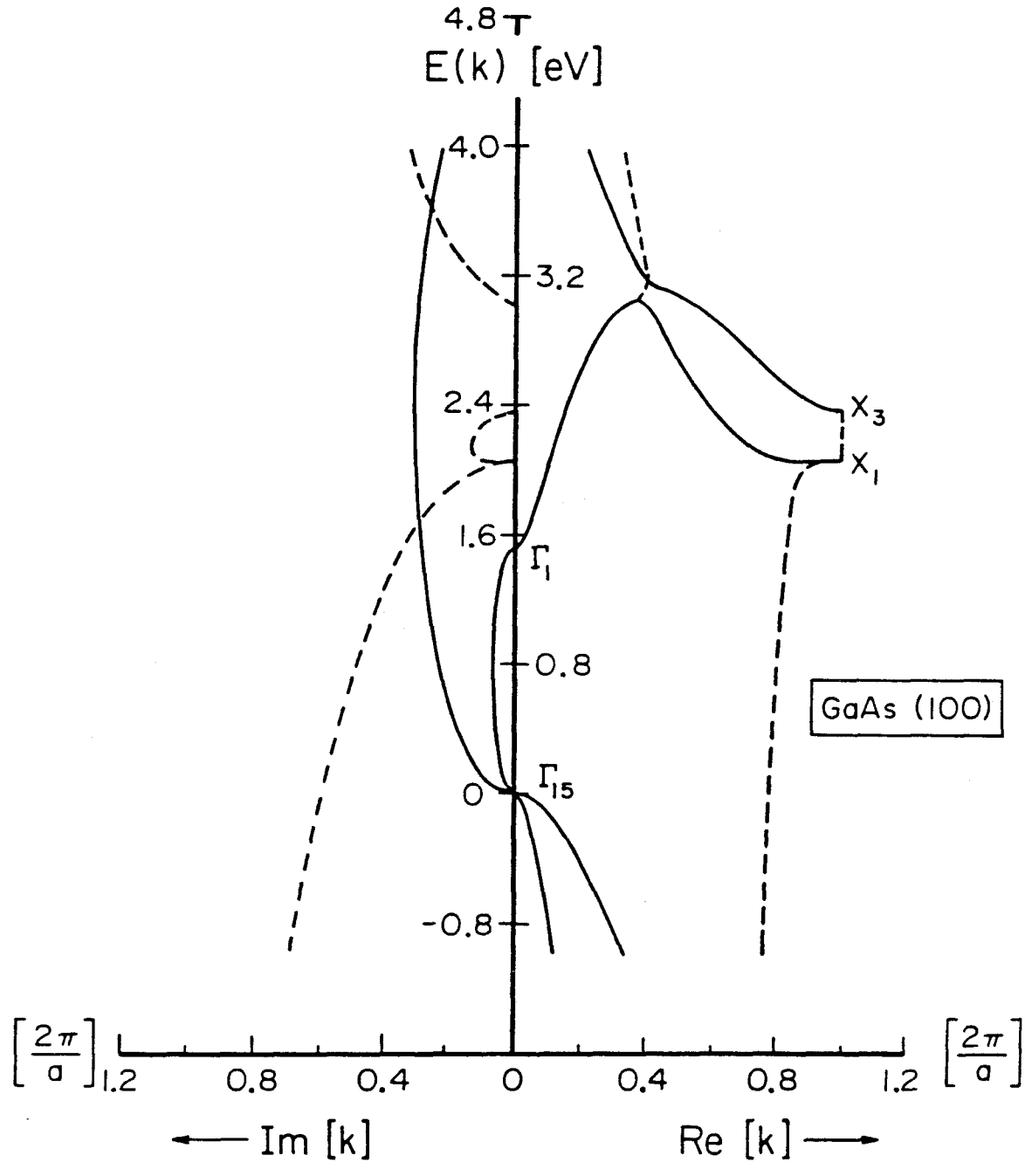

Figure 2: Complex-**k** band structure of GaAs along the (100) direction, respectively. The complex-**k** band structure corresponds to vanishing wavevector parallel to the (100) interface plane, *i.e.* $\mathbf{k}_{||} = \mathbf{0}$. At a given energy E, the purely real values of k_z are indicated by a solid line on the right panel of the figure and the purely imaginary values of k_z are indicated by a solid line on the left panel of the figure. Complex values of k_z are indicated by a dashed line, Re$[k_z]$ being on the right and Im$[k_z]$ being on the left of the figure respectively. The zero of energy is taken to be the GaAs valence band maximum.

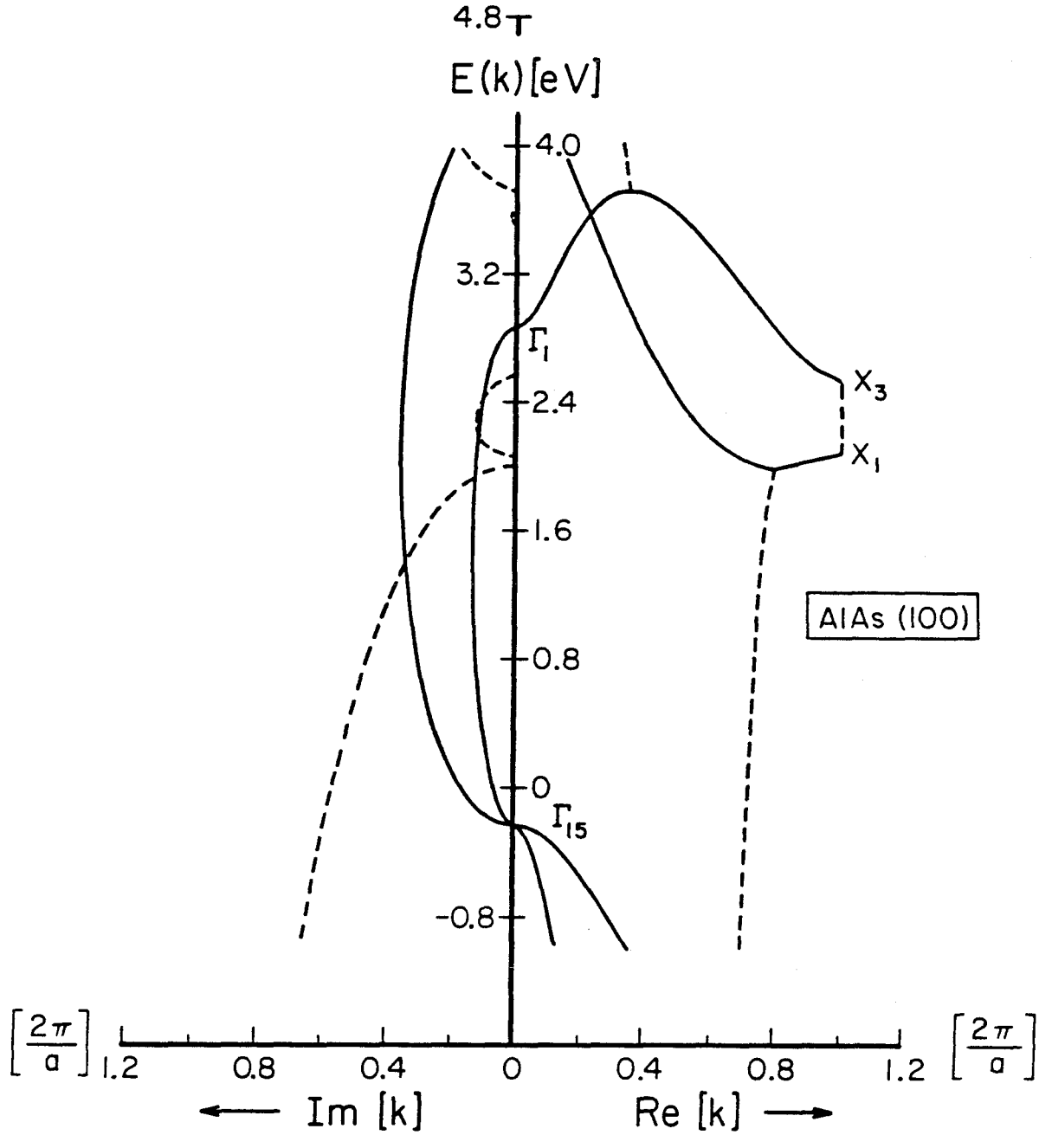

Figure 3: Complex-**k** band structure of AlAs along the (100) direction, respectively. The complex-**k** band structure corresponds to vanishing wavevector parallel to the (100) interface plane, *i.e.* $\mathbf{k}_{\|} = \mathbf{0}$. At a given energy E, the purely real values of k_z are indicated by a solid line on the right panel of the figure and the purely imaginary values of k_z are indicated by a solid line on the left panel of the figure. Complex values of k_z are indicated by a dashed line, $\mathrm{Re}[k_z]$ being on the right and $\mathrm{Im}[k_z]$ being on the left of the figure respectively. The zero of energy is taken to be the GaAs valence band maximum.

is measured with respect to the GaAs conduction band minimum. We consider the case of vanishing parallel wavevector $\mathbf{k}_{\|} = \mathbf{0}$, and composition of $x = 1.0$. Calculations were carried out for different AlAs barrier thicknesses.

For energies of the incoming states near the GaAs conduction band Γ-point, *transmission through the* AlAs *barrier occurs mostly via the coupling to evanescent states that connect to the* AlAs *conduction band at the Γ-point.* In the energy range considered, no propagating Bloch states are available in AlAs and the wavefunction has an evanescent character in the barrier. The AlAs Γ-point minimum is at an energy $E_{\Gamma}^{\mathrm{AlAs}} = 1.35$ eV above the GaAs conduction band minimum. As mentioned in Section (3.3.2), the transmission coefficient vanishes for incoming states derived from near the conduction band Γ-point at an energy equal to $E_{\Gamma}^{\mathrm{GaAs}}$. At this energy, the component of the group velocity normal to the interface vanishes, $\left[\frac{\partial E(\mathbf{k})}{\partial k_z}\right]_{k_z = k_{\Gamma}^{I}} \equiv 0$, and the incoming state $|\mathbf{k}_{\|} E; k_{\Gamma}{}^{I}\rangle$ does not couple to any states in AlAs.

3.3.3.3 Transmission Coefficient vs. $Ga_{1-x}Al_xAs$ Barrier Thickness:

We now examine the *different transport regimes.* Figure 5 shows the total transmission coefficient $T(\mathbf{k}_{\|}, E)$ as a function of the number of monolayers forming the central $Ga_{1-x}Al_xAs$ barrier. Layers are measured in units of $a/2$, where a is the GaAs lattice constant. Energies of the incoming Bloch state $|\mathbf{k}_{\|} E; k_{\Gamma}{}^{I}\rangle$ range from 0.19 eV$\leq E \leq$ 0.69 eV, measured with respect to the GaAs conduction band minimum. The alloy composition is $x = 0.3$ and $\mathbf{k}_{\|} = \mathbf{0}$. The alloy is direct and the Γ-point energy edge of $Ga_{1-x}Al_xAs$ is $E_{\Gamma}^{Ga_{1-x}Al_xAs} \approx 0.41$ eV. Transmission through the $Ga_{1-x}Al_xAs$ barrier is either tunneling or propagating depending on the nature of the Bloch states available for strong coupling in the alloy.

For energies of the incoming state *less than* $E_{\Gamma}^{Ga_{1-x}Al_xAs}$, the avail-

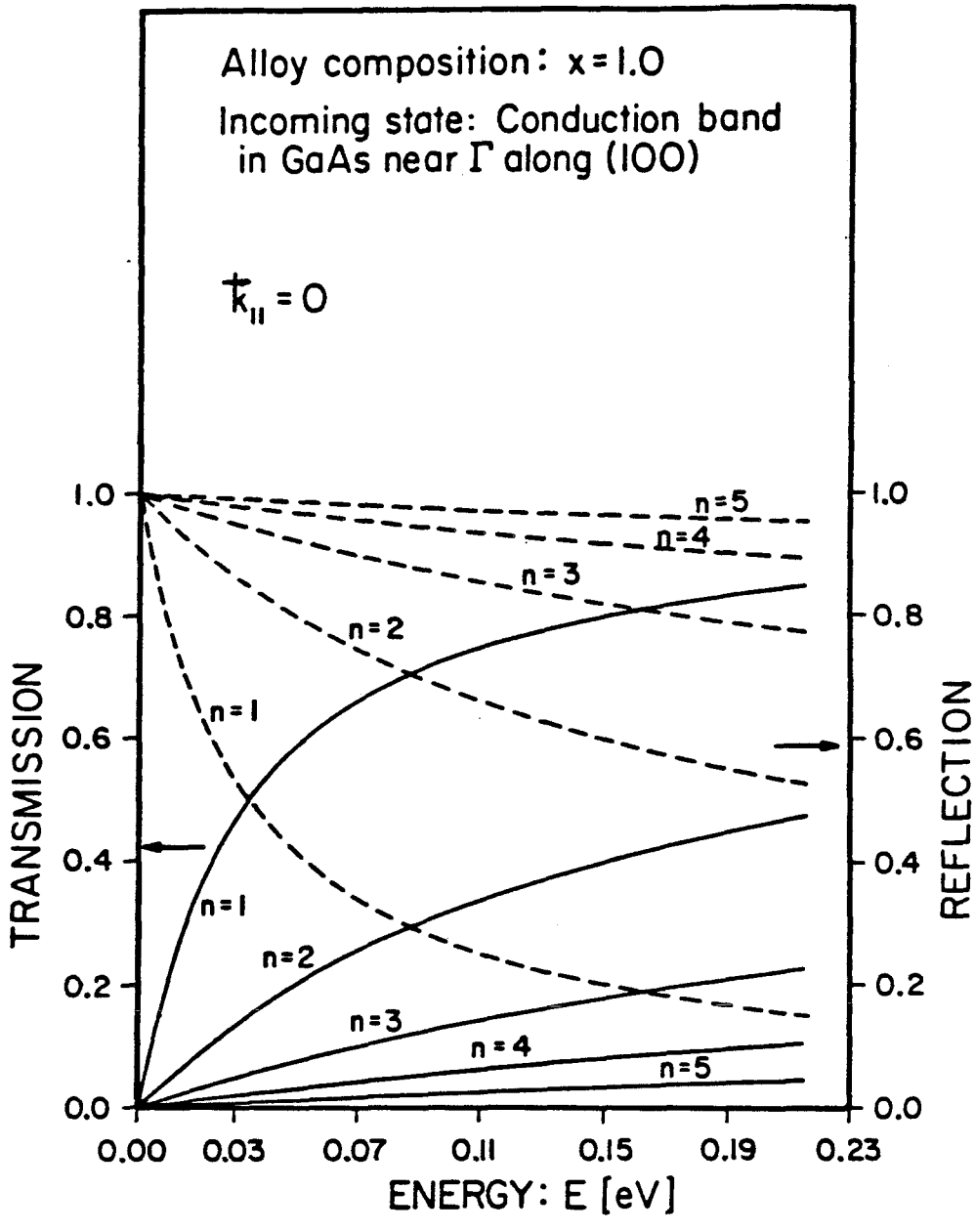

Figure 4: Total transmission (solid line) and reflection (dashed line) coefficients , $T(\mathbf{k}_{\|}, E)$ and $R(\mathbf{k}_{\|}, E)$, as a function of the energy E of the incident Bloch state $|\mathbf{k}_{\|} E; k_{\Gamma}{}^{I}\rangle$, for different $Ga_{1-x}Al_xAs$ barrier thicknesses with a composition of $x = 1.0$. Energy is measured with respect to the GaAs conduction band minimum and $\mathbf{k}_{\|} = \mathbf{0}$. The number of $Ga_{1-x}Al_xAs$ barrier layers is n.

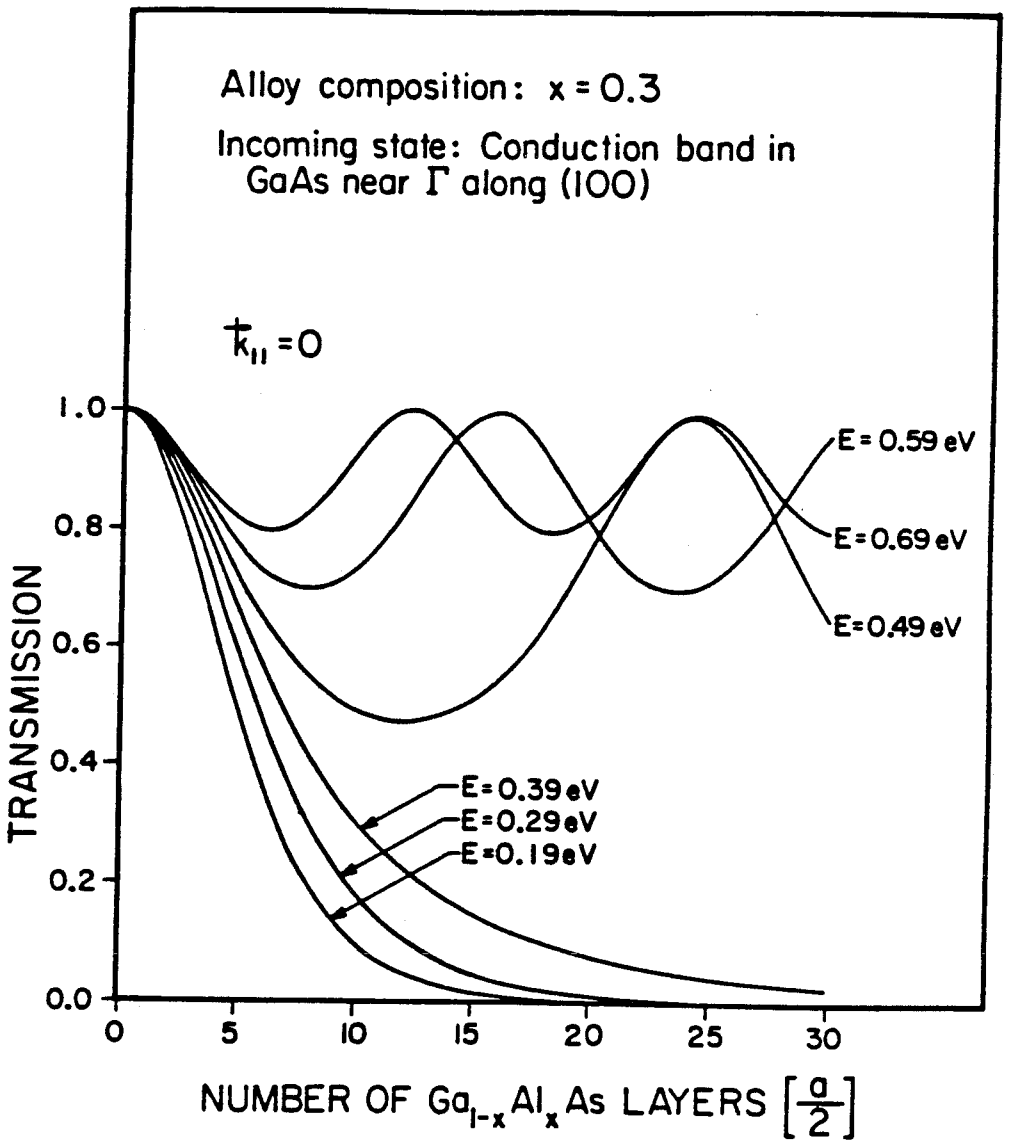

Figure 5: Total transmission coefficient, $T(\mathbf{k}_{\parallel}, E)$, as a function of central $Ga_{1-x}Al_xAs$ barrier thickness for different incoming energies. The incoming Bloch state has no momemtum parallel to the interface, $\mathbf{k}_{\parallel} = \mathbf{0}$. The $Ga_{1-x}Al_xAs$ alloy composition is $x = 0.3$.

able states in the alloy are *gap states* (k_Γ^{II} complex) and the wavefunction is damped in the barrier. However, for energies of the incoming state *greater than* $E_\Gamma^{Ga_{1-x}Al_xAs}$, the available states in the alloy are *band states* (k_Γ^{II} real) and the wavefunction is not damped in the barrier.

Generally, when an incoming state in GaAs is derived from a conduction band extremum, say λ, such that $k_0 \equiv k_\lambda^I$ and $|\mathbf{k}_\parallel E; k_0\rangle \equiv |\mathbf{k}_\parallel E; k_\lambda{}^I\rangle$ the mode of transport (*i.e.*, tunneling or propagating) appears to be determined by the nature of the states in $Ga_{1-x}Al_xAs$ derived from the same conduction band extremum, $|\mathbf{k}_\parallel E; k_\lambda{}^{II}\rangle$. For energies of the incoming state less than the alloy conduction band edge $E_\lambda^{Ga_{1-x}Al_xAs}$, the states that couple strongly in the alloy are gap states ($|\mathbf{k}_\parallel E; k_\lambda{}^{II}\rangle$ evanescent) and hence the wavefunction is damped in the barrier. However, for energies of the incoming state greater than the alloy conduction band edge $E_\lambda^{Ga_{1-x}Al_xAs}$, the states that couple strongly in the alloy are band states ($|\mathbf{k}_\parallel E; k_\lambda{}^{II}\rangle$ propagating) and hence the wavefunction is not damped in the barrier.

o In the *tunneling regime of transport*, transmission occurs mostly via the coupling to the alloy Γ-point *evanescent* states (k_Γ^{II} complex). As seen in Figure 5, the evanescent character of the wavefunction in $Ga_{1-x}Al_xAs$ is reflected in the fact that the transmission coefficient $T(\mathbf{k}_\parallel, E)$ is an exponentially decaying function of the $Ga_{1-x}Al_xAs$ barrier thickness. These observations are similar to those obtained from the thick-barrier WKB approximation[15—16].

o For incoming states with energy *greater than* $E_\Gamma^{Ga_{1-x}Al_xAs}$, transmission occurs mostly via the coupling to the alloy Γ-point *propagating* states (k_Γ^{II} real). The transmission coefficient is unity when the thickness of the $Ga_{1-x}Al_xAs$ barrier contains an integral number of half-wavelengths (determined by k_Γ^{II}) in the barrier region. Under these *resonant scattering* conditions, the states derived from the conduction ba. Γ-point couple strongly to each other and channeling into Bloch

states derived from different conduction band extrema is found to be small. This observation is supported by the original work[2,3] on the transport of Bloch states at a single GaAs-$Ga_{1-x}Al_xAs$ heterojunction.

For energy of the incoming state above $E_\Gamma^{Ga_{1-x}Al_xAs}$, the transmission coefficient is a periodic function of the $Ga_{1-x}Al_xAs$ barrier thickness. Since the wavevector k_Γ^{II} increases with incident Bloch state energy, the period of the transmission amplitude decreases with the energy of the incident Bloch state. The off-resonance transmission amplitudes increase with increasing incident energy. The general qualitative behavior of the transport is similar to that exhibited by plane wave states incident on a rectangular quantum-mechanical barrier[17].

3.3.3.4 Transmission Through X-point Bloch states:

Figure 6 shows the total transmission and reflection coefficients, $T(\mathbf{k}_\parallel, E)$ and $R(\mathbf{k}_\parallel, E)$, as a function of the number of monolayers forming a central AlAs barrier. The energy of the incoming Bloch state $|\mathbf{k}_\parallel E; k_\Gamma{}^I\rangle$ is E =0.51 eV, measured with respect to the GaAs conduction band minimum. The incoming state derived from near the conduction band Γ-point has vanishing parallel momentum, $\mathbf{k}_\parallel = \mathbf{0}$. At this energy the states available for transport in AlAs are *propagating* states near the X-point extremum (k_X^{II} real), and *evanescent* states connecting to the Γ-point (k_Γ^{II} complex) at higher energy. Here again it is found that, for incoming states derived from the GaAs conduction band Γ-point, transmission through the AlAs barrier occurs mostly via the coupling to evanescent states that connect to the AlAs conduction band at the Γ-point. At small AlAs barrier thicknesses, transmission of conduction band Γ-point incoming states is governed by *tunneling*. In this regime, the incoming state $|\mathbf{k}_\parallel E; k_\Gamma{}^I\rangle$ tunnels through the AlAs barrier by coupling to the evanescent Bloch states $|\mathbf{k}_\parallel E; k_\Gamma{}^{II}\rangle$ associated with the conduction

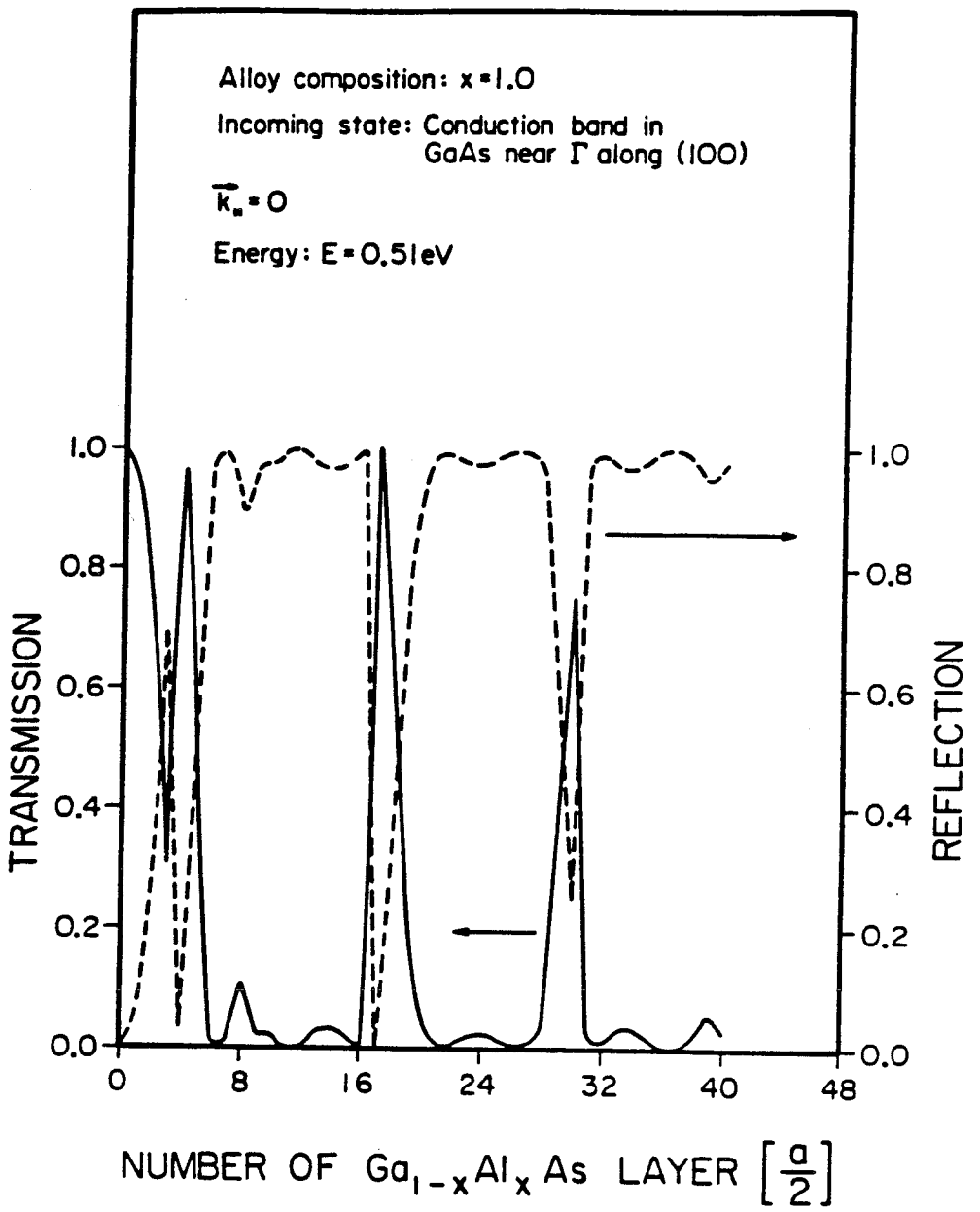

Figure 6: Total transmission (solid line) and reflection (dashed line) coefficients , $T(\mathbf{k}_{\parallel}, E)$ and $R(\mathbf{k}_{\parallel}, E)$, as a function of central AlAs barrier thickness for an energy of $E = 0.51$ eV. Energy is measured with respect to the GaAs conduction band minimum and $\mathbf{k}_{\parallel} = \mathbf{0}$.

band Γ-point minimum. However, it was found that under energetically favorable conditions, transport could exhibit very sharp *resonance scattering* through available propagating X-point states, $|\mathbf{k}_{\|}E; k_X{}^{II}\rangle$. This mode of resonant transport occurs for thick AlAs barriers when the tunneling through Γ-point derived evanescent Bloch states is negligible. *The sharpness of the resonances in this case is an indication of the weakness of the coupling between states derived from the Γ-point and states derived from the X-point.*

3.3.3.5 Transmission Coefficient vs. $Ga_{1-x}Al_xAs$ Alloy Composition:

We now analyse the relative contributions of the X-point and the Γ-point conduction band Bloch states to the transmitted wavefunction as a function of the alloy composition x. Figure 7 shows the transmission coefficients $T_\Gamma(\mathbf{k}_{\|}, E)$ and $T_X(\mathbf{k}_{\|}, E)$ as a function of alloy composition, for two different $Ga_{1-x}Al_xAs$ barrier thicknesses. The energy of the incoming state is $E = 0.69$ eV measured with respect to the GaAs conduction band minimum. For the range of alloy compositions studied, this energy is greater than $E_\Gamma^{Ga_{1-x}Al_xAs}$. At this energy the Γ-point and X-point states in GaAs and $Ga_{1-x}Al_xAs$ are *propagating* ($k_\Gamma^I, k_\Gamma^{II}, k_\Gamma^{III}$ real, and $k_X^I, k_X^{II}, k_X^{III}$ real). The incoming Bloch state has $\mathbf{k}_{\|} = \mathbf{0}$.

As mentioned above, the Γ-point energy edge, $E_\Gamma^{Ga_{1-x}Al_xAs}$, scales linearly with the alloy composition. The composition x is therefore proportional to the Γ-point barrier height at the interface. For the range of alloy compositions studied, the Γ-point energy edge of $Ga_{1-x}Al_xAs$ varies approximately in the range $0 \text{ eV} \leq E_\Gamma^{Ga_{1-x}Al_xAs} \leq 0.47$ eV, above the GaAs Γ-point conduction band minimum. For an energy of the incoming state of $E = 0.69$ eV, the transport regime for incoming states derived from the conduction band Γ-point is propagating since the coupling states in the alloy are propagating Bloch states. Since the energy of

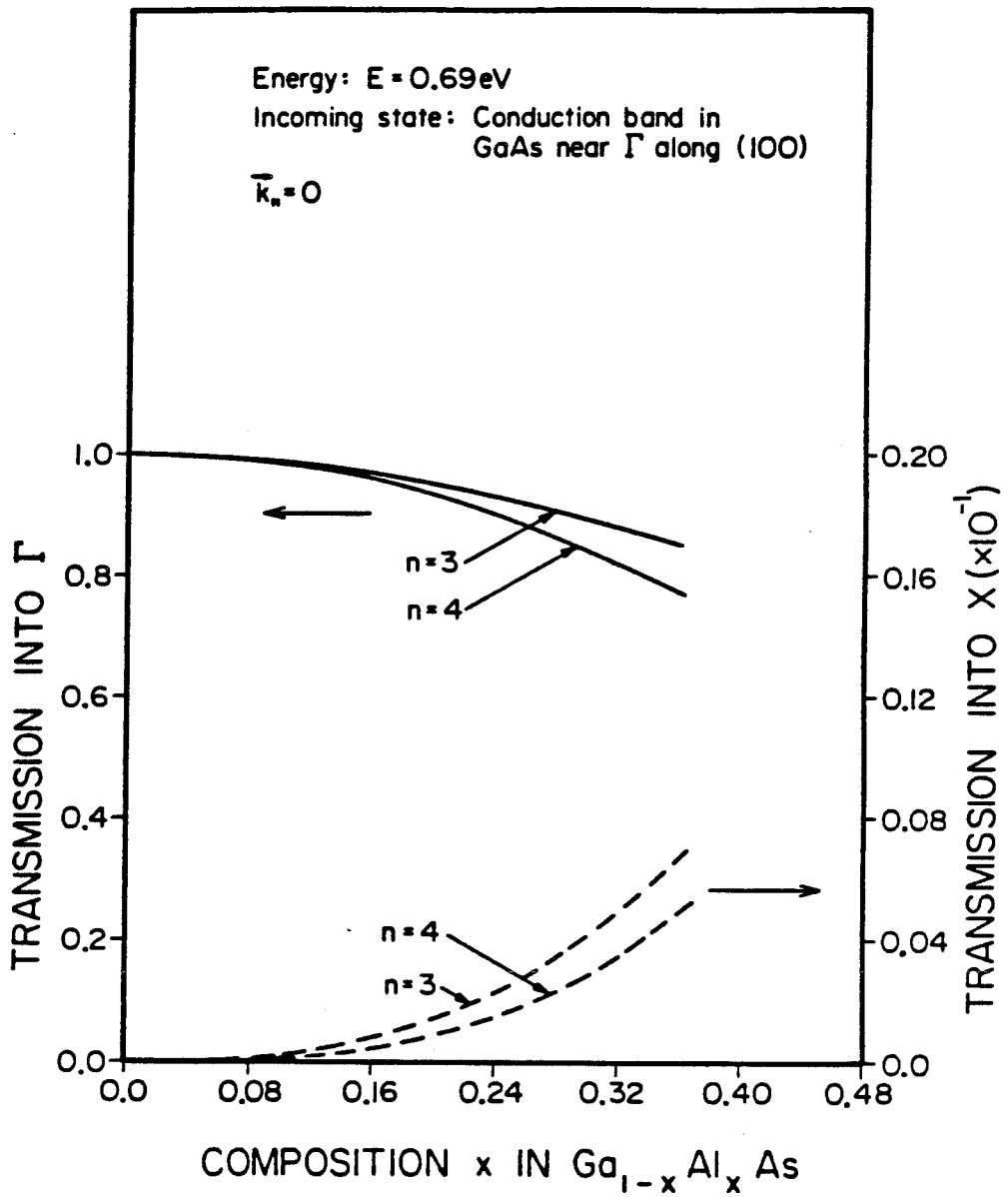

Figure 7: Wavevector-resolved transmission coefficients, $T_\Gamma(\mathbf{k}_\parallel, E)$ (solid line) and $T_X(\mathbf{k}_\parallel, E)$ (dashed line), as a function of $Ga_{1-x}Al_xAs$ alloy composition x for different barrier thicknesses. The energy of the incoming state is $E = 0.69$ eV. The number of $Ga_{1-x}Al_xAs$ barrier layers is n, and $\mathbf{k}_\parallel = \mathbf{0}$.

the incoming state lies above the Γ-point energy edge of the alloy, the transmission amplitude is a weakly dependent function of the barrier height.

As the Al content of $Ga_{1-x}Al_xAs$ increases, transmission into the propagating X-point Bloch states $|\mathbf{k}_{\|}E; k_X{}^{III}\rangle$ increases but remains rather small. States derived from the same extremum of the conduction band appear to couple strongly to each other across the GaAs-$Ga_{1-x}Al_xAs$ interface. *However, states derived from different extrema of the conduction band appear to couple weakly across the* GaAs-$Ga_{1-x}Al_xAs$ *interface.*

3.3.4 Summary and Conclusions:

We have calculated the transport coefficients of Bloch states through GaAs-$Ga_{1-x}Al_xAs$-GaAs double heterojunctions. The model uses complex-**k** band structures and transfer matrix methods in the tight-binding approximation. With these techniques, k_z-resolved transport coefficients can be calculated. This, in turn, allows for a better understanding of the transmission coefficients of Bloch states derived from different extrema of the conduction band in GaAs. The incoming electron is derived from the GaAs conduction band Γ-point. Calculations of transport coefficients associated with various conduction band valleys were carried through as a function of

- the energy of the incoming state,
- thickness of the $Ga_{1-x}Al_xAs$ barrier and
- alloy composition, x, in the $Ga_{1-x}Al_xAs$ barrier.

The major result of this study is that, *states derived from the same extremum of the conduction band appear to couple strongly to each other across the* GaAs-$Ga_{1-x}Al_xAs$ *interface.* Transmission through the $Ga_{1-x}Al_xAs$ barrier is either tunneling or propagating depending on the nature of the Bloch states available for strong coupling in the alloy. For energies of the incoming states near the GaAs conduction band Γ-point, transmission through the $Ga_{1-x}Al_xAs$ barrier occurs mostly via the coupling to states (evanescent or propagating) that connect to the alloy conduction band at the Γ-point.

In the *propagating mode of transport,* resonances in the transmission could possibly be used in GaAs high-speed low-current electronic devices. In an operational mode, it is desirable to populate the low-mass high-velocity GaAs conduction band Γ-point minimum and to depopulate the high-mass low-velocity X and L valleys. These results could provide the basis for an interesting filter for use in

high-speed devices[18].

References

1. J. C. Slater and G. F. Koster, *Phys. Rev.* **94**, 1498 (1954).
2. G. C. Osbourn and D. L. Smith, *Phys. Rev.* **B19**, 2124 (1979).
3. G. C. Osbourn and D. L. Smith, *J. Vac. Sci. Technol.* **16**, 1529 (1979).
4. G. C. Osbourn, *J. Vac. Sci. Technol.* **17**, 1104 (1980).
5. G. C. Osbourn, *J. Vac. Sci. Technol.* **19**, 592 (1981).
6. Y. C. Chang and J. N. Schulman, *Phys. Rev.* **B25**, 3975 (1982).
7. J. N. Schulman and Y. C. Chang, to be published in *Phys. Rev.* **B**.
8. D. H. Lee and J. D. Joannopoulos, *Phys. Rev.* **B23**, 4988 (1981); *Phys. Rev.* **B23**, 4997 (1981).
9. J. Pollmann and S. Pantelides, *Phys. Rev.* **B18**, 5524 (1978).
10. D. H. Lee and J. D. Joannopoulos, *J. Vac. Sci. Technol.* **19**, 355 (1981).
11. Y. C. Chang and J. N. Schulman, *J. Vac. Sci. Technol.* **21**, 540 (1982).
12. P. Vogl, H. P. Hjalmarson, and J. D. Dow, *J. Phys. Chem. Sol.* **44**, 365 (1983).
13. J. N. Schulman and Y. C. Chang, *Phys. Rev.* **B24**, 4445 (1981)
14. H. C. Casey and M. B. Panish, *Heterostructure Lasers* (Academic Press, New York, 1978), Part A, Chapter 4.
15. R. Dingle, W. Weigmann, and C. Henry, *Phys. Rev. Lett.* **33**, 827 (1974).
16. S. M. Sze, *Physics of Semiconductor Devices, 2rd Edition* (Wiley-Interscience, 1981), p. 850
17. L. I. Schiff, *Quantum Mechanics, 3rd Edition* (McGraw-Hill Book Company, 1968), pp. 102-104
18. W. A. Harrison, *Phys. Rev.* **123**, 85 (1961).
19. C. B. Duke, *Tunneling Phenomena in Solids* (Plenum Press, New York,

1969), 31.

CHAPTER 4

ELECTRONIC STRUCTURE OF SEMICONDUCTOR SUPERLATTICES

Section 4.1

INTRODUCTION

4.1.1 Scope of this study

This study is concerned with a *new approach to the theory of semiconductor superlattices* devised specially for the study of *non-local properties*, such as *optical properties.*

Superlattice structures are made by the alternate deposition of layers of two lattice-matched solids. Semiconductor superlattices can be viewed as completely new materials whose electronic and optical properties are not just a combination of the properties of the bulk constituent semiconductors. In fact, it is possible to tailor the electronic and optical properties of semiconductor superlattices over a large range. It is this tailorability that makes semiconductor superlattices vastly more interesting that the corresponding semiconductor alloys.

Due to the alternate arrangement of layers of semiconductor, the superlattice primitive cell in $\mathbf{x}$-space can be made to be much larger than that of the constituent semiconductors. This is accompanied by a corresponding reduction to the Brillouin zone in $\mathbf{k}$-space. This effect is known as *band folding.* The concept of *band folding* often plays an all important role at determining the general qualitative features of the electronic band structure. Thus, in a zeroth-order picture, the *increase in the dimension of the* $\mathbf{x}$*-space primitive cell* translates directly in a *proportional decrease in the dimension of the* $\mathbf{k}$*-space primitive cell, or first Brillouin zone.* This has the effect of folding the quantum number $\mathbf{k}$ associated with the translation group back near the center of the first Brillouin zone. This *folding back of the Brillouin zone* is a completely new property due to the increased repeated distance and does not have its origin in the bulk properties of the constituent semiconductors.

In particular, it is possible to create a direct band gap (*i.e.*, whenever the maximum of the valence band and the minimum of the conduction band occur at the same **k**-point in the Brillouin zone) superlattice out of two indirect semiconductors[1].

The *optical properties* of quantum well structures and semiconductor superlattices have generated a lot of experimental work in the past few years. More specifically, the fabrication of *quantum well lasers*[2] has opened a totally new area of applications. In these quantum well laser systems, quantum mechanical effects are readily observed as the *energy of the light emitted from the quantum well is greater than that of the corresponding bulk solid.* This is one of the examples of the experimental evidence of the existence of energy subbands.

In the light of these new effects, it is imperative to devise a theory that allows for a deeper understanding of the optical properties of semiconductor superlattices. This chapter is devoted to the presentation of a general theoretical formalism well suited for the study of the optical properties of semiconductor superlattices. The formalism presented here will serve as a basis for future studies in the area of the optical properties of semiconductor superlattices.

4.1.2 Outline of Chapter 4

This chapter is concerned with the study of the electronic structure of semiconductor superlattices. *The formalism used is particularly suitable for the study of the optical properties of semiconductor superlattices.*

• The first step leading to realistic superlattice electronic structure is the *accurate calculation of the electronic band structure of the constituent bulk semiconductors.* Within the present formalism, the following procedure allows us to *describe the constituent semiconductors in terms of a single set of basis functions*:

(i) The *local pseudopotential Hamiltonian* of each semiconductor forming the superlattice is expressed in terms of a local pseudopotential Hamiltonian associated with a *reference solid.* A total number of 113 plane waves $\exp(i\mathbf{g}\cdot\mathbf{x})$, where $\mathbf{g}$ is a reciprocal lattice vector, is used.

(ii) We operate a transformation on the local pseudopotential Hamiltonian of each solid in order to *transform from a plane wave representation,* $\exp(i\mathbf{g}\cdot\mathbf{x})$, *to a representation in terms of* $\mathbf{k}_0 = \mathbf{0}$ *basis functions associated with the same reference solid,* $u_m(\mathbf{x})$. We refer to this representation as the $\mathbf{k}\cdot\mathbf{p}$ representation. Thus the Hamiltonian of each solid is now expressed in a $\mathbf{k}\cdot\mathbf{p}$ representation associated with the *same set of* $\mathbf{k}_0 = \mathbf{0}$ *basis functions* $u_m(\mathbf{x})$. This technique has a definite advantage, since no approximations are made when matching the supelattice state function onto the interface plane.

(iii) The $\mathbf{k}\cdot\mathbf{p}$ Hamiltonian of each solid is *truncated down to* $N = 27$ *basis functions* $u_m(\mathbf{x})$. This truncation procedure is very satisfying since *the* $\mathbf{k}\cdot\mathbf{p}$ *representation provides much better convergence than the plane wave representation.* Furthermore the $\mathbf{k}\cdot\mathbf{p}$ Hamiltonian of each solid can be *explicitely calculated in terms of the* $\mathbf{k}_0 = \mathbf{0}$ *basis functions of the reference solid,* $u_m(\mathbf{x})$.

(iv) The complex-**k** energy band structure is then obtained with the *use of a companion matrix whose eigenvector matrix is closely related to the boundary condition matrix* on the superlattice state function. Since we use $N = 27$ basis functions $u_m(\mathbf{x})$ we obtain a total of $2N = 54$ Bloch solutions $|\mathbf{k}_{\|}E; k_{\lambda}^{(j)}\rangle$ with complex wavevectors $k_{\lambda}^{(j)}$ at each parallel momentum $\mathbf{k}_{\|}$ and energy E, in each solid $j = 1, 2$.

(v) The superlattice state function is then expanded in terms of the Bloch solutions $|\mathbf{k}_{\|}E; k_{\lambda}^{(j)}\rangle$ in each solid j. Since the Bloch solutions $|\mathbf{k}_{\|}E; k_{\lambda}^{(j)}\rangle$ are expended in terms of the basis functions $u_m(\mathbf{x})$ of the reference solid, we can express the superlattice state function in terms of the basis functions $u_m(\mathbf{x})$ associated with $\mathbf{k}_0 = \mathbf{0}$. The expansion coefficients are termed the *multi-component envelope functions.* The use of the $\mathbf{k} \cdot \mathbf{p}$ theoretic allows a *description of the superlattice wavefunction in terms of basis functions* $u_m(\mathbf{x})$ *which are exact eigensolutions of the crystal Hamiltonian of the reference solid at* $\mathbf{k}_0 = \mathbf{0}$.

(vi) A suitable set of boundary conditions on the superlattice wavefunction allows us to obtain the complex-**q** energy spectrum of the superlattice, where **q** is the superlattice wavevector that classifies the superlattice solutions. We thus obtain the *complex-***q** *energy band structure of the superlattice.*

• We would like to stress two very attractive features of the above formalism:

(i) The only empirical input parameters are the *local pseudopotential form factor* and *the energy band offsets.*

(ii) The superlattice state function in each solid is expressed in terms of a *set of basis functions* $u_m(\mathbf{x})$ *associated with the same reference solid.* We therefore relax the often used approximation that the $\mathbf{k}_0 = \mathbf{0}$ functions for all semiconductor of the group III-V are the same[3—5], which is clearly a convenient approximation when matching the superlattice state function onto the interface plane.

4.1.3.Summary of the Results of Chapter 4

We have applied the above formalism to the case of the GaAs-Alas superlattice.

• The complex-**k** energy band structure is accurately described by this truncated $\mathbf{k} \cdot \mathbf{p}$ Hamiltonian derived from a more complete local pseudopotential calculation. It is shown that this method provides an efficient way of obtaining the bulk Bloch solutions associated with each solid forming the superlattice in terms of the *same* set of basis functions. The transformation from the *local pseudopotential formalism* to the $\mathbf{k} \cdot \mathbf{p}$ *formalism* allows us to truncate the number of basis functions from 113 plane waves, $\exp(i\mathbf{g} \cdot \mathbf{x})$, down to 27 zone-center functions, $u_m(\mathbf{x})$.

• We also present results for complex-**q** energy band structure for GaAs-AlAs superlattices of different periods. More specifically we study the variation of the superlattice band gap as a function of the number of GaAs monolayers forming the superlattice period, the number of AlAs monolayers being kept fixed.

The formalism presented here will serve as a basis for future studies on the *optical properties of semiconductor superlattices.*

Section 4.2

ELECTRONIC STRUCTURE OF SEMICONDUCTOR SUPERLATTICES

4.2.1 Outline of Section 4.2:

In this section, we develop the theoretical framework to treat the electronic structure of semiconductor superlattices. The electronic spectrum of semiconductor superlattices is obtained via a bulk complex-$\mathbf{k}$ full-zone $\mathbf{k} \cdot \mathbf{p}$ description of the constituent semiconductors. The bulk complex-$\mathbf{k}$ full-zone $\mathbf{k} \cdot \mathbf{p}$ band structure is derived from a local pseudopotential calculation to obtain accurate description of the band structure and of the associated Bloch solutions. Within the pseudopotential and $\mathbf{k} \cdot \mathbf{p}$ scheme, the bulk complex-$\mathbf{k}$ Bloch solutions for the two solids forming the superlattice structure are expanded in terms of the *same set of zone-center functions.*

The complex-$\mathbf{k}$ bulk Bloch states of each semiconductors forms the expansion set for the superlattice wavefunction. The superlattice bandstructure and wavefunction are derived from a *set of boundary conditions imposed on the envelope function at the semiconductor interface.*

4.2.2 Introduction:

The backbone of the theory of the electronic structure of semiconductor superlattice presented here rests on the full-zone $\mathbf{k} \cdot \mathbf{p}$ description of the constituent semiconductors forming the superlattice. A review of the $\mathbf{k} \cdot \mathbf{p}$ theory of bulk semiconductors is presented in Appendix (4.1). In the full-zone $\mathbf{k} \cdot \mathbf{p}$ approach the Bloch state at a *general* $\mathbf{k}$*-point* in the Brillouin zone is expanded in terms of a set of cell-periodic function associated with a *special* $\mathbf{k}$*-point* in the Brillouin zone, $u_n(\mathbf{k}_0; \mathbf{x})$. In the present treatment, we take $\mathbf{k}_0 = \mathbf{0}$ as the special $\mathbf{k}$-point with which the cell periodic basis functions are associated.

The theoretical technique used here is based on the full-zone $\mathbf{k} \cdot \mathbf{p}$ theory derived from a local pseudodopotential approach as developed in Appendix (4.2). In the local pseudopotential approach, the Bloch state at a *general* $\mathbf{k}$*-point* in the Brillouin zone is expanded in terms of a set of plane waves $\exp(i\mathbf{g} \cdot \mathbf{x})$ associated with reciprocal lattice vectors $\mathbf{g}$. The term *pseudopotential* refers to a potential such that the expansion of the Bloch state in terms of the plane waves $\exp(i\mathbf{g} \cdot \mathbf{x})$ will converge fairly rapidly.

The formal connection between the *local pseudopotential description* and the *full-zone* $\mathbf{k} \cdot \mathbf{p}$ *description* is presented in Appendix (4.3). We would like to point out two important advantages of this approach.

o By using a full-zone $\mathbf{k} \cdot \mathbf{p}$ formulation derived from a local pseudopotential description of the two constituent semiconductors, it is possible to *expand the bulk Bloch solutions in each solid in terms of the same set of cell-periodic part of the Bloch functions associated with* $\mathbf{k}_0 = \mathbf{0}$. By doing so, we relax the often used approximation that takes the cell-periodic part of the Bloch functions at the center of the Brillouin zone to be equal.

o By transforming from a local pseudopotential description to a $\mathbf{k} \cdot \mathbf{p}$ description

we *increase the convergence with respect to the number of basis functions used in the description of the band structure and the associated Bloch solutions.*

The basic ingredients of the theory developed below are the complex-**k** bulk Bloch solutions. The superlattice state function is expanded in terms of the bulk Bloch solutions associated with complex-**k** in each solid. The prescription to obtain the complex-**k** energy band structure and states with a knowledge of the full-zone $\mathbf{k} \cdot \mathbf{p}$ Hamiltonian is developed at length in Appendix (4.4).

In the present section, we are mainly concerned with the description of the superlattice state function in terms of the Bloch solutions associated with complex-**k**. Further, we indicate how the expansion coefficients are determined from a *set of boundary conditions on the superlattice state function across the interfaces.* From these boundary conditions it is possible to derive an efficient and accurate way to obtain the *superlattice electronic energy spectrum.*

4.2.3 k.p Theory of Semiconductor Superlattices

4.2.3.1. Superlattice Wavefunction:

The superlattice is made of two lattice-matched solids belonging to the zincblende crystal structure. Let $j = 1, 2$ be a label to identify either one of the two constituent semiconductors forming the superlattice. The set of Bloch states $\{|\mathbf{k}_{\|}E; k_{\lambda}^{(j)}\rangle\}$ in solid j is a solution of the bulk Schrödinger equation:

$$\hat{H}^{(j)}|\mathbf{k}_{\|}E; k_{\lambda}^{(j)}\rangle = E(\mathbf{k}_{\|}, k_{\lambda}^{(j)})|\mathbf{k}_{\|}E; k_{\lambda}^{(j)}\rangle, \tag{1}$$

where $\hat{H}^{(j)}$ refer to the bulk Hamiltonian in solid j, and $[\lambda = 1, \ldots, 2N]$. Note that Eq.(1) is *not an eigenvalue problem*, since we have to find the solutions $k_{\lambda}^{(j)}$ for a given parallel wavevector $\mathbf{k}_{\|}$ and total energy E.

Using the technique outlined in Appendix (4.4), the Bloch solution $|\mathbf{k}_{\|}E; k_{\lambda}^{(j)}\rangle$ associated with the wavevector $k_{\lambda}^{(j)}$ can be expanded in terms of a set of $\mathbf{k}_0 = \mathbf{0}$ basis functions $\{|m\rangle\}$ of a *common reference solid,*

$$\langle \mathbf{x}|\mathbf{k}_{\|}E; k_{\lambda}^{(j)}\rangle \equiv \exp(i\mathbf{k}_{\|}\cdot\mathbf{x}_{\|})\exp(ik_{\lambda}^{(j)}z)u(\mathbf{k}_{\|}, k_{\lambda}^{(j)}; \mathbf{x}), \tag{2.a}$$

$$\langle \mathbf{x}|\mathbf{k}_{\|}E; k_{\lambda}^{(j)}\rangle = \exp(i\mathbf{k}_{\|}\cdot\mathbf{x}_{\|})\exp(ik_{\lambda}^{(j)}z)\sum_{m=1}^{N}\langle \mathbf{x}|m\rangle C^{(j)}(m, k_{\lambda}^{(j)}; \mathbf{k}_{\|}E). \tag{2.b}$$

The basis functions $\langle \mathbf{x}|m\rangle \equiv u_m(\mathbf{x})$ are the same for both solids $j = 1, 2$. Let $\mathbf{C}^{(j)}(k_{\lambda}; \mathbf{k}_{\|}E)$ be the column vector associated with the eigenvalue $k_{\lambda}^{(j)}$ consists of the expansion coefficients $C^{(j)}(m, k_{\lambda}^{(j)}; \mathbf{k}_{\|}E)$ in terms of the $\mathbf{k}_0 = \mathbf{0}$ basis functions in the reference solid. As before, the index m will refer to a $\mathbf{k}_0 = \mathbf{0}$ basis function in the reference solid. Let N be the number of basis functions $\langle \mathbf{x}|m\rangle$ entering in the expansion of the Bloch solution $\langle \mathbf{x}|\mathbf{k}_{\|}E; k_{\lambda}^{(j)}\rangle$.

We now indicate how to construct the superlattice state out of the bulk solutions obtained in the preceding section. Let the superlattice state at fixed parallel

wavevector $\mathbf{k}_\parallel$ and energy E in solid j be $|\mathbf{k}_\parallel E; \mathbf{q}; j\rangle$, where $\mathbf{q}$ is a quantum number that labels the superlattice states. The label $\mathbf{q}$ is referred to as the *superlattice wavevector*. Let the $\hat{\mathbf{z}}$ be the direction normal to the superlattice interfaces.

We now expand the superlattice state $|\mathbf{k}_\parallel E; \mathbf{q}; j\rangle$ on the set of Bloch solutions $\{|\mathbf{k}_\parallel E; k_\lambda^{(j)}\rangle\}$ in each solid j:

$$|\mathbf{k}_\parallel E; \mathbf{q}; j\rangle = \sum_{\lambda=1}^{2N} |\mathbf{k}_\parallel E; k_\lambda^{(j)}\rangle f^{(j)}(k_\lambda^{(j)}, \mathbf{q}; \mathbf{k}_\parallel), \tag{3}$$

where the amplitudes $f^{(j)}(k_\lambda^{(j)}, \mathbf{q}; \mathbf{k}_\parallel)$ indicate the admixture of the bulk Bloch state $|\mathbf{k}_\parallel E; k_\lambda^{(j)}\rangle$ in the superlattice state $|\mathbf{k}_\parallel E; \mathbf{q}; j\rangle$.

As seen above, the Bloch solutions in solid j $\{|\mathbf{k}_\parallel E; k_\lambda^{(j)}\rangle\}$ are described in a zone-center expansion set $\{|m\rangle\}$ which is associated with a common reference solid

Then the superlattice state in solid j can be expressed as a linear combination of zone-center basis functions $\{|m\rangle\}$ of a reference solid. By using explicitly a $\mathbf{x}$-representation, we can expand:

$$\langle \mathbf{x}|\mathbf{k}_\parallel E; \mathbf{q}; j\rangle = \sum_{\lambda=1}^{2N} \langle \mathbf{x}|\mathbf{k}_\parallel E; k_\lambda^{(j)}\rangle f^{(j)}(k_\lambda^{(j)}, \mathbf{q}; \mathbf{k}_\parallel),$$

$$= \sum_{\lambda=1}^{2N} \left[\exp(i\mathbf{k}_\parallel \cdot \mathbf{x}_\parallel) \exp(ik_\lambda^{(j)} z) \sum_{m=1}^{N} \langle \mathbf{x}|m\rangle C^{(j)}(m, k_\lambda^{(j)}; \mathbf{k}_\parallel E) \right] f^{(j)}(k_\lambda^{(j)}, \mathbf{q}; \mathbf{k}_\parallel),$$

$$= \sum_{m=1}^{N} \langle \mathbf{x}|m\rangle \left[\exp(i\mathbf{k}_\parallel \cdot \mathbf{x}_\parallel) \sum_{\lambda=1}^{2N} \exp(ik_\lambda^{(j)} z) C^{(j)}(m, k_\lambda^{(j)}; \mathbf{k}_\parallel E) f^{(j)}(k_\lambda^{(j)}, \mathbf{q}; \mathbf{k}_\parallel) \right],$$

and finally,

$$\langle \mathbf{x}|\mathbf{k}_\parallel E; \mathbf{q}; j\rangle \equiv \sum_{m=1}^{N} \langle \mathbf{x}|m\rangle F^{(j)}(m; \mathbf{k}_\parallel \mathbf{q}; \mathbf{x}), \tag{4}$$

where the functions $F^{(j)}(m; \mathbf{k}_\parallel \mathbf{q}; \mathbf{x})$ are referred to as *multi-component envelope functions* and are defined to be the expression in [...]:

$$F^{(j)}(m; \mathbf{k}_\parallel \mathbf{q}; \mathbf{x}) \equiv \exp(i\mathbf{k}_\parallel \cdot \mathbf{x}_\parallel) \cdot$$

$$\sum_{\lambda=1}^{2N}\left[\exp(ik_{\lambda}^{(j)}z)C^{(j)}(m,k_{\lambda}^{(j)};\mathbf{k}_{\|}E)\right]f^{(j)}(k_{\lambda}^{(j)},\mathbf{q};\mathbf{k}_{\|}), \tag{5}$$

in terms of the basis states at $\mathbf{k}_0 = \mathbf{0}$ in the reference solid, $\{|m\rangle\}$.

4.2.3.2. Equivalent Solutions:

We note that *due to the lack of periodicity of the* $\mathbf{k}\cdot\mathbf{p}$ *Hamiltonian, some of the solutions* $k_\lambda^{(j)}$ *are related to each other by a reciprocal lattice vector* $\mathbf{g}$. Thus, some solutions $|\mathbf{k}_\parallel E; k_\lambda^{(j)}\rangle$ have $\mathrm{Re}\left[k_\lambda^{(j)}\right]$ outside the first Brillouin zone. These solutions are *approximate repeated-zone solutions due to the truncation of the* $\mathbf{k}\cdot\mathbf{p}$ *Hamiltonian.* These bulk solutions whose $\mathrm{Re}\left[k_\lambda^{(j)}\right]$ lie outside the first Brillouin should be equal to the bulk solutions whose $\mathrm{Re}\left[k_\lambda^{(j)}\right]$ lie inside the first Brillouin plus a reciprocal lattice vector $\hat{\mathbf{z}}g_z$. However, since the set of $\mathbf{k}_0 = \mathbf{0}$ basis functions $\{|m\rangle\}$ used in the calculations constitute a truncated set and is not a complete set, these solutions are only approximate, repeated-zone solutions to the solutions inside the first Brillouin zone. In higher-index Brillouin zones, the bulk solutions $\{|\mathbf{k}_\parallel E; k_\lambda^{(j)}\rangle\}$ contain appreciable admixture of zone-center basis functions lying at high energy. Since the set of zone-center basis functions is truncated, these high-energy zone-center basis functions are not include in the expansion set and therefore, the bulk solutions lying in high-order Brillouin zones are poorly described.

We would like to examine Bloch states whose wavevectors are related by a reciprocal lattice vector. A more complete treatment is given in Appendix (4.5) and we point out here only the line of the argument.

Consider two Bloch states associated with the wavevectors

$$\mathbf{k}_\lambda \equiv \mathbf{k}_\parallel + \hat{\mathbf{z}}k_\lambda, \tag{6.a}$$

and

$$\mathbf{k}'_\lambda \equiv \mathbf{k}_\parallel{}' + \hat{\mathbf{z}}k'_\lambda. \tag{6.b}$$

Suppose that $\mathbf{k}_\lambda$ and $\mathbf{k}'_\lambda$ are related by a reciprocal lattice vector, $\mathbf{g}_\mu$,

$$\mathbf{k}_\lambda = \mathbf{k}'_\lambda + \mathbf{g}_\mu, \tag{7.a}$$

where

$$\mathbf{g}_\mu = \mathbf{g}_\parallel + \hat{\mathbf{z}} g_\mu. \tag{7.b}$$

Equations (7) imply that

$$\mathbf{k}_\parallel = \mathbf{k}_\parallel{}' + \mathbf{g}_\parallel, \tag{8.a}$$

and,

$$\hat{\mathbf{z}} k_\lambda = \hat{\mathbf{z}} k'_\lambda + \hat{\mathbf{z}} g_\mu. \tag{8.b}$$

We must consider two cases:

(i) In the case where $\mathbf{g}_\parallel \neq \mathbf{0}$ we have

$$\mathbf{k}_\parallel \neq \mathbf{k}_\parallel{}'. \tag{9}$$

Since the Bloch states correspond to fixed parallel wavevector $\mathbf{k}_\parallel$ and energy E, this situation would correspond to another problem unless the Hamiltonian has some higher symmetry along some directions in the Brillouin zone. We rule out this case.

(i) In the case where $\mathbf{g}_\parallel = \mathbf{0}$ we have

$$\mathbf{k}_\parallel = \mathbf{k}_\parallel{}', \tag{10.a}$$

and,

$$\hat{\mathbf{z}} k_\lambda = \hat{\mathbf{z}} k'_\lambda + \hat{\mathbf{z}} g_\mu. \tag{10.b}$$

In this case the two Bloch states have their wavevectors in the $\hat{\mathbf{z}}$-direction separated by a reciprocal lattice vector. Bloch states $|\mathbf{k}_\parallel E; k_\lambda\rangle$ whose wavevector satisfy Eq.(10) are said to be *equivalent*. Thus *equivalent Bloch states correspond to the same physical situation.*

Then, it seems appropriate to *relabel the solutions* $k_\lambda^{(j)}$ *into sets of non-equivalent Bloch states.* Let us make the change of label for the solutions $k_\lambda^{(j)}$ in

solid $j = 1, 2$

$$k_{\lambda}^{(j)} \rightarrow k_{\gamma\mu}^{(j)}, \tag{11.a}$$

for the wavevector,

$$|\mathbf{k}_{\|} E; k_{\lambda}^{(j)}\rangle \rightarrow |\mathbf{k}_{\|} E; k_{\gamma\mu}^{(j)}\rangle, \tag{11.b}$$

for the associated Bloch states, and,

$$f^{(j)}(k_{\lambda}^{(j)}, \mathbf{q}; \mathbf{k}_{\|}) \rightarrow f^{(j)}(k_{\gamma\mu}^{(j)}, \mathbf{q}; \mathbf{k}_{\|}), \tag{11.c}$$

for the superlattice amplitudes. The meaning of the double label is the following:

- γ labels the sets of non-equivalent Bloch states
- μ labels the equivalent partners within the set γ.

Thus, out of the $2N$ solutions

$$k_{\lambda}^{(j)}, \qquad \lambda = 1, \ldots, 2N, \tag{12.a}$$

$$|\mathbf{k}_{\|} E; k_{\lambda}^{(j)}\rangle, \qquad \lambda = 1, \ldots, 2N, \tag{12.b}$$

let there be $2M < 2N$ sets of non-equivalent solutions

$$k_{\gamma\mu}^{(j)}, \qquad \gamma = 1, \ldots, 2M, \tag{13.a}$$

$$|\mathbf{k}_{\|} E; k_{\gamma\mu}^{(j)}\rangle, \qquad \gamma = 1, \ldots, 2M, \tag{13.b}$$

where the index μ labels the equivalent partner solutions within the set γ,

$$\hat{\mathbf{z}} k_{\gamma\mu'}^{(j)} = \hat{\mathbf{z}} k_{\gamma\mu}^{(j)} + \hat{\mathbf{z}} g_{\mu\mu'}. \tag{13.c}$$

We now would like to determine the number $2M$ of non-equivalent sets γ. As shown in Appendix (4.5), if N is the number of plane waves $\{|\mathbf{g}\rangle\}$ included in

the expansion of the Bloch solutions in the *local pseudopotential formalism* and $M < N$ is the the number of two-dimensional reciprocal lattice vector $\mathbf{g}_{\|}$ included in the expansion set $\{|\mathbf{g})\}$, then the *number of non-equivalent solutions is equal to twice the number M of distinct two-dimensional reciprocal lattice vectors* $\mathbf{g}_{\|}$. Thus, for each $\mathbf{g}_{\|}$ included in the expansion there are two non-equivalent solutions. The other solutions are related to these two by a reciprocal lattice vector $\hat{\mathbf{z}}g_z$ and therefore *correspond to equivalent solutions.* Each different $\mathbf{g}_{\|}$ included in the expansion of the Bloch state gives rise to a set of *non-equivalent Bloch solutions.*

Since *only the non-equivalent solutions are the physically meaningful quantities,* we must solve the boundary conditions only for the non-equivalent states.

Let us now break the total $2N$ solutions $k_{\lambda}^{(j)}$ into $2M < 2N$ sets $k_{\gamma\mu}^{(j)}$ of *non-equivalent solutions.* We *relabel the solutions* $k_{\lambda}^{(j)}$ *into sets of non-equivalent Bloch states.* Let us make the change of label for the solutions $k_{\lambda}^{(j)}$ in solid $j = 1, 2$

$$k_{\lambda}^{(j)} \rightarrow k_{\gamma\mu}^{(j)}, \tag{14.a}$$

for the wavevector,

$$|\mathbf{k}_{\|} E; k_{\lambda}^{(j)}\rangle \rightarrow |\mathbf{k}_{\|} E; k_{\gamma\mu}^{(j)}\rangle, \tag{14.b}$$

for the associated Bloch states, and

$$f^{(j)}(k_{\lambda}^{(j)}, \mathbf{q}; \mathbf{k}_{\|}) \rightarrow f^{(j)}(k_{\gamma\mu}^{(j)}, \mathbf{q}; \mathbf{k}_{\|}), \tag{14.c}$$

for the superlattice amplitudes.

As above, γ labels the sets of non-equivalent Bloch states and μ labels the equivalent partners within the set γ, and $[\gamma = 1, \ldots, 2M]$.

We now rewrite the expansion of the superlattice state function as

$$|\mathbf{k}_{\|}E;\mathbf{q};j\rangle = \sum_{\gamma=1}^{2M}\sum_{\mu}|\mathbf{k}_{\|}E;k_{\gamma\mu}^{(j)}\rangle f^{(j)}(k_{\gamma\mu}^{(j)},\mathbf{q};\mathbf{k}_{\|}). \tag{15}$$

The summation $\sum_{\gamma=1}^{2M}$ is over the $2M$ sets of non-equivalent solutions. The summation $\sum_{\mu}$ is over the partner solutions within the set γ.

The relation between the equivalent partners of a set γ is shown in Appendix (4.5) to be

$$|\mathbf{k}_{\|}E;k_{\gamma\mu}^{(j)}\rangle = \exp\left[i\varphi^{(j)}(\gamma,\mu)\right]|\mathbf{k}_{\|}E;k_{\gamma}^{(j)}\rangle, \tag{16}$$

where the state $|\mathbf{k}_{\|}E;k_{\gamma}^{(j)}\rangle$ belongs to the eigenvalue $k_{\gamma}^{(j)}$ and the state $|\mathbf{k}_{\|}E;k_{\gamma\mu}^{(j)}\rangle$ belongs to the eigenvalue $k_{\gamma\mu}^{(j)}$. The phase $\exp\left[i\varphi^{(j)}(\gamma,\mu)\right]$ relates a Bloch solution outside the first Brillouin, $|\mathbf{k}_{\|}E;k_{\gamma\mu}^{(j)}\rangle$, to a solution inside the first Brillouin zone $|\mathbf{k}_{\|}E;k_{\gamma}^{(j)}\rangle$. As above, we adopt the convention that $\mathrm{Re}\left[k_{\gamma}^{(j)}\right]$ lies inside the first Brillouin zone.

We can now write

$$|\mathbf{k}_{\|}E;\mathbf{q};j\rangle = \sum_{\gamma=1}^{2M}\sum_{\mu}|\mathbf{k}_{\|}E;k_{\gamma\mu}^{(j)}\rangle f^{(j)}(k_{\gamma\mu}^{(j)},\mathbf{q};\mathbf{k}_{\|}), \tag{17.a}$$

or, using

$$|\mathbf{k}_{\|}E;k_{\gamma\mu}^{(j)}\rangle = \exp\left[i\varphi^{(j)}(\gamma,\mu)\right]|\mathbf{k}_{\|}E;k_{\gamma}^{(j)}\rangle, \tag{17.b}$$

we have

$$|\mathbf{k}_{\|}E;\mathbf{q};j\rangle = \sum_{\gamma=1}^{2M}\sum_{\mu}\exp\left[i\varphi^{(j)}(\gamma,\mu)\right]|\mathbf{k}_{\|}E;k_{\gamma}^{(j)}\rangle f^{(j)}(k_{\gamma\mu}^{(j)},\mathbf{q};\mathbf{k}_{\|}), \tag{18.a}$$

or, regrouping,

$$|\mathbf{k}_{\|}E;\mathbf{q};j\rangle = \sum_{\gamma=1}^{2M}|\mathbf{k}_{\|}E;k_{\gamma}^{(j)}\rangle\left[\sum_{\mu}\exp\left[i\varphi^{(j)}(\gamma,\mu)\right]f^{(j)}(k_{\gamma\mu}^{(j)},\mathbf{q};\mathbf{k}_{\|})\right], \tag{18.b}$$

and finally,

$$|\mathbf{k}_{\|}E;\mathbf{q};j\rangle = \sum_{\gamma=1}^{2M} |\mathbf{k}_{\|}E;k_{\gamma}^{(j)}\rangle f^{(j)}(k_{\gamma}^{(j)},\mathbf{q};\mathbf{k}_{\|}), \tag{19.a}$$

where we have defined,

$$f^{(j)}(k_{\gamma}^{(j)},\mathbf{q};\mathbf{k}_{\|}) \equiv \sum_{\mu} \exp\left[i\varphi^{(j)}(\gamma,\mu)\right] f^{(j)}(k_{\gamma\mu}^{(j)},\mathbf{q};\mathbf{k}_{\|}). \tag{19.b}$$

Since *only the non-equivalent solutions correspond to physically distinct situations we only should regard the sum*

$$f^{(j)}(k_{\gamma}^{(j)},\mathbf{q};\mathbf{k}_{\|}) \equiv \sum_{\mu} \exp\left[i\varphi^{(j)}(\gamma,\mu)\right] f^{(j)}(k_{\gamma\mu}^{(j)},\mathbf{q};\mathbf{k}_{\|}), \tag{20}$$

as physically meaningful. Then, within the local pseudopotential formalism, we know that *there are only* $2M$ *physically significant amplitudes,* $f^{(j)}(k_{\gamma}^{(j)},\mathbf{q};\mathbf{k}_{\|})$, *where* M *is the number of distinct* $\mathbf{g}_{\|}$ *included in the expansion of the Bloch state.* The amplitudes $f^{(j)}(k_{\gamma}^{(j)},\mathbf{q};\mathbf{k}_{\|}), [\gamma = 1,\ldots,2M]$ are the quantities of interest.

4.2.3.3 Linear Independence on the Interface Plane:

In the local pseudopotential formalism, *the number of linearly independent plane wave projected onto the interface plane is equal to the number of distinct two-dimensional reciprocal lattice vectors* $\mathbf{g}_{\|}$ *included in the expansion.* It would thus be possible to project the total set of N plane wave $\exp(i\mathbf{g}\cdot\mathbf{x})$ onto a set of M linearly independent plane waves $\exp(i\mathbf{g}_{\|}\cdot\mathbf{x}_{\|})$ in the interface plane. In this case we would solve the boundary conditions for the $2M$ amplitudes $f^{(j)}(k_{\gamma}^{(j)},\mathbf{q};\mathbf{k}_{\|})$. However, another approach would be to solve the boundary conditions for *all the*

$2N$ *amplitudes* $f^{(j)}(k^{(j)}_{\gamma\mu}, \mathbf{q}; \mathbf{k}_{\|})$ *and then to extract the information about the* $2M$ *physically significant non-equivalent amplitudes* $f^{(j)}(k^{(j)}_{\gamma}, \mathbf{q}; \mathbf{k}_{\|})$. By doing so, we use a particular way of dividing the solutions into equivalent and non-equivalent. Since this division is unphysical, it legitimate to do so *given that we are able to extract the physically meaningful solutions in the expansion of the superlattice state function.*

o In the case of a *truncated* $\mathbf{k} \cdot \mathbf{p}$ *description, the solutions outside the first Brillouin are in general poorly described.* But, as mentioned above these out-of-zone solutions are equivalent to some solutions *inside the first Brillouin zone.* The latter are very accurately described within the present formalism. In general *only well-described solutions within the first Brillouin zone are retained in the superlattice state function expansion, the other equivalent solutions are discarded due to their poor description.*

o Special consideration must be given in the case of *solutions right at the first Brillouin zone edge*, that solutions of the form,

$$k^{(j)}_{\gamma\mu} = \pm\frac{1}{2}g_{\mu} \pm i\kappa^{(j)}_{\lambda}, \tag{21}$$

where $\kappa^{(j)}_{\lambda}$ is a real number and g_{μ} is the smallest non-vanishing reciprocal lattice vector. In this case, the description of all the equivalent solutions is equally good and we cannot discard any solution.

4.2.4 Superlattice Complex-q Bandstructure:

We now indicate how the complex-q band structure of the superlattice can be calculated by application of the proper boundary conditions on the superlattice wavefunction, $|\mathbf{k}_{\|}E;\mathbf{q};j\rangle$.

4.2.4.1 Boundary conditions:

The superlattice wavefunction $|\mathbf{k}_{\|}E;\mathbf{q};j\rangle$ is expressed in terms of the *same* set of $\mathbf{k}_0 = \mathbf{0}$ basis functions, $\{|m\rangle\}$, of a reference solid,

$$\langle \mathbf{x}|\mathbf{k}_{\|}E;\mathbf{q};j\rangle \equiv \sum_{m=1}^{N} \langle \mathbf{x}|m\rangle F^{(j)}(m;\mathbf{k}_{\|}\mathbf{q};\mathbf{x}). \tag{22}$$

The superlattice primitive cell is shown in Figure (1). The interface plane has been taken to be at $z_0 = 0$ for convenience.

• The solid (1) extends from $z_0 = -b$ to the *left* of the interface plane up to $z_0 = 0$.

• The solid (2) extends from $z_0 = 0$ up to $z_0 = a$ to the *right* of the interface plane.

Let $\mathbf{R}_0$ be the superlattice period. We apply the following set of boundary conditions on the superlattice wavefunction on both sides of the interface:

(i) Continuity of the superlattice wavefunction at the interface plane $z_0 = 0$

$$\left[\langle \mathbf{x}|\mathbf{k}_{\|}E;\mathbf{q};1\rangle\right]_{z=0} = \left[\langle \mathbf{x}|\mathbf{k}_{\|}E;\mathbf{q};2\rangle\right]_{z=0}. \tag{23.a}$$

(ii) Continuity of the normal derivative of superlattice wavefunction at the interface plane $z_0 = 0$

$$\hat{\mathbf{s}} \cdot \left[\nabla\langle \mathbf{x}|\mathbf{k}_{\|}E;\mathbf{q};1\rangle\right]_{z=0} = \hat{\mathbf{s}} \cdot \left[\nabla\langle \mathbf{x}|\mathbf{k}_{\|}E;\mathbf{q};2\rangle\right]_{z=0}. \tag{23.b}$$

(iii) Bloch theorem for the superlattice wavefunction,

$$\exp(i\mathbf{q}\cdot\mathbf{R}_0)\left[\langle \mathbf{x}|\mathbf{k}_{\|}E;\mathbf{q};1\rangle\right]_{z=-b} = \left[\langle \mathbf{x}|\mathbf{k}_{\|}E;\mathbf{q};2\rangle\right]_{z=a}. \tag{23.c}$$

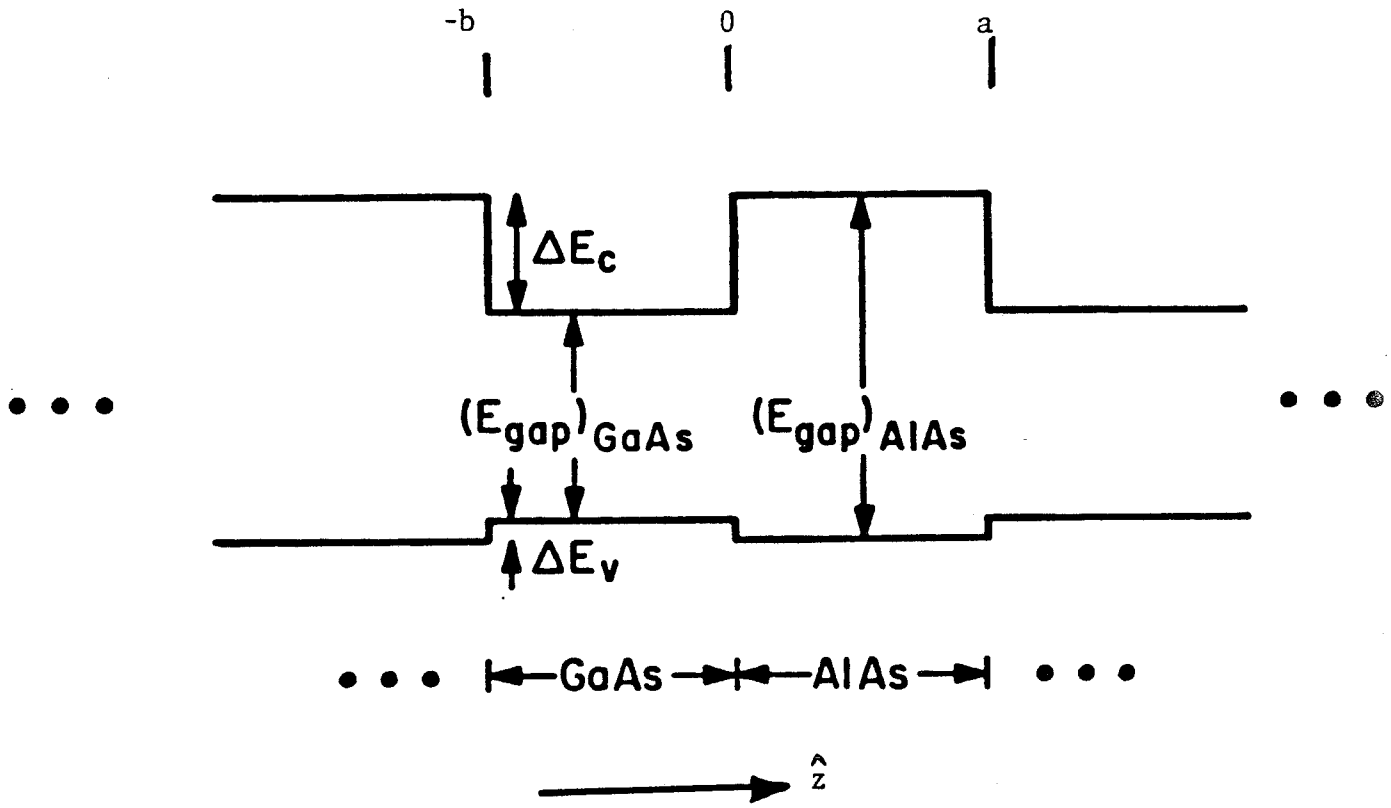

Figure 1: Energy band diagram of a GaAs-AlAs (100) superlattice. The superlattice primitive cell extends from $z_0 = -b$ to the left of the GaAs-AlAs interface, up to $z_0 = a$ to the right of the interface. The GaAs-AlAs interface is taken to be at $z_0 = 0$.

(iv) Bloch theorem for the normal derivative of superlattice wavefunction,

$$\exp(i\mathbf{q}\cdot\mathbf{R}_0)\hat{\mathbf{z}}\cdot\left[\nabla\langle\mathbf{x}|\mathbf{k}_{\|}E;\mathbf{q};1)\right]_{z=-b}=\hat{\mathbf{z}}\cdot\left[\nabla\langle\mathbf{x}|\mathbf{k}_{\|}E;\mathbf{q};2)\right]_{z=a}. \qquad (23.d)$$

Let us now *solve the boundary conditions equations for all the* $2N$ *amplitudes* $f^{(j)}(k^{(j)}_{\gamma\mu},\mathbf{q};\mathbf{k}_{\|})$ *with the provision that we will later extract the* $2M$ *physically meaningful amplitudes* $f^{(j)}(k^{(j)}_{\gamma},\mathbf{q};\mathbf{k}_{\|})$ *out of the* $f^{(j)}(k^{(j)}_{\gamma\mu},\mathbf{q};\mathbf{k}_{\|})$. With this procedure, the set of boundary conditions on the superlattice wavefunction reduces to a *set of boundary conditions on the expansion coefficients of each of the basis functions,* $|m\rangle$. These expansion coefficients are the envelope functions defined by Eqs.(8) in terms of the zone-center basis functions of the reference solid, $\{|m\rangle\}$,

$$F^{(j)}(m;\mathbf{k}_{\|}\mathbf{q};\mathbf{x})\equiv\exp(i\mathbf{k}_{\|}\cdot\mathbf{x}_{\|})\cdot$$

$$\sum_{\gamma\mu=1}^{2N}\left[\exp(ik^{(j)}_{\gamma\mu}z)C^{(j)}(m,k^{(j)}_{\gamma\mu};\mathbf{k}_{\|}E)\right]f^{(j)}(k^{(j)}_{\gamma\mu},\mathbf{q};\mathbf{k}_{\|}). \qquad (24)$$

Then the set of boundary conditions Eq.(10) is equivalent to a set of boundary conditions on each of the the envelope functions, *i.e.*, for $m=1,2,\ldots,N$,

(i) Continuity of the superlattice wavefunction at the interface plane $z_0=0$

$$\left[F^{(1)}(m;\mathbf{k}_{\|}\mathbf{q};\mathbf{x})\right]_{z=0}=\left[F^{(2)}(m;\mathbf{k}_{\|}\mathbf{q};\mathbf{x})\right]_{z=0}, \qquad (25.a)$$

(ii) Continuity of the normal derivative of superlattice wavefunction at the interface plane $z_0=0$

$$\left[\langle\mathbf{x}|m\rangle\hat{\mathbf{z}}\cdot\nabla F^{(1)}(m;\mathbf{k}_{\|}\mathbf{q};\mathbf{x})\right]_{z=0}+\left[F^{(1)}(m;\mathbf{k}_{\|}\mathbf{q};\mathbf{x})\hat{\mathbf{z}}\cdot\nabla\langle\mathbf{x}|m\rangle\right]_{z=0}=$$

$$\left[\langle \mathbf{x}|m\rangle \hat{\mathbf{z}} \cdot \nabla F^{(2)}(m;\mathbf{k}_{\|}\mathbf{q};\mathbf{x})\right]_{z=0} + \left[F^{(2)}(m;\mathbf{k}_{\|}\mathbf{q};\mathbf{x})\hat{\mathbf{z}} \cdot \nabla\langle \mathbf{x}|m\rangle\right]_{z=0} \qquad (25.b)$$

(iii) Bloch theorem for the superlattice wavefunction,

$$\exp(i\mathbf{q}\cdot\mathbf{R}_0)\left[F^{(1)}(m;\mathbf{k}_{\|}\mathbf{q};\mathbf{x})\right]_{z=-b} = \left[F^{(2)}(m;\mathbf{k}_{\|}\mathbf{q};\mathbf{x})\right]_{z=a}, \qquad (25.c)$$

(iv) Bloch theorem for the normal derivative of superlattice wavefunction,

$$\exp(i\mathbf{q}\cdot\mathbf{R}_0)\cdot$$

$$\left[\left[\langle \mathbf{x}|m\rangle \hat{\mathbf{z}} \cdot \nabla F^{(1)}(m;\mathbf{k}_{\|}\mathbf{q};\mathbf{x})\right]_{z=-b} + \left[F^{(1)}(m;\mathbf{k}_{\|}\mathbf{q};\mathbf{x})\hat{\mathbf{z}} \cdot \nabla\langle \mathbf{x}|m\rangle\right]_{z=-b}\right] =$$

$$\left[\left[\langle \mathbf{x}|m\rangle \hat{\mathbf{z}} \cdot \nabla F^{(2)}(m;\mathbf{k}_{\|}\mathbf{q};\mathbf{x})\right]_{z=a} + \left[F^{(2)}(m;\mathbf{k}_{\|}\mathbf{q};\mathbf{x})\hat{\mathbf{z}} \cdot \nabla\langle \mathbf{x}|m\rangle\right]_{z=a}\right] \qquad (25.d)$$

Equations (12a) and (12.b) constitute a set of $2N$ equations. Likewise, Eqs. (12a) and (12.b) constitute a set of $2N$ equations. There is therefore a total of $4N$ equations. Each envelope function, $F^{(j)}(m;\mathbf{k}_{\|}\mathbf{q};\mathbf{x})$, has $2N$ components, *i.e*, $2N$ unknown coefficients $f^{(j)}(k^{(j)}_{\gamma\mu},\mathbf{q};\mathbf{k}_{\|})$ per solid j. Thus the total number of unknown is thus:

$$[2\cdot N] + [2\cdot N] = 4N, \qquad (26)$$

and is equal to the total number of equations.

• We now obtain the normal derivatives of the $\mathbf{k}_0 = \mathbf{0}$ basis functions in the reference material, $\{|m\rangle\}$, *i.e.*, the terms

$$[\hat{\mathbf{z}} \cdot \nabla\langle \mathbf{x}|m\rangle], \qquad (27)$$

in Eqs.(12.b) and (12.d). We can use the fact that the functions $\langle \mathbf{x}|m\rangle$ and $\hat{\mathbf{z}} \cdot \nabla\langle \mathbf{x}|m\rangle$ are periodic functions with the space periodicity of the space lattice . Thus, the function $\hat{\mathbf{z}} \cdot \nabla\langle \mathbf{x}|m\rangle$ can be expanded on a set of periodic functions with the periodicity of the space lattice,

$$\hat{\mathbf{z}} \cdot \nabla\langle \mathbf{x}|m\rangle = \left[\frac{i}{\hbar}\right] \sum_{m'} p_z(m, m')\langle \mathbf{x}|m'\rangle, \tag{28}$$

where $p_z \equiv \hat{\mathbf{z}} \cdot \mathbf{p}$ is the component of the momentum normal to the interface and we used the expression of the momentum operator in $\mathbf{x}$-representation, $\mathbf{p} \equiv -i\hbar\nabla$.

It is straightforward to express the set of boundary conditions of Eqs.(12) in an *eigenvalue system* for the $4N$ unknown coefficients $f^{(j)}(k^{(j)}_{\gamma\mu}, \mathbf{q}; \mathbf{k}_{\|})$, where $j = 1, 2$. By using Eq.(8.a) for the envelope function,

$$F^{(j)}(m; \mathbf{k}_{\|}\mathbf{q}; \mathbf{x}) \equiv \exp(i\mathbf{k}_{\|} \cdot \mathbf{x}_{\|}) \cdot$$

$$\sum_{\gamma\mu=1}^{2N} \left[\exp(ik^{(j)}_{\gamma\mu} z) C^{(j)}(m, k^{(j)}_{\gamma\mu}; \mathbf{k}_{\|} E)\right] f^{(j)}(k^{(j)}_{\gamma\mu}, \mathbf{q}; \mathbf{k}_{\|}), \tag{29}$$

we obtain the following relations for $m = 1, 2, \ldots, N$,

$$\sum_{\gamma\mu=1}^{2N} \left[C^{(1)}(m, k^{(1)}_{\gamma\mu}; \mathbf{k}_{\|} E)\right] f^{(1)}(k^{(1)}_{\gamma\mu}, \mathbf{q}; \mathbf{k}_{\|}) =$$

$$\sum_{\gamma\mu=1}^{2N} \left[C^{(2)}(m, k^{(2)}_{\gamma\mu}; \mathbf{k}_{\|} E)\right] f^{(2)}(k^{(2)}_{\gamma\mu}, \mathbf{q}; \mathbf{k}_{\|}) \tag{30.a}$$

$$\sum_{\gamma\mu=1}^{2N} \left[\sum_{m'} \left[\hbar k^{(1)}_{\gamma\mu} \delta(m, m') + p_z(m, m')\right] C^{(1)}(m', k^{(1)}_{\gamma\mu}; \mathbf{k}_{\|} E)\right] f^{(1)}(k^{(1)}_{\gamma\mu}, \mathbf{q}; \mathbf{k}_{\|}) =$$

$$\sum_{\gamma\mu=1}^{2N}\left[\sum_{m'}\left[\hbar k_{\gamma\mu}^{(2)}\delta(m,m')+p_z(m,m')\right]C^{(2)}(m',k_{\gamma\mu}^{(2)};\mathbf{k}_{\|}E)\right]f^{(2)}(k_{\gamma\mu}^{(2)},\mathbf{q};\mathbf{k}_{\|}) \tag{30.b}$$

$$\exp(i\mathbf{q}\cdot\mathbf{R}_0)\sum_{\gamma\mu=1}^{2N}\left[C^{(1)}(m,k_{\gamma\mu}^{(1)};\mathbf{k}_{\|}E)\exp(-ik_{\gamma\mu}^{(1)}b)\right]f^{(1)}(k_{\gamma\mu}^{(1)},\mathbf{q};\mathbf{k}_{\|})=$$

$$\sum_{\gamma\mu=1}^{2N}\left[C^{(2)}(m,k_{\gamma\mu}^{(2)};\mathbf{k}_{\|}E)\exp(ik_{\gamma\mu}^{(2)}a)\right]f^{(2)}(k_{\gamma\mu}^{(2)},\mathbf{q};\mathbf{k}_{\|}) \tag{30.c}$$

$$\exp(i\mathbf{q}\cdot\mathbf{R}_0)\cdot$$

$$\sum_{\gamma\mu=1}^{2N}\left[\sum_{m'}\left[\hbar k_{\gamma\mu}^{(1)}\delta(m,m')+p_z(m,m')\right]C^{(1)}(m',k_{\gamma\mu}^{(1)};\mathbf{k}_{\|}E)\exp(-ik_{\gamma\mu}^{(1)}b)\right]\cdot$$

$$f^{(1)}(k_{\gamma\mu}^{(1)},\mathbf{q};\mathbf{k}_{\|})=$$

$$\sum_{\gamma\mu=1}^{2N}\left[\sum_{m'}\left[\hbar k_{\gamma\mu}^{(2)}\delta(m,m')+p_z(m,m')\right]C^{(2)}(m',k_{\gamma\mu}^{(2)};\mathbf{k}_{\|}E)\exp(ik_{\gamma\mu}^{(2)}a)\right]\cdot$$

$$f^{(2)}(k_{\gamma\mu}^{(2)},\mathbf{q};\mathbf{k}_{\|}) \tag{30.d}$$

Let us express the set of $4N$ equations given by Eqs.(17) for the $4N$ unknown coefficients $f^{(j)}(k_{\gamma\mu}^{(j)},\mathbf{q};\mathbf{k}_{\|})$ in a matrix form.

To do so, let us define the $[2N]$ -dimensional column vector $\mathbf{f}^{(j)}(\mathbf{q})$ composed of the expansion coefficients $f^{(j)}(k_{\gamma\mu}^{(j)},\mathbf{q};\mathbf{k}_{\|})$ of the envelope function $F^{(j)}(m;\mathbf{k}_{\|}\mathbf{q};\mathbf{x})$.

Also let us define the $[2N\cdot 2N]$ diagonal matrix $\mathbf{D}(k_{\gamma\mu}^{(j)})$ whose matrix elements are the complex-$\mathbf{k}$ values $k_{\gamma\mu}^{(j)}$ in solid j.

We define the $[2N \cdot 2N]$ diagonal matrix $\mathbf{D}(\mathbf{q})$ whose matrix elements are the complex-$\mathbf{q}$ values of the superlattice wavevector.

We also define the $[2N \cdot 2N]$ matrix $\mathbf{M}(\mathbf{k}_{\|}E;j)$ whose first $[N \cdot 2N]$ are the set of Eqs.(13.a) whose second $[N \cdot 2N]$ are the set of Eqs.(13.b).

We can thus write, symbolically,

$$\mathbf{M}(\mathbf{k}_{\|}E;j) \equiv \begin{bmatrix} C^{(j)}(m, k_{\gamma\mu}^{(j)};\mathbf{k}_{\|}E) \\ (\hbar k_{\gamma\mu}^{(j)} + p_z)C^{(j)}(m, k_{\gamma\mu}^{(j)};\mathbf{k}_{\|}E) \end{bmatrix} \tag{31}$$

Thus the set of equations Eqs(13) can be written as

$$\mathbf{M}(\mathbf{k}_{\|}E;1)\cdot\mathbf{f}^{(1)}(\mathbf{q}) = \mathbf{M}(\mathbf{k}_{\|}E;2)\cdot\mathbf{f}^{(2)}(\mathbf{q}),$$

for the set of equations Eqs(17.a) and (17.b) and,

$$\exp\left[i\mathbf{D}(\mathbf{q})\cdot\mathbf{R}_0\right]\cdot\mathbf{M}(\mathbf{k}_{\|}E;1)\cdot\exp\left[-i\mathbf{D}(k_{\gamma\mu}^{(1)})b\right]\cdot\mathbf{f}^{(1)}(\mathbf{q}) =$$

$$\mathbf{M}(\mathbf{k}_{\|}E;2)\cdot\exp\left[i\mathbf{D}(k_{\gamma\mu}^{(2)})a\right]\cdot\mathbf{f}^{(2)}(\mathbf{q})$$

for the set of equations Eqs(17.c) and (17.d). Equations (19) constitute a set of two $[2N \cdot 2N]$ matrix equations to be solved for the two $[2N]$ -dimensional column vectors $\mathbf{f}^{(j)}(\mathbf{q})$ in solids $j = 1, 2$.

It is now a simple matter to express Eqs.(19) as an eigensystem for the column vector $\mathbf{f}^{(1)}(\mathbf{q})$. Inverting Eq.(19.a) we find

$$\mathbf{f}^{(2)}(\mathbf{q}) = \left[\mathbf{M}(\mathbf{k}_{\|}E;2)\right]^{-1}\cdot\mathbf{M}(\mathbf{k}_{\|}E;1)\cdot\mathbf{f}^{(1)}(\mathbf{q}),$$

or, by defining the *transfer matrix* $\mathbf{T}(\mathbf{k}_{\|}E)$ as

$$\mathbf{T}(\mathbf{k}_{\|}E) \equiv \left[\mathbf{M}(\mathbf{k}_{\|}E;2)\right]^{-1}\cdot\mathbf{M}(\mathbf{k}_{\|}E;1), \tag{34}$$

we can write,

$$\mathbf{f}^{(2)}(\mathbf{q}) = \mathbf{T}(\mathbf{k}_{\|}E)\cdot\mathbf{f}^{(1)}(\mathbf{q}), \tag{35.a}$$

or more explicitly,

$$f^{(2)}(k^{(2)}_{\gamma\mu}, \mathbf{q}; \mathbf{k}_\parallel) = \sum_{\gamma'\mu'} \mathbf{T}(k^{(2)}_{\gamma\mu}, k^{(1)}_{\gamma'\mu'}; \mathbf{k}_\parallel E) \cdot f^{(1)}(k^{(1)}_{\gamma'\mu'}, \mathbf{q}; \mathbf{k}_\parallel). \qquad (35.b)$$

• The physical meaning of the transfer matrix $\mathbf{T}(\mathbf{k}_\parallel E)$ is clear: *The transfer matrix indicates the mixing between the different Bloch states* $\{|\mathbf{k}_\parallel E; k^{(j)}_{\gamma\mu})\}$ *across the interface plane.*

Then Eq.(19.b) becomes,

$$\exp\left[i\mathbf{D}(\mathbf{q}) \cdot \mathbf{R}_0\right] \cdot \mathbf{M}(\mathbf{k}_\parallel E; 1) \cdot \exp\left[-i\mathbf{D}(k^{(1)}_{\gamma\mu})b\right] \cdot \mathbf{f}^{(1)}(\mathbf{q}) =$$

$$\mathbf{M}(\mathbf{k}_\parallel E; 2) \cdot \exp\left[i\mathbf{D}(k^{(2)}_{\gamma\mu})a\right] \cdot \mathbf{T}(\mathbf{k}_\parallel E) \cdot \mathbf{f}^{(1)}(\mathbf{q})$$

By rearranging,

$$\exp\left[i\mathbf{D}(\mathbf{q}) \cdot \mathbf{R}_0\right] \cdot \mathbf{f}^{(1)}(\mathbf{q}) =$$

$$\exp\left[i\mathbf{D}(k^{(1)}_{\gamma\mu})b\right] \cdot \left[\mathbf{T}(\mathbf{k}_\parallel E)\right]^{-1} \cdot \exp\left[i\mathbf{D}(k^{(2)}_{\gamma\mu})a\right] \cdot \mathbf{T}(\mathbf{k}_\parallel E) \cdot \mathbf{f}^{(1)}(\mathbf{q}). \qquad (37)$$

Equation (24) constitutes an eigensystem for the column vector $\mathbf{f}^{(1)}(\mathbf{q})$. Diagonalization of the matrix,

$$\exp\left[i\mathbf{D}(k^{(1)}_{\gamma\mu})b\right] \cdot \left[\mathbf{T}(\mathbf{k}_\parallel E)\right]^{-1} \cdot \exp\left[i\mathbf{D}(k^{(2)}_{\gamma\mu})a\right] \cdot \mathbf{T}(\mathbf{k}_\parallel E), \qquad (38.a)$$

yields the complex-$\mathbf{q}$ band structure of the superlattice through the matrix of Bloch factors,

$$\exp\left[i\mathbf{D}(\mathbf{q}) \cdot \mathbf{R}_0\right] \qquad (38.b)$$

Once the set of coefficients $\mathbf{f}^{(1)}(\mathbf{q})$ are known in solid (1), the set of coefficients $\mathbf{f}^{(2)}(\mathbf{q})$ in solid (2), can be calculated with the use of the transfer matrix, $\mathbf{T}(\mathbf{k}_\parallel E)$,

$$\mathbf{f}^{(2)}(\mathbf{q}) = \mathbf{T}(\mathbf{k}_\parallel E) \cdot \mathbf{f}^{(1)}(\mathbf{q}). \qquad (39)$$

4.2.4.2 Truncated Transfer Matrix: Reduced Eigensystem:

As it stands, the eigensystem

$$\exp\left[i\mathbf{D}(\mathbf{q})\cdot\mathbf{R}_0\right]\cdot\mathbf{f}^{(1)}(\mathbf{q}) =$$

$$\exp\left[i\mathbf{D}(k^{(1)}_{\gamma\mu})b\right]\cdot\left[\mathbf{T}(\mathbf{k}_{\|}E)\right]^{-1}\cdot\exp\left[i\mathbf{D}(k^{(2)}_{\gamma\mu})a\right]\cdot\mathbf{T}(\mathbf{k}_{\|}E)\cdot\mathbf{f}^{(1)}(\mathbf{q}). \qquad (40.a)$$

and,

$$\mathbf{f}^{(2)}(\mathbf{q}) = \mathbf{T}(\mathbf{k}_{\|}E)\cdot\mathbf{f}^{(1)}(\mathbf{q}), \qquad (40.b)$$

is a $[2N\cdot 2N]$ eigensystem for the $2N$ superlattices amplitudes $f^{(1)}(k^{(1)}_{\gamma'\mu'},\mathbf{q};\mathbf{k}_{\|})$ and $f^{(2)}(k^{(2)}_{\gamma\mu},\mathbf{q};\mathbf{k}_{\|})$. The index $\gamma\mu$ runs over *all the bulk solutions.*

$$k^{(j)}_{\gamma\mu}, \qquad \gamma\mu = 1,\ldots,2N, \qquad (41.a)$$

corresponding to the Bloch states,

$$|\mathbf{k}_{\|}E;k^{(j)}_{\gamma\mu}\rangle, \qquad \gamma\mu = 1,\ldots,2N. \qquad (41.b)$$

As mentioned above we are interested in a *reduced eigensystem for the non-equivalent solutions,*

$$f^{(j)}(k^{(j)}_{\gamma},\mathbf{q};\mathbf{k}_{\|}) \equiv \sum_{\mu}\exp\left[i\varphi^{(j)}(\gamma,\mu)\right]f^{(j)}(k^{(j)}_{\gamma\mu},\mathbf{q};\mathbf{k}_{\|}), \qquad (42)$$

where $\mathrm{Re}\left[k^{(j)}_{\gamma}\right]$ is in the first Brillouin zone and the sum $\sum_{\mu}$ is over the *equivalent partners belonging to the set* γ. We must therefore extract the physically meaningful $2M$ amplitudes $f^{(j)}(k^{(j)}_{\gamma},\mathbf{q};\mathbf{k}_{\|})$ out of the equivalent $2N$ amplitudes $f^{(j)}(k^{(j)}_{\gamma\mu},\mathbf{q};\mathbf{k}_{\|})$.

The procedure for going from the above $[2N\cdot 2N]$ eigensystem for the $2N$ superlattices amplitudes $f^{(j)}(k^{(j)}_{\gamma\mu},\mathbf{q};\mathbf{k}_{\|})$ to a reduced $[2M\cdot 2M]$ eigensystem for

the $2M$ superlattices amplitudes $f^{(j)}(k_\gamma^{(j)}, \mathbf{q}; \mathbf{k}_\parallel)$ is outlined in Appendix (4.5) for the *local pseudopotential formalism* and in Appendix (4.6) for the *truncated* $\mathbf{k}\cdot\mathbf{p}$ *formalism*.

We give here the general line of the developement:

o By definition, two equivalent wavevectors $k_{\gamma\mu}^{(j)}$ and $k_{\gamma\mu'}^{(j)}$ belonging to the same set γ are related through

$$\hat{\mathbf{z}} k_{\gamma\mu'}^{(j)} = \hat{\mathbf{z}} k_{\gamma\mu}^{(j)} + \hat{\mathbf{z}} g_{\mu\mu'}, \tag{43}$$

where $g_{\mu\mu'}$ is a reciprocal lattice vector. The phase relation between equivalent Bloch states belonging to a given set γ is

$$|\mathbf{k}_\parallel E; k_{\gamma\mu'}^{(j)}\rangle = \exp\left[i\varphi^{(j)}(\gamma, \mu\mu')\right] |\mathbf{k}_\parallel E; k_{\gamma\mu}^{(j)}\rangle, \tag{44}$$

where the state $|\mathbf{k}_\parallel E; k_{\gamma\mu}^{(j)}\rangle$ belongs to the eigenvalue $k_{\gamma\mu}^{(j)}$ and the state $|\mathbf{k}_\parallel E; k_{\gamma\mu'}^{(j)}\rangle$ belongs to the eigenvalue $k_{\gamma\mu'}^{(j)}$.

o We must therefore express the *non-reduced transfer matrix*,

$$\mathbf{T}(k_{\gamma\mu}^{(2)}, k_{\gamma'\mu'}^{(1)}; \mathbf{k}_\parallel E),$$

that couples all the partners $k_{\gamma'\mu'}^{(1)}$ and $k_{\gamma\mu}^{(2)}$ of the non-equivalent sets γ and γ', in terms of a *reduced transfer matrix*,

$$\Omega(k_\gamma^{(2)}, k_{\gamma'}^{(1)}; \mathbf{k}_\parallel E),$$

that relates the states $k_\gamma^{(2)}$ and $k_{\gamma'}^{(1)}$ where *both* $Re\left[k_{\gamma'}^{(1)}\right]$ *and* $Re\left[k_\gamma^{(2)}\right]$ *lie inside the first Brillouin zone.*

o This is done by expressing the proper phase relations between the equivalent partners $k_{\gamma\mu}^{(j)}$ and $k_\gamma^{(j)}$ of the set γ where the solution $k_\gamma^{(j)}$ lies within the first

Brillouin zone. We then perform a sum over all the partners $\sum_{\mu}$ while expressing the phases with respect to the solution $k_{\gamma}^{(j)}$ lying within the first Brillouin zone.

o We arrive at a reduced $[2M \cdot 2M]$ eigensystem for the $2M$ superlattices amplitudes $f^{(j)}(k_{\gamma}^{(j)}, \mathbf{q}; \mathbf{k}_{\parallel})$,

$$f^{(j)}(k_{\gamma}^{(j)}, \mathbf{q}; \mathbf{k}_{\parallel}) \equiv \sum_{\mu} \exp\left[i\varphi^{(j)}(\gamma, \mu)\right] f^{(j)}(k_{\gamma\mu}^{(j)}, \mathbf{q}; \mathbf{k}_{\parallel}), \tag{45}$$

corresponding to the solutions $k_{\gamma}^{(j)}$ lying inside the first Brillouin zone.

o The *reduced eigensystem* takes the following form

$$\exp\left[i\mathbf{D}(\mathbf{q}) \cdot \mathbf{R}_0\right] \cdot \mathbf{f}^{(1)}(\mathbf{q}) =$$

$$\exp\left[i\mathbf{D}(k_{\gamma}^{(1)})b\right] \cdot \left[\Omega(\mathbf{k}_{\parallel}E)\right]^{-1} \cdot \exp\left[i\mathbf{D}(k_{\gamma}^{(2)})a\right] \cdot \Omega(\mathbf{k}_{\parallel}E) \cdot \mathbf{f}^{(1)}(\mathbf{q}), \tag{46.a}$$

and,

$$\mathbf{f}^{(2)}(\mathbf{q}) = \Omega(\mathbf{k}_{\parallel}E) \cdot \mathbf{f}^{(1)}(\mathbf{q}), \tag{46.b}$$

where we have defined the $[2M \cdot 2M]$ *reduced transfer matrix*

$$\Omega(\mathbf{k}_{\parallel}E) \equiv \Omega(k_{\gamma}^{(2)}, k_{\gamma'}^{(1)}; \mathbf{k}_{\parallel}E) \qquad \gamma, \gamma' = 1, \ldots, 2M, \tag{47.a}$$

and the diagonal matrices

$$\exp\left[i\mathbf{D}(k_{\gamma}^{(j)})z\right] \equiv \exp(ik_{\gamma}^{(j)}z) \qquad \gamma = 1, \ldots, 2M. \tag{47.b}$$

The above eigensystem constitutes therefore an eigensystem for the the expansion amplitudes

$$\mathbf{f}^{(1)}(\mathbf{q}) \equiv f^{(1)}(k_{\gamma}^{(1)}, \mathbf{q}; \mathbf{k}_{\parallel}) \qquad \gamma = 1, \ldots, 2M, \tag{48.a}$$

and,

$$\mathbf{f}^{(2)}(\mathbf{q}) \equiv f^{(2)}(k_{\gamma}^{(2)}, \mathbf{q}; \mathbf{k}_{\parallel}) \qquad \gamma = 1, \ldots, 2M, \tag{48.b}$$

where the $2M$ superlattices amplitudes $f^{(j)}(k_{\gamma}^{(j)}, \mathbf{q}; \mathbf{k}_{\parallel})$ are

$$f^{(j)}(k_{\gamma}^{(j)}, \mathbf{q}; \mathbf{k}_{\parallel}) \equiv \sum_{\mu} \exp\left[i\varphi^{(j)}(\gamma, \mu)\right] f^{(j)}(k_{\gamma\mu}^{(j)}, \mathbf{q}; \mathbf{k}_{\parallel}), \tag{49}$$

where $\mathrm{Re}\left[k_{\gamma}^{(j)}\right]$ lies inside the first Brillouin zone for $j = 1, 2$.

4.2.4.3 Actual Truncation of Transfer Matrix:

In the present work, we have performed a *truncation of the transfer matrix to include only those solutions whose real part lies inside the first Brillouin zone.* This can be justified on the grounds that, due to the truncation of the $\mathbf{k} \cdot \mathbf{p}$ Hamiltonian, the out-of-zone solutions are approximately described and should not enter in the expansion of the superlattice state function.

We have proceed as follow:

o The Hamiltonian of each solid forming the superlattice is expressed in terms of a *local pseudopotential Hamiltonian.* The local pseudopotential Hamiltonian is expressed in terms of 113 plane waves $\exp(i\mathbf{g} \cdot \mathbf{x})$.

o From the transformation that diagonalizes the pseudopotential at $\mathbf{k}_0 = \mathbf{0}$, the Hamiltonian is transformed from the $\{|\mathbf{g}\rangle\}$-representation (*local pseudopotentials*) to the $\{|m\rangle\}$-representation ($\mathbf{k} \cdot \mathbf{p}$). The $\mathbf{k} \cdot \mathbf{p}$ Hamiltonian of both solids forming the superlattice is thus expressed in terms of the *same set of basis functions* $\langle \mathbf{x}|m\rangle \equiv u_m(\mathbf{x})$ *associated with the reference solid.* At this point the $\mathbf{k} \cdot \mathbf{p}$ Hamiltonian is truncated to include $N = 27$ basis functions $u_m(\mathbf{x})$ associated with $\mathbf{k}_0 = \mathbf{0}$.

o The complex-$\mathbf{k}$ bandstructure is obtained from this truncated $\mathbf{k}\cdot\mathbf{p}$ Hamiltonian. This produces $2N = 54$ solutions

$$k_{\gamma\mu}^{(j)}, \qquad \gamma\mu = 1, \ldots, 54, \quad (50.a)$$

corresponding to the Bloch states,

$$|\mathbf{k}_\parallel E; k_{\gamma\mu}^{(j)}\rangle, \qquad \gamma\mu = 1, \ldots, 54. \quad (50.b)$$

o The eigensystem derived from the boundary conditions then involves a *non-reduced transfer matrix,*

$$\mathbf{T}(k_{\gamma\mu}^{(2)}, k_{\gamma'\mu'}^{(1)}; \mathbf{k}_\parallel E), \qquad \gamma\mu, \gamma'\mu' = 1, \ldots, 54, \quad (51)$$

that couples all the partners $k^{(1)}_{\gamma'\mu'}$ and $k^{(2)}_{\gamma\mu}$ of the non-equivalent sets γ and γ'.

The *transfer matrix is then truncated to include only* 18 *solutions.* We then obtain a *reduced transfer matrix,*

$$\Omega(k^{(2)}_{\gamma}, k^{(1)}_{\gamma'}; \mathbf{k}_{\|} E), \qquad \gamma, \gamma' = 1, \ldots, 54, (52)$$

that relates the states $k^{(2)}_{\gamma}$ and $k^{(1)}_{\gamma'}$ where *both* $Re\left[k^{(1)}_{\gamma'}\right]$ *and* $Re\left[k^{(2)}_{\gamma}\right]$ *lie inside the first Brillouin zone.* The number 18 corresponds to *twice the number of different* $\mathbf{g}_{\|}$ *contained in the first* 15 *free-electrons plane wave states having reciprocal lattice vectors:*

$$\mathbf{g} = \frac{2\pi}{a}(0,0,0), (\pm 1, \pm 1, \pm 1), \frac{2\pi}{a}(\pm 2, 0, 0), \qquad (53)$$

where a is the bulk lattice constant for the solid under consideration. Thus for each $\mathbf{k}_{\|}$ and E, we obtain a $[18 \cdot 18]$ eigensystem for the 18 superlattices amplitudes $f^{(j)}(k^{(j)}_{\gamma}, \mathbf{q}; \mathbf{k}_{\|})$, corresponding to the solutions $k^{(j)}_{\gamma}$ lying inside the first Brillouin zone. This produces 18 complex-**q** superlattice wavevector.

By using this truncation procedure we discard the following states:

(i) Real-**k** Bloch states with $\mathrm{Re}\left[k^{(j)}_{\gamma\mu}\right] > 2\pi/a$ and $\mathrm{Im}\left[k^{(j)}_{\gamma\mu}\right] = 0$. These out-of-zone real solutions are equivalent to real solutions $k^{(j)}_{\gamma}$ inside the first Brillouin zone.

(ii) Complex-**k** Bloch states with $\mathrm{Re}\left[k^{(j)}_{\gamma\mu}\right] > 2\pi/a$ and $\mathrm{Im}\left[k^{(j)}_{\gamma\mu}\right] \neq 0$. These out-of-zone complex solutions are equivalent to complex solutions $k^{(j)}_{\gamma}$ inside the first Brillouin zone.

(iii) Purely imginary-**k** Bloch states with $\mathrm{Re}\left[k^{(j)}_{\gamma\mu}\right] = 0$ and $\mathrm{Im}\left[k^{(j)}_{\gamma\mu}\right] \neq 0$ and very large. These solutions are *very rapidly decaying solutions that contribute to the superlattice state function only on the interface plane.*

4.2.4.4 Symmetric Truncation of Transfer Matrix:

As mentioned above, special care must be taken whenever the *Bloch solutions lie exactly on the first Brillouin zone,*

$$k_{\gamma\mu}^{(j)} = \pm\frac{1}{2}g_\mu \pm i\kappa_\lambda^{(j)}, \tag{54}$$

where $\kappa_\lambda^{(j)}$ is a real number and g_μ is the smallest non-vanishing reciprocal lattice vector.

To perform a *symmetric truncation of the transfer matrix we must include solutions by pair of inversion and time-reversal.* That is, if

$$k_{\gamma\mu}^{(j)} = K_{\gamma\mu}^{(j)} + iQ_{\gamma\mu}^{(j)}, \tag{55}$$

is a solution lying within the first Brillouin zone, then we must also include, in the reduced eigensystem, the following time-reversed pairs of solutions:

o For the first time-reversed pair,

$$k_{\gamma\mu}^{(j)} = K_{\gamma\mu}^{(j)} + iQ_{\gamma\mu}^{(j)}, \tag{56.a}$$

$$-k_{\gamma\mu}^{(j)^*} = -K_{\gamma\mu}^{(j)} + iQ_{\gamma\mu}^{(j)}. \tag{56.b}$$

o For the second time-reversed pair,

$$-k_{\gamma\mu}^{(j)} = -K_{\gamma\mu}^{(j)} - iQ_{\gamma\mu}^{(j)}, \tag{56.c}$$

$$k_{\gamma\mu}^{(j)^*} = K_{\gamma\mu}^{(j)} - iQ_{\gamma\mu}^{(j)}, \tag{56.d}$$

We refer to Appendix (5.1) to show that *the time-reversed partner of a Bloch state associated with wavevector* k_λ *is a Bloch state associated with wavevector* $-k_\lambda^*$, *to within a phase factor* $\exp(i\varphi)$.

Let $k_{\gamma 0}$ be a solution on the first Brillouin zone edge,

$$k_{\gamma 0} \equiv \frac{1}{2} g_0 + i\kappa_\gamma, \tag{57}$$

where g_0 is the smallest non-vanishing reciprocal lattice vector. The two time-reversed pairs are

o For the first time-reversed pair,

$$k_{\gamma 0} \equiv \frac{1}{2} g_0 + i\kappa_\gamma, \tag{58.a}$$

$$-k^*_{\gamma 0} \equiv -\frac{1}{2} g_0 + i\kappa_\gamma. \tag{58.b}$$

o For the second time-reversed pair,

$$-k_{\gamma 0} \equiv -\frac{1}{2} g_0 - i\kappa_\gamma, \tag{58.c}$$

$$k^*_{\gamma 0} \equiv \frac{1}{2} g_0 - i\kappa_\gamma. \tag{58.b}$$

From these four solutions we construct the *symmetrized linear combinations*, writing $|k_\lambda\rangle$ for the Bloch state $|\mathbf{k}_\parallel E; k_\lambda\rangle$,

o For the first time-reversed pair,

$$|k_{\gamma 0}, -k^*_{\gamma 0}, \pm\rangle \equiv |k_{\gamma 0}\rangle \pm |-k^*_{\gamma 0}\rangle, \tag{59.a}$$

associated with the time-reversed pair,

$$\left(k_{\gamma 0}, -k^*_{\gamma 0}\right). \tag{59.b}$$

o For the second time-reversed pair,

$$|-k_{\gamma 0}, k^*_{\gamma 0}, \pm\rangle \equiv |-k_{\gamma 0}\rangle \pm |k^*_{\gamma 0}\rangle, \tag{60.a}$$

associated with the time-reversed pair,

$$\left(-k_{\gamma 0}, k^{*}_{\gamma 0}\right). \tag{60.b}$$

Only one symmetrized linear combination was retained for the expansion of the superlattice state function. This approach has the advantage of *producing a symmetric truncation of the transfer matrix whereby time-reversed pairs are included in the expansion of the superlattice state function.* Some basic symmetry properties of the transfer matrix are discussed in Appendix (4.7)

4.2.5 Results

In this section we present some results obtained from the above formalism. We apply the formalism to the GaAs-AlAs (100) superlattice.

4.2.5.1 Complex-k Bulk Bandstructure: k · p Theory

We first analyse the complex-**k** band structure of bulk GaAs and bulk AlAs.

• Figures (1) and (2) show a typical complex-**k** band structure for GaAs and AlAs, respectively, as obtained by the **k**·**p** method outlined above. Only the energy bands within the first Brillouin zone are shown. The complex-**k** band structure corresponds to vanishing wavevector parallel to the (100) interface plane, *i.e.*, $\mathbf{k}_{\parallel} = \mathbf{0}$. At a given energy E, the purely real values of k_z are indicated by a solid line on the right panel of the figure and the purely imaginary values of k_z are indicated by a solid line on the left panel of the figure. Complex values of k_z are indicated by a dashed line, $\mathrm{Re}[k_z]$ being on the right and $\mathrm{Im}[k_z]$ being on the left of the figure respectively. The origin of the energies is taken to correspond to the top of the GaAs valence band. The top of the AlAs valence band is therefore shifted down by the *valence band offset*,

$$\Delta E_v = 0.15\Big[E^{\mathrm{AlAs}}(\Gamma) - E^{\mathrm{GaAs}}(\Gamma)\Big]. \tag{61}$$

Numerically we have, $\Delta E_v = 0.266\mathrm{eV}$.

As mentioned above this band structure is obtained from a local pseudopotential calculation including 113 plane waves $\exp(i\mathbf{g}\cdot\mathbf{x})$. Then the Hamiltonian is transformed from the $\{|\mathbf{g}\rangle\}$-representation (pseudopotentials) to the $\{|m\rangle\}$-representation ($\mathbf{k}\cdot\mathbf{p}$) in terms of basis functions of a *common reference solid*. The $\mathbf{k}\cdot\mathbf{p}$ Hamiltonian is then truncated down to include $N = 27$ basis functions

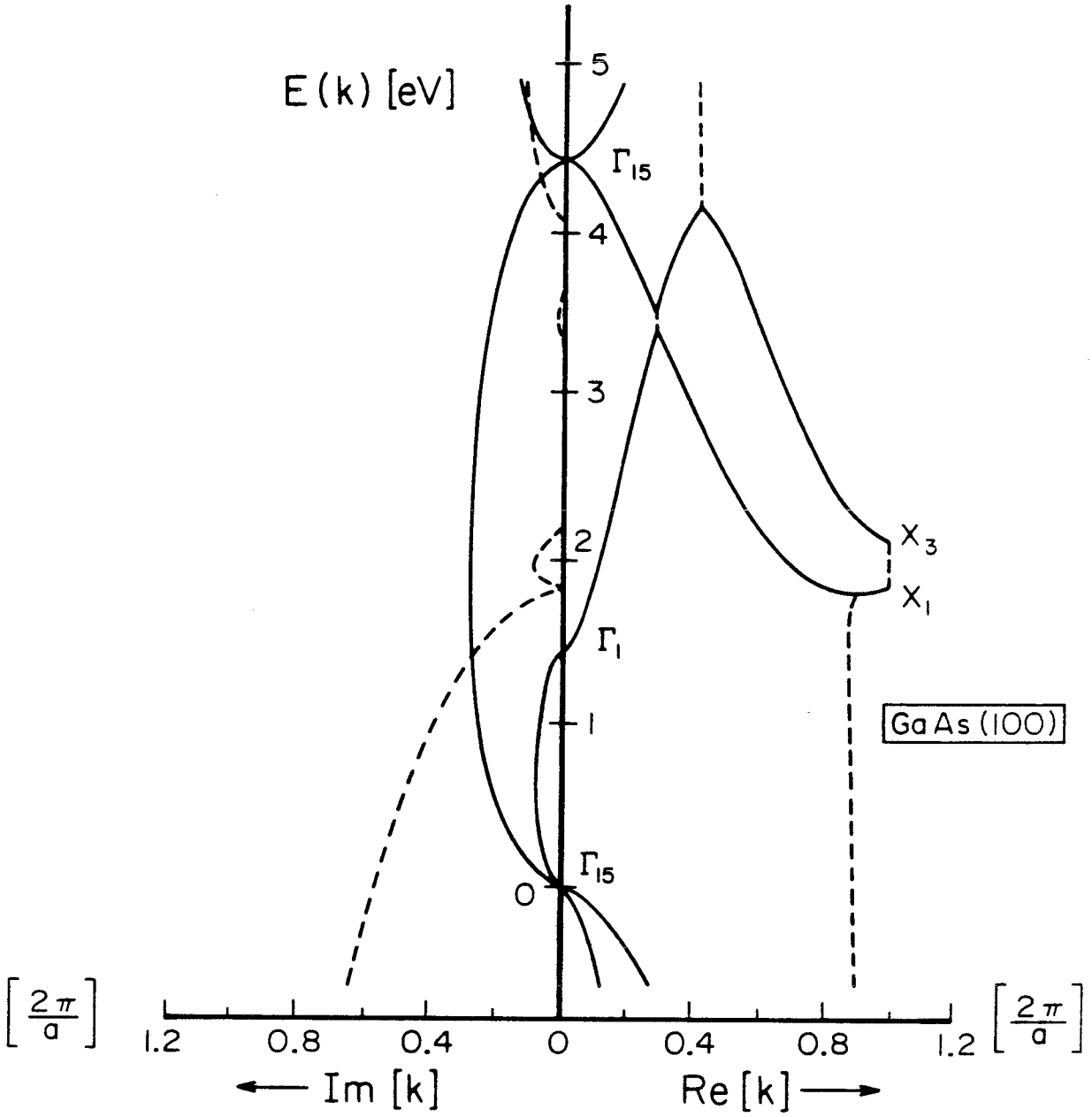

Figure 2: Complex-**k** band structure of GaAs along the (100) direction, respectively. Only the energy bands within the first Brillouin zone are shown. The complex-**k** band structure corresponds to vanishing wavector parallel to the (100) interface plane, *i.e.* $\mathbf{k}_{\parallel} = \mathbf{0}$. At a given energy E, the purely real values of k_z are indicated by a solid line on the right panel of the figure and the purely imaginary values of k_z are indicated by a solid line on the left panel of the figure. Complex values of k_z are indicated by a dashed line, $\mathrm{Re}[k_z]$ being on the right and $\mathrm{Im}[k_z]$ being on the left of the figure respectively. The zero of energy is taken at the top of the GaAs valence band maximum.

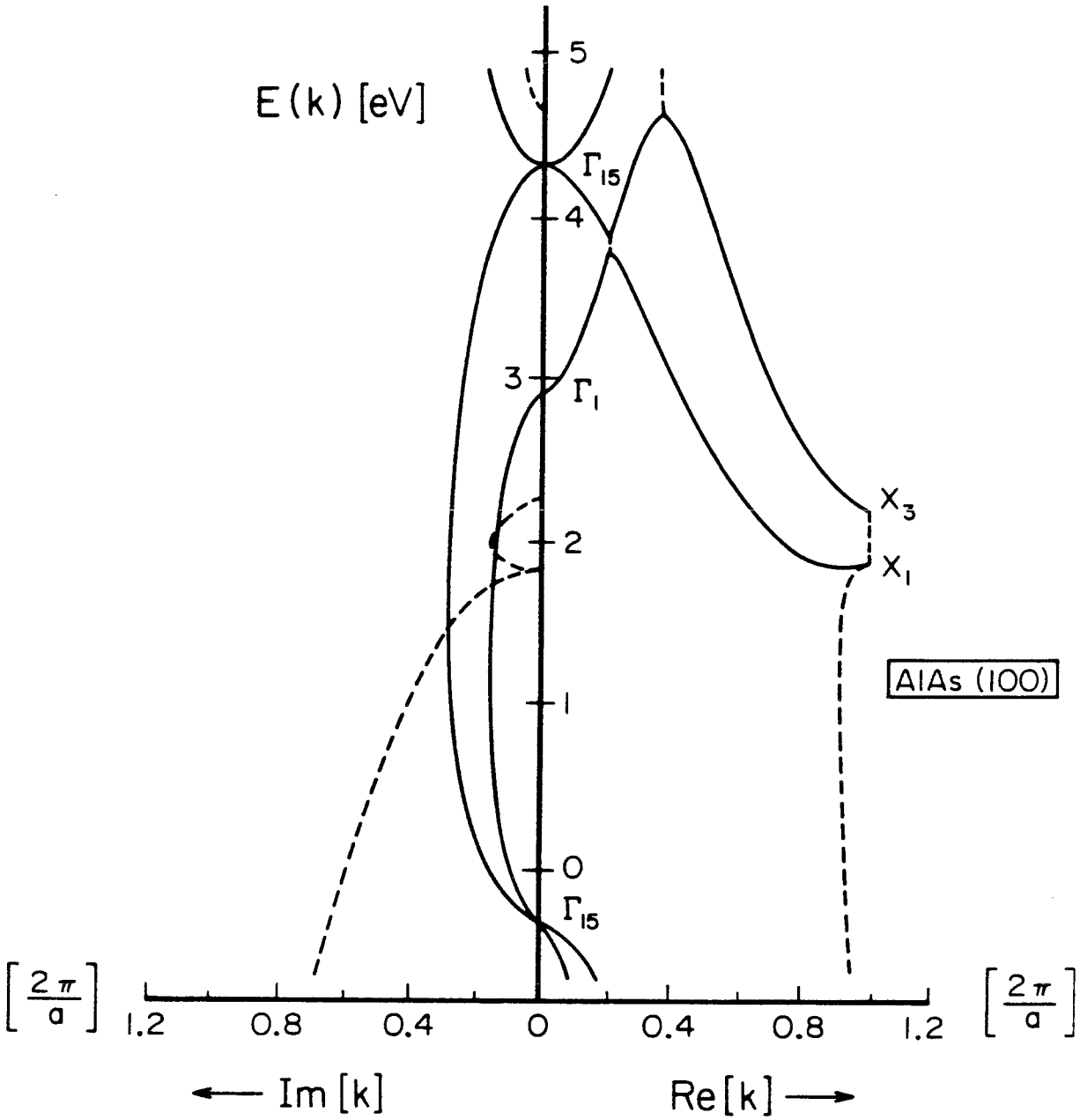

Figure 3: Complex-**k** band structure of AlAs along the (100) direction, respectively. Only the energy bands within the first Brillouin zone are shown. The complex-**k** band structure corresponds to vanishing wavevector parallel to the (100) interface plane, *i.e.* $\mathbf{k}_{||} = \mathbf{0}$. At a given energy E, the purely real values of k_z are indicated by a solid line on the right panel of the figure and the purely imaginary values of k_z are indicated by a solid line on the left panel of the figure. Complex values of k_z are indicated by a dashed line, $\mathrm{Re}[k_z]$ being on the right and $\mathrm{Im}[k_z]$ being on the left of the figure respectively. The zero of energy is taken at the top of the GaAs valence band maximum.

$u_m(\mathbf{x})$. Out of the $2N = 54$ solutions obtained,

$$k_{\gamma\mu}^{(j)}, \qquad \gamma\mu = 1, \ldots, 54, (62.a)$$

corresponding to the Bloch states,

$$|\mathbf{k}_\parallel E; k_{\gamma\mu}^{(j)}\rangle, \qquad \gamma\mu = 1, \ldots, 54, (62.b)$$

we only plotted 10 solutions $k_\gamma^{(j)}$ whose real part lies within the first Brillouin zone.

The symmetry of the Bloch states at $\mathbf{k} = \mathbf{0}$ and $\mathbf{k} = 2\pi/a(0, 0, 1)$ are indicated. One the right panel, which shows Re$[k_z]$, we can identify, in solid lines, the heavy-hole (Δ_5^v) and the light-hole (Δ_1^v) bands and the two lowest conduction band (Δ_1^c) . On the left panel, which shows Im$[k_z]$, we can identify two major bands for which k_z is *purely imaginary.* Both of these bands originate from the top of the valence band and *connect real bands across the energy gap.* The band of Δ_1 symmetry connects the *light-hole band* and the *first conduction band* across the energy gap. The band of Δ_5 symmetry connects the *heavy-hole band* and the *second conduction band* across the energy gap. We can also identify *complex bands* for which both Re$[k_z]$ and Im$[k_z]$ are non-zero. These bands are indicated by pairs of dashed lines. These bands emanate from the X-point. One complex band of special interest is the band that connects the points X_1^c and X_3^c. This complex band is of the form,

$$k_\gamma^{(j)} = \pm\frac{1}{2}g_z \pm i\kappa_\lambda^{(j)}, \qquad (63.a)$$

where $\kappa_\lambda^{(j)}$ is a real number and

$$g_z = \frac{4\pi}{a}(0, 0, 1) \qquad (63.b)$$

is the smallest non-vanishing reciprocal lattice vector.

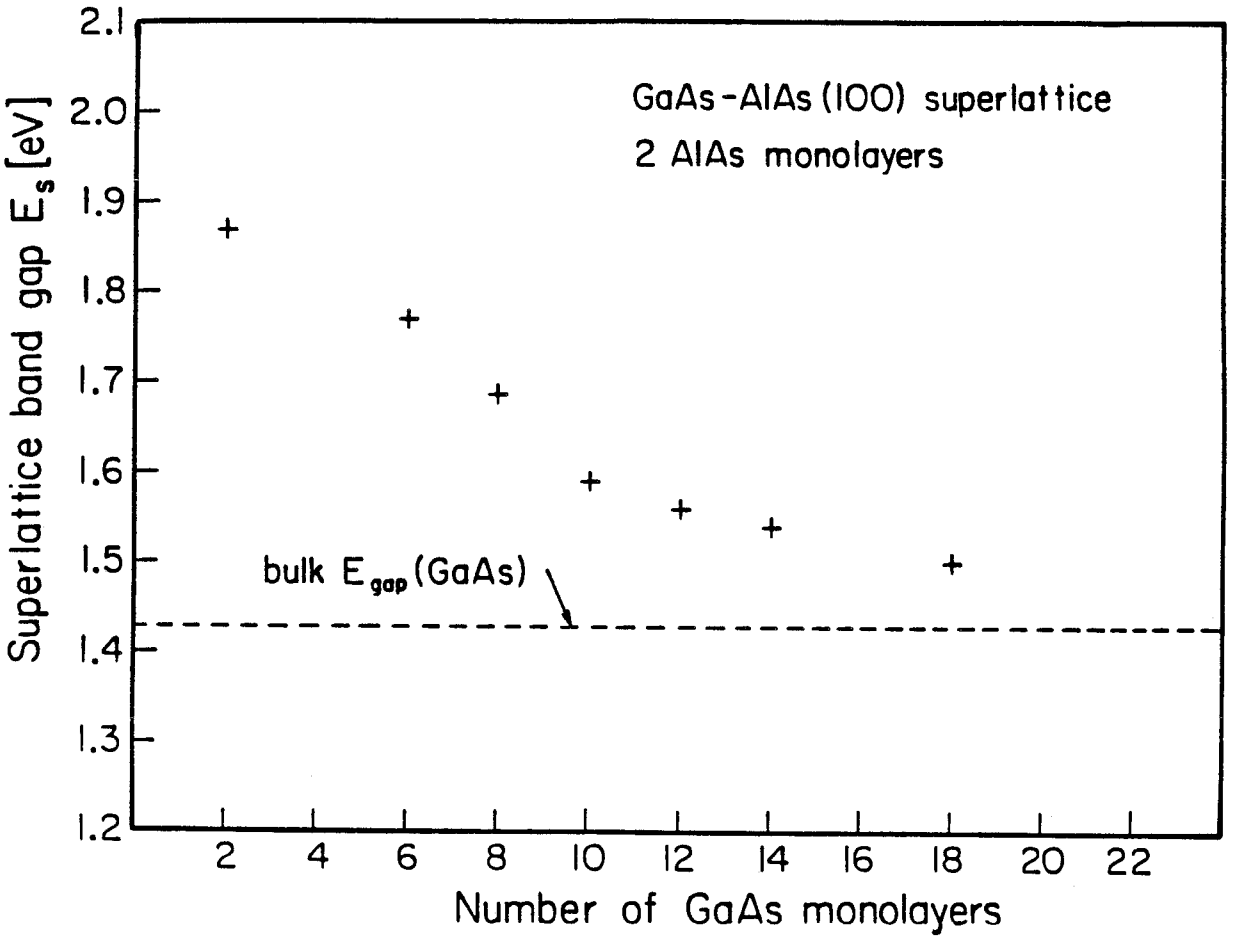

Figure 4: GaAs-AlAs (100) superlattice energy band gap as a function of the number of GaAs monolayers forming the superlattice period. The superlattice period consists of 2 monolayers of AlAs.

4.2.5.2 Superlattice Energy Gap:

We used the procedure described above to study the GaAs-AlAs superlatices grown along the (100) direction. GaAs-AlAs (100) superlattice energy band gap as a function of the number of GaAs monolayers forming the superlattice period. Monolayers are in units of $a/2$, where a is the lattice constant of bulk GaAs and AlAs. The superlattice period consists of 2 monolayers of AlAs. As seen in the figure, the *superlattice band gap decreases when the number of GaAs monolayers increases in the superlattice period*, the number of AlAs monolayers being kept fixed.

The superlattice state at the conduction band edges is derived from the lowest conduction band Δ_1^c of GaAs. At the energy corresponding to the superlattice conduction band minimum, the Bloch solutions forming the superlattice state are propagating states derived from the first conduction band. The AlAs Bolch solutions derived from the X-point lie higher in energy and do not contribute substantially to the lowest superlattice state.

4.2.6 Summary and Conclusions:

We have developed a new formalism for the study of the optical properties of semiconductor superlattices. This formalism is essentially based on a *local pseudopotential formulation* and on the $\mathbf{k} \cdot \mathbf{p}$ *theory.* We summarize the major ingredients of the theory.

• An accurate description of the bulk constituents semiconductors forming the superlattice is obtained. This is done using a set of 113 plane waves, $\exp(i\mathbf{g}\cdot\mathbf{x})$, in the expansion of the bulk Bloch solutions within the local pseudopotential formalism.

A transformation from the *local pseudopotential formalism* to the $\mathbf{k} \cdot \mathbf{p}$ *formalism* is then performed. At this point, *the* $\mathbf{k} \cdot \mathbf{p}$ *Hamiltonian of both constituent semiconductors is expressed in terms of the same set of* $\mathbf{k}_0 = \mathbf{0}$ *basis functions,* $u_m(\mathbf{x})$. This results relaxes the often used approximation the the $\mathbf{k}_0 = \mathbf{0}$ basis functions for all III-V semiconductors are the same.

The complex-$\mathbf{k}$ energy band structure is then obtained within the $\mathbf{k} \cdot \mathbf{p}$ formalism. Due to the nice convergence features of the $\mathbf{k} \cdot \mathbf{p}$ formalism, it is legitimate, at this point, to truncate the $\mathbf{k} \cdot \mathbf{p}$ Hamiltonian from 113 basis functions down to 27 basis functions $u_m(\mathbf{x})$. Each bulk Bloch soultions, associated with real or complex values of $\mathbf{k}$, is then expanded in terms of the *same* set of $\mathbf{k}_0 = \mathbf{0}$ basis functions.

The superlattice state function is then expanded in terms of the bulk Bloch solutions associated with complex-$\mathbf{k}$ in each solid. A set of realistic boundary conditions is then applied on the superlattice state function and formulated in terms of *eigensystem* for the superlattice state function. The eigenvalues of this eigensystem are the complex values of $\mathbf{q}$, the superlattice wavevector.

It is therefore possible to obtain the *complex-*$\mathbf{q}$ *energy band structure of the superlattice* without having to perform energy searches.

The method is applied to the study of the superlattice band gap as a function

of the number of GaAs monolayers forming the superlattice period.

References

1. G. C. Osbourn, *J. Vac. Sci. Technol.* **21**, 469 (1982).
2. See for example, N. Holonyak, Jr., B. A. Vojak, W. D. Laidig, K. Hess, J. J. Coleman, and P. D. Dapkus, *Appl. Phys. Lett.* **37**, 136 (1980).
3. S. R. White and L. J. Sham, *Phys. Rev. Lett.* **47**, 879 (1981).
4. G. Bastard, *Phys. Rev.* **B25**, 7584 (1982).
5. M. Altarelli, *Phys. Rev.* **B28**, 842 (1983).

APPENDICES

CHAPTER 2

ENERGY SPECTRUM OF SHALLOW DONORS IN $Ga_{1-x}Al_xAs$-GaAs-$Ga_{1-x}Al_xAs$ QUANTUM WELL STRUCTURES

APPENDIX 2.1

Effective-mass theory: Bulk Semiconductors

In this appendix, we develop the theory necessary for the study of shallow Coulomb centers within quantum well structures. For the cases treated here, the constituent semiconductors forming the quantum well structure are *direct, i.e* solids for which the maximum of the valence band is believed to be located at the same value of $\mathbf{k}$ as the minimum of the conduction band. Therefore a single-valley effective mass theory is adequate for the electronic structures investigated here. The back-bone of the treatment resides in the multi-valley effective mass theory (EMT) for shallow impurity states in bulk semiconductors as was first developed by Kohn[1].

The EMT was first developped to treat the motion of an electron in the Coulomb potential of an impurity atom imbeded within a perfectly crystalline host solid. The Schrödinger equation for the impurity electron wavefunction, $|\Psi\rangle$, is:

$$\hat{H}|\Psi\rangle = E|\Psi\rangle, \tag{1}$$

where the Hamiltonian $\hat{H}$ is the sum of the unperturbed Hamiltonian , $\hat{H}^0$, corresponding to the host solid, plus the impurity potential, $U(\mathbf{x})$,

$$\hat{H} \equiv \hat{H}^0 + U(\mathbf{x}). \tag{2}$$

The eigenfunctions for the unperturbed problem are the set of Bloch functions, $\{|n\mathbf{k}\rangle\}$, associated with the energy eigenvalue spectrum $E_n(\mathbf{k})$ forming the host

solid band structure:

$$\hat{H}^0|n\mathbf{k}\rangle = E_n(\mathbf{k})|n\mathbf{k}\rangle. \tag{3}$$

In $\mathbf{x}$-space representation, the Bloch function $|n\mathbf{k}\rangle$ is of the form

$$\langle\mathbf{x}|n\mathbf{k}\rangle = \exp(i\mathbf{k}\cdot\mathbf{x})u_n(\mathbf{k};\mathbf{x}), \tag{4}$$

where $u_n(\mathbf{k};\mathbf{x})$ is a function periodic in the $\mathbf{x}$-space lattice and is referred to as the *cell-periodic part of the Bloch function*

$$u_n(\mathbf{k};\mathbf{x}+\mathbf{R}) = u_n(\mathbf{k};\mathbf{x}), \tag{5}$$

where $\mathbf{R}$ is a Bravais lattice vector generating the $\mathbf{x}$-space lattice. The index n is the band index that labels the eigensolutions of Eq.(3) and $\hbar\mathbf{k}$ is the crystal momentum. The Bloch solutions $\{|n\mathbf{k}\rangle\}$ are orthogonal with respect to band index n and wavevector $\mathbf{k}$,

$$\langle n\mathbf{k}|n'\mathbf{k}'\rangle = \delta(n,n')\delta^3(\mathbf{k}-\mathbf{k}'), \tag{6.a}$$

or,

$$\int d^3\mathbf{x}\, u_n^*(\mathbf{k};\mathbf{x})u_{n'}(\mathbf{k}';\mathbf{x})\exp\left[i(\mathbf{k}'-\mathbf{k})\cdot\mathbf{x}\right] = \delta(n,n')\delta^3(\mathbf{k}-\mathbf{k}'). \tag{6.b}$$

Since the cell-periodic functions, $u_n(\mathbf{k};\mathbf{x})$ are periodic in the direct lattice (*cf.* Eq.(5)), we can expand these functions on a set of plane waves $\exp(i\mathbf{g}\cdot\mathbf{x})$ associated with the reciprocal lattice,

$$u_n(\mathbf{k};\mathbf{x}) = \sum_{\mathbf{g}} C_n(\mathbf{k};\mathbf{g})\exp(i\mathbf{g}\cdot\mathbf{x}), \tag{7}$$

where $\mathbf{g}$ is a set of reciprocal lattice vector generating the reciprocal lattice. The set of coefficients $C_n(\mathbf{k};\mathbf{g})$ is obtained by inverting Eq.(7),

$$C_n(\mathbf{k};\mathbf{g}) = \int d^3\mathbf{x} u_n(\mathbf{k};\mathbf{x}) \exp(-i\mathbf{g}\cdot\mathbf{x}) \tag{8}$$

The Bloch solutions $\{|n\mathbf{k}\rangle\}$ of Eq.(4) can now be written as

$$\langle\mathbf{x}|n\mathbf{k}\rangle = \exp(i\mathbf{k}\cdot\mathbf{x}) u_n(\mathbf{k};\mathbf{x}), \tag{8.a}$$

$$\langle\mathbf{x}|n\mathbf{k}\rangle = \exp(i\mathbf{k}\cdot\mathbf{x}) \sum_{\mathbf{g}} C_n(\mathbf{k};\mathbf{g}) \exp(i\mathbf{g}\cdot\mathbf{x}). \tag{8.b}$$

With a knowledge of the unperturbed crystal eigensolutions, $\{|n\mathbf{k}\rangle\}$, the impurity electron state ,$|\Psi\rangle$, is constructed from a linear combination of the host solid Bloch states,

$$|\Psi\rangle = \sum_n \int \frac{d^3\mathbf{k}}{(2\pi)^3} F_n(\mathbf{k}) |n\mathbf{k}\rangle, \tag{9}$$

where the integral is over the first Brillouin zone and the sum runs over all bands. The expansion coefficients, $F_n(\mathbf{k})$, are called the envelope functions and indicate the degree of mixing of the Bloch states $|n\mathbf{k}\rangle$ in the expansion Eq.(9). The Schrödinger equation for the impurity electron, Eq. (1), can be transformed in matrix equation in the coefficients $F_n(\mathbf{k})$ by replacing the expansion of Eq.(9) into Eq.(1) and by projecting onto the Bloch state $\langle n\mathbf{k}|$:

$$[E_n(\mathbf{k}) - E] F_n(\mathbf{k}) + \sum_{n'} \int \frac{d^3\mathbf{k}'}{(2\pi)^3} \langle n\mathbf{k}|U(\mathbf{x})|n'\mathbf{k}'\rangle F_{n'}(\mathbf{k}') = 0, \tag{10}$$

where

$$\langle n\mathbf{k}|U(\mathbf{x})|n'\mathbf{k}'\rangle \equiv \int d^3\mathbf{x} \langle n\mathbf{k}|\mathbf{x}\rangle U(\mathbf{x}) \langle\mathbf{x}|n'\mathbf{k}'\rangle, \tag{11.a}$$

or, using Eq.(4)

$$\langle n\mathbf{k}|U(\mathbf{x})|n'\mathbf{k}'\rangle = \int d^3\mathbf{x} u_n^*(\mathbf{k};\mathbf{x}) U(\mathbf{x}) u_{n'}(\mathbf{k}';\mathbf{x}) \exp\left[i(\mathbf{k}' - \mathbf{k})\cdot\mathbf{x}\right]. \tag{11.b}$$

Eq.(10) is the single-valley effective mass equation (EME) for the envelope functions $F_n(\mathbf{k})$. The matrix equation (10) contains a *diagonal* part:

$$[E_n(\mathbf{k}) - E]\, F_n(\mathbf{k})$$

since $\hat{H}^0$ is diagonal in the $\{|n\mathbf{k}\rangle\}$-representation, and a *off-diagonal* part:

$$\sum_{n'} \int \frac{d^3\mathbf{k}'}{(2\pi)^3} \langle n\mathbf{k}|U(\mathbf{x})|n'\mathbf{k}'\rangle F_{n'}(\mathbf{k}'),$$

which is associated with the scattering between the two Bloch states $|n\mathbf{k}\rangle$ and $|n'\mathbf{k}'\rangle$ by the Coulomb potential $U(\mathbf{x})$.

As Eq.(10) stands, it constitutes an infinite set of coupled integral equations for the envelope functions $F_n(\mathbf{k})$. To find which values of $\mathbf{k}$ and $\mathbf{k}'$ are mixed by the perturbing potential $U(\mathbf{x})$, it is instructive to expand the product $u_n^*(\mathbf{k};\mathbf{x})u_{n'}(\mathbf{k}';\mathbf{x})$ on a set of plane waves associated with the reciprocal lattice $\mathbf{g}$ as in Eq.(7),

$$u_n^*(\mathbf{k};\mathbf{x})u_{n'}(\mathbf{k}';\mathbf{x}) = \sum_{\mathbf{g}} C_{nn'}(\mathbf{k}\mathbf{k}';\mathbf{g}) \exp(i\mathbf{g}\cdot\mathbf{x}). \tag{12.a}$$

As in the expansion of Eq.(6) only reciprocal lattice vectors enter in the expansion since the product $u_n^*(\mathbf{k};\mathbf{x})u_{n'}(\mathbf{k}';\mathbf{x})$ is a periodic function with the periodicity of the direct lattice $\mathbf{R}$. The set of coefficients $C_{nn'}(\mathbf{k}\mathbf{k}';\mathbf{g})$ is given by the inversion of Eq.(12),

$$C_{nn'}(\mathbf{k}\mathbf{k}';\mathbf{g}) = \int d^3\mathbf{x} u_n^*(\mathbf{k};\mathbf{x})u_{n'}(\mathbf{k}';\mathbf{x}) \exp(-i\mathbf{g}\cdot\mathbf{x}). \tag{12.b}$$

The Coulomb scattering matrix elements $\langle n\mathbf{k}|U(\mathbf{x})|n'\mathbf{k}'\rangle$ can then be expanded in the following way:

$$\langle n\mathbf{k}|U(\mathbf{x})|n'\mathbf{k}'\rangle = \sum_{\mathbf{g}} C_{nn'}(\mathbf{k}\mathbf{k}';\mathbf{g}) U_{nn'}(\mathbf{k} - \mathbf{k}' - \mathbf{g}), \tag{13}$$

where $U_{nn'}(\mathbf{k}-\mathbf{k}'-\mathbf{g})$ is the Fourier transform of the Coulomb potential,

$$U_{nn'}(\mathbf{k}-\mathbf{k}'-\mathbf{g}) = -\left[\frac{4\pi e^2}{\epsilon|\mathbf{k}-\mathbf{k}'-\mathbf{g}|^2}\right], \tag{14}$$

for

$$U(\mathbf{x}) = -\frac{e^2}{\epsilon|\mathbf{x}|}. \tag{15}$$

Here ϵ is the static dielectric constant of the host solid and $|\mathbf{x}|$ is the distance measured from the Coulomb center. The set of EME for the envelope functions, $F_n(\mathbf{k})$, then becomes:

$$[E_n(\mathbf{k})-E]F_n(\mathbf{k}) + \sum_{n'}\sum_{\mathbf{g}}\int \frac{d^3\mathbf{k}'}{(2\pi)^3} C_{nn'}(\mathbf{k}\mathbf{k}';\mathbf{g})U_{nn'}(\mathbf{k}-\mathbf{k}'-\mathbf{g})F_{n'}(\mathbf{k}') = 0. \tag{16}$$

The Coulomb attraction of the impurity atom is greatly reduced by the static dielectric constant, ϵ, of the host solid. We anticipate the set of equations Eq.(16), will have solutions for which $F_n(\mathbf{k})$ has small amplitude unless $n = 0$ and $\mathbf{k}-\mathbf{k}'$ is small, *i.e.*,

$$|\mathbf{k}-\mathbf{k}'| \ll |\mathbf{g}|. \tag{17}$$

Also, we assume that

$$|U_{nn'}(\mathbf{k}-\mathbf{k}'-\mathbf{g})| \ll |U_{nn'}(\mathbf{k}-\mathbf{k}')|, \tag{18}$$

by the explicit form of $U_{nn'}(\mathbf{k}-\mathbf{k}'-\mathbf{g})$ given by Eq.(14). As a consequence, all the $\mathbf{g}\neq 0$ terms are dropped in Eq.(16) and we set, for $n' = n = 0$,

$$C(\mathbf{k}\mathbf{k}';\mathbf{g}=\mathbf{0}) \approx C(\mathbf{k}\mathbf{k};\mathbf{g}=\mathbf{0}) = 1. \tag{19.a}$$

The equality in Eq.(19) is exact and is a direct consequence of Eq.(12.b) and of the normalization condition

$$\langle n\mathbf{k}|n'\mathbf{k}'\rangle = \delta(n,n')\delta^3(\mathbf{k}-\mathbf{k}'), \tag{19.b}$$

Equation (20) assumes that the function $u_0(\mathbf{k};\mathbf{x})$ for $n = 0$ does not vary appreciably over the range of $\mathbf{k}$ values for which the envelope function $F(\mathbf{k}) \equiv F_0(\mathbf{k})$ has large amplitude. The above approximation is essentially equivalent to taking the cell-periodic function $u_0(\mathbf{k};\mathbf{x})$ as constant in Eq.(7).

Furthermore, we expand the unperturbed eigenenergies $E_0(\mathbf{k})$ of the band $n = 0$ about the extremum $\mathbf{k} = \mathbf{0}$ up to order $\mathbf{k}^2$,

$$E_0(\mathbf{k}) = E_0(\mathbf{k} = \mathbf{0}) + \frac{\hbar^2}{2m^*}\mathbf{k}^2, \tag{20}$$

where m^* is the effective mass associated with Bloch states derived from near the conduction band extremum. Within the set of approximations mentioned above, the EME becomes:

$$\left[\frac{\hbar^2}{2m^*}\mathbf{k}^2 - E_b\right]F(\mathbf{k}) + \int \frac{d^3\mathbf{k}'}{(2\pi)^3}U(\mathbf{k}-\mathbf{k}')F(\mathbf{k}') = 0, \tag{21}$$

where $E_b \equiv E - E_0(\mathbf{k} = \mathbf{0})$ is the energy of the impurity state measured with respect to the host solid band edge. This simplified version of the EME can be transformed in $\mathbf{x}$-space by introducing the Fourier transform of the envelope function $F(\mathbf{k})$:

$$F(\mathbf{x}) = \int \frac{d^3\mathbf{k}}{(2\pi)^3}F(\mathbf{k})\exp(i\mathbf{k}\cdot\mathbf{x}). \tag{22}$$

By Fourier transforming Eq.(20), we obtain:

$$\left[\frac{-\hbar^2}{2m^*}\nabla_{\mathbf{x}}^2 - E_b\right]F(\mathbf{x}) + U(\mathbf{x})F(\mathbf{x}) = 0, \tag{23}$$

which indicates that $F(\mathbf{x})$ is the solution of a hydrogenic-like EME in which the Coulomb potential has been reduced by a factor ϵ.

The EMT has been particularly successful in the study of shallow donor states in direct band gap semiconductors. Within these solids, the eigenenergy spectrum

corresponding to Eq.(17) is close to the simple Hydrogen atom Rydberg series, where the free-electron mass m is replaced by the effective mass m^* and the vacuum dielecric constant ϵ_0 has been replaced by the host solid dielectric constant ϵ, *i.e.*, $m \rightarrow m^*$ and $\epsilon_0 \rightarrow \epsilon$:

$$E_n^* = \frac{1}{n^2}\left[\frac{e^2}{\epsilon}\right]^2\left[\frac{m^*}{2\hbar^2}\right], \qquad n = 1, 2, 3, \ldots (24.a)$$

or,

$$E_n^* = \left[\frac{\epsilon_0}{\epsilon}\right]^2\left[\frac{m^*}{m}\right]E_n \ll E_n \qquad (24.b)$$

where E_n is the Hydrogen atom Rydberg series. The corresponding Bohr orbit associated with the impurity electron ground state is similarly modified to read:

$$a^* = \left[\frac{\epsilon}{e^2}\right]\left[\frac{\hbar^2}{m^*}\right], \qquad (25.a)$$

or,

$$a^* = \left[\frac{\epsilon}{\epsilon_0}\right]\left[\frac{m}{m^*}\right]a_0 \gg a_0 \qquad (25.b)$$

where a_0 is the Hydrogen atom Bohr orbit. The most spectacular success of the EMT has been in the theory of shallow donors states in GaAs. In this case, the relations Eqs.(22) and (23) have been verified experimentally to hold to a high degree of accuracy[2]. In GaAs, we have $m^* = 0.067m$ and $\epsilon = 13.1\epsilon_0$ such that the binding energy ($n = 1$ in Eq.(21)) is of the order of $|E_b| \approx 5.311$ meV. Similarly the donor ground state Bohr orbit is of the order of $a^* \approx 100$ Å. Thus, the donor ground state wavefunction extends over a large number of primitive cells in **x**-space.

Typically, for shallow donors the envelope function $F(\mathbf{k})$ extends appreciably in **k**-space only to values of the order of

$$k_0 \approx \left[\frac{1}{a^*}\right]. \qquad (26)$$

For shallow donors in GaAs, this value corresponds to approximately to 1% of the Brillouin zone. An estimate of the validity of retaining only the $n = 0$ term in Eq.(16) can be made by transforming Eq.(16) to read, for $\mathbf{g} = \mathbf{0}$,

$$F_n(\mathbf{k}) = -\left[\frac{1}{E_n(\mathbf{k}) - E}\right] \int \frac{d^3\mathbf{k}'}{(2\pi)^3} U_{n0}(\mathbf{k} - \mathbf{k}') F_0(\mathbf{k}') = 0, \tag{27}$$

which gives, in order of magnitude,

$$|F_n(\mathbf{k})| \approx \left[\frac{|E_b|}{E_g}\right]\left[\frac{a_0}{a^*}\right]|F_0(\mathbf{k})|, \tag{28}$$

where E_g is the band gap energy.

References

1. W. Kohn, *Solid-State Physics*, ed. F. Seitz and D. Turnbull, Vol. 5, (Academic, New York 1968), pp. 257-320.
2. G. E. Stilman, D. M. Larsen, C. M. Wolfe, and R. C. Brandt, *Solid State Commun.* **9**, 2245 (1971).

APPENDIX 2.2

The purpose of this appendix is twofold.

• First, we develop the effective-mass equation for shallow impurities in quantum well structures.

• Second, we indicate the procedure to solve the effective-mass equation for the impurity envelope function within a variational formalism.

2.2.1 Effective-mass theory: Quantum Well Structures

In this section of the appendix, we develop the effective-mass equation for shallow impurities in quantum well structures. Having described the effective-mass theory formalism for bulk semiconductors, we now turn to the application of this technique in the calculation of the electronic spectrum of shallow impurity states in quantum well structures. Since the bulk periodicity is broken by the introduction of an interface, the wavevector $\mathbf{k}$ that labels the Bloch state solutions $\{|n\mathbf{k}\rangle\}$ of the bulk solid is *not a good quantum number anymore.*

Consider the case for which the quantum axis normal to the interface is along the $\hat{\mathbf{z}}$ direction. The wavevector $\mathbf{k}$ can now be decomposed on a component parallel to the interface, $\mathbf{k}_{\|}$, and a quantized component normal to the interface, $\hat{\mathbf{z}}k_n$:

$$\mathbf{k} = \mathbf{k}_{\|} + \hat{\mathbf{z}}k_n, \tag{1}$$

with

$$\mathbf{k}_{\|} = \hat{\mathbf{x}}k_x + \hat{\mathbf{y}}k_y, \tag{2}$$

being the component of the wavevector $\mathbf{k}$ parallel to the interface plane. Since the translational symmetry of the bulk solid is preserved parallel to the interface, the component $\mathbf{k}_{\|}$ still remains a good quantum number to label the Bloch solutions. The component of the wavevector perpendicular to the interface, $\hat{\mathbf{z}}k_n$, is now quantized in discrete values associated to the energy levels of a particle confined within a one-dimensional quantum well. The total energy, E, of the Bloch state is also a good quantum number to label the solutions.

In the case of quantum well structures, and in the spirit of the EMA outlined in Appendix (2.1), we now label the Bloch solutions of the bulk Hamiltonian $\hat{H}^0$ by $\{|n\mathbf{k}_{\|}\rangle\}$, where the index n labels the energy subbands associated with the one-dimensional confining quantum well and $\mathbf{k}_{\|}$ labels the component of the wavevector parallel to the interface. The Schrödinger equation for the unperturbed problem is now:

$$\hat{H}^0|n\mathbf{k}_{\|}\rangle = E_n(\mathbf{k}_{\|})|n\mathbf{k}_{\|}\rangle, \tag{3}$$

where now the unperturbed Hamiltonian, $\hat{H}^0$, can be decomposed in the following way:

$$\hat{H}^0 \equiv \hat{H}^0(\mathbf{k}_{\|}) + \hat{H}^0(z). \tag{4}$$

The Hamiltonian $\hat{H}^0(\mathbf{k}_{\|})$ gives rise to a two-dimensional energy dispersion, $E^0(\mathbf{k}_{\|})$, and the Hamiltonian $\hat{H}^0(z)$ contains the confining quantum well potential, $V(z)$,

$$\hat{H}^0(z) \equiv \frac{-\hbar^2}{2m^*}\left[\frac{\partial^2}{\partial z^2}\right] + V(z). \tag{5}$$

Accordingly, the energy eigenvalue spectrum, $E_n(\mathbf{k}_{\|})$, can be decomposed in

$$E_n(\mathbf{k}_{\|}) = E^0(\mathbf{k}_{\|}) + E_n(\hat{\mathbf{z}}k_n). \tag{6}$$

The energy function $E^0(\mathbf{k}_{\|})$ represents the *two-dimensional energy dispersion relation.* The series of solutions $E_n(\hat{\mathbf{z}}k_n)$ label the *energy levels associated with*

quantum well Hamiltonian $\hat{H}^0(z)$. In the case where $V(z)$ represents a simple rectangular potential well, the discrete energy levels $E_n(\hat{\mathbf{z}}k_n)$ are of the form

$$E_n(\hat{\mathbf{z}}k_n) \equiv \frac{\hbar^2}{2m^*}{k_n}^2, \tag{7}$$

where the set of $\hat{\mathbf{z}}k_n$ represent the discrete values of the wavevector normal to the interface plane.

As seen by Eq.(6), the energy eigenvalue spectrum is dispersionless in the $\hat{\mathbf{z}}$-direction, *i.e.*, the energy function $E_n(\mathbf{k}_{\|})$ contains no k_z dependence. This is a direct consequence of the fact that we are considering a single quantum well and therefore the overlap vanishes in the $\hat{\mathbf{z}}$-direction. The energy dispersion relation, $E_n(\mathbf{k}_{\|})$, consists of a series of two-dimensional subbands, $E^0(\mathbf{k}_{\|})$, belonging to the energy levels $E_n(\hat{\mathbf{z}}k_n)$ of the quantum well.

Within the effective-mass approximation, the cell-periodic functions are assumed to remain constant in the small range of $\mathbf{k}$-space for which the envelope has large amplitude. Therefore, the Bloch solutions of Eq.(3) can approximately be written as a product:

$$|n\mathbf{k}_{\|}\rangle \approx |\mathbf{k}_{\|}\rangle|n\rangle, \tag{8.a}$$

or, in $\mathbf{x}$-representation,

$$\langle\mathbf{x}|n\mathbf{k}_{\|}\rangle \approx \exp(i\mathbf{k}_{\|}\cdot\mathbf{x}_{\|})\varphi_n(z), \tag{8.b}$$

with

$$\langle\mathbf{x}|\mathbf{k}_{\|}\rangle \equiv \exp(i\mathbf{k}_{\|}\cdot\mathbf{x}_{\|}), \tag{8.c}$$

and,

$$\langle z|n\rangle \equiv \varphi_n(z), \tag{8.d}$$

where $\mathbf{x}_{\|}$ is a two-dimensional position vector parallel to the interface plane,

$$\mathbf{x}_{\|} = \hat{\mathbf{x}}x + \hat{\mathbf{y}}y, \tag{9.a}$$

and

$$\mathbf{x} = \mathbf{x}_{\|} + \hat{\mathbf{z}} z, \tag{9.b}$$

In the well model, the functions $\varphi_n(z)$ are eigenstates of the one-dimensional operator $\hat{H}^0(z)$,

$$\hat{H}^0(z)\varphi_n(z) = \left[\frac{\hbar^2}{2m^*}{k_n}^2\right]\varphi_n(z). \tag{10}$$

As for bulk semiconductors, we must solve the Schrödinger equation for the defect wavefunction in the presence of a Coulombic potential $U(\mathbf{x})$,

$$\hat{H}|\Psi\rangle = E|\Psi\rangle, \tag{11}$$

where, as in Appendix (2.1), the Hamiltonian $\hat{H}$ is the sum of the unperturbed solid Hamiltonian , $\hat{H}^0$, plus the impurity potential, $U(\mathbf{x})$,

$$\hat{H} \equiv \hat{H}^0 + U(\mathbf{x}). \tag{12}$$

As in the case for bulk, the impurity wavefunction, $|\Psi\rangle$, is expanded on the set of Bloch solutions, $\{|n\mathbf{k}_{\|}\rangle\}$, of Eq.(3),

$$|\Psi\rangle = \sum_n \int \frac{d^2\mathbf{k}_{\|}}{(2\pi)^2} F_n(\mathbf{k}_{\|})|n\mathbf{k}_{\|}\rangle, \tag{13}$$

where the summation now runs over all the subbands n associated with the quantum well. By substitution of the expansion Eq(12) into the Schrödiger equation Eq.(10), and by projecting onto the Bloch solution $\langle n\mathbf{k}_{\|}|$, we obtain the matrix equation for the envelope function, $F_n(\mathbf{k}_{\|})$,

$$\left[E_n(\mathbf{k}_{\|}) - E\right]F_n(\mathbf{k}_{\|}) + \sum_{n'} \int \frac{d^2\mathbf{k}_{\|}'}{(2\pi)^2} \langle n\mathbf{k}_{\|}|U(\mathbf{x})|n'\mathbf{k}_{\|}'\rangle F_{n'}(\mathbf{k}_{\|}') = 0, \tag{14}$$

where

$$\langle n\mathbf{k}_{\|}|U(\mathbf{x})|n'\mathbf{k}_{\|}{}'\rangle \equiv \int d^2\mathbf{x}_{\|}.dz\langle n\mathbf{k}_{\|}|\mathbf{x}\rangle U(\mathbf{x})\langle\mathbf{x}|n'\mathbf{k}_{\|}{}'\rangle. \tag{15}$$

More explicitly, we have, using Eq.(7.b):

$$\langle n\mathbf{k}_{\|}|U(\mathbf{x})|n'\mathbf{k}_{\|}{}'\rangle = \int d^2\mathbf{x}_{\|}.dz\varphi_n^*(z)\exp(-i\mathbf{k}_{\|}\cdot\mathbf{x}_{\|})U(\mathbf{x})\varphi_{n'}(z)\exp(i\mathbf{k}_{\|}{}'\cdot\mathbf{x}_{\|}) \tag{16}$$

As in the case for bulk semiconductors, the matrix equation (14) contains a *diagonal* part:

$$\left[E^0(\mathbf{k}_{\|}) + E_n(\hat{\mathbf{z}}k_n) - E\right]F_n(\mathbf{k}_{\|})$$

since $\hat{H}^0$ is diagonal in the $\{|n\mathbf{k}_{\|}\rangle\}$-representation, and a *off-diagonal* part:

$$\sum_{n'}\int\frac{d^2\mathbf{k}_{\|}{}'}{(2\pi)^2}\langle n\mathbf{k}_{\|}|U(\mathbf{x})|n'\mathbf{k}_{\|}{}'\rangle F_{n'}(\mathbf{k}_{\|}{}'),$$

which represents the scattering between between the Bloch states $|n\mathbf{k}_{\|}\rangle$ and $|n'\mathbf{k}_{\|}{}'\rangle$ by the Coulomb potential $U(\mathbf{x})$.

2.2.2 Variational solution of the Effective-mass equations

We now develop the formalism necessary to solve the effective-mass equation Eq.(14) by a variational method.

2.2.2.1 Crystal momentum representation:

In order to obtain a variational formulation of the effective-mass equations in the crystal momentum representation (**k**-space), we first expand the two-dimensional envelope function, $F_n(\mathbf{k}_\parallel)$, on a set of orthogonal variational orbitals $\{\Xi_\mu(\mathbf{k}_\parallel)\}$ in the following way:

$$F_n(\mathbf{k}_\parallel) = \sum_\mu A_\mu^n \Xi_\mu(\mathbf{k}_\parallel). \tag{17}$$

Substituting the variational expansion Eq.(15) in the effective-mass equation Eq.(14) and projecting onto the basis function $\langle\Xi_\mu(\mathbf{k}_\parallel)|$ in $\mathbf{k}_\parallel$-space we obtain the matrix equation to be solved for the expansion coefficients A_μ^n in the $\{\Xi_\mu(\mathbf{k}_\parallel)\}$-representation,

$$\sum_{n'\mu'} \hat{H}_{nn'}^{\mu\mu'}(E) A_{\mu'}^{n'} = 0, \tag{18}$$

where the matrix elements $\hat{H}_{nn'}^{\mu\mu'}(E)$ contain the energy E and are defined to be

$$\hat{H}_{nn'}^{\mu\mu'}(E) \equiv T_{nn'}^{\mu\mu'}(E) + U_{nn'}^{\mu\mu'}, \tag{19.a}$$

where the kinetic energy term is

$$T_{nn'}^{\mu\mu'}(E) \equiv \langle\Xi_\mu(\mathbf{k}_\parallel)|\big[E_n(\mathbf{k}_\parallel) - E\big]|\Xi_\mu(\mathbf{k}_\parallel)\rangle\delta(n,n'), \tag{19.b}$$

$$T_{nn'}^{\mu\mu'}(E) \equiv \left[\int \frac{d^2\mathbf{k}_\parallel}{(2\pi)^2}\Xi_\mu^*(\mathbf{k}_\parallel)\big[E_n(\mathbf{k}_\parallel) - E\big]\Xi_{\mu'}(\mathbf{k}_\parallel)\right]\delta(n,n'), \tag{19.c}$$

and the Coulomb term is

$$U_{nn'}^{\mu\mu'} \equiv \int d^2\mathbf{x}_\parallel . dz\, \xi_\mu^*(\mathbf{x}_\parallel)\varphi_n^*(z) U(\mathbf{x}) \xi_{\mu'}(\mathbf{x}_\parallel)\varphi_{n'}(z), \tag{19.d}$$

where we have defined the two-dimensional Fourier transform

$$\xi_\mu(\mathbf{x}_\parallel) \equiv \int \frac{d^2\mathbf{k}_\parallel}{(2\pi)^2} \Xi_\mu(\mathbf{k}_\parallel) \exp(i\mathbf{k}_\parallel \cdot \mathbf{x}_\parallel). \tag{20}$$

Note that the kinetic energy term, $T_{nn'}^{\mu\mu'}(E)$, is evaluated in $\mathbf{k}$-space, whereas the Coulomb potential energy term, $U_{nn'}^{\mu\mu'}$, is evaluated in $\mathbf{x}$-space. The set of functions $\{\xi_\mu(\mathbf{x}_\parallel)\}$ is simply the two-dimensional Fourier transforms of the basis functions $\{\Xi_\mu(\mathbf{k}_\parallel)\}$ used in the crystal momentum representation of Eq.(17)

2.2.2.2 Wannier representation:

We now wish to give an equivalent expansion of the envelope functions expanded in Wannier representation ($\mathbf{x}$-space). As in Eq.(12) the defect wavefunction is expanded on the set of solutions $\{|n\mathbf{k}_\parallel\rangle\}$ corresponding to the unperturbed problem:

$$|\Psi\rangle = \sum_n \int \frac{d^2\mathbf{k}_\parallel}{(2\pi)^2} F_n(\mathbf{k}_\parallel) |n\mathbf{k}_\parallel\rangle. \tag{21}$$

by using the $\mathbf{x}$-representation of the Bloch solutions, Eq(7.b):

$$\langle \mathbf{x}|n\mathbf{k}_\parallel\rangle \approx \exp(i\mathbf{k}_\parallel \cdot \mathbf{x}_\parallel)\varphi_n(z), \tag{22}$$

we obtain

$$\langle \mathbf{x}|\Psi\rangle = \sum_n \int \frac{d^2\mathbf{k}_\parallel}{(2\pi)^2} F_n(\mathbf{k}_\parallel) \exp(i\mathbf{k}_\parallel \cdot \mathbf{x}_\parallel)\varphi_n(z). \tag{23}$$

By regrouping terms,

$$\langle \mathbf{x}|\Psi\rangle = \sum_n \left[\int \frac{d^2\mathbf{k}_\parallel}{(2\pi)^2} F_n(\mathbf{k}_\parallel) \exp(i\mathbf{k}_\parallel \cdot \mathbf{x}_\parallel) \right] \varphi_n(z), \tag{24}$$

or

$$\langle \mathbf{x}|\Psi\rangle = \sum_n F_n(\mathbf{x}_\parallel)\varphi_n(z), \tag{25}$$

where the envelope function $F_n(\mathbf{x}_\parallel)$ is the two-dimensional Fourier transform of $F_n(\mathbf{k}_\parallel)$ defined by,

$$F_n(\mathbf{x}_\parallel) \equiv \int \frac{d^2\mathbf{k}_\parallel}{(2\pi)^2} F_n(\mathbf{k}_\parallel) \exp(i\mathbf{k}_\parallel \cdot \mathbf{x}_\parallel). \tag{26}$$

As in the crystal-momentum representation, the envelope function in $\mathbf{x}$-space is expanded on the set of variational orbitals $\{\xi_\mu(\mathbf{x}_\parallel)\}$,

$$F_n(\mathbf{x}_\parallel) = \sum_\mu A_\mu^n \xi_\mu(\mathbf{x}_\parallel), \tag{27}$$

and the defect wavefunction can now be written as,

$$\langle \mathbf{x}|\Psi\rangle = \sum_n F_n(\mathbf{x}_\parallel)\varphi_n(z), \tag{28}$$

$$\langle \mathbf{x}|\Psi\rangle = \sum_{n\mu} A_\mu^n \xi_\mu(\mathbf{x}_\parallel)\varphi_n(z). \tag{29}$$

In this representation, the matrix equation to be solved for the expansion coefficients A_μ^n:

$$\sum_{n'\mu'} \hat{H}_{nn'}^{\mu\mu'}(E) A_{\mu'}^{n'} = 0, \tag{30}$$

where now the matrix elements $\hat{H}_{nn'}^{\mu\mu'}(E)$ are defined to be

$$\hat{H}_{nn'}^{\mu\mu'}(E) \equiv T_{nn'}^{\mu\mu'}(E) + U_{nn'}^{\mu\mu'}, \tag{31.a}$$

where the kinetic energy term has been Fourier transformed,

$$T_{nn'}^{\mu\mu'}(E) \equiv \langle \xi_\mu(\mathbf{x}_\parallel)|\big[E_n(\mathbf{x}_\parallel) - E\big]|\xi_\mu(\mathbf{x}_\parallel)\rangle \delta(n,n'), \tag{31.b}$$

$$T_{nn'}^{\mu\mu'}(E) \equiv \left[\int d^2\mathbf{x}_\parallel\, \xi_\mu^*(\mathbf{x}_\parallel)\big[E_n(\mathbf{x}_\parallel) - E\big] \Xi_{\mu'}(\mathbf{k}_\parallel)\right]\delta(n,n'), \tag{31.c}$$

and the Coulomb term is still given by

$$U_{nn'}^{\mu\mu'} \equiv \int d^2\mathbf{x}_{\parallel}.dz\,\xi_{\mu}^{*}(\mathbf{x}_{\parallel})\varphi_{n}^{*}(z)U(\mathbf{x})\xi_{\mu'}(\mathbf{x}_{\parallel})\varphi_{n'}(z), \tag{31.d}$$

where we have defined the two-dimensional Fourier transform of the kinetic energy term:

$$E_n(\mathbf{x}_{\parallel}) \equiv \int \frac{d^2\mathbf{k}_{\parallel}}{(2\pi)^2} E_n(\mathbf{k}_{\parallel})\exp(i\mathbf{k}_{\parallel}\cdot\mathbf{x}_{\parallel}), \tag{32.a}$$

with,

$$E_n(\mathbf{x}_{\parallel}) \equiv \frac{-\hbar^2}{2m^*}\nabla_{\mathbf{x}_{\parallel}}^2 + \frac{\hbar^2}{2m^*}{k_n}^2, \tag{32.b}$$

where $\nabla_{\mathbf{x}_{\parallel}}^2$ is a two-dimensional Laplacian operator.

Thus, diagonalization of the matrix $\hat{H}_{nn'}^{\mu\mu'}(E)$ in the representation $\{\xi_{\mu}(\mathbf{x}_{\parallel})\}$, yields the energy eigenvalues E, and the energy eigenstates through the expansion

$$\langle\mathbf{x}|\Psi\rangle = \sum_{n\mu} A_{\mu}^{n}\xi_{\mu}(\mathbf{x}_{\parallel})\varphi_{n}(z). \tag{33}$$

APPENDIX 2.3

Hamiltonian for Shallow Donors in $Ga_{1-x}Al_xAs$-GaAs-$Ga_{1-x}Al_xAs$ Quantum Well Structures

The purpose of this appendix is to give an explicit expression for the Hamiltonian for a shallow Coulombic donor in $Ga_{1-x}Al_xAs$-GaAs-$Ga_{1-x}Al_xAs$ quantum well structures.

The effective-mass Hamiltonian corresponding to a Coulomb center located at a distance c from the center of a finite quantum well of width $2a$ along the $\hat{\mathbf{z}}$ direction (the $\hat{\mathbf{z}}$-axis is normal to the interface plane) and height V_0 (see Figure 1 for geometry) is:

$$\hat{H}(1) = \frac{-\hbar^2}{2m_1^*}\nabla_{\mathbf{x}}^2 + U_1(\mathbf{x}) \qquad \ldots\text{in region (1),}(1.a)$$

$$\hat{H}(2) = \frac{-\hbar^2}{2m_2^*}\nabla_{\mathbf{x}}^2 + U_2(\mathbf{x}) + V_0 \qquad \ldots\text{in region (2),}(1.b)$$

$$\hat{H}(3) = \frac{-\hbar^2}{2m_2^*}\nabla_{\mathbf{x}}^2 + U_3(\mathbf{x}) + V_0 \qquad \ldots\text{in region (3),}(1.c)$$

where m_1^* refers to the bulk GaAs (well material) effective mass and m_2^* refers to the interpolated effective mass in $Ga_{1-x}Al_xAs$ (barrier material). Since the bulk dielectric constants of GaAs and $Ga_{1-x}Al_xAs$, ϵ_1 and ϵ_2 respectively, differ slightly, the Hamiltonian must include terms due to electrostatic image charges. The potentials $U_1(\mathbf{x})$, $U_2(\mathbf{x})$ and $U_3(\mathbf{x})$ represent the Coulomb interaction between

the electron and the impurity ion as well as the ion image charge. When the origin is taken to be on the ionized donor, the left and right boundaries of the quantum well are respectively $z_0 = -[a + c]$ and $z_0 = [a - c]$. We let the dielectric mismatch between GaAs and $Ga_{1-x}Al_xAs$ be expressed as:

$$p \equiv \frac{[\epsilon_1 - \epsilon_2]}{[\epsilon_1 + \epsilon_2]}, \tag{2.a}$$

$$p' \equiv \frac{2\epsilon_1}{[\epsilon_1 + \epsilon_2]}, \tag{2.b}$$

and the positions of the ion image charges along the $\hat{\mathbf{z}}$-axis to be:

$$z_0^+(n) = 2\left(\left(n - \left[\frac{n+1}{2}\right]\right)(a+c) + \left[\frac{n+1}{2}\right](a-c)\right), \tag{3.a}$$

$$z_0^-(n) = -2\left(\left[\frac{n+1}{2}\right](a+c) + \left(n - \left[\frac{n+1}{2}\right]\right)(a-c)\right), \tag{3.b}$$

where

$$[x] \equiv \textit{integer part of } x. \tag{3.c}$$

Letting

$$\rho = \sqrt{x^2 + y^2}, \tag{4.a}$$

and

$$|\mathbf{x}| = \sqrt{\rho^2 + z^2}, \tag{4.b}$$

the potential energy in region (1) can be written as:

$$U_1(\mathbf{x}) = -\frac{e^2}{\epsilon_1 |\mathbf{x}|} + v_1^+(\mathbf{x}) + v_1^-(\mathbf{x}), \tag{4.c}$$

where

$$v_1^+(\mathbf{x}) = \left[-\frac{e^2}{\epsilon_1}\right] \sum_{n=1}^{\infty} p^n \left[\rho^2 + \left[z - z_0^+(n)\right]^2\right]^{-1/2}, \tag{4.d}$$

$$v_1^-(\mathbf{x}) = \left[-\frac{e^2}{\epsilon_1}\right] \sum_{n=1}^{\infty} p^n \left[\rho^2 + \left[z - z_0^-(n)\right]^2\right]^{-1/2}, \qquad (4.e)$$

for the electron-ion potential.

In region (2), the potential energy can be expressed as:

$$U_2(\mathbf{x}) = \left[-\frac{e^2}{\epsilon_2}\right] p' \sum_{n=0}^{\infty} p^n \left[\rho^2 + \left[z - z_0^+(n)\right]^2\right]^{-1/2}, \qquad (4.f)$$

for the electron-ion potential.

In region (3), the potential energy can be expressed as:

$$U_3(\mathbf{x}) = \left[-\frac{e^2}{\epsilon_2}\right] p' \sum_{n=0}^{\infty} p^n \left[\rho^2 + \left[z - z_0^-(n)\right]^2\right]^{-1/2}, \qquad (4.g)$$

for the electron-ion potential.

APPENDICES

CHAPTER 3

ELECTRONIC TRANSPORT THROUGH SEMICONDUCTOR DOUBLE HETEROJUNCTION STRUCTURES

APPENDIX 3.1

The purpose of this appendix is threefold.

- First, we develop the empirical tight-binding theory for bulk solid.
- Second, we study the the special case of zincblende semiconductors.
- Finally, we list the set of empirical tight-binding interactions used for GaAs and AlAs.

3.1.1 Empirical Tight-binding Theory of Bulk Solids

In this part of the appendix, we describe the empirical tight-binding method used to provide a description of the electronic band structure of a solid. This method was first suggested by Bloch[1] in 1928. In this method, the set of Bloch solutions, $\{|n\mathbf{k}\rangle\}$, associated with the energy eigenvalue spectrum $E_n(\mathbf{k})$ forming the solid band structure,

$$\hat{H}_0|n\mathbf{k}\rangle = E_n(\mathbf{k})|n\mathbf{k}\rangle, \tag{1}$$

is expanded in a Wannier representation consisting of a *set of Bloch sums*, $\{|\alpha\nu;\mathbf{k}\rangle\}$, in the form:

$$|n\mathbf{k}\rangle = \sum_{\alpha\nu} C(\alpha\nu;n\mathbf{k})|\alpha\nu;\mathbf{k}\rangle, \tag{2}$$

The Bloch sums $\{|\alpha\nu;\mathbf{k}\rangle\}$ consist of a sum of atomic orbitals $\{|\alpha\nu;\mathbf{R}\rangle\}$ located within the primitive cell labelled by $\mathbf{R}$ and modulated by the appropriate Bloch factor, $\exp(i\mathbf{k}\cdot\mathbf{R})$,

$$|\alpha\nu;\mathbf{k}\rangle \equiv \frac{1}{\sqrt{N}}\sum_{\mathbf{R}} \exp(i\mathbf{k}\cdot\mathbf{R})|\alpha\nu;\mathbf{R}\rangle, \tag{3}$$

where $|\alpha\nu;\mathbf{R}\rangle$ consists of an atomic orbital of symmetry α on an atom of type ν within the primitive cell labelled by the translation vector $\mathbf{R}$. N is the number of primitive cells in the lattice. More explicitly, we write,

$$\langle\mathbf{x}|\alpha\nu;\mathbf{R}\rangle \equiv \phi_{\alpha\nu}(\mathbf{x}-\mathbf{d}_\nu-\mathbf{R}), \tag{4}$$

where $\phi_{\alpha\nu}(\mathbf{x}-\mathbf{d}_\nu-\mathbf{R})$ is an atomic orbital of symmetry α on an atom of type ν located at the position $\mathbf{d}_\nu$ within the primitive cell labelled by the translation vector $\mathbf{R}$. The set of vectors $[\mathbf{R},\mathbf{d}_\nu]$ spans the whole three-dimensional crystal.

When the local orbital representation, $\{|\alpha\nu;\mathbf{R}\rangle\}$, is used, the Schrödinger equation Eq.(1) for the Bloch solutions $\{|n\mathbf{k}\rangle\}$ can be transformed into a generalized eigenvalue problem of the form

$$\sum_{\alpha'\nu'}\left[\hat{H}_0(\alpha\nu,\alpha'\nu';\mathbf{k})-E_n(\mathbf{k})S(\alpha\nu,\alpha'\nu';\mathbf{k})\right]C(\alpha'\nu';n\mathbf{k})=0, \tag{5}$$

where the *Hamiltonian matrix elements* $\hat{H}_0(\alpha\nu,\alpha'\nu';\mathbf{k})$ are defined to be:

$$\hat{H}_0(\alpha\nu,\alpha'\nu';\mathbf{k}) \equiv \frac{1}{N}\sum_{\mathbf{R}}\exp(i\mathbf{k}\cdot\mathbf{R})\hat{H}_0(\alpha\nu,\alpha'\nu';\mathbf{R}), \tag{6.a}$$

and the *overlap matrix elements* $S(\alpha\nu,\alpha'\nu';\mathbf{k})$ are defined to be:

$$S(\alpha\nu,\alpha'\nu';\mathbf{k}) \equiv \frac{1}{N}\sum_{\mathbf{R}}\exp(i\mathbf{k}\cdot\mathbf{R})S(\alpha\nu,\alpha'\nu';\mathbf{R}). \tag{6.b}$$

In Eq.(6) the matrix elements $\hat{H}_0(\alpha\nu,\alpha'\nu';\mathbf{R})$ and $S(\alpha\nu,\alpha'\nu';\mathbf{R})$ are simply the *Hamiltonian* matrix elements and the *overlap* matrix elements between two local orbitals $|\alpha\nu;\mathbf{R}\rangle$ and $|\alpha'\nu';\mathbf{R}'\rangle$, *i.e.*,

$$\hat{H}_0(\alpha\nu,\alpha'\nu';\mathbf{R}-\mathbf{R}') \equiv \langle\alpha\nu;\mathbf{R}|\hat{H}_0|\alpha'\nu';\mathbf{R}'\rangle, \tag{7.a}$$

or,

$$\hat{H}_0(\alpha\nu,\alpha'\nu';\mathbf{R}-\mathbf{R}') \equiv \int d^3\mathbf{x}\,\phi^*_{\alpha\nu}(\mathbf{x}-\mathbf{d}_\nu-\mathbf{R})\hat{H}_0\phi_{\alpha'\nu'}(\mathbf{x}-\mathbf{d}_{\nu'}-\mathbf{R}'), \tag{7.b}$$

and

$$S(\alpha\nu, \alpha'\nu'; \mathbf{R} - \mathbf{R}') \equiv \langle \alpha\nu; \mathbf{R} | \alpha'\nu'; \mathbf{R}' \rangle, \tag{7.c}$$

or,

$$S(\alpha\nu, \alpha'\nu'; \mathbf{R} - \mathbf{R}') \equiv \int d^3\mathbf{x} \phi^*_{\alpha\nu}(\mathbf{x} - \mathbf{d}_\nu - \mathbf{R}) \phi_{\alpha'\nu'}(\mathbf{x} - \mathbf{d}_{\nu'} - \mathbf{R}'). \tag{7.d}$$

As seen by Eq.(5) the size of the matrix to be diagonalized is $N_\alpha \cdot N_\nu$ where N_α is the number of atomic orbitals per atom and N_ν is the number of atoms in the primitive cell. Thus, *the order of the secular matrix is equal to the total number of orbitals in the primitive cell.* Solution of the matrix equation Eq.(5) in the local orbital representation $\{|\alpha\nu; \mathbf{R}\rangle\}$ yields the energy bands $E_n(\mathbf{k})$ and the Bloch functions $\{|n\mathbf{k}\rangle\}$ in terms of the expansion coefficients $C(\alpha\nu; n\mathbf{k})$,

$$|n\mathbf{k}\rangle = \sum_{\alpha\nu} C(\alpha\nu; n\mathbf{k}) |\alpha\nu; \mathbf{k}\rangle, \tag{8.a}$$

or, using Eq(3),

$$|n\mathbf{k}\rangle = \frac{1}{\sqrt{N}} \sum_{\alpha\nu} C(\alpha\nu; n\mathbf{k}) \left[\sum_{\mathbf{R}} \exp(i\mathbf{k} \cdot \mathbf{R}) |\alpha\nu; \mathbf{R}\rangle \right]. \tag{8.b}$$

In the expansion of the Bloch sums $\{|\alpha\nu; \mathbf{k}\rangle\}$ in terms if the local atomic orbitals, $\{|\alpha\nu; \mathbf{R}\rangle\}$,

$$|\alpha\nu; \mathbf{k}\rangle = \frac{1}{\sqrt{N}} \sum_{\mathbf{R}} \exp(i\mathbf{k} \cdot \mathbf{R}) |\alpha\nu; \mathbf{R}\rangle, \tag{9}$$

the sum over the translational lattice vectors $\mathbf{R}$ must be carried to convergence, at each wavevector $\mathbf{k}$. As it stands, the direct evaluation of the Hamiltonian and overlap matrix elements, $\hat{H}_0(\alpha\nu, \alpha'\nu'; \mathbf{R} - \mathbf{R}')$ and $S(\alpha\nu, \alpha'\nu'; \mathbf{R} - \mathbf{R}')$, is too cumbersome due to the large number of multicenter integrals.

However, Slater and Koster[2] suggested that the method outlined above, also known as the linear combination of atomic orbitals method (LCAO), could be used effectively as an *interpolation scheme.* If, for example, more powerful band structure calculation techniques are used to obtain the solutions of Eq.(1) at high-symmetry **k**-points in the Brillouin zone, then the LCAO matrix elements $\hat{H}_0(\alpha\nu, \alpha'\nu'; \mathbf{R} - \mathbf{R}')$ can be treated as parameters to be fitted to the accurately known energies $E_n(\mathbf{k})$ at these high-symmetry points. Thus when the Hamiltonian matrix elements $\hat{H}_0(\alpha\nu, \alpha'\nu'; \mathbf{R} - \mathbf{R}')$ are treated as *disposable parameters*, a simple diagonalization of the matrix equation Eq.(5) will give the energy eigenvalues $E_n(\mathbf{k})$ and the Bloch functions $\{|n\mathbf{k}\rangle\}$ in the local orbital representation, $\{|\alpha\nu; \mathbf{R}\rangle\}$. The method outlined above is referred to as the empirical tight-binding method (ETBM) due to the fact that the matrix elements $\hat{H}_0(\alpha\nu, \alpha'\nu'; \mathbf{R} - \mathbf{R}')$ appearing in the matrix equation Eq.(5) are treated as parameters to be fitted to energy eigenvalues obtained by more detailed calculations at high-symmetry **k**-points in the Brillouin zone.

We now discuss some of the basic assumptions of the ETBM when used in the study of the electronic structure of tetrehedral semiconductors.

(i) The basis set $\{|\alpha\nu; \mathbf{R}\rangle\}$ used is usually restricted to a small number of orbital symmetries α on each atom ν. Typically four orbitals per atom are used, *i.e.*, $\alpha = s, p_x, p_y, p_z$. This set is often referred to as a *minimum basis set*, or the sp^3 model. The adequacy of the use of one s orbital and three p orbital has been examined in detail by Kane[3] and Chadi[4]. Both of these authors used a pseudopotential Hamiltonian and verified the minimum number of LCAO necessary to reproduce the energy band structure $E_n(\mathbf{k})$ obtained in the plane-wave-basis calculation. They found that the use of s and p orbitals is quite adequate for the valence band and the lowest-lying conduction bands. In the calculations presented

below, the minimum basis set mentioned above is increased so as to include an excited s-like orbital denoted s^*. We therefore use five orbitals per atom in the sp^3s^* model.

(ii) Orbitals centered on different atoms are assumed to be orthonormal, *i.e.*,

$$S(\alpha\nu, \alpha'\nu'; \mathbf{R} - \mathbf{R}') = \delta(\alpha, \alpha')\delta(\nu, \nu')\delta^3(\mathbf{R} - \mathbf{R}'), \tag{10.a}$$

so that

$$S(\alpha\nu, \alpha'\nu'; \mathbf{k}) = \delta(\alpha, \alpha')\delta(\nu, \nu'). \tag{10.b}$$

The neglect of the overlap matrix elements has be justified by Anderson[5] in the case of molecular systems. There exists a set of orbitals which represent the *exact* solutions of the one-electron problem. These orbitals are *not orthogonal* but nevertheless satisfy a secular equation of the form Eq.(5) with a *diagonal* overlap matrix $S(\alpha\nu, \alpha'\nu'; \mathbf{k})$. Of course, in that case the Hamiltonian matrix $\hat{H}_0(\alpha\nu, \alpha'\nu'; \mathbf{k})$ appearing in Eq.(5) is not the matrix elements of the true Hamiltonian, but rather those of a non-Hermitian pseudo Hamiltonian. It it therefore justified to *assume* that $S(\alpha\nu, \alpha'\nu'; \mathbf{k}) = \delta(\alpha, \alpha')\delta(\nu, \nu')$, provided that the Hamiltonian matrix $\hat{H}_0(\alpha\nu, \alpha'\nu'; \mathbf{k})$ is not interpreted as the matrix elements of the true Hamiltonian.

(iii) Only first (and sometimes second) nearest-neighbors are retained in the construction of the Bloch sums $|\alpha\nu; \mathbf{k}\rangle$ in Eq.(2). This implies that the summations of Eqs.(6) neglect the interactions $\hat{H}_0(\alpha\nu, \alpha'\nu'; \mathbf{R})$ and the overlap $S(\alpha\nu, \alpha'\nu'; \mathbf{R})$ after the first or the second nearest-neighbors shells. Again this can be justified partly if we regard the interactions $\hat{H}_0(\alpha\nu, \alpha'\nu'; \mathbf{R})$ as effective average interactions rather than as the matrix elements of the true Hamiltonian $\hat{H}_0$. In the applications discussed below, only first nearest-neighbors interactions are retained within the sp^3s^* model. Furthermore, it is assumed that the Hamiltonian has *local cylindrical symmetry about the axis connecting pairs of interacting atoms.*

3.1.2 Application to Zincblende Semiconductors

As an application of the ETBM as a method of band structure calculations, we consider more specifically the case of semiconductors with the zincblende structure. The zincblende structure consists of a *face-centered space lattice* with primitive translation vectors

$$\mathbf{a}_1 = \left[\frac{a}{2}\right](\hat{\mathbf{x}} + \hat{\mathbf{y}}), \tag{11.a}$$

$$\mathbf{a}_2 = \left[\frac{a}{2}\right](\hat{\mathbf{y}} + \hat{\mathbf{z}}), \tag{11.b}$$

$$\mathbf{a}_3 = \left[\frac{a}{2}\right](\hat{\mathbf{x}} + \hat{\mathbf{z}}), \tag{11.c}$$

where a is the length of the side of the conventional cubic unit cell. The reciprocal lattice is body-centered cubic with primitive reciprocal lattice vectors

$$\mathbf{b}_1 = \left[\frac{1}{2}\right]\left[\frac{4\pi}{a}\right](+\hat{\mathbf{x}} + \hat{\mathbf{y}} - \hat{\mathbf{z}}), \tag{12.a}$$

$$\mathbf{b}_2 = \left[\frac{1}{2}\right]\left[\frac{4\pi}{a}\right](+\hat{\mathbf{x}} - \hat{\mathbf{y}} + \hat{\mathbf{z}}), \tag{12.b}$$

$$\mathbf{b}_3 = \left[\frac{1}{2}\right]\left[\frac{4\pi}{a}\right](-\hat{\mathbf{x}} + \hat{\mathbf{y}} + \hat{\mathbf{z}}), \tag{12.c}$$

where $[4\pi/a]$is the length of the conventional cubic unit cell in $\mathbf{k}$-space.

In the case of the zincblende structure, the primitive cell contains two different basis atoms with coordinates

$$\mathbf{d}_a = \mathbf{0}, \tag{13.a}$$

and,

$$\mathbf{d}_c = \left[\frac{a}{4}\right](\hat{\mathbf{x}} + \hat{\mathbf{y}} + \hat{\mathbf{z}}), \tag{13.b}$$

where $\mathbf{d}_a$ and $\mathbf{d}_c$ represent the coordinates of the anion (Ga,Al,In...) and the cation (As,Sb,...), respectively. The anion has been arbitrarily placed at the origin of the

primitive cell. Since we are considering five atomic orbitals per atom,

$$\alpha \equiv s, s^*, p_x, p_y, p_z, \tag{14}$$

then we have ten atomic orbitals per primitive cell and the matrix equation Eq.(5) is a 10×10.

Let $\mathbf{C}(\nu; n\mathbf{k})$ represent the five-dimensional column vector consisting of the coefficients $C(\alpha\nu; n\mathbf{k})$ associated with the basis atom of type ν, *i.e.*,

$$\mathbf{C}(\nu; n\mathbf{k}) \equiv C(\alpha\nu; n\mathbf{k}), \qquad \alpha \equiv s, s^*, p_x, p_y, p_z. \tag{15.a}$$

And let $\mathbf{H}(\nu\nu'; \mathbf{k})$ represent the 5×5 tight-binding interaction matrix consisting of the interactions $\hat{H}_0(\alpha\nu, \alpha'\nu'; \mathbf{k})$, between the atoms ν and ν', *i.e.*,

$$\mathbf{H}(\nu\nu'; \mathbf{k}) \equiv \hat{H}_0(\alpha\nu, \alpha'\nu'; \mathbf{k}), \qquad \alpha', \alpha \equiv s, s^*, p_x, p_y, p_z. \tag{15.b}$$

Then, the secular equation Eq.(5) can be written in the following matrix form

$$\begin{bmatrix} \mathbf{H}(aa; \mathbf{k}) & \mathbf{H}(ac; \mathbf{k}) \\ \mathbf{H}(ca; \mathbf{k}) & \mathbf{H}(cc; \mathbf{k}) \end{bmatrix} \cdot \begin{bmatrix} \mathbf{C}(a; n\mathbf{k}) \\ \mathbf{C}(c; n\mathbf{k}) \end{bmatrix} = E_n(\mathbf{k}) \begin{bmatrix} \mathbf{C}(a; n\mathbf{k}) \\ \mathbf{C}(c; n\mathbf{k}) \end{bmatrix} \tag{16}$$

In Eq.(16) the subscripts $\nu = a$ and $\nu = c$ refer to the *anion* and *cation*, respectively.

3.1.3 Empirical Tight-Binding Parameters

We now present the empirical tight-binding model used to obtain the electronic band structure of GaAs and $Ga_{1-x}Al_xAs$. As mentioned above the model uses five orbitals per atom and tight-binding interactions up to first nearest-neighbors are retained. The sp^3s^* used here is similar to that of Vogl *et al.*[4].

Tables 1 and 2 show the set of empirical tight-binding Hamiltonian matrix elements for GaAs and AlAs in the sp^3s^* model. The interactions showed stand for the following matrix elements:

$$E(s;\nu) \equiv \langle s\nu;\mathbf{R}|\hat{H}_0|s\nu;\mathbf{R}\rangle, \tag{17.a}$$

$$E(p;\nu) \equiv \langle p_x\nu;\mathbf{R}|\hat{H}_0|p_x\nu;\mathbf{R}\rangle, \tag{17.b}$$

$$E(s^*;\nu) \equiv \langle s^*\nu;\mathbf{R}|\hat{H}_0|s^*\nu;\mathbf{R}\rangle, \tag{17.c}$$

$$V(s;s) \equiv 4\langle sa;\mathbf{R}|\hat{H}_0|sc;\mathbf{R}\rangle, \tag{17.d}$$

$$V(p_x;p_x) \equiv 4\langle p_x a;\mathbf{R}|\hat{H}_0|p_x c;\mathbf{R}\rangle, \tag{17.e}$$

$$V(p_x;p_y) \equiv 4\langle p_x a;\mathbf{R}|\hat{H}_0|p_y c;\mathbf{R}\rangle, \tag{17.f}$$

$$V(s,a;p,c) \equiv 4\langle sa;\mathbf{R}|\hat{H}_0|p_x c;\mathbf{R}\rangle, \tag{17.g}$$

$$V(s^*,a;p,c) \equiv 4\langle s^* a;\mathbf{R}|\hat{H}_0|p_x c;\mathbf{R}\rangle, \tag{17.h}$$

$$V(p,a;s^*,c) \equiv 4\langle p_x a;\mathbf{R}|\hat{H}_0|s^* c;\mathbf{R}\rangle, \tag{17.i}$$

where $\nu = a, c$ for the anion (As) or cation (Ga,Al), and $\mathbf{R}$ labels the primitive cell. Thus, we have a total of 13 parameters: 6 on-site energies, $E(s,a)$, $E(s,c)$, $E(s^*,a)$, $E(s^*,c)$, $E(p,a)$, and $E(p,s)$; and 7 transfer tight-binding matrix elements, $V(s;s)$, $V(p_x,p_x)$, $V(p_x,p_y)$, $V(s,a;p_x,c)$, $V(p_x,a;s,c)$, $V(s^*,a;p_x,c)$, and $V(p_x,a;s^*,c)$.

In Eq.(6), the matrices $\mathbf{H}(aa;\mathbf{k})$ and $\mathbf{H}(cc;\mathbf{k})$ represent the anion-anion and cation-cation self energies, respectively, and the matrices $\mathbf{H}(ac;\mathbf{k})$ and $\mathbf{H}(ca;\mathbf{k})$

Interaction	(eV)
$E(s;a)$	-8.3431
$E(p;a)$	1.0414
$E(s;c)$	-2.7150
$E(p;c)$	3.6686
$E(s^*;a)$	8.5914
$E(s^*;c)$	6.7386
$V(s;s)$	-6.4513
$V(p_x;p_x)$	1.9546
$V(p_x;p_y)$	5.0779
$V(s,a;p,c)$	4.4800
$V(s,c;p,a)$	5.7839
$V(s^*,a;p,c)$	4.8422
$V(p,a;s^*,c)$	4.8077

Table 1. Empirical tight-binding interactions for GaAs. The model used includes first nearest-neighbors interactions and five atomic orbitals per atoms, sp^3s^*. The notation for the tight-binding interactions is described in the text.

Interaction	(eV)
$E(s;a)$	-7.5273
$E(p;a)$	0.9833
$E(s;c)$	-1.0790
$E(p;c)$	3.5867
$E(s^*;a)$	7.4833
$E(s^*;c)$	6.7267
$V(s;s)$	-6.6642
$V(p_x;p_x)$	1.8780
$V(p_x;p_y)$	4.2919
$V(s,a;p,c)$	5.1106
$V(s,c;p,a)$	5.4965
$V(s^*,a;p,c)$	4.5216
$V(p,a;s^*,c)$	4.9950

Table 2. Empirical tight-binding interactions for AlAs. The model used includes first nearest-neighbors interactions and five atomic orbitals per atoms, sp^3s^*. The notation for the tight-binding interactions is described in the text.

represent the anion-cation and cation-anion transfer interaction matrices, respectively. Diagonalization of the matrix Eq.(16) for each wavevector $\mathbf{k}$ yields the energy eigenvalues $E_n(\mathbf{k})$ and the expansion coefficients $C(\alpha\nu; n\mathbf{k})$ of the Bloch states $\{|n\mathbf{k}\rangle\}$ in terms of the Bloch sums $\{|\alpha\nu; \mathbf{k}\rangle\}$,

$$|n\mathbf{k}\rangle = \sum_{\alpha\nu} C(\alpha\nu; n\mathbf{k})|\alpha\nu; \mathbf{k}\rangle. \tag{18}$$

In the case of the alloy $Ga_{1-x}Al_xAs$, we use the *virtual crystal approximation*. In this method the empirical tight-binding interactions are *weighted according to the alloy composition* x.

References

1. F. Bloch, *Z. Physik* **52**, 555 (1928).

2. J. C. Slater and G. F. Koster, *Phys. Rev.* **94**, 1498 (1954).

3. E. O. Kane, *Phys. Rev.* **B 13**, 3478 (1976).

4. P. Vogl, H. P. Hjalmarson, and J. D. Dow, *J. Phys. Chem. Solids* **44**, 365 (1983).

APPENDIX 3.2

The purpose of this appendix is twofold.

• In the first part of this appendix, we give a detailed derivation of the *transfer matrix method* used in the sudy of interfaces systems.

• In the second part, we make the distinction between *layer orbitals* and *sublayer orbitals.*

3.2.1 Transfer Matrix Theory

The purpose of this part of the appendix is to give a detailed derivation of the transfer matrix method as used within the empirical tight-binding theory.

Interface systems are most easily studied in terms of planar orbitals. Before defining the planar orbital, let us first introduce the notion of sublayer. A sublayer consists of the *smallest number of adjacent atomic planes parallel to the interface such that each sublayer interacts with the same number of other sublayers on each side.* In the cases treated here, *i.e.*, (100) and (111) interfaces, we can view the sublayer as being a *single atomic plane* (either a anion atomic plane or a cation atomic plane).

Let us define a *planar orbital* corresponding to an atomic orbital of symmetry α within the sublayer labelled by σ to be the two-dimensional Bloch sum

$$|\alpha\sigma;\mathbf{k}_{\|}\rangle \equiv \frac{1}{\sqrt{N_{\|}}}\sum_{\mathbf{R}_{\|}} \exp(i\mathbf{k}_{\|}\cdot\mathbf{R}_{\|})|\alpha;\mathbf{R}_{\|}\sigma\rangle, \tag{1}$$

where $\mathbf{R}_{\|}$ is a two-dimensional primitive lattice translation vector and σ labels the sublayer in the $\hat{\mathbf{z}}$-direction. $N_{\|}$ is the number of two-dimensional primitive cells in

the crystal. Let there be N_α orbitals of symmetry α per two-dimensional primitive cell.

The localized orbital $|\alpha;\mathbf{R}_\parallel\sigma\rangle$ is simply

$$\langle\mathbf{x}|\alpha;\mathbf{R}_\parallel\sigma\rangle \equiv \phi_\alpha(\mathbf{x}-\mathbf{R}_\parallel-\mathbf{d}_\alpha{}^\sigma), \tag{2}$$

where $\phi_\alpha(\mathbf{x}-\mathbf{R}_\parallel-\mathbf{d}_\alpha{}^\sigma)$ is the local orbital of atomic symmetry α located at position $\mathbf{d}_\alpha{}^\sigma$ within the two-dimensional primitive cell labelled by $\mathbf{R}_\parallel$ and in the sublayer σ. The position $\mathbf{d}_\alpha{}^\sigma$ can be decomposed into a component *parallel* to the interface and a component *perpendicular* to the interface. Thus, we write

$$\mathbf{d}_\alpha{}^\sigma \equiv \mathbf{f}_\alpha{}^\sigma + \hat{\mathbf{z}}\sigma a_0, \tag{3}$$

where $\mathbf{f}_\alpha{}^\sigma$ is a two-dimensional position vector parallel to the interface and $\hat{\mathbf{z}}\sigma a_0$ is the component perpendicular to the interface which specifies the distance of the sublayer σ from the origin. The sublayer is labelled by σ, and a_0 is the distance separating adjacent sublayers. The set of vectors $\left[\mathbf{R}_\parallel, \mathbf{d}_\alpha{}^\sigma\right]$ spans the whole three-dimensional crystal.

Having defined the *two-dimensional Bloch sum*, $|\alpha\sigma;\mathbf{k}_\parallel\rangle$, it is clear that we can also define the *three-dimensional Bloch sum* $|\alpha;\mathbf{k}_\parallel k_z\rangle$ corresponding to the wavevector

$$\mathbf{k} \equiv \mathbf{k}_\parallel + \hat{\mathbf{z}}k_z, \tag{4}$$

by summing over the sublayers σ with the appropriate Bloch factors $\exp(ik_z\sigma a_0)$,

$$|\alpha;\mathbf{k}_\parallel k_z\rangle \equiv \frac{1}{\sqrt{N_z}}\sum_\sigma \exp(ik_z\sigma a_0)|\alpha\sigma;\mathbf{k}_\parallel\rangle, \tag{5.a}$$

or, using Eq.(2)

$$|\alpha;\mathbf{k}_\parallel k_z\rangle \equiv \frac{1}{\sqrt{N}}\sum_\sigma \exp(ik_z\sigma a_0)\sum_{\mathbf{R}_\parallel}\exp(i\mathbf{k}_\parallel\cdot\mathbf{R}_\parallel)|\alpha;\mathbf{R}_\parallel\sigma\rangle, \tag{5.b}$$

where $N \equiv N_{\|} \cdot N_z$ is the total number of primitive cells in the crystal. Eq.(5.b) simply corresponds to the bulk case for the Bloch sum

$$|\alpha\nu;\mathbf{k}\rangle \equiv \frac{1}{\sqrt{N}} \sum_{\mathbf{R}} \exp(i\mathbf{k}\cdot\mathbf{R})|\alpha\nu;\mathbf{R}\rangle, \tag{6}$$

where the summation has been broken into a two-dimensional part $\sum_{\mathbf{R}_{\|}}$ and a one-dimensional part $\sum_{\sigma}$.

Let us define $|\Psi(\mathbf{k}_{\|}E;\sigma)\rangle$ as the tight-binding electronic wavefunction of the Hamiltonian $\hat{H}$, evaluated on the sublayer σ. The wavefunction $|\Psi(\mathbf{k}_{\|}E;\sigma)\rangle$, corresponding to a given parallel wavevector $\mathbf{k}_{\|}$ and energy E and evaluated on the sublayer σ is simply constructed out of a *linear combination of the two-dimensional planar orbitals*, $\{|\alpha\sigma;\mathbf{k}_{\|}\rangle\}$, as defined by Eq (4). We write the expansion of $|\Psi(\mathbf{k}_{\|}E;\sigma)\rangle$ as

$$|\Psi(\mathbf{k}_{\|}E;\sigma)\rangle \equiv \sum_{\alpha=1}^{N_a} C(\alpha\sigma;\mathbf{k}_{\|})|\alpha\sigma;\mathbf{k}_{\|}\rangle, \tag{7}$$

where the expansion coefficients $C(\alpha\sigma;\mathbf{k}_{\|})$ indicate the degree of mixing of the planar orbitals $\{|\alpha\sigma;\mathbf{k}_{\|}\rangle\}$. Of course, in order to obtain the wavefunction over all space, we must add the contribution on each individual sublayer,

$$|\Psi(\mathbf{k}_{\|}E)\rangle \equiv \sum_{\sigma} |\Psi(\mathbf{k}_{\|}E;\sigma)\rangle, \tag{8.a}$$

or, using Eq.(7),

$$|\Psi(\mathbf{k}_{\|}E)\rangle \equiv \sum_{\sigma} \left[\sum_{\alpha=1}^{N_a} C(\alpha\sigma;\mathbf{k}_{\|})|\alpha\sigma;\mathbf{k}_{\|}\rangle \right]. \tag{8.b}$$

We now introduce the transfer matrix as it is proposed by Schulman and Chang[1]. Let N_σ be the number of sublayers that interact on one side with a given

sublayer, *i.e.*, a given sublayer σ has non-zero tight binding matrix elements only with N_σ other sublayers on one side.

Let us solve the Schrödinger equation on a given sublayer σ,

$$\hat{H}|\Psi(\mathbf{k}_\parallel E;\sigma)\rangle = E|\Psi(\mathbf{k}_\parallel E;\sigma)\rangle, \tag{9}$$

where the wavefunction $|\Psi(\mathbf{k}_\parallel E;\sigma)\rangle$ on the sublayer σ is expanded in terms of layer orbitals $\{|\alpha\sigma;\mathbf{k}_\parallel\rangle\}$ as in Eq.(3). The Hamiltonian $\hat{H}$ is the interface Hamiltonian.

Let us now define the $[N_\alpha \cdot N_\alpha]$ tight-binding matrix that couples the layer orbitals on sublayers σ and σ' as $\mathbf{H}_E(\sigma,\sigma';\mathbf{k}_\parallel)$ with matrix elements

$$\left[\mathbf{H}_E(\sigma,\sigma';\mathbf{k}_\parallel)\right]_{\alpha,\alpha'} \equiv \langle\alpha\sigma;\mathbf{k}_\parallel|\left[\hat{H}-E\right]|\alpha'\sigma';\mathbf{k}_\parallel\rangle. \tag{10}$$

Let us also define $\mathbf{C}(\sigma;\mathbf{k}_\parallel)$ be the column vector of dimension N_α corresponding to the coefficients $C(\alpha\sigma;\mathbf{k}_\parallel)$ on sublayer σ. With these definitions, Schrödinger equation Eq.(9) can be cast into a matrix form

$$\sum_{m=-N_\sigma}^{N_\sigma} \mathbf{H}_E(\sigma,\sigma+m;\mathbf{k}_\parallel)\cdot\mathbf{C}(\sigma+m;\mathbf{k}_\parallel) = 0, \tag{11}$$

where the summation is over all the sublayer m that interacts with a given sublayer σ. The $[N_\alpha \cdot N_\alpha]$ matrix $\mathbf{H}_E(\sigma,\sigma+m;\mathbf{k}_\parallel)$ couples the $[2N_\sigma+1]$ sublayers entering in the summation. The summation can be broken into two parts

$$\mathbf{H}_E(\sigma,\sigma+N_\sigma;\mathbf{k}_\parallel)\cdot\mathbf{C}(\sigma+N_\sigma;\mathbf{k}_\parallel) +$$

$$\sum_{m=-N_\sigma}^{N_\sigma-1} \mathbf{H}_E(\sigma,\sigma+m;\mathbf{k}_\parallel)\cdot\mathbf{C}(\sigma+m;\mathbf{k}_\parallel) = 0, \tag{12}$$

where the term $m = N_\sigma$ has been singled out. By multiplying by $\mathbf{H}_E(\sigma,\sigma+N_\sigma;\mathbf{k}_\parallel)^{-1}$, we obtain

$$\mathbf{C}(\sigma+N_\sigma;\mathbf{k}_\parallel) = -\mathbf{H}_E(\sigma,\sigma+N_\sigma;\mathbf{k}_\parallel)^{-1}\cdot$$

$$\sum_{m=-N_\sigma}^{N_\sigma-1} \mathbf{H}_E(\sigma, \sigma+m; \mathbf{k}_\parallel) \cdot \mathbf{C}(\sigma+m; \mathbf{k}_\parallel) = 0, \tag{13}$$

which relates the column vector $\mathbf{C}(\sigma + N_\sigma; \mathbf{k}_\parallel)$ on the sublayer $\sigma + N_\sigma$ to the column vectors $\mathbf{C}(\sigma + m; \mathbf{k}_\parallel)$ on the precedent $2N_\sigma$ sublayers,

$$m = -N_\sigma, -N_\sigma + 1, \ldots, N_\sigma - 1. \tag{14}$$

The matrix that allows us to obtain the column vector $\mathbf{C}(\sigma; \mathbf{k}_\parallel)$ on sublayer σ in terms of previous column vectors is called a *transfer matrix. The transfer matrix is defined in terms of sublayers.*

3.2.2 Layer Orbitals

In the second part of this appendix we distinguish between *layer orbitals* and *sublayer orbitals*.

If the set of equations (14) can be iterated $2N_\sigma$ times, then, by a product of transfer matrices, we can relate the set of $2N_\sigma$ coefficients

$$\mathbf{C}(\sigma + N_\sigma; \mathbf{k}_\parallel), \mathbf{C}(\sigma + N_\sigma + 1; \mathbf{k}_\parallel), \ldots, \mathbf{C}(\sigma + 3N_\sigma - 1; \mathbf{k}_\parallel), \tag{15.a}$$

to the set of $2N_\sigma$ original coefficients

$$\mathbf{C}(\sigma - N_\sigma; \mathbf{k}_\parallel), \mathbf{C}(\sigma - N_\sigma + 1; \mathbf{k}_\parallel), \ldots, \mathbf{C}(\sigma + N_\sigma - 1; \mathbf{k}_\parallel). \tag{15.b}$$

In that case, the two sets of coefficients have no sublayer in common and the product of transfer matrices that allows us to *completely decouple the two set of sublayers* can be viewed as transferring the electronic wavefunction over *layers*, or *groups of sublayers*. This is equivalent to the idea of principal layers introduced by Lee and Joannopoulos[2]. In the following, a layer Σ will be composed of $2N_\sigma$ sublayers σ.

In the systems considered below, a sublayer will consist of a single monoatomic plane and a layer can be viewed as a group of monoatomic planes. With this in mind, the equation,

$$\mathbf{C}(\Sigma; \mathbf{k}_\parallel) \equiv \mathbf{T}(\Sigma; \mathbf{k}_\parallel) \cdot \mathbf{C}(\Sigma - 1; \mathbf{k}_\parallel), \tag{16}$$

will refer to the transfer between layers Σ and $\Sigma - 1$, *i.e.*, groups of sublayers.

The transfer matrix $\mathbf{T}(\Sigma; \mathbf{k}_\parallel)$ transfers over layers and is just the product of transfer matrices that transfer over sublayers, $\mathbf{T}(\sigma; \mathbf{k}_\parallel)$.

By a simple extention, we can define a *layer orbital* in the same way as we defined a *sublayer orbital* by Eq.(2).

The following example will make clear the distinction between layers and sublayers. Figure (1) illustrates the case of the (100) interface in zincblende semiconductor. Shown in Figure (1) are the atomic positions in a zincblende structure projected on a (100) plane. Fractions denote height above base in units of the length of the conventional cubic unit cell, a. The open circles represent cations (*i.e.*, Ga, Al) and the filled circles represent anions (*i.e.*, As). The open circles represent cations (*i.e.*, Ga, Al) and the filled circles represent anions (*i.e.*, As). The points 0 and $\frac{1}{2}$ are on the cation face-centered cubic space lattice. The points $\frac{1}{4}$ and $\frac{3}{4}$ are on the anion face-centered cubic space lattice displaced from the cation face-centered lattice by $\frac{1}{4}(\hat{\mathbf{x}}+\hat{\mathbf{y}}+\hat{\mathbf{z}})$.

In Figure (1) we define the layer Σ in terms of the $2N_\sigma = 2$ sublayers σ and indicate how the product of two sublayer transfer matrices $\mathbf{T}(\sigma;\mathbf{k}_\parallel)$ allows us to obtain the layer transfer matrix $\mathbf{T}(\Sigma;\mathbf{k}_\parallel)$.

Let $\mathbf{C}(\Sigma;\mathbf{k}_\parallel)$ designate the column vector consisting of the atomic orbitals on the *cation* sublayer σ within the layer Σ. Let $\mathbf{A}(\Sigma;\mathbf{k}_\parallel)$ designate the column vector consisting of the atomic orbitals on the *anion* sublayer σ within the layer Σ.

By application of a sublayer transfer matrix, we obtain,

$$\begin{bmatrix}\mathbf{C}(\Sigma;\mathbf{k}_\parallel)\\ \mathbf{A}(\Sigma;\mathbf{k}_\parallel)\end{bmatrix} = [\mathbf{T}(1)]\cdot\begin{bmatrix}\mathbf{A}(\Sigma-1;\mathbf{k}_\parallel)\\ \mathbf{C}(\Sigma;\mathbf{k}_\parallel)\end{bmatrix}. \tag{17.a}$$

The sublayer transfer matrix $\mathbf{T}(1)$ transfer from one anion sublayer to the adjacent cation sublayer.

Application of another transfer matrix yields.

$$\begin{bmatrix}\mathbf{C}(\Sigma;\mathbf{k}_\parallel)\\ \mathbf{A}(\Sigma;\mathbf{k}_\parallel)\end{bmatrix} = [\mathbf{T}(1)]\cdot[\mathbf{T}(2)]\cdot\begin{bmatrix}\mathbf{C}(\Sigma-1;\mathbf{k}_\parallel)\\ \mathbf{A}(\Sigma-1;\mathbf{k}_\parallel)\end{bmatrix}. \tag{17.b}$$

In this case, *the two column vectors have been completely decoupled and have no sublayer in common.* Thus the product of the two sublayer transfer

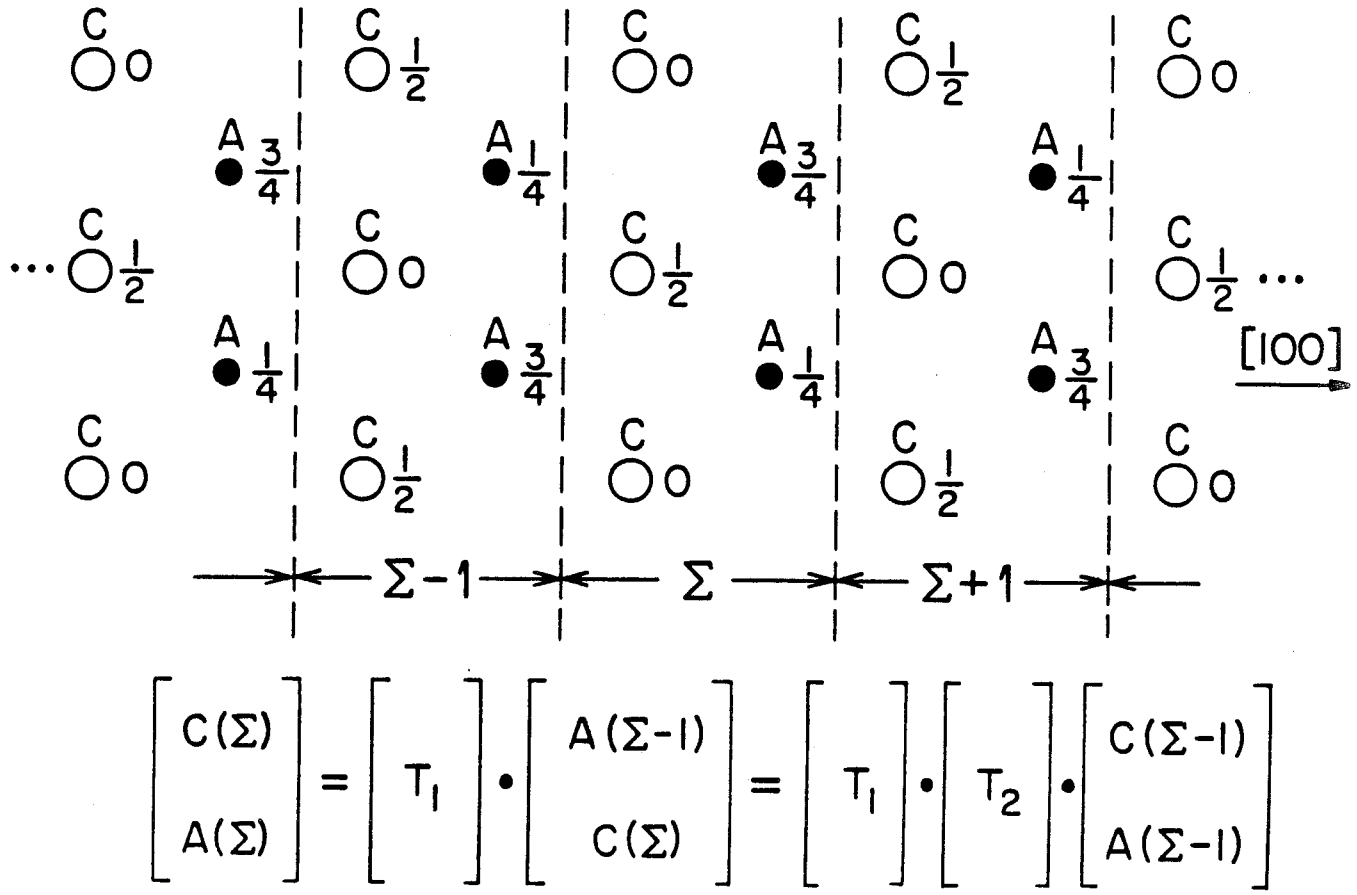

Figure 1. Atomic positions in a zincblende structure projected on a (100) plane. Fractions denote height above base in units of the length of the conventional cubic unit cell, a. The open circles represent cations (*i.e.* Ga, Al) and the filled circles represent anions (*i.e.* As). The points 0 and $\frac{1}{2}$ are on the cation face-centered cubic space lattice. The points $\frac{1}{4}$ and $\frac{3}{4}$ are on the anion face-centered cubic space lattice displaced from the cation face-centered lattice by $\frac{1}{4}(\hat{\mathbf{x}} + \hat{\mathbf{y}} + \hat{\mathbf{z}})$.

matrices,

$$\mathbf{T}(\Sigma; \mathbf{k}_{\|}) \equiv [\mathbf{T}(1)] \cdot [\mathbf{T}(2)], \tag{18}$$

allows the transfer from one *layer* to the other.

References

1. J. N. Schulman and Y. C. Chang, *Phys. Rev.* **B27**, 2346 (1983).

2. D. H. Lee and J. D. Joannopoulos, *Phys. Rev.* **B23**, 4988 (1981), *Phys. Rev.* **B23**, 4997 (1981).

APPENDIX 3.3

This appendix serves two purposes:

• In the first part of this appendix, we indicate how the *complex-***k** *band structure* of a solid can be determined given a knowledge of the transfer matrix within the empirical tight-binding method.

• In the second part of the appendix, we give the transformation rule to express the interface tight-binding wavefunction either in a *complex-***k** *bulk solutions representation* or in a *planar orbital representation.*

3.3.1 Complex-k Bandstructure

In this part of the appendix, we indicate the prescription to obtain the complex-**k** solutions $\{|\mathbf{k}_{\|}E;k_z\rangle\}$ in the planar orbital representation $\{|\alpha\sigma;\mathbf{k}_{\|}\rangle\}$ once the transfer matrix is known.

Consider the case for which the axis normal to the interface is along the $\hat{\mathbf{z}}$ direction. The wavevector **k** can now be decomposed on a *component parallel* to the interface, $\mathbf{k}_{\|}$, and a *component normal* to the interface, $\hat{\mathbf{z}}k_z$:

$$\mathbf{k} = \mathbf{k}_{\|} + \hat{\mathbf{z}}k_z, \tag{1.a}$$

with

$$\mathbf{k}_{\|} = \hat{\mathbf{x}}k_x + \hat{\mathbf{y}}k_y, \tag{1.b}$$

being the component of the wavevector **k** parallel to the interface plane. Since the translational symmetry of the bulk solid is preserved parallel to the interface, *the*

component $\mathbf{k}_{\|}$ *still remains a good quantum number for the Bloch solutions and remains real.* The total energy ,E, of the Bloch state is also a good quantum number to label the solutions. It is more convenient, when dealing with an interface system, to label the Bloch state solutions by $\{|\mathbf{k}_{\|}E;k_z\rangle\}$, with

$$\hat{H}_0|\mathbf{k}_{\|}E;k_z\rangle = E(\mathbf{k}_{\|},k_z)|\mathbf{k}_{\|}E;k_z\rangle. \tag{3}$$

In Eq.(3) we labelled the Bloch states $|\mathbf{k}_{\|}E;k_z\rangle$ in the extended zone scheme and therefore we got rid of the band index, n, that appears in Eq.(1.1). It is important to realize that Eq.(3) is *not an eigenvalue problem*, since for a given $\mathbf{k}_{\|}$ and $E(\mathbf{k}_{\|},k_z)$ there exists a finite number of k_z, real or complex, for which the Bloch state $|\mathbf{k}_{\|}E;k_z\rangle$ is a solution of Eq.(3). As mentioned above, the component of the wavevector parallel to the interface, $\mathbf{k}_{\|}$, and the total energy, E, can be used to label the solutions of Eq.(3). However, the component k_z is not a conserved quantity across the interface and cannot be used to label the solutions of Eq.(3). We now show how to obtain all the solutions of Eq.(3) for k_z real or complex within the ETBM framework. In this case the spectrum $E(\mathbf{k}_{\|},k_z)$ is referred to as a complex-$\mathbf{k}$ band structure.

Let us define $|\mathbf{k}_{\|}E;k_z,\sigma\rangle$ the Bloch solution of Eq.(3) evaluated on the sublayer σ. Let the bulk primitive cell be made up of, say, L sublayers in the $\hat{\mathbf{z}}$-direction. Then, after being transferred over the L sublayers, the bulk Bloch state on sublayer $L\sigma$, $|\mathbf{k}_{\|}E;k_z,\sigma+L\rangle$ has to be equal to the Bloch state on sublayer σ, $|\mathbf{k}_{\|}E;k_z,\sigma\rangle$, multiplied by the Bloch factor $\exp(ik_zLa_0)$, *i.e.*,

$$|\mathbf{k}_{\|}E;k_z,\sigma+L\rangle \equiv \exp(ik_zLa_0)|\mathbf{k}_{\|}E;k_z,\sigma\rangle. \tag{4}$$

With this information, we arrive at an *eigenvalue problem* for the solution of Eq.(3.3). We write $\mathbf{T}(\sigma;\mathbf{k}_{\|})$ as the transfer matrix that gives the coefficients

$\mathbf{C}(\sigma;\mathbf{k}_\parallel)$ on sublayer σ in terms of the coefficients $\mathbf{C}(\sigma-1;\mathbf{k}_\parallel)$ of the preceding sublayer $[\sigma-1]$,

$$\mathbf{C}(\sigma;\mathbf{k}_\parallel) \equiv \mathbf{T}(\sigma;\mathbf{k}_\parallel)\cdot\mathbf{C}(\sigma-1;\mathbf{k}_\parallel). \tag{5}$$

Successive transfers then lead to the set

$$\mathbf{C}(\sigma+L;\mathbf{k}_\parallel) = \left[\mathbf{T}(\sigma+L;\mathbf{k}_\parallel)\right]\cdot\mathbf{C}(\sigma+L-1;\mathbf{k}_\parallel),$$

$$\mathbf{C}(\sigma+L;\mathbf{k}_\parallel) = \left[\mathbf{T}(\sigma+L;\mathbf{k}_\parallel)\cdot\mathbf{T}(\sigma+L-1;\mathbf{k}_\parallel)\right]\cdot\mathbf{C}(\sigma+L-2;\mathbf{k}_\parallel),$$

$$\cdots$$

$$\cdots$$

$$\cdots$$

$$\mathbf{C}(\sigma+L;\mathbf{k}_\parallel) = \left[\mathbf{T}(\sigma+L;\mathbf{k}_\parallel)\cdot\mathbf{T}(\sigma+L-1;\mathbf{k}_\parallel)\cdot\ldots\cdot\mathbf{T}(\sigma+1;\mathbf{k}_\parallel)\right]\cdot\mathbf{C}(\sigma;\mathbf{k}_\parallel), \tag{6}$$

where a *product of L transfer matrices* is included in $[\ldots]$.

But we also know, by Eq.(2.12), that

$$\mathbf{C}(\sigma+L;\mathbf{k}_\parallel) \equiv [\exp(ik_zLa_0)]\,\mathbf{C}(\sigma;\mathbf{k}_\parallel), \tag{7}$$

must be true for the Bloch theorem to be realized.

By combining Eq.(2.14) and Eq.(2.15) we arrive at the *eigenvalue problem,*

$$\left[\mathbf{T}(\sigma+L;\mathbf{k}_\parallel)\cdot\mathbf{T}(\sigma+L-1;\mathbf{k}_\parallel)\cdot\ldots\cdot\mathbf{T}(\sigma+1;\mathbf{k}_\parallel)\right]\cdot\mathbf{C}(\sigma;\mathbf{k}_\parallel) =$$

$$[\exp(ik_zLa_0)]\,\mathbf{C}(\sigma;\mathbf{k}_\parallel), \tag{8}$$

for the $[N_\alpha]$-dimensional column vector $\mathbf{C}(\sigma;\mathbf{k}_\parallel)$ composed of the coefficients $C(\alpha\sigma;\mathbf{k}_\parallel)$ on sublayer σ.

The eigenvalues of this eigensystem are simply the components of the wavevector $\mathbf{k}$ normal to the interface, through the Bloch factor, $[\exp(ik_z La_0)]$.

By direct diagonalization of the following product of L transfer matrices

$$\left[\mathbf{T}(\sigma + L; \mathbf{k}_{\|}) \cdot \mathbf{T}(\sigma + L - 1; \mathbf{k}_{\|}) \cdot \ldots \cdot \mathbf{T}(\sigma + 1; \mathbf{k}_{\|})\right] , \tag{9}$$

it is possible to find the $[2N_\sigma \cdot N_\alpha] \equiv 2N$ complex values of k_z for each parallel wavevector $\mathbf{k}_{\|}$ and energy E. We can therefore label the allowed complex-k_z wavevectors by

$$k_z \equiv k_\lambda \qquad [\lambda = 1, 2, \ldots, 2N], (10.a)$$

and the corresponding Bloch states by

$$|\mathbf{k}_{\|} E; k_z\rangle \equiv |\mathbf{k}_{\|} E; k_\lambda\rangle \qquad [\lambda = 1, 2, \ldots, 2N]. (10.b)$$

Let $\mathbf{S}(\mathbf{k}_{\|})$ be the $[2N_\sigma \cdot N_\alpha]$ eigenvector matrix that diagonalizes the product of L transfer matrices

$$\left[\mathbf{T}(\sigma + L; \mathbf{k}_{\|}) \cdot \mathbf{T}(\sigma + L - 1; \mathbf{k}_{\|}) \cdot \ldots \cdot \mathbf{T}(\sigma + 1; \mathbf{k}_{\|})\right] \tag{11}$$

in the planar orbital representation $\{|\alpha\sigma; \mathbf{k}_{\|}\rangle\}$.

The meaning of the matrix $\mathbf{S}(\mathbf{k}_{\|})$ is simple: Is it the *eigenvector matrix of coefficients for the expansion of the bulk Bloch states* $\{|\mathbf{k}_{\|} E; k_\lambda\rangle\}$ *in the planar orbital representation* $\{|\alpha\sigma; \mathbf{k}_{\|}\rangle\}$. The eigenvector matrix $\mathbf{S}(\mathbf{k}_{\|})$ that diagonalizes the product of L transfer matrices, allows us to transform the description of the electronic wavefunction from the planar orbital representation $\{|\alpha\sigma; \mathbf{k}_{\|}\rangle\}$ to the Bloch states representation $\{|\mathbf{k}_{\|} E; k_\lambda\rangle\}$.

In terms of *layer* we can state that, the eigenvector matrix $\mathbf{S}(\mathbf{k}_{\|})$ in composed of the column vectors $S(\alpha\sigma, k_\lambda; \mathbf{k}_{\|})$ that are simply the expansion of the Bloch state

$|\mathbf{k}_{\|}E; k_\lambda\ , \Sigma\rangle$ corresponding to $k_z \equiv k_\lambda$ in terms of the planar orbitals $\{|\alpha\sigma; \mathbf{k}_{\|}\rangle\}$. Thus the Bloch state with $k_z = k_\lambda$ on layer Σ can be written as

$$|\mathbf{k}_{\|}E; k_\lambda\ , \Sigma\rangle = \exp(ik_\lambda\ \Sigma a_0) \sum_{\sigma=1}^{2N_\sigma} \cdot$$

$$\left[\sum_{\alpha=1}^{N_\alpha} S(\alpha\sigma, k_\lambda\ ; \mathbf{k}_{\|})|\alpha\sigma; \mathbf{k}_{\|}\rangle\right] \qquad [\lambda = 1, \ldots, 2N]. \quad (12)$$

where the index σ labels the $2N_\sigma$ sublayers forming the layer Σ.

3.3.2 Connections between Complex-k Solutions and Planar Orbitals

In this second section of the appendix, we outline briefly the correspondence between the *bulk Bloch states representation* $\{|\mathbf{k}_{\|}E;k_z\rangle\}$ and the *planar orbital representation* $\{|\alpha\sigma;\mathbf{k}_{\|}\rangle\}$.

On a given layer Σ, the electron wavefunction, $|\Psi(\mathbf{k}_{\|}E;\Sigma)\rangle$, can be expanded in a *planar orbital representation* as in Eq.(3.5)

$$|\Psi(\mathbf{k}_{\|}E;\Sigma)\rangle = \sum_{\alpha=1}^{N_\alpha}\sum_{\sigma=1}^{2N_\sigma} C(\alpha\sigma;\mathbf{k}_{\|})|\alpha\sigma;\mathbf{k}_{\|}\rangle, \tag{13}$$

where the expansion coefficients $C(\alpha\sigma;\mathbf{k}_{\|})$ indicate the admixture of the planar orbitals $\{|\alpha\sigma;\mathbf{k}_{\|}\rangle\}$ in the wavefunction $|\Psi(\mathbf{k}_{\|}E;\Sigma)\rangle$. The sum is over all the subalyers σ forming the layer Σ.

On the other hand, we could use as the expansion set the set of *bulk Bloch states* $\{|\mathbf{k}_{\|}E;k_\lambda\ ,\Sigma\rangle\}$ evaluated on the layer Σ,

$$|\Psi(\mathbf{k}_{\|}E;\Sigma)\rangle = \sum_{\lambda=1}^{2N} A(k_\lambda\ ;\mathbf{k}_{\|},E)|\mathbf{k}_{\|}E;k_\lambda\ ,\Sigma\rangle, \tag{14}$$

where now the expansion coefficients $A(k_\lambda\ ;\mathbf{k}_{\|},E)$ indicate the admixture of the bulk Bloch states $\{|\mathbf{k}_{\|}E;k_\lambda\ ,\Sigma\rangle\}$ in the wavefunction $|\Psi(\mathbf{k}_{\|}E;\Sigma)\rangle$.

But, as seen in the preceding we can relate the *bulk Bloch states* on a layer Σ and the *planar orbitals* on that same layer by

$$|\mathbf{k}_{\|}E;k_\lambda\ ,\Sigma\rangle = \exp(ik_\lambda\ \Sigma a_0)\sum_{\sigma=1}^{2N_\sigma}\cdot$$

$$\left[\sum_{\alpha=1}^{N_\alpha} S(\alpha\sigma,k_\lambda\ ;\mathbf{k}_{\|})|\alpha\sigma;\mathbf{k}_{\|}\rangle\right] \qquad [\lambda=1,\ldots,2N], \tag{15}$$

where the $[2N_\sigma \cdot N_\alpha]$ eigenvector matrix $\mathbf{S}(\mathbf{k}_\parallel)$ diagonalizes the product of L transfer matrices

$$\left[\mathbf{T}(\sigma+L;\mathbf{k}_\parallel)\cdot\mathbf{T}(\sigma+L-1;\mathbf{k}_\parallel)\cdot\ldots\cdot\mathbf{T}(\sigma+1;\mathbf{k}_\parallel)\right], \tag{16}$$

in the planar orbital representation.

By combining Eqs(3.2) and (3.3) we have

$$|\Psi(\mathbf{k}_\parallel E;\Sigma)\rangle = \sum_{\lambda=1}^{2N} A(k_\lambda;\mathbf{k}_\parallel,E)|\mathbf{k}_\parallel E;k_\lambda,\Sigma\rangle, \tag{17.a}$$

$$|\Psi(\mathbf{k}_\parallel E;\Sigma)\rangle = \sum_{\lambda=1}^{2N} A(k_\lambda;\mathbf{k}_\parallel,E)\cdot$$

$$\left[\exp(ik_\lambda\,\Sigma a_0)\sum_{\alpha=1}^{N_\alpha}\sum_{\sigma=1}^{2N_\sigma} S(\alpha\sigma,k_\lambda;\mathbf{k}_\parallel)|\alpha\sigma;\mathbf{k}_\parallel\rangle\right], \tag{17.b}$$

$$|\Psi(\mathbf{k}_\parallel E;\Sigma)\rangle = \sum_{\alpha=1}^{N_\alpha}\sum_{\sigma=1}^{2N_\sigma}\cdot$$

$$\left[\sum_{\lambda=1}^{2N} S(\alpha\sigma,k_\lambda;\mathbf{k}_\parallel)\exp(ik_\lambda\,\Sigma a_0)A(k_\lambda;\mathbf{k}_\parallel,E)\right]|\alpha\sigma;\mathbf{k}_\parallel\rangle. \tag{18.c}$$

And, by comparing with Eq.(3.1),

$$|\Psi(\mathbf{k}_\parallel E;\Sigma)\rangle = \sum_{\alpha=1}^{N_\alpha}\sum_{\sigma=1}^{2N_\sigma} C(\alpha\sigma;\mathbf{k}_\parallel)|\alpha\sigma;\mathbf{k}_\parallel\rangle, \tag{19}$$

we find that the expansion coefficients $C(\alpha\sigma;\mathbf{k}_\parallel)$ of the planar orbital expansion are related to the amplitudes $A(k_\lambda;\mathbf{k}_\parallel,E)$ of the bulk Bloch states representations by

$$C(\alpha\sigma;\mathbf{k}_\parallel) \equiv \sum_{\lambda=1}^{2N} S(\alpha\sigma,k_\lambda;\mathbf{k}_\parallel)\exp(ik_\lambda\,\Sigma a_0)A(k_\lambda;\mathbf{k}_\parallel,E), \tag{20}$$

where the sublayer σ is within the layer Σ.

We can also write Eq.(3.6) as the matrix equation,

$$\mathbf{C}(\Sigma;\mathbf{k}_{\|}) \equiv \mathbf{S}(\Sigma;\mathbf{k}_{\|}) \cdot \mathbf{A}(\mathbf{k}_{\|}), \tag{21}$$

where the colunm vector $\mathbf{C}(\Sigma;\mathbf{k}_{\|})$ is composed of the coefficients $C(\alpha\sigma;\mathbf{k}_{\|})$ of the atomic orbitals α on the sublayer σ belonging to the layer Σ. The $[2N_\sigma \cdot N_\alpha]$ matrix $\mathbf{S}(\Sigma;\mathbf{k}_{\|})$ is formed of the column vectors $S(\alpha\sigma, k_\lambda\ ;\mathbf{k}_{\|})$ and has matrix elements

$$S(\alpha\sigma, k_\lambda\ , \Sigma;\mathbf{k}_{\|}) \equiv S(\alpha\sigma, k_\lambda\ ;\mathbf{k}_{\|}) \exp(ik_\lambda\ \Sigma a_0), \tag{22}$$

where the sublayer σ belongs to the layer Σ. The column vector $\mathbf{A}(\mathbf{k}_{\|})$ is composed of the $2N$ coefficients $A(k_\lambda\ ;\mathbf{k}_{\|}, E)$ of the bulk Bloch states representation $\{|\mathbf{k}_{\|} E; k_\lambda\ \rangle\}$.

Appendix 3.4

Calculation of Transport Coefficients: Tight-Binding Transfer Matrix Method

The purpose of this appendix is to obtain the transport coefficients for electrons through a semiconductor double heterojunction structure. The formalism utilizes the complex-**k** band structure and the transfer matrix method within the *empirical tight-binding method.*

3.4.1 Tight-Binding Wavefunction and Transfer Matrix

Let the incoming Bloch state $|\mathbf{k}_{\|}E;k_0\rangle$ with real wavevector k_0 be incident from the left in GaAs onto the GaAs-$Ga_{1-x}Al_xAs$ interface. The total wavefunction on a given layer Σ composed of the $2N_\sigma$ sublayers σ, can be written as[1]:

$$|\Psi(\mathbf{k}_{\|}E;\Sigma)\rangle = |\mathbf{k}_{\|}E;k_0\ ,\Sigma\rangle + \sum_{\lambda=1}^{2N} A^{(I)}(k_\lambda\ ;\mathbf{k}_{\|},E)|\mathbf{k}_{\|}E;k_\lambda\ ,\Sigma\rangle \quad \text{region I } (1.a)$$

$$|\Psi(\mathbf{k}_{\|}E;\Sigma)\rangle = \sum_{\alpha=1}^{N_\alpha}\sum_{\sigma=1}^{2N_\sigma} C^{(I-II)}(\alpha\sigma;\mathbf{k}_{\|},E)|\alpha\sigma;\mathbf{k}_{\|}\rangle \qquad \text{interface I-II } (1.b)$$

$$|\Psi(\mathbf{k}_{\|}E;\Sigma)\rangle = \sum_{\lambda=1}^{2N} A^{(II)}(k_\lambda\ ;\mathbf{k}_{\|},E)|\mathbf{k}_{\|}E;k_\lambda\ ,\Sigma\rangle \qquad \text{region II } (1.c)$$

$$|\Psi(\mathbf{k}_{\|}E;\Sigma)\rangle = \sum_{\alpha=1}^{N_\alpha}\sum_{\sigma=1}^{2N_\sigma} C^{(II-III)}(\alpha\sigma;\mathbf{k}_{\|},E)|\alpha\sigma;\mathbf{k}_{\|}\rangle \qquad \text{interface II-III } (1.d)$$

$$|\Psi(\mathbf{k}_{\|}E;\Sigma)\rangle = \sum_{\lambda=1}^{2N} A^{(III)}(k_\lambda\ ;\mathbf{k}_{\|},E)|\mathbf{k}_{\|}E;k_\lambda\ ,\Sigma\rangle \qquad \text{region III } (1.e)$$

• The expansion coefficients $A^{(I)}(k_\lambda;\mathbf{k}_\parallel,E)$, $A^{(II)}(k_\lambda;\mathbf{k}_\parallel,E)$ and $A^{(III)}(k_\lambda;\mathbf{k}_\parallel,E)$ are associated with the bulk Bloch states representation, $\{|\mathbf{k}_\parallel E;k_z\rangle\}$, in regions I, II and III, respectively.

• The expansion coefficients $C^{(I-II)}(\alpha\sigma;\mathbf{k}_\parallel,E)$ and $C^{(II-III)}(\alpha\sigma;\mathbf{k}_\parallel,E)$ are associated with the planar orbital representation, $\{|\alpha\sigma;\mathbf{k}_\parallel\rangle\}$, across the interfaces.

We now explain the procedure to obtain the transport coefficients within the tight-binding transfer matrix framework outlined above. First let us define the *layer-dependent* matrix $\mathbf{S}(\Sigma;\mathbf{k}_\parallel)$ to be simply the eigenvector matrix with matrix elements,

$$S(\alpha\sigma,k_\lambda\ ,\Sigma;\mathbf{k}_\parallel)\equiv S(\alpha\sigma,k_\lambda\ ;\mathbf{k}_\parallel)\exp(ik_\lambda\ \Sigma a_0), \tag{2}$$

where the sublayer σ is within the layer Σ. With this definition, the relation derived in Appendix (3.2) between the expansion coefficients for the planar orbital representation and the bulk Bloch states representation,

$$C(\alpha\sigma;\mathbf{k}_\parallel)\equiv\sum_{\lambda=1}^{2N}S(\alpha\sigma,k_\lambda\ ;\mathbf{k}_\parallel)\exp(ik_\lambda\ \Sigma a_0)A(k_\lambda\ ;\mathbf{k}_\parallel,E), \tag{3}$$

can be written in matrix form as

$$\mathbf{C}(\Sigma;\mathbf{k}_\parallel)\equiv\mathbf{S}(\Sigma;\mathbf{k}_\parallel)\cdot\mathbf{A}(\mathbf{k}_\parallel), \tag{4}$$

where the column vector $\mathbf{A}(\mathbf{k}_\parallel)$ is formed by the $2N$ expansion coefficients, $A(k_\lambda;\mathbf{k}_\parallel,E)$. The column vector $\mathbf{C}(\Sigma;\mathbf{k}_\parallel)$ is composed of the coefficients, $C(\alpha\sigma;\mathbf{k}_\parallel)$, for the atomic orbitals α on the sublayers σ belonging to the layer Σ. The GaAs-$Ga_{1-x}Al_xAs$-GaAs DHS is schematically represented in Figure (1) of Section (2.2). Let the central $Ga_{1-x}Al_xAs$ barrier region be composed of n layers.

• In the last layer of the bulk region I, we can write, dropping the label $\mathbf{k}_\parallel$ altogether,

$$\mathbf{C}^{(I)}(0)=\mathbf{S}^{(I)}(0)\cdot\mathbf{A}^{(I)}, \tag{5.a}$$

where the origin of region I (*i.e.*, $\Sigma = 0$), has been taken on the last layer of region I.

• On the first layer of the barrier region II, we have

$$\mathbf{C}^{(II)}(0) = \mathbf{S}^{(II)}(0) \cdot \mathbf{A}^{(II)}, \tag{5.b}$$

where the origin of region II has been taken on the first layer of region II. But the first layer of region II can be expressed in terms of the last layer of region I by the transfer matrix equation,

$$\mathbf{C}^{(II)}(0) = \mathbf{T}^{(I-II)} \cdot \mathbf{C}^{(I)}(0), \tag{5.c}$$

where the transfer matrix $\mathbf{T}^{(I-II)}$ relates the coefficients of the last layer of region I to the coefficients on the first layer of region II. By combining Eqs(8.b) and (8.c) we have

$$\mathbf{A}^{(II)} = \left[\mathbf{S}^{(II)}(0)\right]^{-1} \cdot \mathbf{T}^{(I-II)} \cdot \mathbf{C}^{(I)}(0). \tag{5.d}$$

• Similarly, on the last layer of the barrier region II, *i.e.*, layer $n-1$, we have

$$\mathbf{C}^{(II)}(n-1) = \mathbf{S}^{(II)}(n-1) \cdot \mathbf{A}^{(II)}, \tag{5.e}$$

• and on the first layer of region III we have,

$$\mathbf{C}^{(III)}(0) = \mathbf{S}^{(III)}(0) \cdot \mathbf{A}^{(III)}, \tag{5.f}$$

where the origin of region III (*i.e.*, $\Sigma = 0$), has been taken on the first layer of region III.

• Again, the first layer of region III can be expressed in terms of the last layer of region II by the transfer matrix equation,

$$\mathbf{C}^{(III)}(0) = \mathbf{T}^{(II-III)} \cdot \mathbf{C}^{(II)}(n-1), \tag{5.g}$$

where the transfer matrix $\mathbf{T}^{(II-III)}$ relates the coefficients of the last layer of region II to the coefficients on the first layer of region III.

• Then, the coefficients of the bulk states in region III, $\mathbf{A}^{(III)}$ can be related to the coefficients of the bulk Bloch states on region I, by

$$\mathbf{A}^{(III)} = \left[\mathbf{S}^{(III)}(0)\right]^{-1} \cdot \mathbf{C}^{(III)}(0), \tag{5.h}$$

$$= \left[\mathbf{S}^{(III)}(0)\right]^{-1} \cdot \mathbf{T}^{(II-III)} \cdot \mathbf{C}^{(II)}(n-1), \tag{5.i}$$

$$= \left[\mathbf{S}^{(III)}(0)\right]^{-1} \cdot \mathbf{T}^{(II-III)} \cdot \mathbf{S}^{(II)}(n-1) \cdot \mathbf{A}^{(II)}, \tag{5.j}$$

$$= \left[\mathbf{S}^{(III)}(0)\right]^{-1} \cdot \mathbf{T}^{(II-III)} \cdot \mathbf{S}^{(II)}(n-1) \cdot \left[\mathbf{S}^{(II)}(0)\right]^{-1} \cdot \mathbf{T}^{(I-II)} \cdot \mathbf{C}^{(I)}(0), \tag{5.k}$$

and finally

$$\mathbf{A}^{(III)} \equiv \mathbf{M}(\mathbf{k}_{\|}E) \cdot \mathbf{A}^{(I)}, \tag{5.l}$$

where the matrix $\mathbf{M}(\mathbf{k}_{\|}E)$ is defined to be

$$\mathbf{M}(\mathbf{k}_{\|}E) \equiv \left[\mathbf{S}^{(III)}(0)\right]^{-1} \cdot \mathbf{T}^{(II-III)} \cdot \mathbf{S}^{(II)}(n-1) \cdot \left[\mathbf{S}^{(II)}(0)\right]^{-1} \cdot \mathbf{T}^{(I-II)} \cdot \mathbf{S}^{(I)}(0). \tag{5.m}$$

3.4.1 Boundary Conditions

We have now to impose the proper *boundary conditions* on the incoming and the outgoing states. Suppose that the column vector $\mathbf{A}(\mathbf{k}_{\|})$, formed by the $2N$ expansion coefficients $A(k_\lambda\ ;\mathbf{k}_{\|},E)$ corresponding to the $2N$ bulk solutions $\{|\mathbf{k}_{\|}E;k_\lambda\ \rangle\}$, is ordered such that the solutions corresponding to $\mathrm{Im}[k_\lambda\ ]>0$ are *above* those for which $\mathrm{Im}[k_\lambda\ ]<0$. Then we write

$$\mathbf{A}^{(I)} \equiv \begin{bmatrix} \mathbf{A}^{(I,+)} \\ \mathbf{A}^{(I,-)} \end{bmatrix}, \tag{6.a}$$

in region I, and

$$\mathbf{A}^{(III)} \equiv \begin{bmatrix} \mathbf{A}^{(III,+)} \\ \mathbf{A}^{(III,-)} \end{bmatrix}, \tag{6.b}$$

The matrix equation Eq.(5.1) can now be expressed in the form,

$$\begin{bmatrix} \mathbf{A}^{(III,+)} \\ \mathbf{A}^{(III,-)} \end{bmatrix} = \begin{bmatrix} \mathbf{M}(+,+) & \mathbf{M}(+,-) \\ \mathbf{M}(-,+) & \mathbf{M}(-,-) \end{bmatrix} \cdot \begin{bmatrix} \mathbf{A}^{(I,+)} \\ \mathbf{A}^{(I,-)} \end{bmatrix}. \tag{7}$$

We now impose the boundary conditions that there are *no growing states at* $z=+\infty$ *and at* $z=-\infty$. This translates into,

$$\mathbf{A}^{(I)} \equiv \begin{bmatrix} \mathbf{0} \\ \mathbf{A}^{(I,-)} \end{bmatrix}, \tag{8.a}$$

in region I, and

$$\mathbf{A}^{(III)} \equiv \begin{bmatrix} \mathbf{A}^{(III,+)} \\ \mathbf{0} \end{bmatrix}, \tag{8.b}$$

We now have to solve the matrix equation,

$$\begin{bmatrix} \mathbf{A}^{(III,+)} \\ \mathbf{0} \end{bmatrix} = \begin{bmatrix} \mathbf{M}(+,+) & \mathbf{M}(+,-) \\ \mathbf{M}(-,+) & \mathbf{M}(-,-) \end{bmatrix} \cdot \begin{bmatrix} \mathbf{0} \\ \mathbf{A}^{(I,-)} \end{bmatrix}, \tag{9}$$

for the column vector of the *outgoing state*,

$$\mathbf{A}^{(III)} \equiv \begin{bmatrix} \mathbf{A}^{(III,+)} \\ \mathbf{0} \end{bmatrix}, \tag{10.b}$$

given that the column vector for the *incoming state*,

$$\mathbf{A}^{(I)} \equiv \begin{bmatrix} \mathbf{0} \\ \mathbf{A}^{(I,-)} \end{bmatrix}, \tag{10.a}$$

is known.

References

1. G. C. Osbourn and D. L. Smith, *Phys. Rev.* **B19**, 2124 (1979).

APPENDICES

CHAPTER 4

ELECTRONIC STRUCTURE OF SEMICONDUCTOR SUPERLATTICES

APPENDIX 4.1

In this appendix, we review the $\mathbf{k}\cdot\mathbf{p}$ perturbation theory of bulk semiconductor as a mean of calculating energy band structure. Most of the derivations presented here can be found in the review article by Kane[1] and in standard solid-state physics texts[2].

This appendix contains two subsections.

- In the first subsection we derive the set of $\mathbf{k}\cdot\mathbf{p}$ equations when the cell-periodic part of the Bloch state is expanded on a set of cell-periodic functions at $\mathbf{k}=\mathbf{k}_0$.
- In the second subsection, we consider the special case whereby $\mathbf{k}_0=\mathbf{0}$.

k.p Theory of Bulk Semiconductors

Given that the set of Bloch states $\{|n\mathbf{k}\rangle\}$ are solutions to the Schrödinger equation for the bulk solid:

$$\hat{H}|n\mathbf{k}\rangle = E_n(\mathbf{k})|n\mathbf{k}\rangle. \tag{1}$$

The Hamiltonian is

$$\hat{H} = \frac{1}{2m}\mathbf{p}^2 + V(\mathbf{x}), \tag{2}$$

where $V(\mathbf{x}+\mathbf{R}) = V(\mathbf{x})$ is the crystal potential which has the symmetry of the crystal space group. The momentum operator is $\mathbf{p} \equiv -i\hbar\nabla$. The energy eigenvalues, $E_n(\mathbf{k})$, for the band structure of bulk solid. The Bloch states are of the form,

$$\langle\mathbf{x}|n\mathbf{k}\rangle = \exp(i\mathbf{k}\cdot\mathbf{x})u_n(\mathbf{k};\mathbf{x}), \tag{3}$$

where $u_n(\mathbf{k};\mathbf{x})$ is the cell-periodic part of the Bloch function:

$$u_n(\mathbf{k};\mathbf{x}+\mathbf{R}) = u_n(\mathbf{k};\mathbf{x}), \tag{4}$$

where $\mathbf{R}$ is a Bravais lattice vector generating the $\mathbf{x}$-space lattice. The index n is the band index and $\hbar\mathbf{k}$ is the crystal momentum. We now wish to obtain the eigenvalue equation for the cell-periodic part of the Bloch function, $u_n(\mathbf{k};\mathbf{x})$, by direct substitution of the form Eq.(3) into the Schrödinger equation Eq.(1):

$$\left[\frac{1}{2m}\mathbf{p}^2 + V(\mathbf{x})\right]\exp(i\mathbf{k}\cdot\mathbf{x})u_n(\mathbf{k};\mathbf{x}) = E_n(\mathbf{k})u_n(\mathbf{k};\mathbf{x}). \tag{5}$$

By commuting the plane wave $\exp(i\mathbf{k}\cdot\mathbf{x})$ across the Hamiltonian, we arrive at:

$$\hat{H}(\mathbf{k})u_n(\mathbf{k};\mathbf{x}) = E_n(\mathbf{k})u_n(\mathbf{k};\mathbf{x}), \tag{6}$$

where the Hamiltonian $\hat{H}(\mathbf{k})$ is defined to be :

$$\hat{H}(\mathbf{k}) \equiv \frac{1}{2m}(\mathbf{p}+\hbar\mathbf{k})^2 + V(\mathbf{x}), \tag{7.a}$$

or,

$$\hat{H}(\mathbf{k}) \equiv \frac{1}{2m}\mathbf{p}^2 + \frac{\hbar}{m}\mathbf{k}\cdot\mathbf{p} + \frac{\hbar^2}{2m}\mathbf{k}^2 + V(\mathbf{x}). \tag{7.b}$$

The form of the Hamiltonian $\hat{H}(\mathbf{k})$ corresponds to a *gauge transformation*,

$$\hat{H}(\mathbf{k}) \equiv \hat{H}(\mathbf{p}+\mathbf{k};\mathbf{x}) \equiv \exp(-i\mathbf{k}\cdot\mathbf{x})\cdot\hat{H}(\mathbf{p};\mathbf{x})\cdot\exp(i\mathbf{k}\cdot\mathbf{x}). \tag{7.c}$$

4.1.1 Expansion on set of functions at $\mathbf{k}= \mathbf{k}_0$

For any wavevector $\mathbf{k}$, the cell-periodic functions $u_n(\mathbf{k};\mathbf{x})$ form a complete set for any function having the periodicity of the crystal potential, $V(\mathbf{x})$. Thus the cell-periodic function $u_n(\mathbf{k};\mathbf{x})$ associated with any wavevector $\mathbf{k}$ can be expanded on the set of cell-periodic functions $\{u_{n'}(\mathbf{k}_0;\mathbf{x})\}$ belonging to the different bands n' and associated with a particular wavevector $\mathbf{k}_0$,

$$u_n(\mathbf{k};\mathbf{x}) = \sum_{n'} u_{n'}(\mathbf{k}_0;\mathbf{x}) C(nn';\mathbf{k}\mathbf{k}_0), \tag{8}$$

so that the Bloch solutions of Eq.(1) become

$$\langle \mathbf{x}|n\mathbf{k}\rangle = \exp(i\mathbf{k}\cdot\mathbf{x}) \sum_{n'} u_{n'}(\mathbf{k}_0;\mathbf{x}) C(nn';\mathbf{k}\mathbf{k}_0). \tag{9}$$

The amplitudes $C(nn';\mathbf{k}\mathbf{k}_0)$ indicate the mixing of the $\mathbf{k}_0$ basis states, $u_{n'}(\mathbf{k}_0;\mathbf{x})$ belonging to the different bands n'. The $\mathbf{k} = \mathbf{k}_0$ cell-periodic basis functions ,$\{u_n(\mathbf{k}_0;\mathbf{x})\}$, are solutions of the $\mathbf{k} = \mathbf{k}_0$ Schrödinger equation, Eq (5):

$$\hat{H}(\mathbf{k}_0) u_n(\mathbf{k}_0;\mathbf{x}) = E_n(\mathbf{k}_0) u_n(\mathbf{k}_0;\mathbf{x}), \tag{10}$$

where the Hamiltonian for $\mathbf{k} = \mathbf{k}_0$, $\hat{H}(\mathbf{k}_0)$ is simply the Hamiltonian $\hat{H}(\mathbf{k})$ in Eq. (7) with $\mathbf{k} = \mathbf{k}_0$:

$$\hat{H}(\mathbf{k}_0) \equiv \frac{1}{2m}\mathbf{p}^2 + \frac{\hbar}{m}\mathbf{k}_0\cdot\mathbf{p} + \frac{\hbar^2}{2m}\mathbf{k}_0{}^2 + V(\mathbf{x}). \tag{11}$$

Thus, at a general $\mathbf{k}$, we can split the $\mathbf{k}$-dependent Hamiltonian defined in Eq. (7) into a $\mathbf{k}$-independent term, $\hat{H}(\mathbf{k}_0)$, and a $\mathbf{k}$-dependent term:

$$\hat{H}(\mathbf{k}) \equiv \frac{1}{2m}\mathbf{p}^2 + \frac{\hbar}{m}\mathbf{k}\cdot\mathbf{p} + \frac{\hbar^2}{2m}\mathbf{k}^2 + V(\mathbf{x}), \tag{12.a}$$

$$\hat{H}(\mathbf{k}) \equiv \hat{H}(\mathbf{k}_0) + \frac{\hbar}{m}(\mathbf{k}-\mathbf{k}_0)\cdot\mathbf{p} + \frac{\hbar^2}{2m}(\mathbf{k}^2 - \mathbf{k}_0{}^2), \tag{12.b}$$

with

$$\hat{H}(\mathbf{k}_0) \equiv \frac{1}{2m}\mathbf{p}^2 + \frac{\hbar}{m}\mathbf{k}_0 \cdot \mathbf{p} + \frac{\hbar^2}{2m}{\mathbf{k}_0}^2 + V(\mathbf{x}). \tag{12.c}$$

Eq. (6) can be put in matrix equation by using the expansion Eq. (8) for the cell-periodic function ,$u_n(\mathbf{k};\mathbf{x})$, and by projecting onto the $\mathbf{k}_0$ basis state, $u_n^*(\mathbf{k}_0;\mathbf{x})$,

$$\sum_{n'} \hat{H}(nn';\mathbf{k}\mathbf{k}_0)C(nn';\mathbf{k}\mathbf{k}_0) = E_n(\mathbf{k})C(nn';\mathbf{k}\mathbf{k}_0), \tag{13}$$

where the matrix elements $\hat{H}(nn';\mathbf{k}\mathbf{k}_0)$ are defined to be

$$\hat{H}(nn';\mathbf{k}\mathbf{k}_0) \equiv \left[E_n(\mathbf{k}_0) + \frac{\hbar^2}{2m}(\mathbf{k}^2 - {\mathbf{k}_0}^2)\right]\delta(n,n') + \frac{\hbar}{m}(\mathbf{k}-\mathbf{k}_0)\cdot\mathbf{p}(n,n';\mathbf{k}_0), \tag{14}$$

with the momentum matrix element between two $\mathbf{k}_0$ basis states given by:

$$\mathbf{p}(n,n';\mathbf{k}_0) \equiv \int d^3\mathbf{x}\, u_n^*(\mathbf{k}_0;\mathbf{x})\mathbf{p}u_{n'}(\mathbf{k}_0;\mathbf{x}), \tag{15}$$

the integration being over the primitive cell on which the $\mathbf{k}_0$ basis states are normalized.

The matrix equation Eq. (13) is the eigenvalue equation for a general cell-periodic at wavevector $\mathbf{k}$, $u_n(\mathbf{k};\mathbf{x})$, when the $\mathbf{k}_0$ basis functions $\{u_n(\mathbf{k}_0;\mathbf{x})\}$ are taken as the expansion set. Although Eq. (13) can be solved for any wavevector $\mathbf{k}$, it is most useful when $\mathbf{k}$ is near $\mathbf{k}_0$ such that the non-diagonal part of the Hamiltonian $\hat{H}(nn';\mathbf{k}\mathbf{k}_0)$,

$$\frac{\hbar}{m}(\mathbf{k}-\mathbf{k}_0)\cdot\mathbf{p}(n,n';\mathbf{k}_0)$$

is small.

4.1.2 Expansion on set of functions at k= 0

In the special case where the basis functions $\{u_n(\mathbf{k}_0;\mathbf{x})\}$ are taken to be at the center of the Brillouin zone, *i.e.*, $\mathbf{k}_0 = \mathbf{0}$, the above expressions take on a particularly simple form. In this case, the expansion Eq. (8) becomes:

$$u_n(\mathbf{k};\mathbf{x}) = \sum_{n'} u_{n'}(\mathbf{x})C(nn';\mathbf{k}), \tag{16}$$

so that the Bloch solutions of Eq.(1) become

$$\langle \mathbf{x}|n\mathbf{k}\rangle = \exp(i\mathbf{k}\cdot\mathbf{x})\sum_{n'} u_{n'}(\mathbf{x})C(nn';\mathbf{k}), \tag{17}$$

dropping the index $\mathbf{k}_0 = \mathbf{0}$ altogether.

The set of zone-center basis functions $\{u_n(\mathbf{x})\}$ satisfy the $\mathbf{k}_0 = \mathbf{0}$ Schrödinger equation, Eq.(10):

$$\hat{H}_0 u_n(\mathbf{x}) = E_n(\mathbf{0})u_n(\mathbf{x}), \tag{18}$$

where the $\mathbf{k}_0 = \mathbf{0}$ Hamiltonian, $\hat{H}_0$ is simply:

$$\hat{H}_0 \equiv \frac{1}{2m}\mathbf{p}^2 + V(\mathbf{x}). \tag{19}$$

Thus the equation for $u_n(\mathbf{x})$ associated with $\mathbf{k}_0 = \mathbf{0}$ has the symmetry of the crystal potential $V(\mathbf{x})$ which is the symmetry of the crystal space group.

The set of energies $E_n(\mathbf{0})$ corresponds to the energies of the Bloch states at the center of the Brillouin zone. For a general $\mathbf{k}$, the Schrödinger equation becomes:

$$\hat{H}(\mathbf{k})u_n(\mathbf{k};\mathbf{x}) = E_n(\mathbf{k})u_n(\mathbf{k};\mathbf{x}), \tag{20}$$

where the $\mathbf{k}$-dependent Hamiltonian, $\hat{H}(\mathbf{k})$, has the simple form:

$$\hat{H}(\mathbf{k}) \equiv \hat{H}_0 + \frac{\hbar}{m}\mathbf{k}\cdot\mathbf{p} + \frac{\hbar^2}{2m}\mathbf{k}^2. \tag{21}$$

The Hamiltonian $\hat{H}_0$ is simply the $\mathbf{k}_0 = \mathbf{0}$ Hamiltonian of Eq. (19). The kinetic energy term,

$$\frac{\hbar^2}{2m}\mathbf{k}^2$$

is simply a c-number that produces a shift in the energy eigenvalues $E_n(\mathbf{k})$. The term

$$\frac{\hbar}{m}\mathbf{k}\cdot\mathbf{p}$$

is referred to as the $\mathbf{k}\cdot\mathbf{p}$ Hamiltonian.

In the special case where $\mathbf{k}_0 = \mathbf{0}$ the matrix equation Eq. (13) becomes, in terms of the zone-center expansion set $\{u_n(\mathbf{x})\}$,

$$\sum_{n'} \hat{H}(nn';\mathbf{k})C(nn';\mathbf{k}) = E_n(\mathbf{k})C(nn';\mathbf{k}), \tag{22}$$

where the matrix elements $\hat{H}(nn';\mathbf{k})$ are defined to be

$$\hat{H}(nn';\mathbf{k}) \equiv \left[E_n(\mathbf{0}) + \frac{\hbar^2}{2m}\mathbf{k}^2\right]\delta(n,n') + \frac{\hbar}{m}\mathbf{k}\cdot\mathbf{p}(n,n'), \tag{23}$$

with the momentum matrix element between zone-center basis states given by:

$$\mathbf{p}(n,n') \equiv \int d^3\mathbf{x}\, u_n^*(\mathbf{x})\mathbf{p}u_{n'}(\mathbf{x}). \tag{24}$$

Since the operator $\mathbf{p}$ transforms according to a *vector representation*, the Hamiltonian matrix $\hat{H}(nn';\mathbf{k})$ *can have non-diagonal elements only between zone-center states* $u_n(\mathbf{x})$ *of opposite parity.*

Direct diagonalization of the $\mathbf{k}\cdot\mathbf{p}$ Hamiltonian matrix $\hat{H}(nn';\mathbf{k})$ of Eq.(22) yields the energy eigenvalues $E_n(\mathbf{k})$ across the entire Brillouin zone. Furthermore, the eigenvector matrix consisting of the expansion coefficients, $C(nn';\mathbf{k})$, are used to construct the Bloch states:

$$\begin{aligned}\langle\mathbf{x}|n\mathbf{k}\rangle &= \exp(i\mathbf{k}\cdot\mathbf{x})u_n(\mathbf{k};\mathbf{x}),\\ \langle\mathbf{x}|n\mathbf{k}\rangle &= \exp(i\mathbf{k}\cdot\mathbf{x})\sum_{n'} u_{n'}(\mathbf{x})C(nn';\mathbf{k}),\end{aligned} \tag{25}$$

in terms of the zone-center expansion set $\{u_n(\mathbf{x})\}$ at $\mathbf{k}_0 = \mathbf{0}$.

References

1. E. O. Kane, *Physics of III-V Compounds*, edited by A. C. Beer and R. K. Willardson (Academic, New York, 1966), Vol. 1, p. 75
2. C. Kittel, *Quantum Theory of Solids* , (John Wiley, New York, 1963) p. 182.

APPENDIX 4.2

Pseudopotentials formulation:

The purpose of this appendix is twofold,

• First, we give a brief description of the pseudopotential theory as it is used for the calculation of the electronic band structure of bulk crystalline solids. This appendix is a collection of results regarding the *local pseudopotential theory.* The major derivation and the theoretical justifications can be found in the review articles by Cohen and Heine[1].

• Secondly, we treat the specialized case of semiconductor with the diamond or zincblende structure.

4.2.1 Pseudopotential Theory of Bulk Semiconductors

Briefly, a *pseudopotential is a potential such that an expansion of the pseudo Bloch states* $\{|\text{pseudo}; n\mathbf{k}\rangle\}$ *in terms of plane waves* $\{|\mathbf{g}\rangle\}$ *associated with reciprocal lattice vector* $\mathbf{g}$*, will converge.* We briefly outline below the procedure.

Given that the set of pseudo Bloch states $\{|\text{pseudo}; n\mathbf{k}\rangle\}$ are solutions to the Schrödinger equation for the bulk solid:

$$\hat{H}^{\text{pseudo}}|\text{pseudo}; n\mathbf{k}\rangle = E_n(\mathbf{k})|\text{pseudo}; n\mathbf{k}\rangle. \tag{1}$$

The pseudo Hamiltonian is

$$\hat{H}^{\text{pseudo}} = \frac{1}{2m}\mathbf{p}^2 + V_{\text{pseudo}}(\mathbf{x}), \tag{2}$$

where $V_{\text{pseudo}}(\mathbf{x}+\mathbf{R}) = V_{\text{pseudo}}(\mathbf{x})$ is a pseudopotential which has the symmetry of the crystal space group. The momentum operator is $\mathbf{p} \equiv -i\hbar\nabla$. The energy eigenvalues, $E_n(\mathbf{k})$, are the same for the set of pseudo Bloch states and the set of true Bloch states. The pseudo Bloch states $\{|\text{pseudo}; n\mathbf{k}\rangle\}$ are *smoothly varying in the core regions in contrast with the true Bloch states* $\{|n\mathbf{k}\rangle\}$.

We now expand the pseudo Bloch solutions of Eq.(1), $\{|\text{pseudo}; n\mathbf{k}\rangle\}$, in terms of a set of plane waves $\{|\mathbf{g}\rangle\}$,

$$|\text{pseudo}; n\mathbf{k}\rangle = \exp(i\mathbf{k}\cdot\mathbf{x})\sum_{\mathbf{g}}|\mathbf{g}\rangle C^{(n)}(\mathbf{g},\mathbf{k}), \tag{3}$$

where, in the $\mathbf{x}$-representation, we define the plane wave associated with the reciprocal lattice vector $\mathbf{g}$ as,

$$\langle\mathbf{x}|\mathbf{g}\rangle \equiv \exp(i\mathbf{g}\cdot\mathbf{x}) \tag{4}$$

By substitution of the plane wave expansion Eq.(3) in Schrödinger equation,

$$\hat{H}^{\text{pseudo}}|\text{pseudo}; n\mathbf{k}\rangle = E_n(\mathbf{k})|\text{pseudo}; n\mathbf{k}\rangle, \tag{5}$$

we arrive at the matrix equation,

$$\sum_{\mathbf{g}'}\hat{H}^{\text{pseudo}}_{\text{local}}(\mathbf{g}\mathbf{g}';\mathbf{k})C^{(n)}(\mathbf{g}',\mathbf{k}) = E_n(\mathbf{k})C^{(n)}(\mathbf{g},\mathbf{k}). \tag{6}$$

We define the pseudopotential form factors $V(\mathbf{g})$ as the Fourier amplitudes of the pseudopotential $V_{\text{pseudo}}(\mathbf{x})$,

$$V_{\text{pseudo}}(\mathbf{x}) = \sum_{\mathbf{g}}\exp(i\mathbf{g}\cdot\mathbf{x})V(\mathbf{g}). \tag{7}$$

The pseudopotential form factors $V(\mathbf{g})$ can be written as a product of an *structure factor* $S_\alpha(\mathbf{g})$ and a *atomic form factor* $V_\alpha(\mathbf{g})$, associated with the atomic species

α,

$$V_{\text{pseudo}}(\mathbf{x}) = \sum_{\mathbf{g}} \exp(i\mathbf{g}\cdot\mathbf{x})V(\mathbf{g}). \tag{8}$$

where

$$V(\mathbf{g}) = \sum_{\alpha} S_\alpha(\mathbf{g})V_\alpha(\mathbf{g}), \tag{9}$$

where the sum is over all the atomic species α within the primitive cell.

• The *structure factors* $S_\alpha(\mathbf{g})$ associated with the plane wave $\mathbf{g}$ are defined as,

$$S_\alpha(\mathbf{g}) \equiv \frac{1}{N_\alpha} \sum_{j} \exp(i\mathbf{g}\cdot\mathbf{d}_\alpha^j), \tag{10}$$

where N_α is the number of atomic species present. The sum $\sum_j$ is over all the primitive cells, and $\mathbf{d}_\alpha^j$ is the position vector associated with the atomic species α within the primitive cell j.

• The *atomic form factors* $V_\alpha(\mathbf{g})$ are the Fourier transforms of the atomic pseudopotentials $V_\alpha(\mathbf{x})$ associated with the atomic species α,

$$V_\alpha(\mathbf{g}) \equiv \frac{1}{\Omega_\alpha} \int d^3\mathbf{x} \exp(-i\mathbf{g}\cdot\mathbf{x})V_\alpha(\mathbf{x}), \tag{11}$$

where Ω_α is the atomic volume.

4.2.2 Local and Non-Local Pseudopotentials

The purpose of this section is to make a distinction between *local pseudopotentials* and *non-local pseudopotentials.* In order to do so, let us first define what is meant by an *orthogonalized plane wave* (OPW). We define an OPW as a *plane wave that has been orthogonalized to the core states of the atom,*

$$|\text{opw};\mathbf{k}+\mathbf{g}\rangle \equiv \left[1-\sum_c |\varphi_c\rangle\langle\varphi_c|\right]|\text{pw};\mathbf{k}+\mathbf{g}\rangle, \tag{12}$$

where $|\text{pw};\mathbf{k}+\mathbf{g}\rangle$ is simply the *plane wave*

$$\langle\mathbf{x}|\text{pw};\mathbf{k}+\mathbf{g}\rangle \equiv \exp\left[i(\mathbf{k}+\mathbf{g})\cdot\mathbf{x}\right], \tag{13}$$

and $|\varphi_c\rangle$ stands for the core state whose eigenenergy is E_c. The sum $\sum_c$ runs over all the core states of all the atoms.

In the OPW representation the *pseudopotential operator* $\hat{V}^{\text{opw}}$ can be written as

$$\hat{V}^{\text{opw}} \equiv V(\mathbf{x}) + \sum_c \left[E_n(\mathbf{k}) - E_c\right]|\varphi_c\rangle\langle\varphi_c|, \tag{14}$$

where the potential $V(\mathbf{x})$ stands for the *true crystal potential.* More specifically, by using the definition of $|\text{opw};\mathbf{k}+\mathbf{g}\rangle$, we can write the matrix elements,

$$V^{\text{opw}}(\mathbf{g}\mathbf{g}';\mathbf{k}) \equiv \langle\text{opw};\mathbf{k}+\mathbf{g}|\hat{V}^{\text{opw}}|\text{opw};\mathbf{k}+\mathbf{g}'\rangle, \tag{15}$$

$$V^{\text{opw}}(\mathbf{g}\mathbf{g}';\mathbf{k}) \equiv V(\mathbf{g}\mathbf{g}') + \sum_c \left[E_n(\mathbf{k}) - E_c\right]\langle\text{pw};\mathbf{k}+\mathbf{g}|\varphi_c\rangle\langle\varphi_c|\text{pw};\mathbf{k}+\mathbf{g}'\rangle. \tag{16}$$

The operator $\hat{V}^{\text{opw}}$ is a *non-local operator* due to the non-locality of the operator $|\varphi_c\rangle\langle\varphi_c|$. Thus the pseudopotential $\hat{V}^{\text{opw}}$ depends

- on the *energy eigenvalues* $E_n(\mathbf{k})$, and
- on the *l-angular momentum components* present in the core states $|\varphi_c\rangle$.

In the *local pseudopotential approximation* used in the present work, *we neglect the l-angular momentum dependence of the pseudopotential operator* $\hat{V}^{\text{opw}}$. Within the *local pseudopotential approximation*, the pseudopotential Hamiltonian matrix in the plane wave representation, is simply

$$\hat{H}^{\text{pseudo}}_{\text{local}}(\mathbf{g}\mathbf{g}';\mathbf{k}) = \frac{\hbar^2}{2m}[\mathbf{k}+\mathbf{g}]^2\delta^3(\mathbf{g}-\mathbf{g}') + V(\mathbf{g}\mathbf{g}') \tag{17}$$

where the off-diagonal matrix elements $V(\mathbf{g}\mathbf{g}')$ are the *pseudopotentials form factors.*

This local pseudopotential approach has proven to be adequate to explain most of the optical data available for semiconductor compounds[2].

Furthermore, if we take the atomic pseudopotentials to be spherically symmetric,

$$V_\alpha(\mathbf{x}) \equiv V_\alpha(|\mathbf{x}|), \tag{18}$$

then the pseudopotential form factors $V(\mathbf{g}\mathbf{g}')$ *depend only on the magnitude of* $\mathbf{g}$,

$$V(\mathbf{g}\mathbf{g}') \equiv V(|\mathbf{g}-\mathbf{g}'|). \tag{19}$$

In the *empirical local pseudopotential method* used within the context of this work, the pseudopotential form factors, $V(|\mathbf{g}-\mathbf{g}'|)$ are empirical parameters fitted to the optical data.

3.2.3 Application to Diamond and Zincblende Structures

In the case of semiconductors with the diamond or zincblende structure, the above treatment may be specialized. Suppose a semiconductor whose stoichiometry is $a^N c^{8-N}$, where the atomic species $\alpha \equiv a$ represents an *anion* and the atomic species $\alpha \equiv c$ represents a *cation*. Then the pseudopotential form factor can be written as the sum of a *symmetric* part $V^{(S)}(\mathbf{g})$ and an *antisymmetric* part $V^{(A)}(\mathbf{g})$,

$$V(\mathbf{g}) = \sum_{\alpha} S_\alpha(\mathbf{g}) V_\alpha(\mathbf{g}), \tag{20}$$

or,

$$V(\mathbf{g}) = V^{(S)}(\mathbf{g}) \cos(\mathbf{g} \cdot \mathbf{d}_0) + iV^{(A)}(\mathbf{g}) \sin(\mathbf{g} \cdot \mathbf{d}_0), \tag{21}$$

where the *symmetric part* is given by

$$V^{(S)}(\mathbf{g}) = \frac{1}{2}[V_a(\mathbf{g}) + V_c(\mathbf{g})], \tag{22}$$

and the *antisymmetric part* is given by

$$V^{(A)}(\mathbf{g}) = \frac{1}{2}[V_a(\mathbf{g}) - V_c(\mathbf{g})]. \tag{23}$$

The origin in the calculation of the structure factor $S_\alpha(\mathbf{g})$ is symmetrically taken to be halfway between the anion-cation bond,

$$\mathbf{d}_0 \equiv \left[\frac{a}{8}\right](\hat{\mathbf{x}} + \hat{\mathbf{y}} + \hat{\mathbf{z}}), \tag{24}$$

and a is the length of the conventional cubic unit cell.

It is clear that for the diamond structure with O_h symmetry, the antisymmetric part of the pseudopotential form factor vanishes,

$$V^{(A)}(\mathbf{g})(O_h) \equiv 0. \tag{25}$$

References

1. M. L. Cohen, and V. Heine, *Solid State Physics*, edited by H. Ehrenreich, F. Seitz, and D. Turnbull, (Academic, New York, 1970), Vol. 24, p. 38.
2. M. L. Cohen and T. K. Bergstresser, *Phys. Rev.* **141**, 789 (1966).

APPENDIX 4.3

Pseudopotentials and $\mathbf{k} \cdot \mathbf{p}$ formulations:

The purpose of this appendix is twofold,

• First, we relate the $\mathbf{k} \cdot \mathbf{p}$ and pseudopotentials formulations as presented in Appendices (4.1) and (4.2).

• Secondly, we describe the procedure used to express the $\mathbf{k}_0 = \mathbf{0}$ basis function of two zincblende semiconductors in terms of the $\mathbf{k}_0 = \mathbf{0}$ basis function of a *reference solid*.

4.3.1 Connection between Pseudopotential and $\mathbf{k} \cdot \mathbf{p}$ Theories of Bulk Semiconductors

From the preceding two Appendices, it is clear that the set of $\mathbf{k}_0 = \mathbf{0}$ states, $\{|m\rangle\}$ can be expanded in terms of the set of plane waves $\{|\mathbf{g}\rangle\}$, where $\mathbf{g}$ is a reciprocal lattice vector,

$$|m\rangle = \sum_{\mathbf{g}} |\mathbf{g}\rangle U(\mathbf{g}, m). \tag{1}$$

In $\mathbf{x}$-representation, we have explicitly

$$\langle \mathbf{x}|m\rangle \equiv u_m(\mathbf{x}), \tag{2.a}$$

for the $\mathbf{k}_0 = \mathbf{0}$ basis functions, and

$$\langle \mathbf{x}|\mathbf{g}\rangle \equiv \exp(i\mathbf{g} \cdot \mathbf{x}), \tag{2.b}$$

for the plane waves.

For a complete set $\{|m\rangle\}$ we have the *closure relation*

$$\sum_m |m\rangle\langle m| = \mathbf{1}, \tag{3}$$

which, in the $\{|\mathbf{g}\rangle\}$-representation, translates into

$$\sum_m U(\mathbf{g}, m) \cdot \left[U(\mathbf{g}', m)\right]^\dagger = \delta^3(\mathbf{g} - \mathbf{g}'). \tag{4}$$

The transformation matrix $U(\mathbf{g}, m)$ allows us to transform from the $\{|\mathbf{g}\rangle\}$-representation to the $\{|m\rangle\}$-representation. Thus, we can transform from the local pseudopotential formulation to the $\mathbf{k}\cdot\mathbf{p}$ formulation with the help of the **U** matrix,

$$\hat{H}(mm';\mathbf{k}) = \sum_{\mathbf{g}}\sum_{\mathbf{g}'} [U(\mathbf{g}, m)]^\dagger \hat{H}^{\text{pseudo}}_{\text{local}}(\mathbf{g}\mathbf{g}';\mathbf{k}) U(\mathbf{g}', m'), \tag{5}$$

• In the $\{|\mathbf{g}\rangle\}$-representation the Hamiltonian matrix is given by the local pseudopotential Hamiltonian,

$$\hat{H}^{\text{pseudo}}_{\text{local}}(\mathbf{g}\mathbf{g}';\mathbf{k}) \equiv \frac{\hbar^2}{2m}[\mathbf{k}+\mathbf{g}]^2\delta^3(\mathbf{g}-\mathbf{g}') + V(\mathbf{g}\mathbf{g}'), \tag{6}$$

where the off-diagonal matrix elements $V(\mathbf{g}\mathbf{g}')$ are the pseudopotential form factors.

• In the $\{|m\rangle\}$-representation the Hamiltonian matrix is given by the $\mathbf{k}\cdot\mathbf{p}$ Hamiltonian,

$$\hat{H}(mm';\mathbf{k}) \equiv \left[E_m(\mathbf{0}) + \frac{\hbar^2}{2m}\mathbf{k}^2\right]\delta(m,m') + \frac{\hbar}{m}\mathbf{k}\cdot\langle m|\mathbf{p}|m'\rangle + \Delta V(mm'), \tag{7}$$

where the perturbation potential in the $\{|m\rangle\}$-representation is

$$\Delta V(mm') = \sum_{\mathbf{g}}\sum_{\mathbf{g}'} [U(\mathbf{g}, m)]^\dagger \Delta V(\mathbf{g}\mathbf{g}') U(\mathbf{g}', m'), \tag{8.a}$$

and the momemtum matrix element between zone-center basis states given as above by:

$$\langle m|\mathbf{p}|m'\rangle \equiv \int d^3\mathbf{x} u^*_m(\mathbf{x})\mathbf{p}u_{m'}(\mathbf{x}). \tag{8.b}$$

and $E_m(\mathbf{0})$ is the energy of the state $|m\rangle$ at $\mathbf{k}_0 = \mathbf{0}$.

We will make extensive use of the transformation relation Eq.(3) in the following section.

It is a simple matter to find the transformation matrix **U**. The matrix **U** is the *eigenvector matrix that diagonalizes the local pseudopotential Hamiltonian,*

$$\hat{H}^{\text{pseudo}}_{\text{local}}(\mathbf{gg}';\mathbf{k}) = \frac{\hbar^2}{2m}[\mathbf{k}+\mathbf{g}]^2\delta^3(\mathbf{g}-\mathbf{g}') + V(\mathbf{gg}'), \tag{9.a}$$

at $\mathbf{k} = \mathbf{0}$,

$$\left[\hat{H}(mm';\mathbf{k})\right]_{\mathbf{k}=\mathbf{0}} = \left[\sum_{\mathbf{g}}\sum_{\mathbf{g}'}[U(\mathbf{g},m)]^\dagger \hat{H}^{\text{pseudo}}_{\text{local}}(\mathbf{gg}';\mathbf{k})U(\mathbf{g}',m')\right]_{\mathbf{k}=\mathbf{0}}, \tag{9.b}$$

$$\left[\hat{H}(mm';\mathbf{k})\right]_{\mathbf{k}=\mathbf{0}} = E_m(\mathbf{0})\delta(m,m'). \tag{9.c}$$

4.3.2 Reference Solid:

4.3.2.1 Pseudopotential Formalism

In this second part of the Appendix(4.3) we describe the prescription to express the $\mathbf{k}_0 = \mathbf{0}$ basis function of two zincblende solids in terms of the $\mathbf{k}_0 = \mathbf{0}$ basis functions of a reference solid. The procedure is rather well exemplified within the *local pseudopotential* formalism.

• Suppose a zincblende semiconductor whose stoichiometry is $a^N c^{8-N}$, where the atomic species $\alpha \equiv a$ represents an *anion* and the atomic species $\alpha \equiv c$ represents a *cation*. Consider a solid $j = 1, 2$ described in terms of a local pseudopotential Hamiltonian of the form

$$\hat{H}^{(j)}(\mathbf{g}\mathbf{g}';\mathbf{k}) \equiv \frac{\hbar^2}{2m}[\mathbf{k}+\mathbf{g}]^2\delta^3(\mathbf{g}-\mathbf{g}') + V^{(j)}(\mathbf{g}\mathbf{g}'), \tag{10.a}$$

The pseudopotential form factor $V^{(j)}(\mathbf{g})$ can be written as the sum of a *symmetric* part $V^{(j;S)}(\mathbf{g})$ and an *antisymmetric* part $V^{(j;A)}(\mathbf{g})$,

$$V^{(j)}(\mathbf{g}) = V^{(j;S)}(\mathbf{g})\cos(\mathbf{g}\cdot\mathbf{d}_0) + iV^{(j;A)}(\mathbf{g})\sin(\mathbf{g}\cdot\mathbf{d}_0), \tag{10.b}$$

where the *symmetric part* is given by

$$V^{(j;S)}(\mathbf{g}) = \frac{1}{2}\left[V_a^{(j)}(\mathbf{g}) + V_c^{(j)}(\mathbf{g})\right], \tag{11.a}$$

and the *antisymmetric part* is given by

$$V^{(j;A)}(\mathbf{g}) = \frac{1}{2}\left[V_a^{(j)}(\mathbf{g}) - V_c^{(j)}(\mathbf{g})\right]. \tag{11.b}$$

The origin in the calculation of the structure factor is symmetrically taken to be halfway between the anion-cation bond,

$$\mathbf{d}_0 \equiv \left[\frac{a}{8}\right](\hat{\mathbf{x}}+\hat{\mathbf{y}}+\hat{\mathbf{z}}), \tag{12}$$

and a is the length of the conventional cubic unit cell.

We now wish to express the Hamiltonian $\hat{H}^{(j)}(\mathbf{gg}';\mathbf{k})$ in terms of a Hamiltonian $\hat{H}^{(0)}(\mathbf{gg}';\mathbf{k})$ associated with a reference solid. Suppose that the reference solid is described in terms of a local pseudopotential Hamiltonian of the form,

$$\hat{H}^{(0)}(\mathbf{gg}';\mathbf{k}) \equiv \frac{\hbar^2}{2m}[\mathbf{k}+\mathbf{g}]^2\delta^3(\mathbf{g}-\mathbf{g}') + V^{(0)}(\mathbf{gg}'). \tag{13}$$

Let us take the reference solid Hamiltonian to be the *average of the local pseudopotential Hamiltonians* $\hat{H}^{(j)}(\mathbf{gg}';\mathbf{k})$ *in each solid* $j = 1, 2$

$$\hat{H}^{(0)}(\mathbf{gg}';\mathbf{k}) \equiv \frac{1}{2}\sum_{j=1}^{2}\hat{H}^{(j)}(\mathbf{gg}';\mathbf{k}). \tag{14}$$

The pseudopotential form factor $V^{(0)}(\mathbf{g})$ can be written as the sum of a *symmetric* part $V^{(0;S)}(\mathbf{g})$ and an *antisymmetric* part $V^{(0;A)}(\mathbf{g})$,

$$V^{(0)}(\mathbf{g}) = V^{(0;S)}(\mathbf{g})\cos(\mathbf{g}\cdot\mathbf{d}_0) + iV^{(0;A)}(\mathbf{g})\sin(\mathbf{g}\cdot\mathbf{d}_0), \tag{15.a}$$

where the *symmetric part* is given by

$$V^{(0;S)}(\mathbf{g}) = \frac{1}{2}\sum_{j=1}^{2}V^{(j;S)}(\mathbf{g}) \tag{15.b}$$

and the *antisymmetric part* is given by

$$V^{(0;A)}(\mathbf{g}) = \frac{1}{2}\sum_{j=1}^{2}V^{(j;A)}(\mathbf{g}). \tag{15.c}$$

• The Hamiltonian of solid $j = 1, 2$ can now be written as a sum of the reference Hamiltonian $\hat{H}^{(0)}(\mathbf{gg}';\mathbf{k})$, plus a perturbation term $\Delta V^{(j)}(\mathbf{gg}')$,

$$\hat{H}^{(j)}(\mathbf{gg}';\mathbf{k}) = \hat{H}^{(0)}(\mathbf{gg}';\mathbf{k}) + \Delta V^{(j)}(\mathbf{gg}'). \tag{16}$$

The perturbation pseudopotential form factor $\Delta V^{(j)}(\mathbf{g})$ can be written as the sum of a *symmetric* part $\Delta V^{(j;S)}(\mathbf{g})$ and an *antisymmetric* part $\Delta V^{(j;A)}(\mathbf{g})$,

$$\Delta V^{(j)}(\mathbf{g}) = \Delta V^{(j;S)}(\mathbf{g})\cos(\mathbf{g}\cdot\mathbf{d}_0) + i\Delta V^{(j;A)}(\mathbf{g})\sin(\mathbf{g}\cdot\mathbf{d}_0), \tag{17.a}$$

where the *symmetric part* is given by

$$\Delta V^{(j;S)}(\mathbf{g}) = \frac{1}{2}\left[V^{(j;S)}(\mathbf{g}) - V^{(i;S)}(\mathbf{g})\right], \tag{17.b}$$

and the *antisymmetric part* is given by

$$\Delta V^{(j;A)}(\mathbf{g}) = \frac{1}{2}\left[V^{(j;A)}(\mathbf{g}) - V^{(i;A)}(\mathbf{g})\right]. \tag{17.c}$$

We have now expressed the local pseudopotential Hamiltonians $\hat{H}^{(j)}(\mathbf{g}\mathbf{g}';\mathbf{k})$ of the two solids $j = 1, 2$ in terms of the local pseudopotential Hamiltonians $\hat{H}^{(0)}(\mathbf{g}\mathbf{g}';\mathbf{k})$ of the reference solid.

4.3.2.2 $\mathbf{k} \cdot \mathbf{p}$ Formalism

In this section we wish to translate the results of the preceding section from the pseudopotential to the $\mathbf{k} \cdot \mathbf{p}$ formalism using the transformation matrix, U.

• Let the set of $\mathbf{k}_0 = \mathbf{0}$ basis function $\{|m\rangle\}$ refer to *reference solid*. At each $\mathbf{k}$, we can transform the Hamiltonian of the reference solid from the $\{|\mathbf{g}\rangle\}$-representation to the $\{|m\rangle\}$-representation with the U matrix,

$$\hat{H}^{(0)}(mm';\mathbf{k}) = \sum_{\mathbf{g}} \sum_{\mathbf{g}'} [U(\mathbf{g},m)]^{\dagger} \hat{H}^{(0)}(\mathbf{g}\mathbf{g}';\mathbf{k}) U(\mathbf{g}',m'), \tag{18}$$

where $\hat{H}^{(0)}(mm';\mathbf{k})$ is the Hamiltonian of the reference solid in the $\{|m\rangle\}$-representation. *At the special point* $\mathbf{k} = \mathbf{0}$ *the set of function* $\{|m\rangle\}$ *are eigenstates of* $\hat{H}^{(0)}(mm';\mathbf{k})$ *and the matrix* $\hat{H}^{(0)}(mm';\mathbf{k})$ *is diagonal,*

$$\left[\hat{H}^{(0)}(mm';\mathbf{k})\right]_{\mathbf{k}=\mathbf{0}} = \left[\sum_{\mathbf{g}} \sum_{\mathbf{g}'} [U(\mathbf{g},m)]^{\dagger} \hat{H}^{(0)}(\mathbf{g}\mathbf{g}';\mathbf{k}) U(\mathbf{g}',m')\right]_{\mathbf{k}=\mathbf{0}}, \tag{19.a}$$

$$\left[\hat{H}^{(0)}(mm';\mathbf{k})\right]_{\mathbf{k}=\mathbf{0}} = E_m(\mathbf{0})\delta(m,m'). \tag{19.b}$$

Thus, the $\{|m\rangle\}$-representation is the representation that diagonalizes the $\mathbf{k} \cdot \mathbf{p}$ Hamiltonian of the reference solid $\hat{H}^{(0)}(mm';\mathbf{k})$ at $\mathbf{k} = \mathbf{0}$.

• We now express the Hamiltonian of the solids $j = 1, 2$ in the $\{|m\rangle\}$-representation that diagonalizes $\hat{H}^{(0)}(mm';\mathbf{k})$ at $\mathbf{k} = \mathbf{0}$. From the preceding section, we have

$$\hat{H}^{(j)}(mm';\mathbf{k}) = \sum_{\mathbf{g}} \sum_{\mathbf{g}'} [U(\mathbf{g},m)]^{\dagger} \hat{H}^{(j)}(\mathbf{g}\mathbf{g}';\mathbf{k}) U(\mathbf{g}',m'), \tag{20.a}$$

but,

$$\hat{H}^{(j)}(\mathbf{g}\mathbf{g}';\mathbf{k}) = \hat{H}^{(0)}(\mathbf{g}\mathbf{g}';\mathbf{k}) + \Delta V^{(j)}(\mathbf{g}\mathbf{g}'), \tag{20.b}$$

therefore,

$$\hat{H}^{(j)}(mm';\mathbf{k}) = \sum_{\mathbf{g}}\sum_{\mathbf{g}'}[U(\mathbf{g},m)]^{\dagger}\Big[\hat{H}^{(0)}(\mathbf{g}\mathbf{g}';\mathbf{k}) + \Delta V^{(j)}(\mathbf{g}\mathbf{g}')\Big]U(\mathbf{g}',m'), \quad (20.c)$$

and finally, we can write explicitly,

$$\hat{H}^{(j)}(mm';\mathbf{k}) \equiv \left[E_m(\mathbf{0}) + \frac{\hbar^2}{2m}\mathbf{k}^2\right]\delta(m,m') + \frac{\hbar}{m}\mathbf{k}\cdot\langle m|\mathbf{p}|m'\rangle + \Delta V^{(j)}(mm'), \quad (20.d)$$

where the perturbation potential in the $\{|m\rangle\}$-representation is

$$\Delta V^{(j)}(mm') = \sum_{\mathbf{g}}\sum_{\mathbf{g}'}[U(\mathbf{g},m)]^{\dagger}\Delta V^{(j)}(\mathbf{g}\mathbf{g}')U(\mathbf{g}',m'). \quad (20.e)$$

We see that *in a $\{|m\rangle\}$-representation in which the reference Hamiltonian $\hat{H}^{(0)}(mm';\mathbf{k})$ is diagonal, the Hamiltonian of solid (j) contains a non-diagonal perturbation term* $\Delta V^{(j)}(mm')$. In general the Hamiltonian $\hat{H}^{(0)}(mm';\mathbf{k})$ of the reference solid and the Hamiltonian $\hat{H}^{(j)}(mm';\mathbf{k})$ for the solids $j = 1, 2$ will have T_d symmetry associated with the zincblende structure.

APPENDIX 4.4

The purpose of this appendix is twofold.

• First we review the full-zone $\mathbf{k} \cdot \mathbf{p}$ theory as it is used to obtain accurate energy bandstructure throughout the first Brillouin zone. The $\mathbf{k} \cdot \mathbf{p}$ Hamiltonian is derived from a local pseudopotential Hamiltonian.

• Second, we indicate the prescription to obtain the complex-$\mathbf{k}$ energy band structure of a solid within the full-zone $\mathbf{k} \cdot \mathbf{p}$ theory. We introduce the *companion matrix*, whose eigenvectors play a crucial role in the application of the *boundary conditions* for the superlattice wavefunction.

We collect these derivations in a single appendix since they are intimately interconnected.

4.4.1 Full-zone k.p Method: Reference Solid

4.4.1.1 Advantage of $\mathbf{k} \cdot \mathbf{p}$ Approach:

The $\mathbf{k} \cdot \mathbf{p}$ method has been particularly successful to describe the features of the band structure near the band edges to great accuracy. We have derived a $\mathbf{k} \cdot \mathbf{p}$ Hamiltonian from a local pseudopotential Hamiltonian in order to describe accurately the electronic band structure of each constituent semiconductor with a small number of basis function associated with the symmetry point $\mathbf{k}_0 = \mathbf{0}$.

In Appendix (4.3), we related the set of $\mathbf{k}_0 = \mathbf{0}$ states, $\{|m\rangle\}$, of the *reference solid* to the set of plane waves $\{|\mathbf{g}\rangle\}$, where $\mathbf{g}$ is a reciprocal lattice vector, through

$$|m\rangle = \sum_{\mathbf{g}} |\mathbf{g}\rangle U(\mathbf{g}, m). \tag{1}$$

Where, in the **x**-representation, we write

$$\langle \mathbf{x}|m\rangle \equiv u_m(\mathbf{x}), \tag{2.a}$$

for the $\mathbf{k}_0 = \mathbf{0}$ basis functions, and

$$\langle \mathbf{x}|\mathbf{g}\rangle \equiv \exp(i\mathbf{g}\cdot\mathbf{x}), \tag{2.b}$$

for the plane waves. As was shown in Appendix (4.3), the transformation matrix **U** allows us to transform from the $\{|\mathbf{g}\rangle\}$-representation to the $\{|m\rangle\}$-representation.

The local pseudopotential Hamiltonian $\hat{H}^{(j)}(\mathbf{g}\mathbf{g}';\mathbf{k})$ of the two solids $j = 1, 2$ is expressed in terms of the local pseudopotential Hamiltonians $\hat{H}^{(0)}(\mathbf{g}\mathbf{g}';\mathbf{k})$ of the reference solid,

$$\hat{H}^{(j)}(\mathbf{g}\mathbf{g}';\mathbf{k}) = \hat{H}^{(0)}(\mathbf{g}\mathbf{g}';\mathbf{k}) + \Delta V^{(j)}(\mathbf{g}\mathbf{g}'). \tag{3}$$

where the term $\Delta V^{(j)}(\mathbf{g}\mathbf{g}')$ is a perturbation term.

The perturbation pseudopotential form factor $\Delta V^{(j)}(\mathbf{g})$ can be written as the sum of a *symmetric* part $\Delta V^{(j;S)}(\mathbf{g})$ and an *antisymmetric* part $\Delta V^{(j;A)}(\mathbf{g})$,

$$\Delta V^{(j)}(\mathbf{g}) = \Delta V^{(j;S)}(\mathbf{g})\cos(\mathbf{g}\cdot\mathbf{d}_0) + i\Delta V^{(j;A)}(\mathbf{g})\sin(\mathbf{g}\cdot\mathbf{d}_0), \tag{4.a}$$

where the *symmetric part* is given by

$$\Delta V^{(j;S)}(\mathbf{g}) = \frac{1}{2}\left[V^{(j;S)}(\mathbf{g}) - V^{(i;S)}(\mathbf{g})\right], \tag{4.b}$$

and the *antisymmetric part* is given by

$$\Delta V^{(j;A)}(\mathbf{g}) = \frac{1}{2}\left[V^{(j;A)}(\mathbf{g}) - V^{(i;A)}(\mathbf{g})\right]. \tag{4.c}$$

We can transform from the $\{|\mathbf{g}\rangle\}$-representation to the $\{|m\rangle\}$-representation through the **U** matrix,

$$\hat{H}^{(j)}(mm';\mathbf{k}) = \sum_{\mathbf{g}}\sum_{\mathbf{g}'} [U(\mathbf{g},m)]^{\dagger}\hat{H}^{(j)}(\mathbf{g}\mathbf{g}';\mathbf{k})U(\mathbf{g}',m'), \tag{5.a}$$

but,

$$\hat{H}^{(j)}(\mathbf{g}\mathbf{g}';\mathbf{k}) = \hat{H}^{(0)}(\mathbf{g}\mathbf{g}';\mathbf{k}) + \Delta V^{(j)}(\mathbf{g}\mathbf{g}'), \tag{5.b}$$

therefore,

$$\hat{H}^{(j)}(mm';\mathbf{k}) = \sum_{\mathbf{g}}\sum_{\mathbf{g}'} [U(\mathbf{g},m)]^{\dagger}\left[\hat{H}^{(0)}(\mathbf{g}\mathbf{g}';\mathbf{k}) + \Delta V^{(j)}(\mathbf{g}\mathbf{g}')\right]U(\mathbf{g}',m'). \tag{5.c}$$

We can also write explicitly,

$$\hat{H}^{(j)}(mm';\mathbf{k}) \equiv \left[E_m(\mathbf{0}) + \frac{\hbar^2}{2m}\mathbf{k}^2\right]\delta(m,m') + \frac{\hbar}{m}\mathbf{k}\cdot\langle m|\mathbf{p}|m'\rangle + \Delta V^{(j)}(mm'), \tag{6}$$

where the perturbation potential in the $\{|m\rangle\}$-representation is

$$\Delta V^{(j)}(mm') = \sum_{\mathbf{g}}\sum_{\mathbf{g}'} [U(\mathbf{g},m)]^{\dagger}\Delta V^{(j)}(\mathbf{g}\mathbf{g}')U(\mathbf{g}',m'). \tag{7}$$

There are many reasons that make the $\mathbf{k}\cdot\mathbf{p}$ approach very attractive:

- the *convergence* is excellent for relatively *small numbers* of $\mathbf{k}_0 = \mathbf{0}$ basis functions,
- the $\mathbf{k}\cdot\mathbf{p}$ Hamiltonian $\hat{H}^{(j)}(mm';\mathbf{k})$ can be *explicitly constructed* once the transformation matrix **U** is knowm,
- the basis functions at $\mathbf{k}_0 = \mathbf{0}$ *of a single reference solid* can be used to describe the electronic structure of two different semiconductors.
- the advantage of using a *single reference solid* is clear: *The Bloch states in both component semiconductors forming the superlattice are expanded in terms of a common reference solid.* This approach has definite advantage when the superlattice state function has to be matched across the interfaces.

4.4.1.2 Truncation from Pseudopotential to k · p Formulation:

In practice the following procedure is used to derive the $\mathbf{k} \cdot \mathbf{p}$ Hamiltonian $\hat{H}^{(j)}(mm';\mathbf{k})$ for each solid $j = 1, 2$,

• Given the local pseudopotential Hamiltonian of each solid $j = 1, 2$,

$$\hat{H}^{(j)}(\mathbf{g}\mathbf{g}';\mathbf{k}) \equiv \frac{\hbar^2}{2m}[\mathbf{k}+\mathbf{g}]^2\delta^3(\mathbf{g}-\mathbf{g}') + V^{(j)}(\mathbf{g}\mathbf{g}'), \tag{8}$$

the local pseudopotential Hamiltonian of the reference solid is constructed from the *average of the Hamiltonian of each solid*,

$$\hat{H}^{(0)}(\mathbf{g}\mathbf{g}';\mathbf{k}) \equiv \frac{1}{2}\sum_{j=1}^{2}\hat{H}^{(j)}(\mathbf{g}\mathbf{g}';\mathbf{k}). \tag{9}$$

A total number of 113 plane waves $\{|\mathbf{g}\rangle\}$ are used to construct the local pseudopotential Hamiltonians $\hat{H}^{(j)}(\mathbf{g}\mathbf{g}';\mathbf{k})$, and $\hat{H}^{(0)}(\mathbf{g}\mathbf{g}';\mathbf{k})$. The plane waves $\{|\mathbf{g}\rangle\}$ used in the calculations are those associated with the reciprocal lattice vectors,

$$\mathbf{g} = \frac{2\pi}{a}(0,0,0), \frac{2\pi}{a}(\pm1,\pm1,\pm1),$$
$$\frac{2\pi}{a}(\pm2,0,0), \frac{2\pi}{a}(\pm2,\pm2,0),$$
$$\frac{2\pi}{a}(\pm1,\pm1,\pm3), \frac{2\pi}{a}(\pm2,\pm2,\pm2),$$
$$\frac{2\pi}{a}(\pm4,0,0), \frac{2\pi}{a}(\pm3,\pm3,\pm1),$$
$$\frac{2\pi}{a}(\pm4,\pm2,0),$$

where a is the bulk lattice constant for the solid under consideration.

• The local pseudopotential Hamiltonian of the *reference solid is diagonalized at* $\mathbf{k} = \mathbf{0}$,

$$\left[\hat{H}^{(0)}(mm';\mathbf{k})\right]_{\mathbf{k}=\mathbf{0}} = \left[\sum_{\mathbf{g}}\sum_{\mathbf{g}'}[U(\mathbf{g},m)]^{\dagger}\hat{H}^{(0)}(\mathbf{g}\mathbf{g}';\mathbf{k})U(\mathbf{g}',m')\right]_{\mathbf{k}=\mathbf{0}}, \tag{10.a}$$

$$\left[\hat{H}^{(0)}(mm';\mathbf{k})\right]_{\mathbf{k}=\mathbf{0}} = E_m(\mathbf{0})\delta(m,m'). \tag{10.b}$$

The eigenvector matrix **U** is the transformation matrix that allows the transformation from the $\{|\mathbf{g}\rangle\}$-representation to the $\{|m\rangle\}$-representation of the *reference solid.*

• Once the transformation matrix **U** is known, the $\mathbf{k}\cdot\mathbf{p}$ Hamiltonian of each solid $\hat{H}^{(j)}(mm';\mathbf{k})$ is obtained from the local pseudopotential Hamiltonian $\hat{H}^{(j)}(\mathbf{g}\mathbf{g}';\mathbf{k})$,

$$\hat{H}^{(j)}(mm';\mathbf{k}) = \sum_{\mathbf{g}}\sum_{\mathbf{g}'}[U(\mathbf{g},m)]^{\dagger}\hat{H}^{(j)}(\mathbf{g}\mathbf{g}';\mathbf{k})U(\mathbf{g}',m'), \tag{11.a}$$

or, using

$$\hat{H}^{(j)}(\mathbf{g}\mathbf{g}';\mathbf{k}) = \hat{H}^{(0)}(\mathbf{g}\mathbf{g}';\mathbf{k}) + \Delta V^{(j)}(\mathbf{g}\mathbf{g}'), \tag{11.b}$$

$$\hat{H}^{(j)}(mm';\mathbf{k}) = \sum_{\mathbf{g}}\sum_{\mathbf{g}'}[U(\mathbf{g},m)]^{\dagger}\left[\hat{H}^{(0)}(\mathbf{g}\mathbf{g}';\mathbf{k}) + \Delta V^{(j)}(\mathbf{g}\mathbf{g}')\right]U(\mathbf{g}',m'), \tag{11.c}$$

• It is impractical to transform from the $\{|\mathbf{g}\rangle\}$-representation to the $\{|m\rangle\}$-representation with the **U** at each **k** point since a large number of plane waves $\{|\mathbf{g}\rangle\}$ are involved in the construction of the Hamiltonians $\hat{H}^{(0)}(\mathbf{g}\mathbf{g}';\mathbf{k})$ and $\hat{H}^{(j)}(\mathbf{g}\mathbf{g}';\mathbf{k})$ for $j = 1, 2$. On the other hand, it is a simple matter to *construct explicitly the Hamiltonian* $\hat{H}^{(j)}(mm';\mathbf{k})$ *with the eigenvector matrix* $U(\mathbf{g},m)$.

As seen in Appendix (4.3), the explicit form of the Hamiltonian of the solid j in the $\{|m\rangle\}$-representation of the reference solid is,

$$\hat{H}^{(j)}(mm';\mathbf{k}) \equiv \left[E_m(\mathbf{0}) + \frac{\hbar^2}{2m}\mathbf{k}^2\right]\delta(m,m') + \frac{\hbar}{m}\mathbf{k}\cdot\langle m|\mathbf{p}|m'\rangle + \Delta V^{(j)}(mm'), \tag{12.a}$$

where the perturbation potential in the $\{|m\rangle\}$-representation is

$$\Delta V^{(j)}(mm') = \sum_{\mathbf{g}} \sum_{\mathbf{g}'} [U(\mathbf{g}, m)]^{\dagger} \Delta V^{(j)}(\mathbf{g}\mathbf{g}') U(\mathbf{g}', m'), \tag{12.b}$$

and the momentum matrix element between zone-center basis states given as above by:

$$\langle m|\mathbf{p}|m'\rangle \equiv \int d^3\mathbf{x} u^*_m(\mathbf{x}) \mathbf{p} u_{m'}(\mathbf{x}). \tag{12.c}$$

Once the Hamiltonian is expressed in the $\{|m\rangle\}$-representation only the first 27 $\mathbf{k}_0 = \mathbf{0}$ are retained to provide the description of the electronic band structure of the solid j. The 27 zone-center basis functions, $\{|m\rangle\}$, are derived from the free-electrons plane wave states having reciprocal lattice vectors:

$$\mathbf{g} = \frac{2\pi}{a}(0,0,0), (\pm 1, \pm 1, \pm 1), \frac{2\pi}{a}(\pm 2, 0, 0), \frac{2\pi}{a}(\pm 2, \pm 2, 0), \tag{13}$$

where a is the bulk lattice constant for the solid under consideration.

• Table 1 show the set of $\mathbf{k}_0 = \mathbf{0}$ basis functions used in the calculations and the plane waves $\mathbf{g}$ from which they originate. The $\mathbf{k}_0 = \mathbf{0}$ basis states are labelled according to their irreducible representation. The reference solid has T_d symmetry.

• In Table 2 we show the set of $\mathbf{k}_0 = \mathbf{0}$ basis functions along with their atomic characters. The following phase convention is adopted: *functions at* $\mathbf{k}_0 = \mathbf{0}$ *are taken to be real.* The top of the valence band is taken to be the origin of energies.

Using the procedure outlined above, the Bloch states $|\mathbf{k}\rangle$ are expanded on the zone-center basis states associated with $\mathbf{k}_0 = \mathbf{0}$

$$\langle \mathbf{x}|\mathbf{k}\rangle = \exp(i\mathbf{k}\cdot\mathbf{x}) u(\mathbf{k};\mathbf{x}),$$

$$\langle \mathbf{x}|\mathbf{k}\rangle = \exp(i\mathbf{k}\cdot\mathbf{x}) \sum_m \langle \mathbf{x}|m\rangle C(m;\mathbf{k}). \tag{14}$$

The energy eigenvalues $E(\mathbf{k})$ and the Bloch states $|\mathbf{k}\rangle$ are obtained by solving Schrödinger equation,

$$\hat{H}|\mathbf{k}\rangle = E(\mathbf{k})|\mathbf{k}\rangle. \tag{15}$$

In order to obtain the bandstructure $E(\mathbf{k})$ and the eigensolutions $|\mathbf{k}\rangle$, we must solve the eigenvalue problem Eq.(13.a) in the zone-center representation $\{|m\rangle\}$ using the expansion Eq.(12):

$$\sum_m \hat{H}(mm';\mathbf{k})C(m';\mathbf{k}) = E(\mathbf{k})C(m';\mathbf{k}), \tag{16}$$

where the matrix elements $\hat{H}(mm';\mathbf{k})$ are defined to be

$$\hat{H}(mm';\mathbf{k}) \equiv \left[E_m(\mathbf{0}) + \frac{\hbar^2}{2m}\mathbf{k}^2\right]\delta(m,m') + \frac{\hbar}{m}\mathbf{k}\cdot\langle m|\mathbf{p}|m'\rangle + \Delta V(mm'), \tag{17}$$

where the perturbation potential in the $\{|m\rangle\}$-representation is

$$\Delta V(mm') = \sum_{\mathbf{g}}\sum_{\mathbf{g}'}[U(\mathbf{g},m)]^{\dagger}\Delta V(\mathbf{g}\mathbf{g}')U(\mathbf{g}',m'), \tag{18.a}$$

and the momentum matrix element between zone-center basis states given as above by:

$$\langle m|\mathbf{p}|m'\rangle \equiv \int d^3\mathbf{x}\, u^*_m(\mathbf{x})\mathbf{p}u_{m'}(\mathbf{x}), \tag{18.b}$$

where we have dropped the index j that labels the solid.

The parameters needed are the energies of the zone-center states, $E_m(\mathbf{0})$, the momentum matrix elements $\langle m|\mathbf{p}|m'\rangle$ between the zone-center states, and the perturbation potential $\Delta V(mm')$. In the bandstructure calculation presented here, these parameters are calculated from the local pseudopotential transformation matrix, $U(\mathbf{g},m)$, as outlined above. As mentioned above, the $\mathbf{k}\cdot\mathbf{p}$ Hamiltonian,

$$\frac{\hbar}{m}\mathbf{k}\cdot\mathbf{p}, \tag{19}$$

$\mathbf{k}_0 = \mathbf{0}$ state	Reciprocal lattice vector $\mathbf{g}$ $[2\pi/a]$
Γ_1	$(0,0,0)$
Γ_{15}	$(\pm 1, \pm 1, \pm 1)$
Γ_1	$(\pm 1, \pm 1, \pm 1)$
Γ_{15}	$(\pm 1, \pm 1, \pm 1)$
Γ_1	$(\pm 1, \pm 1, \pm 1)$
Γ_{12}	$(\pm 2, 0, 0)$
Γ_{15}	$(\pm 2, 0, 0)$
Γ_1	$(\pm 2, 0, 0)$
Γ_{25}	$(\pm 2, \pm 2, 0)$
Γ_{15}	$(\pm 2, \pm 2, 0)$
Γ_{12}	$(\pm 2, \pm 2, 0)$
Γ_{15}	$(\pm 2, \pm 2, 0)$
Γ_1	$(\pm 2, \pm 2, 0)$

Table 1. Set of 27 $\mathbf{k}_0 = \mathbf{0}$ cell-periodic basis functions used in the full-zone $\mathbf{k} \cdot \mathbf{p}$ calculation with the plane waves from which they are derived.

$\mathbf{k}_0 = \mathbf{0}$ state	Atomic symmetry
Γ_1	$[s]$
Γ_{15}	$[p]$
Γ_1	$[s]$
Γ_{15}	$[p]$
Γ_1	$[s]$
Γ_{12}	$[d]$
Γ_{15}	$[d]$
Γ_1	$[s]$
Γ_{25}	$[f]$
Γ_{15}	$[f]$
Γ_{12}	$[f]$
Γ_{15}	$[f]$
Γ_1	$[f]$

Table 2. Set of 27 $\mathbf{k}_0 = \mathbf{0}$ cell-periodic basis functions used in the full-zone $\mathbf{k} \cdot \mathbf{p}$ calculation with their atomic symmetries.

can only couple states of opposite parity due to the fact that the momentum operator **p** transforms according to a *vector representation.* In homopolar diamond semiconductors with O_h symmetry, basis states at $\mathbf{k}_0 = \mathbf{0}$ have definite parity due to the inversion symmetry with respect to the two basis atoms within the primitive cell. However, in heteropolar zincblende semiconductors with T_d symmetry, the *lack of inversion symmetry implies that the basis states at* $\mathbf{k}_0 = \mathbf{0}$ *do not have definite parity.*

Tables 3 and 4 show the energies $E_n(\mathbf{0})$ for the various $\mathbf{k}_0 = \mathbf{0}$ basis functions for GaAs and AlAs, respectively.

$\mathbf{k}_0 = \mathbf{0}$ Energies	[eV]
$E(\Gamma_1)$	-12.198
$E(\Gamma_{15})$	0.0
$E(\Gamma_1)$	1.433
$E(\Gamma_{15})$	4.437
$E(\Gamma_1)$	8.048
$E(\Gamma_{12})$	8.673
$E(\Gamma_{15})$	12.767
$E(\Gamma_1)$	14.234
$E(\Gamma_{25})$	26.751
$E(\Gamma_{15})$	27.329
$E(\Gamma_{12})$	27.620
$E(\Gamma_{15})$	28.0
$E(\Gamma_1)$	28.167

Table 3. Energies of the 27 $\mathbf{k}_0 = \mathbf{0}$ cell-periodic basis functions for GaAs. Energies are expressed in eV.

$\mathbf{k}_0 = \mathbf{0}$ Energies	[eV]
$E(\Gamma_1)$	-11.662
$E(\Gamma_{15})$	0.0
$E(\Gamma_1)$	3.205
$E(\Gamma_{15})$	4.577
$E(\Gamma_1)$	9.122
$E(\Gamma_{12})$	8.418
$E(\Gamma_{15})$	13.0
$E(\Gamma_1)$	14.755
$E(\Gamma_{25})$	26.411
$E(\Gamma_{15})$	27.702
$E(\Gamma_{12})$	27.538
$E(\Gamma_{15})$	29.03
$E(\Gamma_1)$	30.03

Table 4. Energies of the 27 $\mathbf{k}_0 = \mathbf{0}$ cell-periodic basis functions for AlAs. Energies are expressed in eV.

4.4.2 Complex-k Bandstructure : k.p Theory

Having described the $\mathbf{k} \cdot \mathbf{p}$ formalism for bulk semiconductors, we now turn to the application of this technique in the calculation of the electronic spectrum of semiconductor superlattices. The expansion set for the superlattice state consists of the bulk Bloch states associated with complex values of the wavevector $\mathbf{k}$. Since the bulk periodicity is broken by the introduction of a series of interfaces, the wavevector $\mathbf{k}$ that labels the Bloch state solutions $\{|\mathbf{k}\rangle\}$ is not restricted to take on only real values.

Consider the case for which the superlattice axis normal to the interface is along the $\hat{\mathbf{z}}$ direction. The wavevector $\mathbf{k}$ can now be decomposed on a component parallel to the interface, $\mathbf{k}_{\|}$, and a component normal to the interface, $\hat{\mathbf{z}}k_z$:

$$\mathbf{k} = \mathbf{k}_{\|} + \hat{\mathbf{z}}k_z, \tag{1}$$

with

$$\mathbf{k}_{\|} = \hat{\mathbf{x}}k_x + \hat{\mathbf{y}}k_y, \tag{2}$$

being the component of the wavevector $\mathbf{k}$ parallel to the interface plane.

Since the translational symmetry of the bulk solid is preserved parallel to the interface, the component $\mathbf{k}_{\|}$ still remains a good quantum number for the Bloch solutions. The total energy, E, of the Bloch state is also a good quantum number to label the solutions. It is more convenient, when dealing with an interface system to label the Bloch state solutions $\{|\mathbf{k}\rangle\}$ by $\{|\mathbf{k}_{\|}E; k_z\rangle\}$. Then, Schrödinger equation,

$$\hat{H}|\mathbf{k}\rangle = E(\mathbf{k})|\mathbf{k}\rangle, \tag{3.a}$$

becomes

$$\hat{H}|\mathbf{k}_{\|}E; k_z\rangle = E(\mathbf{k}_{\|}, k_z)|\mathbf{k}_{\|}E; k_z\rangle. \tag{3.b}$$

In Eq.(3) we labelled the Bloch states $|\mathbf{k}_{\|}E;k_z\rangle$ in the extended zone scheme and therefore we got rid of the band index, n. It is important to realize that Eq.(3) is *not an eigenvalue problem*, since for a given $\mathbf{k}_{\|}$ and $E(\mathbf{k}_{\|},k_z)$ there exists a finite number of k_z, real or complex, for which the Bloch state $|\mathbf{k}_{\|}E;k_z\rangle$ is a solution of Eq.(3). As mentioned above, the component of the wavevector parallel to the interface, $\mathbf{k}_{\|}$, and the total energy, E, can be used to label the solutions of Eq.(3). However, the component k_z is not a conserved quantity across the interface and cannot be used to label the solutions of Eq.(3). We now show how to obtain all the solutions of Eq.(3) for k_z real or complex within the $\mathbf{k}\cdot\mathbf{p}$ theoretical framework. In this case the spectrum $E(\mathbf{k}_{\|},k_z)$ is referred to as a complex-$\mathbf{k}$ bandstructure.

Following the procedure outlined in Appendix (4.1), we use the set $\{|m)\}$ of zone-center basis states ($\mathbf{k}_0=\mathbf{0}$) of the *reference solid*, as the expansion set for the Bloch solutions $\{|\mathbf{k}_{\|}E;k_z\rangle\}$:

$$\langle\mathbf{x}|\mathbf{k}_{\|}E;k_z\rangle \equiv \exp(i\mathbf{k}_{\|}\cdot\mathbf{x}_{\|})\exp(ik_zz)u(\mathbf{k}_{\|},k_z;\mathbf{x}),$$

$$\langle\mathbf{x}|\mathbf{k}_{\|}E;k_z\rangle = \exp(i\mathbf{k}_{\|}\cdot\mathbf{x}_{\|})\exp(ik_zz)\sum_m\langle\mathbf{x}|m)C(m,k_z;\mathbf{k}_{\|}E), \tag{4}$$

where $\mathbf{x}_{\|}$ is a two-dimensional position vector parallel to the interface plane,

$$\mathbf{x}_{\|} = \hat{\mathbf{x}}x+\hat{\mathbf{y}}y. \tag{5}$$

The ket $|m)$ designates a cell-periodic zone-center basis state associated with $\mathbf{k}_0=\mathbf{0}$, in the *reference solid*,

$$\langle\mathbf{x}|m) \equiv u_m(\mathbf{x}). \tag{6}$$

- Let $\hat{H}_E$ be a matrix containing the energy $E(\mathbf{k}_{\|},k_z)$:

$$\hat{H}_E \equiv \hat{H}-E(\mathbf{k}_{\|},k_z). \tag{7}$$

Direct substitution of the expansion Eq.(4) into Eq.(3), and projection onto the zone-center basis state $\langle m|$, yields the matrix equation in terms of the zone-center basis function $\{|m\rangle\}$:

$$\sum_{m'} \hat{H}_E(mm'; \mathbf{k}_\parallel k_z) C(m', k_z; \mathbf{k}_\parallel E) = 0, \tag{8}$$

where the matrix elements $\hat{H}_E(mm'; \mathbf{k}_\parallel k_z)$ are defined to be

$$\hat{H}_E(mm'; \mathbf{k}_\parallel k_z) \equiv \left[E_m(\mathbf{0}) + \frac{\hbar^2}{2m}\mathbf{k}^2 - E(\mathbf{k}_\parallel, k_z) \right] \delta(m, m')$$

$$+ \frac{\hbar}{m}\mathbf{k} \cdot \langle m|\mathbf{p}|m'\rangle + \Delta V(mm'). \tag{9}$$

The non-diagonal part of the Hamiltonian corresponds to the momentum matrix element between zone-center basis states given by:

$$\langle m|\mathbf{p}|m'\rangle \equiv \int d^3\mathbf{x} u^*_m(\mathbf{x}) \mathbf{p} u_{m'}(\mathbf{x}). \tag{10}$$

The perturbation potential is related to the difference between the local pseudopotential of the solid under consideration, $\hat{H}^{(j)}(\mathbf{g}\mathbf{g}'; \mathbf{k})$, and that of the reference solid, $\hat{H}^{(0)}(\mathbf{g}\mathbf{g}'; \mathbf{k})$,

$$\Delta V(mm') = \sum_{\mathbf{g}} \sum_{\mathbf{g}'} [U(\mathbf{g}, m)]^\dagger \Delta V(\mathbf{g}\mathbf{g}') U(\mathbf{g}', m'). \tag{11}$$

4.4.2.1 Complex-k Bandstructure : Eigenvalue Problem

In order to transform Eq(8) into an eigenvalue problem, we now introduce a companion matrix whose diagonalization, at each parallel wavevector $\mathbf{k}_{\|}$ and total energy $E(\mathbf{k}_{\|}, k_z)$, gives all the set of allowed perpendicular wavevectors, k_z.

To simplify the notation, let us introduce *atomic units* such that

$$\hbar \equiv 1, \tag{12.a}$$

$$m \equiv \frac{1}{2}, \tag{12.b}$$

and, consequently,

$$\frac{\hbar^2}{2m} \equiv 1, \tag{12.c}$$

and

$$\frac{\hbar}{m} \equiv 2, \tag{12.d}$$

• Let us first rewrite Eq.(8) in matrix form:

$$\mathbf{H}_E(\mathbf{k}_{\|}, k_z) \cdot \mathbf{C}(k_z; \mathbf{k}_{\|} E) = 0, \tag{13}$$

where $\mathbf{H}_E(\mathbf{k}_{\|}, k_z)$ is the matrix $\hat{H}_E$ in the zone-center representation, $\{|m\rangle\}$. The column vector $\mathbf{C}(k_z; \mathbf{k}_{\|} E)$ is the set of coefficients $C(m, k_z; \mathbf{k}_{\|} E)$ associated with k_z. The index m labels the zone-center basis functions of the reference solid.

Let us now define the column vector:

$$K(m, k_z; \mathbf{k}_{\|} E) \equiv \sum_{m'} \left[k_z \delta(m, m') + p_z(m, m') \right] C(m', k_z; \mathbf{k}_{\|} E), \tag{14.a}$$

or, in matrix form,

$$\mathbf{K}(k_z; \mathbf{k}_{\|} E) \equiv [k_z \mathbf{1} + p_z] \cdot \mathbf{C}(k_z; \mathbf{k}_{\|} E), \tag{14.b}$$

or,

$$-p_z \cdot \mathbf{C}(k_z; \mathbf{k}_\parallel E) + \mathbf{K}(k_z; \mathbf{k}_\parallel E) = k_z \cdot \mathbf{C}(k_z; \mathbf{k}_\parallel E), \tag{14.c}$$

where the matrix p_z has matrix elements, in the $\{|m\rangle\}$-representation,

$$p_z \equiv p_z(m, m') \equiv \langle m|p_z|m'\rangle, \tag{14.d}$$

and **1** is the unit matrix.

With the above definitions, the matrix $\mathbf{H}_E(\mathbf{k}_\parallel, k_z)$ appearing in Eq.(7) can be factorized in the following way:

$$\hat{H}_E(mm'; \mathbf{k}_\parallel k_z) \equiv \left[E_m(\mathbf{0}) + \mathbf{k}^2 - E(\mathbf{k}_\parallel, k_z)\right] \delta(m, m')$$

$$+2\mathbf{k} \cdot \langle m|\mathbf{p}|m'\rangle + \Delta V(mm'), \tag{15.a}$$

$$= \left[E_m(\mathbf{0}) + \mathbf{k}_\parallel{}^2 + k_z{}^2 - E(\mathbf{k}_\parallel, k_z)\right] \delta(m, m')$$

$$+2\mathbf{k}_\parallel \cdot \langle m|\mathbf{p}_\parallel|m'\rangle + 2k_z \cdot \langle m|p_z|m'\rangle + \Delta V(mm'). \tag{15.b}$$

Let us write the above equation in *matrix form* and extract from it an eigensystem for the column vector,

$$\begin{bmatrix} \mathbf{C}(k_z; \mathbf{k}_\parallel E) \\ \mathbf{K}(k_z; \mathbf{k}_\parallel E) \end{bmatrix} \equiv \begin{bmatrix} \mathbf{C}(k_z; \mathbf{k}_\parallel E) \\ (\mathbf{k} + \mathbf{p})\mathbf{C}(k_z; \mathbf{k}_\parallel E) \end{bmatrix}. \tag{16}$$

We can write, in matrix form,

$$\mathbf{H}_E(\mathbf{k}_\parallel, k_z) \equiv \left[E_m(\mathbf{0}) + \mathbf{k}^2 - E(\mathbf{k}_\parallel, k_z)\right] \mathbf{1} + 2\mathbf{k} \cdot \mathbf{p} + \Delta V, \tag{17.a}$$

$$= \left[E_m(\mathbf{0}) + \mathbf{k}_\parallel{}^2 + k_z{}^2 - E(\mathbf{k}_\parallel, k_z)\right] \mathbf{1} + 2\mathbf{k}_\parallel \cdot \mathbf{p}_\parallel + 2k_z \cdot p_z + \Delta V. \tag{17.b}$$

where the matrices p_z and $\mathbf{p}_{\|}$ are, in the $\{|m\rangle\}$-representation,

$$p_z \equiv \langle m|p_z|m'\rangle, \tag{18.a}$$

and

$$\mathbf{p}_{\|} \equiv \langle m|\mathbf{p}_{\|}|m'\rangle. \tag{18.b}$$

Let us define the matrix $\mathbf{H}_E^{(0)}(\mathbf{k}_{\|})$ as

$$\mathbf{H}_E^{(0)}(\mathbf{k}_{\|}) \equiv \left[E_m(\mathbf{0}) + {\mathbf{k}_{\|}}^2 - E(\mathbf{k}_{\|}, k_z)\right]\mathbf{1} + 2\mathbf{k}_{\|} \cdot \mathbf{p}_{\|} + \Delta V. \tag{19}$$

Now, we can write the eigensystem

$$\mathbf{H}_E(\mathbf{k}_{\|}, k_z) \cdot \mathbf{C}(k_z; \mathbf{k}_{\|}E) = 0, \tag{20.a}$$

as

$$\mathbf{H}_E^{(0)}(\mathbf{k}_{\|}) \cdot \mathbf{C}(k_z; \mathbf{k}_{\|}E) + \left[{k_z}^2 + 2k_z \cdot p_z\right] \cdot \mathbf{C}(k_z; \mathbf{k}_{\|}E) = 0. \tag{20.b}$$

Let us write

$$\left[{k_z}^2 + 2k_z \cdot p_z\right] \cdot \mathbf{C}(k_z; \mathbf{k}_{\|}E) = k_z \cdot [k_z + 2p_z] \cdot \mathbf{C}(k_z; \mathbf{k}_{\|}E), \tag{21.a}$$

$$= k_z \cdot [(k_z + p_z) + p_z] \cdot \mathbf{C}(k_z; \mathbf{k}_{\|}E) \tag{21.b}$$

$$\equiv k_z \cdot \mathbf{K}(k_z; \mathbf{k}_{\|}E) + k_z \cdot p_z \cdot \mathbf{C}(k_z; \mathbf{k}_{\|}E). \tag{21.c}$$

Now, we can write

$$k_z \cdot p_z \cdot \mathbf{C}(k_z; \mathbf{k}_{\|}E) = p_z \cdot [(k_z + p_z) - p_z] \cdot \mathbf{C}(k_z; \mathbf{k}_{\|}E), \tag{22.a}$$

$$= p_z \cdot (k_z + p_z) \cdot \mathbf{C}(k_z; \mathbf{k}_{\|}E) - {p_z}^2 \cdot \mathbf{C}(k_z; \mathbf{k}_{\|}E), \tag{22.b}$$

$$\equiv p_z \cdot \mathbf{K}(k_z; \mathbf{k}_{\|}E) - {p_z}^2 \cdot \mathbf{C}(k_z; \mathbf{k}_{\|}E), \tag{22.c}$$

and finally,

$$\left[k_z{}^2 + 2k_z \cdot p_z\right] \cdot \mathbf{C}(k_z; \mathbf{k}_\parallel E) = [k_z + p_z] \cdot \mathbf{K}(k_z; \mathbf{k}_\parallel E) - p_z{}^2 \cdot \mathbf{C}(k_z; \mathbf{k}_\parallel E) \quad (22.d)$$

Thus, we can write

$$\left[\mathbf{H}_E^{(0)}(\mathbf{k}_\parallel) - p_z{}^2\right] \cdot \mathbf{C}(k_z; \mathbf{k}_\parallel E) + [k_z + p_z] \cdot \mathbf{K}(k_z; \mathbf{k}_\parallel E) = 0, \quad (23.a)$$

or,

$$\left[-\mathbf{H}_E^{(0)}(\mathbf{k}_\parallel) + p_z{}^2\right] \cdot \mathbf{C}(k_z; \mathbf{k}_\parallel E) - p_z \cdot \mathbf{K}(k_z; \mathbf{k}_\parallel E) = k_z \cdot \mathbf{K}(k_z; \mathbf{k}_\parallel E) = 0 \quad (23.b)$$

We thus have the following eigensystem,

$$-p_z \cdot \mathbf{C}(k_z; \mathbf{k}_\parallel E) + \mathbf{K}(k_z; \mathbf{k}_\parallel E) = k_z \cdot \mathbf{C}(k_z; \mathbf{k}_\parallel E), \quad (24.a)$$

$$\left[-\mathbf{H}_E^{(0)}(\mathbf{k}_\parallel) + p_z{}^2\right] \cdot \mathbf{C}(k_z; \mathbf{k}_\parallel E) - p_z \cdot \mathbf{K}(k_z; \mathbf{k}_\parallel E) = k_z \cdot \mathbf{K}(k_z; \mathbf{k}_\parallel E). \quad (24.b)$$

• In matrix form, we obtain,

$$\begin{bmatrix} -p_z & \mathbf{1} \\ -\mathbf{H}^{(1)}(\mathbf{k}_\parallel) & -p_z \end{bmatrix} \cdot \begin{bmatrix} \mathbf{C}(k_z; \mathbf{k}_\parallel E) \\ \mathbf{K}(k_z; \mathbf{k}_\parallel E) \end{bmatrix} = k_z \cdot \begin{bmatrix} \mathbf{C}(k_z; \mathbf{k}_\parallel E) \\ \mathbf{K}(k_z; \mathbf{k}_\parallel E) \end{bmatrix} \quad (25)$$

where we have defined the matrix

$$\mathbf{H}^{(1)}(\mathbf{k}_\parallel) \equiv \mathbf{H}_E^{(0)}(\mathbf{k}_\parallel) + p_z{}^2, \quad (26.a)$$

or,

$$\mathbf{H}^{(1)}(\mathbf{k}_\parallel) \equiv \left[E_m(\mathbf{0}) + \mathbf{k}_\parallel{}^2 - E(\mathbf{k}_\parallel, k_z)\right]\mathbf{1} + 2\mathbf{k}_\parallel \cdot \mathbf{p}_\parallel + \Delta V + p_z{}^2. \quad (26.b)$$

The matrix

$$\begin{bmatrix} -p_z & \mathbf{1} \\ -\mathbf{H}^{(1)}(\mathbf{k}_\parallel) & -p_z \end{bmatrix}, \quad (26.c)$$

is called the *companion matrix*.

It is now possible to solve the eigensystem,

$$\begin{bmatrix} -p_z & \mathbf{1} \\ -\mathbf{H}^{(1)}(\mathbf{k}_\parallel) & -p_z \end{bmatrix} \cdot \begin{bmatrix} \mathbf{C}(k_z;\mathbf{k}_\parallel E) \\ \mathbf{K}(k_z;\mathbf{k}_\parallel E) \end{bmatrix} = k_z \cdot \begin{bmatrix} \mathbf{C}(k_z;\mathbf{k}_\parallel E) \\ \mathbf{K}(k_z;\mathbf{k}_\parallel E) \end{bmatrix}, \tag{27}$$

for the allowed values of k_z at fixed $\mathbf{k}_\parallel$ and $E(\mathbf{k}_\parallel, k_z)$: Direct diagonalization of the companion matrix gives the values of k_z and the expansion coefficients $C(m, k_z; \mathbf{k}_\parallel E)$ appearing in the expansion of Eq.(4) for the Bloch solutions $|\mathbf{k}_\parallel E; k_z\rangle$ in terms of the zone-center basis functions $\{|m\rangle\}$.

4.4.2.2 Eigenvector Matrix of Companion Matrix:

In this subsection, we would like to study more closely the *eigenvector matrix that diagonalizes the companion matrix.*

We note that the size of the companion matrix appearing in Eq.(26) is *twice* the size of the matrices $\mathbf{H}_E(\mathbf{k}_\parallel, k_z)$, $\mathbf{H}_E^{(0)}(\mathbf{k}_\parallel)$, and $\mathbf{H}^{(1)}(\mathbf{k}_\parallel)$. This is due to the fact that the Hamiltonian $\mathbf{H}_E(\mathbf{k}_\parallel, k_z)$ contains kinetic energy terms going like ${k_z}^2$. The procedure outlined above is identical to the technique by which one can transform a m-th order linear differential equation into a set of m first-order linear differential equations. Suppose that the number of zone-center basis functions appearing in the expansion of the Bloch state $|\mathbf{k}_\parallel E; k_z\rangle$ of Eq.(4) is N, *i.e.*, the expansion set is $[\{|m\rangle\}, m = 1, \ldots, N.]$ Therefore, the diagonalization of the companion matrix, Eq.(14), will produce $2N$ complex values of k_z for each $\mathbf{k}_\parallel$ and $E(\mathbf{k}_\parallel, k_z)$. In what follows, we denote the finite number of complex values of k_z by:

$$k_z \equiv k_\lambda, \qquad \lambda = 1, \ldots, 2N, (28.a)$$

and the associated Bloch states by:

$$|\mathbf{k}_\parallel E; k_z\rangle \equiv |\mathbf{k}_\parallel E; k_\lambda\rangle, \qquad \lambda = 1, \ldots, 2N, (28.b)$$

at each $\mathbf{k}_\parallel$ and $E(\mathbf{k}_\parallel, k_z)$.

The matrix of eigenvectors, formed by the column vectors $\mathbf{C}(k_\lambda; \mathbf{k}_\parallel E)$ and consisting of the expansion coefficients, $C(m, k_\lambda; \mathbf{k}_\parallel E)$, is *not a square matrix.* The *columns* of $\mathbf{C}(k_\lambda; \mathbf{k}_\parallel E)$ label the $2N$ solutions Eq.(14), *i.e.*,

$$k_z \equiv k_\lambda, \qquad \lambda = 1, \ldots, 2N, (29.a)$$

and the *rows* of $\mathbf{C}(k_\lambda; \mathbf{k}_\parallel E)$ label the N basis functions at $\mathbf{k}_0 = \mathbf{0}$, *i.e.*,

$$\{|m\rangle\}, \qquad m = 1, \ldots, N. (29.b)$$

The expansion of the Bloch states in solid $j = 1, 2$, $\{|\mathbf{k}_{\|}E; k_{\lambda}^{(j)}\rangle\}$, $[\lambda = 1, \ldots, 2N]$ can now be written as:

$$\langle \mathbf{x}|\mathbf{k}_{\|}E; k_{\lambda}^{(j)}\rangle \equiv \exp(i\mathbf{k}_{\|} \cdot \mathbf{x}_{\|}) \exp(ik_{\lambda}^{(j)} z) u(\mathbf{k}_{\|}, k_{\lambda}; \mathbf{x}),$$

$$\langle \mathbf{x}|\mathbf{k}_{\|}E; k_{\lambda}^{(j)}\rangle = \exp(i\mathbf{k}_{\|} \cdot \mathbf{x}_{\|}) \exp(ik_{\lambda}^{(j)} z) \sum_{m=1}^{N} \langle \mathbf{x}|m\rangle C^{(j)}(m, k_{\lambda}^{(j)}; \mathbf{k}_{\|}E). \qquad (30)$$

where $C^{(j)}(m, k_{\lambda}^{(j)}\ \mathbf{k}_{\|}E)$ is the set of coefficients associated with the eigenvalue $k_{\lambda}^{(j)}$ in solid j. The index m labels the zone-center basis functions of the reference solid. The complex-$\mathbf{k}$ band structure, $E(\mathbf{k}_{\|}, k_{\lambda})$, and Bloch states, $\{|\mathbf{k}_{\|}E; k_{\lambda}\rangle\}$, are obtained by diagonalization of the companion matrix, Eq.(26) within the full-zone $\mathbf{k} \cdot \mathbf{p}$ scheme described in Section 4.4.1. Within this framework, 27 zone-center states $\{|m\rangle\}$ constitute the expansion set for the Bloch states $\{|\mathbf{k}_{\|}E; k_{\lambda}\rangle\}$, *i.e.*, $N = 27$. Out of the $2N = 54$ Bloch states obtained,

$$\{|\mathbf{k}_{\|}E; k_{\lambda}\rangle\}, \qquad \lambda = 1, \ldots, 2N.$$

• We now examine the eigenvector matrix that diagonalizes the companion matrix and gives it physical significance.

Let $\mathbf{M}(\mathbf{k}_{\|}E; j)$ be *the eigenvector matrix that diagonalizes the companion matrix in solid* $j = 1, 2$,

$$\mathbf{M}(\mathbf{k}_{\|}E; j) \equiv \begin{bmatrix} \mathbf{C}^{(j)}(k_{\lambda}; \mathbf{k}_{\|}E) \\ (\mathbf{k} + \mathbf{p})\mathbf{C}^{(j)}(k_{\lambda}; \mathbf{k}_{\|}E) \end{bmatrix}, \qquad (31)$$

for $j = 1, 2$. The column vector $\mathbf{C}^{(j)}(k_{\lambda}; \mathbf{k}_{\|}E)$ is the set of coefficients $C^{(j)}(m, k_{\lambda}^{(j)}; \mathbf{k}_{\|}E)$ associated with the eigenvalue $k_{\lambda}^{(j)}$ in solid $j = 1, 2$. The index m labels the zone-center basis functions of the reference solid.

As they stand, the matrices $\mathbf{M}(\mathbf{k}_{\|}E; j)$ are expressed in the $\mathbf{k}_0 = \mathbf{0}$ basis $\{|m\rangle\}$ of the reference solid. We can express the $\mathbf{M}(\mathbf{k}_{\|}E; j)$ matrices in the plane

wave basis, $\{|\mathbf{g}\rangle\}$, with the use of the transformation matrix $\mathbf{U}$,

$$\mathbf{M}(\mathbf{k}_{\|}E;j) \equiv \begin{bmatrix} \mathbf{U} & \mathbf{0} \\ \mathbf{0} & \mathbf{U} \end{bmatrix} \cdot \begin{bmatrix} \mathbf{C}^{(j)}(k_{\lambda};\mathbf{k}_{\|}E) \\ (\mathbf{k}+\mathbf{p})\mathbf{C}^{(j)}(k_{\lambda};\mathbf{k}_{\|}E) \end{bmatrix}, \tag{32}$$

where we have performed the left multiplication,

$$C^{(j)}(\mathbf{g}, k_{\lambda}^{(j)};\mathbf{k}_{\|}E) \equiv \sum_{n=1}^{N} U(\mathbf{g},m)\cdot C^{(j)}(m, k_{\lambda}^{(j)};\mathbf{k}_{\|}E), \tag{33}$$

to transform bases.

It is to be shown in Chapter (4) then *the eigenvector matrix that diagonalizes the companion matrix is the matrix obtained by applying the boundary conditions on the superlattice state function.* The matrices $\mathbf{M}(\mathbf{k}_{\|}E;j)$ play a crucial role in the theory presented in Chapter (4).

4.4.2.3 Symmetry Properties of Bloch Solutions: Time-reversal

We pause here to point out some of the *symmetry properties* of the expansion coefficients $C(m, k_\lambda; \mathbf{k}_\| E)$ appearing in the expansion Eq.(28).

• Let us consider the case of $\mathbf{k}_\| = \mathbf{0}$. The Bloch state $\langle \mathbf{x}|\mathbf{k}_\| E; k_\lambda\rangle$ can be expanded in terms of the $\mathbf{k}_0 = \mathbf{0}$ basis functions,

$$\psi(k_\lambda; \mathbf{x}) = \exp(ik_\lambda z) \sum_{m=1}^{N} u_m(\mathbf{x}) C(m, k_\lambda), \tag{34}$$

where we have written $\psi(k_\lambda; \mathbf{x})$ for $\langle \mathbf{x}|\mathbf{k}_\| E; k_\lambda\rangle$ at $\mathbf{k}_\| = \mathbf{0}$ for simplicity.

According to Appendix A, the *degenerate time-reversed* state is simply the *complex conjugate in the absence of spin-orbit.* Then we can write the time-reversed partner of $\psi(k_\lambda; \mathbf{x})$ as

$$\psi^*(k_\lambda; \mathbf{x}) = \exp(-ik_\lambda^* z) \sum_{m=1}^{N} u_m^*(\mathbf{x}) C^*(m, k_\lambda), \tag{35.a}$$

or,

$$\psi^*(k_\lambda; \mathbf{x}) = \exp\left[i(-k_\lambda^*)z\right] \sum_{m=1}^{N} u_m^*(\mathbf{x}) C^*(m, k_\lambda). \tag{35.b}$$

We can also write the Bloch solution $\psi(-k_\lambda^*; \mathbf{x})$ associated with the wavevector $-k_\lambda^*$ as,

$$\psi(-k_\lambda^*; \mathbf{x}) = \exp\left[i(-k_\lambda^*)z\right] \sum_{m=1}^{N} u_m(\mathbf{x}) C(m, -k_\lambda^*). \tag{36}$$

Therefore, the time-reversed partner of a Bloch state with wavevector k_λ is a Bloch state with wavevector $-k_\lambda^*$, to within a phase factor, $\exp(i\varphi)$.

We can then relate the time-reversed pair of Bloch states as,

$$\psi^*(k_\lambda; \mathbf{x}) \equiv \exp(-i\varphi)\psi(-k_\lambda^*; \mathbf{x}), \tag{37.a}$$

or,

$$\psi(k_\lambda;\mathbf{x}) \equiv \exp(i\varphi)\psi^*(-k_\lambda^*;\mathbf{x}), \tag{37.b}$$

to within a constant phase factor, $\exp(-i\varphi)$.

By comparing Eq.(35) and Eq.(36), we have

$$\psi^*(k_\lambda;\mathbf{x}) \equiv \exp(-i\varphi)\psi(-k_\lambda^*;\mathbf{x}), \tag{38.a}$$

or, explicitly,

$$\exp\left[i(-k_\lambda^*)z\right]\sum_{m=1}^{N} u_m^*(\mathbf{x})C^*(m,k_\lambda) = \exp(-i\varphi)\exp\left[i(-k_\lambda^*)z\right]\sum_{m=1}^{N} u_m(\mathbf{x})C(m,-k_\lambda^*), \tag{38.b}$$

or,

$$\sum_{m=1}^{N} u_m^*(\mathbf{x})C^*(m,k_\lambda) = \exp(-i\varphi)\sum_{m=1}^{N} u_m(\mathbf{x})C(m,-k_\lambda^*), \tag{38.c}$$

and finally, by complex conjugating,

$$\sum_{m=1}^{N} u_m(\mathbf{x})C(m,k_\lambda) = \exp(i\varphi)\sum_{m=1}^{N} u_m^*(\mathbf{x})C^*(m,-k_\lambda^*). \tag{38.d}$$

According to the *phase convention* we have that $\mathbf{k}_0 = \mathbf{0}$ basis functions have no definite parity and are taken to be *real.* Then we have,

$$u_m^*(\mathbf{x}) = u_m(\mathbf{x}). \tag{39.a}$$

$$C(m,k_\lambda) = \exp(i\varphi)C^*(m,-k_\lambda^*). \tag{39.b}$$

To determine the phase factor $\exp(i\varphi)$, we adopted the following phase convention on the expansion coefficients, *the maximum component of the coefficient* $C(m,k_\lambda)$ *is taken to be real and positive.* Since the maximum component of $C(m,k_\lambda)$ and $C^*(m,-k_\lambda^*)$ occurs for the same index m, then we have that

$$C(m,k_\lambda) = C^*(m,-k_\lambda^*), \tag{40}$$

which fixes the phase factor to be

$$\exp(i\varphi) \equiv 1. \tag{41}$$

4.4.2.4 Normalization of Bloch Solutions: Complex Conjugation

We now indicate how the *normalization of the Bloch solutions is done.* As is shown in Appendix (A), *when the wavevector* k_λ *is complex, if the cell-periodic function* $u_m(\mathbf{k};\mathbf{x})$ *is a solution of the Hamiltonian* $\hat{H}(\mathbf{k})$ *then the cell-periodic function* $u_{m'}(\mathbf{k}^*;\mathbf{x})$ *is a solution of the adjoint operator,* $\hat{H}(\mathbf{k})^\dagger$, where the Hamiltonian $\hat{H}(\mathbf{k})$ is defined to be :

$$\hat{H}(\mathbf{k}) \equiv \frac{1}{2m}(\mathbf{p} + \hbar\mathbf{k})^2 + V(\mathbf{x}), \tag{41.a}$$

or,

$$\hat{H}(\mathbf{k}) \equiv \frac{1}{2m}\mathbf{p}^2 + \frac{\hbar}{m}\mathbf{k}\cdot\mathbf{p} + \frac{\hbar^2}{2m}\mathbf{k}^2 + V(\mathbf{x}). \tag{41.b}$$

This is due to the fact that, for $\mathbf{k}$ complex,

$$\hat{H}(\mathbf{k})^\dagger \equiv \hat{H}(\mathbf{k}^*). \tag{42}$$

Thus we must normalize the solution associated with the wavevector k_λ with the solution associated with k_λ^*. The Bloch solutions

$$|\mathbf{k}_\parallel E; k_z\rangle \equiv |\mathbf{k}_\parallel E; k_\lambda\rangle, \qquad \lambda = 1,\ldots,2N, \tag{43.a}$$

corresponding to the wavevectors,

$$k_z \equiv k_\lambda, \qquad \lambda = 1,\ldots,2N, \tag{43.b}$$

were normalized such that

$$\sum_{m=1}^{N} [C(m,k_\lambda)]^* \cdot C(m,k_\lambda^*) = 1. \tag{44}$$

References

1. M. Cardona, and F. H. Pollak, *Phys. Rev.* **142**, 530 (1966).

2. F. H. Pollak, and M. Cardona, *J. Phys. Chem. Solids* **27**, 423 (1966).

3. F. H. Pollak, C. W. Higginbothham, and M. Cardona, *Proc. Int. Conf. Semiconductor Physics*, (Kyoto) 206 (1966).

APPENDIX 4.5

The purpose of this appendix is twofold.

• First, we analyse the situation in which the Bloch solutions associated with complex values of $\mathbf{k}$ are *equivalent*, *i.e.*, when the solutions are related by a reciprocal lattice vector $\mathbf{g}$.

• Second, we look more closely at the *boundary conditions imposed on the superlattice state function.* We show that the *number of linearly independent functions projected onto the interface plane is closely related to the the number of non-equivalent Bloch states.*

We collect these derivations in a single appendix since they are intimately interconnected.

4.5.1 EQUIVALENT SOLUTIONS

4.5.1.1 Pseudopotential and $\mathbf{k}\cdot\mathbf{p}$ Approaches:

We have seen in Appendix (4.4) that the Bloch solutions in the solid $j = 1, 2$ associated with the (real or complex) wavevector $k_\lambda^{(j)}$, $\{|\mathbf{k}_\parallel E; k_\lambda^{(j)}\rangle\}$, could be expanded in terms of $\mathbf{k}_0 = \mathbf{0}$ basis functions, $\{|m\rangle\}$, of a reference solid,

$$\langle \mathbf{x}|\mathbf{k}_\parallel E; k_\lambda^{(j)}\rangle = \exp(i\mathbf{k}_\parallel \cdot \mathbf{x}_\parallel)\exp(ik_\lambda^{(j)} z)\sum_{m=1}^{N}\langle \mathbf{x}|m\rangle C^{(j)}(m, k_\lambda^{(j)}; \mathbf{k}_\parallel E). \qquad (1)$$

where $C^{(j)}(m, k_\lambda^{(j)}; \mathbf{k}_\parallel E)$ is the set of coefficients associated with the eigenvalue $k_\lambda^{(j)}$ in solid j. In the $\mathbf{x}$-representation, we write

$$\langle \mathbf{x}|m\rangle \equiv u_m(\mathbf{x}), \qquad (2)$$

for the $\mathbf{k}_0 = \mathbf{0}$ basis functions. The index m labels the zone-center basis functions of the reference solid.

Is is also possible to carry out this expansion on a set of plane waves $\{|\mathbf{g}\rangle\}$ associated with the reciprocal lattice,

$$\langle \mathbf{x}|\mathbf{k}_{\|}E; k_{\lambda}^{(j)}\rangle = \exp(i\mathbf{k}_{\|}\cdot\mathbf{x}_{\|})\exp(ik_{\lambda}^{(j)}z)\sum_{\mathbf{g}}\langle \mathbf{x}|\mathbf{g}\rangle C^{(j)}(\mathbf{g}, k_{\lambda}^{(j)}; \mathbf{k}_{\|}E), \tag{3}$$

where, in the $\mathbf{x}$-representation, we write

$$\langle \mathbf{x}|\mathbf{g}\rangle \equiv \exp(i\mathbf{g}\cdot\mathbf{x}), \tag{4}$$

for the plane waves. The relation between the sets of coefficients $C^{(j)}(m, k_{\lambda}^{(j)}; \mathbf{k}_{\|}E)$ and $C^{(j)}(\mathbf{g}, k_{\lambda}^{(j)}; \mathbf{k}_{\|}E)$ is obtained through the matrix $U(\mathbf{g}, m)$

$$C^{(j)}(\mathbf{g}, k_{\lambda}^{(j)}; \mathbf{k}_{\|}E) = \sum_{m} U(\mathbf{g}, m)C^{(j)}(m, k_{\lambda}^{(j)}; \mathbf{k}_{\|}E). \tag{5}$$

The matrix $\mathbf{U}$ is the eigenvector matrix that diagonalizes the local pseudopotential Hamiltonian of the reference solid $\hat{H}^{(0)}(\mathbf{g}\mathbf{g}'; \mathbf{k})$ at $\mathbf{k} = \mathbf{0}$,

$$\left[\hat{H}^{(0)}(mm'; \mathbf{k})\right]_{\mathbf{k}=\mathbf{0}} = \left[\sum_{\mathbf{g}}\sum_{\mathbf{g}'}[U(\mathbf{g}, m)]^{\dagger}\hat{H}^{(0)}(\mathbf{g}\mathbf{g}'; \mathbf{k})U(\mathbf{g}', m')\right]_{\mathbf{k}=\mathbf{0}}, \tag{6.a}$$

$$\left[\hat{H}^{(0)}(mm'; \mathbf{k})\right]_{\mathbf{k}=\mathbf{0}} = E_m(\mathbf{0})\delta(m, m'). \tag{6.b}$$

The eigenvector matrix $\mathbf{U}$ is the transformation matrix that allows the transformation from the $\{|\mathbf{g}\rangle\}$-representation to the $\{|m\rangle\}$-representation of the *reference solid*. Once the transformation matrix $\mathbf{U}$ is known, the $\mathbf{k}\cdot\mathbf{p}$ Hamiltonian of each solid $\hat{H}^{(j)}(mm'; \mathbf{k})$ is obtained from the local pseudopotential Hamiltonian $\hat{H}^{(j)}(\mathbf{g}\mathbf{g}'; \mathbf{k})$,

$$\hat{H}^{(j)}(mm'; \mathbf{k}) = \sum_{\mathbf{g}}\sum_{\mathbf{g}'}[U(\mathbf{g}, m)]^{\dagger}\hat{H}^{(j)}(\mathbf{g}\mathbf{g}'; \mathbf{k})U(\mathbf{g}', m'), \tag{7.a}$$

or, using

$$\hat{H}^{(j)}(\mathbf{g}\mathbf{g}';\mathbf{k}) = \hat{H}^{(0)}(\mathbf{g}\mathbf{g}';\mathbf{k}) + \Delta V^{(j)}(\mathbf{g}\mathbf{g}'), \tag{7.b}$$

$$\hat{H}^{(j)}(mm';\mathbf{k}) = \sum_{\mathbf{g}}\sum_{\mathbf{g}'}[U(\mathbf{g},m)]^{\dagger}\left[\hat{H}^{(0)}(\mathbf{g}\mathbf{g}';\mathbf{k}) + \Delta V^{(j)}(\mathbf{g}\mathbf{g}')\right]U(\mathbf{g}',m'). \tag{7.c}$$

As mentioned in Appendix (4.4), if N is the number of $\mathbf{k}_0 = \mathbf{0}$ basis functions $\{|m\rangle\}$ of plane waves $\{|\mathbf{g}\rangle\}$ then the number of solutions $k_\lambda^{(j)}$ in solid $j = 1, 2$ is $2N$. This is due to the quadratic term in k_z in both the $\mathbf{k}\cdot\mathbf{p}$

$$\hat{H}^{(j)}(mm';\mathbf{k}) \equiv \left[E_m(\mathbf{0}) + \frac{\hbar^2}{2m}\mathbf{k}^2\right]\delta(m,m') + \frac{\hbar}{m}\mathbf{k}\cdot\langle m|\mathbf{p}|m'\rangle + \Delta V^{(j)}(mm'), \tag{8.a}$$

or the local pseudopotential

$$\hat{H}^{(j)}(\mathbf{g}\mathbf{g}';\mathbf{k}) \equiv \frac{\hbar^2}{2m}[\mathbf{k}+\mathbf{g}]^2\delta^3(\mathbf{g}-\mathbf{g}') + V^{(j)}(\mathbf{g}\mathbf{g}'), \tag{8.b}$$

Hamiltonians.

It should be note that *due to inherent lack of periodicity of both the* $\mathbf{k}\cdot\mathbf{p}$ *or the pseudopotential Hamiltonian, some of the solutions* $k_\lambda^{(j)}$ *will be related to each other by a reciprocal lattice vector* $\mathbf{g}$. Thus the diagonalization of the companion matrix produces states $|\mathbf{k}_\parallel E; k_\lambda^{(j)}\rangle$ whose $\mathrm{Re}\left[k_\lambda^{(j)}\right]$ lie outside the first Brillouin zone. These solutions are *approximate repeated-zone solutions due the truncation of the* $\mathbf{k}\cdot\mathbf{p}$ *or local pseudopotential Hamiltonians.*

4.5.1.2 Equivalent states:

In this subsection we would like to examine Bloch states whose wavevectors are related by a reciprocal lattice vector.

Consider two Bloch states associated with the wavevectors

$$\mathbf{k}_\lambda \equiv \mathbf{k}_\parallel + \hat{\mathbf{z}} k_\lambda, \tag{9.a}$$

and

$$\mathbf{k}'_\lambda \equiv \mathbf{k}_\parallel{}' + \hat{\mathbf{z}} k'_\lambda. \tag{9.b}$$

Suppose that $\mathbf{k}_\lambda$ and $\mathbf{k}'_\lambda$ are related by a reciprocal lattice vector, $\mathbf{g}_\mu$,

$$\mathbf{k}_\lambda = \mathbf{k}'_\lambda + \mathbf{g}_\mu, \tag{10.a}$$

where

$$\mathbf{g}_\mu = \mathbf{g}_\parallel + \hat{\mathbf{z}} g_\mu. \tag{10.b}$$

Equations (10) imply that

$$\mathbf{k}_\parallel = \mathbf{k}_\parallel{}' + \mathbf{g}_\parallel, \tag{11.a}$$

and,

$$\hat{\mathbf{z}} k_\lambda = \hat{\mathbf{z}} k'_\lambda + \hat{\mathbf{z}} g_\mu. \tag{11.b}$$

- We must consider two cases:

(i) In the case where $\mathbf{g}_\parallel \neq \mathbf{0}$ we have

$$\mathbf{k}_\parallel \neq \mathbf{k}_\parallel{}'. \tag{12}$$

Since the Bloch states correspond to fixed parallel wavevector $\mathbf{k}_\parallel$ and energy E, this situation would correspond to another problem unless the Hamiltonian has some higher symmetry along some directions in the Brillouin zone. We rule out this case.

(i) In the case where $\mathbf{g}_{\|} = \mathbf{0}$ we have

$$\mathbf{k}_{\|} = \mathbf{k}_{\|}', \tag{13.a}$$

and,

$$\hat{\mathbf{z}} k_{\lambda} = \hat{\mathbf{z}} k_{\lambda}' + \hat{\mathbf{z}} g_{\mu}. \tag{13.b}$$

In this case the two Bloch states have their wavevectors in the $\hat{\mathbf{z}}$-direction separated by a reciprocal lattice vector. Bloch states $|\mathbf{k}_{\|} E; k_{\lambda}\rangle$ whose wavevector satisfy Eq.(10) are said to be *equivalent.* Thus *equivalent Bloch states correspond to the same physical situation.*

• Then, it seems appropriate to *relabel the solutions* $k_{\lambda}^{(j)}$ *into sets of non-equivalent Bloch states.* Let us make the change of label for the solutions $k_{\lambda}^{(j)}$ in solid $j = 1, 2$

$$k_{\lambda}^{(j)} \rightarrow k_{\gamma\mu}^{(j)}, \tag{14.a}$$

for the wavevector, and

$$|\mathbf{k}_{\|} E; k_{\lambda}^{(j)}\rangle \rightarrow |\mathbf{k}_{\|} E; k_{\gamma\mu}^{(j)}\rangle, \tag{14.b}$$

for the associated Bloch states. The meaning of the double label $\gamma\mu$ is the following:

- γ labels the sets of non-equivalent Bloch states
- μ labels the equivalent partners within the set γ.

Thus, out of the $2N$ solutions

$$k_{\lambda}^{(j)}, \qquad \lambda = 1, \ldots, 2N, \tag{15.a}$$

$$|\mathbf{k}_{\|} E; k_{\lambda}^{(j)}\rangle, \qquad \lambda = 1, \ldots, 2N, \tag{15.b}$$

let there be $2M < 2N$ sets of non-equivalent solutions

$$k_{\gamma\mu}^{(j)}, \qquad \gamma = 1, \ldots, 2M, \tag{16.a}$$

$$|\mathbf{k}_{\|} E; k^{(j)}_{\gamma\mu}\rangle, \qquad \gamma = 1, \ldots, 2M, \quad (16.b)$$

where the index μ labels the equivalent partner solutions within the set γ,

$$\hat{\mathbf{z}} k^{(j)}_{\gamma\mu'} = \hat{\mathbf{z}} k^{(j)}_{\gamma\mu} + \hat{\mathbf{z}} g_{\mu\mu'}, \quad (16.c)$$

4.5.1.3 Equivalent states: Counting

The purpose of this subsection is to determine the *number of non-equivalent states*, or, in other words, to determine the number $2M$ of non-equivalent solution sets $k_{\gamma\mu}^{(j)}$ out of the total number $2N$ of solutions $k_{\lambda}^{(j)}$, in solid $j = 1, 2$.

The argument is most easily carried through within the *local pseudopotential formalism*. For notational simplicity, let us use *atomic units* whereby,

$$\hbar \equiv 1, \tag{17.a}$$

$$m \equiv \frac{1}{2}, \tag{17.b}$$

and, consequently,

$$\frac{\hbar^2}{2m} \equiv 1, \tag{18.a}$$

and

$$\frac{\hbar}{m} \equiv 2, \tag{18.b}$$

Let the Bloch state $|n\mathbf{k}\rangle$ be expanded onto the set of plane waves $\{|\mathbf{g}\rangle\}$

$$|n\mathbf{k}\rangle = \exp(i\mathbf{k}\cdot\mathbf{x}) \sum_{\mathbf{g}} |\mathbf{g}\rangle C^{(n)}(\mathbf{g},\mathbf{k}). \tag{19}$$

Then, Schrödinger equation,

$$\hat{H}|n\mathbf{k}\rangle = E_n(\mathbf{k})|n\mathbf{k}\rangle, \tag{20.a}$$

can be transformed into a matrix equation in the $\{|\mathbf{g}\rangle\}$-representation,

$$\sum_{\mathbf{g}'} \hat{H}^{(j)}(\mathbf{g}\mathbf{g}';\mathbf{k}) C^{(n)}(\mathbf{g}',\mathbf{k}) = E_n(\mathbf{k}) C^{(n)}(\mathbf{g},\mathbf{k}), \tag{20.b}$$

or,

$$\sum_{\mathbf{g}'} \left[\hat{H}^{(j)}(\mathbf{g}\mathbf{g}';\mathbf{k}) - E_n(\mathbf{k})\delta^3(\mathbf{g}-\mathbf{g}') \right] C^{(n)}(\mathbf{g}',\mathbf{k}) = 0, \tag{20.c}$$

where the Hamiltonian of solid j in the local pseudopotential form is given by

$$\hat{H}^{(j)}(\mathbf{g}\mathbf{g}';\mathbf{k}) \equiv (\mathbf{k}+\mathbf{g})^2\delta^3(\mathbf{g}-\mathbf{g}') + V^{(j)}(\mathbf{g}\mathbf{g}'), \tag{21}$$

and $V^{(j)}(\mathbf{g}\mathbf{g}')$ are the *pseudopotential form factors.*

Let now consider the quantity,

$$\hat{H}^{(j)}(\mathbf{g}\mathbf{g}';\mathbf{k}) - E(\mathbf{k})\delta^3(\mathbf{g}-\mathbf{g}') =$$

$$\left[(\mathbf{k}+\mathbf{g})^2 - E(\mathbf{k})\right]\delta^3(\mathbf{g}-\mathbf{g}') + V^{(j)}(\mathbf{g}\mathbf{g}'), \tag{22}$$

in the limit where $E_n(\mathbf{k}) \to -\infty$. In that limit, we can neglect the pseudopotential form factors, $V^{(j)}(\mathbf{g}\mathbf{g}')$, and the matrix

$$\hat{H}^{(j)}(\mathbf{g}\mathbf{g}';\mathbf{k}) - E(\mathbf{k})\delta^3(\mathbf{g}-\mathbf{g}')$$

is now *diagonal in the* $\{|\mathbf{g}\rangle\}$*-representation,*

$$\hat{H}^{(j)}(\mathbf{g}\mathbf{g}';\mathbf{k}) - E(\mathbf{k})\delta^3(\mathbf{g}-\mathbf{g}') \to \left[(\mathbf{k}+\mathbf{g})^2 - E(\mathbf{k})\right]\delta^3(\mathbf{g}-\mathbf{g}'). \tag{23}$$

Now, since we must solve for the wavevector $\mathbf{k}$ at fixed energy $E_n(\mathbf{k})$, the problem

$$\sum_{\mathbf{g}'}\left[\hat{H}^{(j)}(\mathbf{g}\mathbf{g}';\mathbf{k}) - E_n(\mathbf{k})\delta^3(\mathbf{g}-\mathbf{g}')\right] C^{(n)}(\mathbf{g}',\mathbf{k}) = 0, \tag{24}$$

is *not an eigenvalue problem.* The allowed values of $\mathbf{k}$ at fixed $E_n(\mathbf{k})$ are found whenever the above equation possesses a solution. The above system has a solution whenever the determinant of the matrix vanishes, *i.e.*,

$$|\hat{H}^{(j)}(\mathbf{g}\mathbf{g}';\mathbf{k}) - E_n(\mathbf{k})\delta^3(\mathbf{g}-\mathbf{g}')| = 0, \tag{25}$$

Let us restrict ourselves to the case whereby $\mathbf{k}_{\|}$ remains real and k_z is allowed to be complex. Now, since the matrix $\hat{H}^{(j)}(\mathbf{g}\mathbf{g}';\mathbf{k})$ is *diagonal*, the condition

$$|\hat{H}^{(j)}(\mathbf{g}\mathbf{g}';\mathbf{k}) - E_n(\mathbf{k})\delta^3(\mathbf{g}-\mathbf{g}')| = 0, \tag{26}$$

simply reduces to

$$\Pi_{\mathbf{g}}\left[(\mathbf{k}+\mathbf{g})^2 - E_n(\mathbf{k})\right] = 0, \tag{27}$$

or

$$\Pi_{\mathbf{g}}\left[\left(\mathbf{k}_{\|}+\mathbf{g}_{\|}\right)^2 + (k_z+g_z)^2 - E_n(\mathbf{k})\right] = 0, \tag{28}$$

where we have written,

$$\mathbf{g} = \mathbf{g}_{\|} + \hat{\mathbf{z}}g_z. \tag{29}$$

Thus, the allowed values of k_z are

$$k_z = -g_z \pm \sqrt{E_n(\mathbf{k}) - \left(\mathbf{k}_{\|}+\mathbf{g}_{\|}\right)^2}. \tag{30}$$

Let N be the number of plane waves $\{|\mathbf{g}\rangle\}$ included in the expansion

$$|n\mathbf{k}\rangle = \exp(i\mathbf{k}\cdot\mathbf{x})\sum_{\mathbf{g}}|\mathbf{g}\rangle C^{(n)}(\mathbf{g},\mathbf{k}), \tag{31}$$

and let $M < N$ be the the number of two-dimensional reciprocal lattice vector $\mathbf{g}_{\|}$ included in the expansion set $\{|\mathbf{g}\rangle\}$. It is clear that the *number if non-equivalent solutions of the form*

$$k_z = -g_z \pm \sqrt{E_n(\mathbf{k}) - \left(\mathbf{k}_{\|}+\mathbf{g}_{\|}\right)^2}, \tag{32}$$

is equal to twice the number M of distinct two-dimensional reciprocal lattice vectors $\mathbf{g}_{\|}$. Thus, for each $\mathbf{g}_{\|}$ included in the expansion there are *two* non-equivalent solutions ($\pm$ sign). The other solutions are related to these two by

a reciprocal lattice vector $\hat{\mathbf{z}}g_z$ and therefore *correspond to equivalent solutions.* Each different $\mathbf{g}_{\|}$ included in the expansion of the Bloch state gives rise to a set of *non-equivalent Bloch solutions.*

Thus, out of the $2N$ solutions

$$k_{\lambda}^{(j)}, \qquad \lambda = 1, \ldots, 2N, (33.a)$$

$$|\mathbf{k}_{\|} E; k_{\lambda}^{(j)}\rangle, \qquad \lambda = 1, \ldots, 2N, (33.b)$$

there are $2M < 2N$ sets of non-equivalent solutions associated with the M different values of $\mathbf{g}_{\|}$ included in the expansion,

$$k_{\gamma\mu}^{(j)}, \qquad \gamma = 1, \ldots, 2M, (34.a)$$

$$|\mathbf{k}_{\|} E; k_{\gamma\mu}^{(j)}\rangle, \qquad \gamma = 1, \ldots, 2M. (34.b)$$

The index μ labels the equivalent partner solutions within the set γ,

$$\hat{\mathbf{z}}k_{\gamma\mu'}^{(j)} = \hat{\mathbf{z}}k_{\gamma\mu}^{(j)} + \hat{\mathbf{z}}g_{\mu\mu'}, \qquad (34.c)$$

4.5.1.4 Relation Between Equivalent Solutions:

The purpose of this section is to examine the relation between equivalent solutions, *i.e.*, solutions related to each other by a reciprocal lattice vector $\hat{\mathbf{z}}g_z$. Again, this is most easily done within the local pseudopotential formalism[1].

4.5.1.4.1 Equivalent Solutions: k Real

Consider the expansion of the Bloch state $|n\mathbf{k}\rangle$ in terms of the set of plane waves $\{|\mathbf{g}\rangle\}$,

$$|n\mathbf{k}\rangle = \exp(i\mathbf{k}\cdot\mathbf{x})\sum_{\mathbf{g}}|\mathbf{g}\rangle C^{(n)}(\mathbf{g},\mathbf{k}). \tag{35}$$

Then, Schrödinger equation,

$$\hat{H}|n\mathbf{k}\rangle = E_n(\mathbf{k})|n\mathbf{k}\rangle, \tag{36.a}$$

can be transformed into a matrix equation in the $\{|\mathbf{g}\rangle\}$-representation,

$$\sum_{\mathbf{g}'}\hat{H}^{(j)}(\mathbf{g}\mathbf{g}';\mathbf{k})C^{(n)}(\mathbf{g}',\mathbf{k}) = E_n(\mathbf{k})C^{(n)}(\mathbf{g},\mathbf{k}), \tag{36.b}$$

or

$$\sum_{\mathbf{g}'}\left[\hat{H}^{(j)}(\mathbf{g}\mathbf{g}';\mathbf{k}) - E_n(\mathbf{k})\delta^3(\mathbf{g}-\mathbf{g}')\right]C^{(n)}(\mathbf{g}',\mathbf{k}) = 0, \tag{36.c}$$

where the Hamiltonian of solid j in the local pseudopotential form is given by

$$\hat{H}^{(j)}(\mathbf{g}\mathbf{g}';\mathbf{k}) \equiv (\mathbf{k}+\mathbf{g})^2\delta^3(\mathbf{g}-\mathbf{g}') + V^{(j)}(\mathbf{g}\mathbf{g}'), \tag{37}$$

and $V^{(j)}(\mathbf{g}\mathbf{g}')$ are the *pseudopotential form factors.*

Now, consider the expansion of the Bloch state $|n\mathbf{k}+\mathbf{g}_0\rangle$, related to $|n\mathbf{k}\rangle$ by the reciprocal lattice vector $\mathbf{g}_0$, in terms of the set of plane waves $\{|\mathbf{g}\rangle\}$,

$$|n\mathbf{k}+\mathbf{g}_0\rangle = \exp\left[i(\mathbf{k}+\mathbf{g}_0)\cdot\mathbf{x}\right]\sum_{\mathbf{g}}|\mathbf{g}\rangle C^{(n)}(\mathbf{g},\mathbf{k}+\mathbf{g}_0). \tag{38}$$

Then, Schrödinger equation,

$$\hat{H}|n\mathbf{k}+\mathbf{g}_0\rangle = E_n(\mathbf{k}+\mathbf{g}_0)|n\mathbf{k}+\mathbf{g}_0\rangle, \tag{39.a}$$

can be transformed into a matrix equation in the $\{|\mathbf{g}\rangle\}$-representation,

$$\sum_{\mathbf{g}'} \hat{H}^{(j)}(\mathbf{g}\mathbf{g}';\mathbf{k}+\mathbf{g}_0)C^{(n)}(\mathbf{g}',\mathbf{k}+\mathbf{g}_0) = E_n(\mathbf{k}+\mathbf{g}_0)C^{(n)}(\mathbf{g},\mathbf{k}+\mathbf{g}_0), \tag{39.b}$$

or

$$\sum_{\mathbf{g}'}\left[\hat{H}^{(j)}(\mathbf{g}\mathbf{g}';\mathbf{k}+\mathbf{g}_0) - E_n(\mathbf{k}+\mathbf{g}_0)\delta^3(\mathbf{g}-\mathbf{g}')\right] C^{(n)}(\mathbf{g}',\mathbf{k}+\mathbf{g}_0) = 0, \tag{39.c}$$

where the Hamiltonian of solid j in the local pseudopotential form is given by

$$\hat{H}^{(j)}(\mathbf{g}\mathbf{g}';\mathbf{k}+\mathbf{g}_0) \equiv (\mathbf{k}+\mathbf{g}_0+\mathbf{g})^2\delta^3(\mathbf{g}-\mathbf{g}') + V^{(j)}(\mathbf{g}\mathbf{g}'), \tag{40}$$

and $V^{(j)}(\mathbf{g}\mathbf{g}')$ are the *pseudopotential form factors.*

Now by comparing the local pseudopotential Hamiltonian corresponding to $|n\mathbf{k}\rangle$,

$$\hat{H}^{(j)}(\mathbf{g}\mathbf{g}';\mathbf{k}) \equiv (\mathbf{k}+\mathbf{g})^2\delta^3(\mathbf{g}-\mathbf{g}') + V^{(j)}(\mathbf{g}\mathbf{g}'), \tag{41.a}$$

and the local pseudopotential Hamiltonian corresponding to $|n\mathbf{k}+\mathbf{g}_0\rangle$

$$\hat{H}^{(j)}(\mathbf{g}\mathbf{g}';\mathbf{k}+\mathbf{g}_0) \equiv (\mathbf{k}+\mathbf{g}_0+\mathbf{g})^2\delta^3(\mathbf{g}-\mathbf{g}') + V^{(j)}(\mathbf{g}\mathbf{g}'), \tag{41.b}$$

it is clear that by making the substitution

$$\mathbf{k}\rightarrow\mathbf{k}+\mathbf{g}_0, \tag{42.a}$$

the resulting equation is the same as if we had made the replacements,

$$\mathbf{g}\rightarrow\mathbf{g}+\mathbf{g}_0, \tag{42.b}$$

and,

$$\mathbf{g}' \rightarrow \mathbf{g}' + \mathbf{g}_0, \tag{42.c}$$

and keeping $\mathbf{k}$ fixed.

Thus *in the pseudopotential formalism, the secular equations for the Bloch states* $|n\mathbf{k}\rangle$ *and* $|n\mathbf{k}+\mathbf{g}_0\rangle$, *where* $\mathbf{g}_0$ *is a reciprocal lattice vector, are the same to within a rearrangemant of the rows of the secular matrix.* We conclude that the eigenvectors $C^{(n)}(\mathbf{g},\mathbf{k})$ and $C^{(n)}(\mathbf{g},\mathbf{k}+\mathbf{g}_0)$ differ by at most a phase factor $\exp[i\varphi(\mathbf{k},\mathbf{g}_0)]$,

$$C^{(n)}(\mathbf{g},\mathbf{k}+\mathbf{g}_0) = \exp[i\varphi(\mathbf{k},\mathbf{g}_0)]\, C^{(n)}(\mathbf{g}+\mathbf{g}_0,\mathbf{k}), \tag{43.a}$$

and belong to the same energy eigenvalue,

$$E_n(\mathbf{k}+\mathbf{g}_0) = E_n(\mathbf{k}). \tag{43.b}$$

Given the relation

$$C^{(n)}(\mathbf{g},\mathbf{k}+\mathbf{g}_0) = \exp[i\varphi(\mathbf{k},\mathbf{g}_0)]\, C^{(n)}(\mathbf{g}+\mathbf{g}_0,\mathbf{k}), \tag{44}$$

between the *expansion coefficients*, we derive the relation between the *Bloch solutions* $|n\mathbf{k}+\mathbf{g}_0\rangle$ and $|n\mathbf{k}\rangle$.

Consider the expansion ,

$$|n\mathbf{k}+\mathbf{g}_0\rangle = \exp[i(\mathbf{k}+\mathbf{g}_0)\cdot\mathbf{x}] \sum_{\mathbf{g}} |\mathbf{g}\rangle C^{(n)}(\mathbf{g},\mathbf{k}+\mathbf{g}_0), \tag{45.a}$$

or explicitly, in $\mathbf{x}$-representation,

$$|n\mathbf{k}+\mathbf{g}_0\rangle = \exp[i(\mathbf{k}+\mathbf{g}_0)\cdot\mathbf{x}] \sum_{\mathbf{g}} \exp(i\mathbf{g}\cdot\mathbf{x}) C^{(n)}(\mathbf{g},\mathbf{k}+\mathbf{g}_0), \tag{45.b}$$

$$= \exp(i\mathbf{k}\cdot\mathbf{x}) \sum_{\mathbf{g}} \exp\left[i(\mathbf{g}+\mathbf{g}_0)\right] C^{(n)}(\mathbf{g}, \mathbf{k}+\mathbf{g}_0), \tag{45.c}$$

$$= \exp(i\mathbf{k}\cdot\mathbf{x}) \sum_{\mathbf{g}} \exp\left[i(\mathbf{g}+\mathbf{g}_0)\right] \exp\left[i\varphi(\mathbf{k}, \mathbf{g}_0)\right] C^{(n)}(\mathbf{g}+\mathbf{g}_0, \mathbf{k}), \tag{45.d}$$

or, by letting

$$\mathbf{g} \rightarrow \mathbf{g} + \mathbf{g}_0, \tag{46}$$

we have

$$= \exp\left[i\varphi(\mathbf{k}, \mathbf{g}_0)\right] \exp(i\mathbf{k}\cdot\mathbf{x}) \sum_{\mathbf{g}} \exp(i\mathbf{g}\cdot\mathbf{x}) C^{(n)}(\mathbf{g}, \mathbf{k}), \tag{47.a}$$

$$\equiv \exp\left[i\varphi(\mathbf{k}, \mathbf{g}_0)\right] |n\mathbf{k}\rangle. \tag{47.b}$$

We can thus write the relation between *equivalent Bloch solutions* as

$$|n\mathbf{k}+\mathbf{g}_0\rangle = \exp\left[i\varphi(\mathbf{k}, \mathbf{g}_0)\right] |n\mathbf{k}\rangle. \tag{48}$$

4.5.1.4.2 Equivalent Solutions: k Complex

We now consider the case where $\mathbf{k}$ takes on complex values. Let the wavevectors $k^{(j)}_{\gamma\mu}$ and $k^{(j)}_{\gamma\mu'}$, in solid $j = 1, 2$, belong to the same set γ and be related through

$$\hat{\mathbf{z}} k^{(j)}_{\gamma\mu'} = \hat{\mathbf{z}} k^{(j)}_{\gamma\mu} + \hat{\mathbf{z}} g_{\mu\mu'}. \tag{49}$$

We can relate the expansion coefficients, $C^{(j)}(\mathbf{g}, k^{(j)}_{\gamma\mu}; \mathbf{k}_{\|} E)$ and $C^{(j)}(\mathbf{g}, k^{(j)}_{\gamma\mu'}; \mathbf{k}_{\|} E)$ in the $\{|\mathbf{g}\rangle\}$-representation,

$$C^{(j)}(\mathbf{g}, k^{(j)}_{\gamma\mu'}; \mathbf{k}_{\|} E) \equiv C^{(j)}(\mathbf{g}, k^{(j)}_{\gamma\mu} + g_{\mu\mu'}; \mathbf{k}_{\|} E)$$

$$= C^{(j)}(\mathbf{g} + \hat{\mathbf{z}} g_{\mu\mu'}, k^{(j)}_{\gamma\mu}; \mathbf{k}_{\|} E) \exp\left[i\varphi^{(j)}(\gamma, \mu\mu')\right]. \tag{50}$$

And, the relation between equivalent Bloch states belonging to a given set γ is

$$|\mathbf{k}_{\|}E;k_{\gamma\mu'}^{(j)}\rangle = \exp\left[i\varphi^{(j)}(\gamma,\mu\mu')\right]|\mathbf{k}_{\|}E;k_{\gamma\mu}^{(j)}\rangle, \tag{51.a}$$

where the state $|\mathbf{k}_{\|}E;k_{\gamma\mu}^{(j)}\rangle$ belongs to the eigenvalue $k_{\gamma\mu}^{(j)}$ and the state $|\mathbf{k}_{\|}E;k_{\gamma\mu'}^{(j)}\rangle$ belongs to the eigenvalue $k_{\gamma\mu'}^{(j)}$, and,

$$\hat{\mathbf{z}}k_{\gamma\mu'}^{(j)} = \hat{\mathbf{z}}k_{\gamma\mu}^{(j)} + \hat{\mathbf{z}}g_{\mu\mu'}. \tag{51.b}$$

From now on, we adopt the convention that the eigenvalue $k_{\gamma}^{(j)}$ *has its real part within the first Brillouin zone*, in solid $j = 1, 2$. That is, $\mathrm{Re}\left[k_{\gamma}^{(j)}\right]$ lies inside the first Brillouin zone. We label the equivalent partner solutions of $k_{\gamma}^{(j)}$ by $k_{\gamma\mu}^{(j)}$. Then we have

$$|\mathbf{k}_{\|}E;k_{\gamma\mu}^{(j)}\rangle = \exp\left[i\varphi^{(j)}(\gamma,\mu)\right]|\mathbf{k}_{\|}E;k_{\gamma}^{(j)}\rangle, \tag{52}$$

where the state $|\mathbf{k}_{\|}E;k_{\gamma}^{(j)}\rangle$ belongs to the eigenvalue $k_{\gamma}^{(j)}$ within the first Brillouin zone and the state $|\mathbf{k}_{\|}E;k_{\gamma\mu}^{(j)}\rangle$ belongs to the eigenvalue $k_{\gamma\mu}^{(j)}$. The phase $\exp\left[i\varphi^{(j)}(\gamma,\mu)\right]$ relates a Bloch solution outside the first Brillouin, $|\mathbf{k}_{\|}E;k_{\gamma\mu}^{(j)}\rangle$, to a solution inside the first Brillouin zone $|\mathbf{k}_{\|}E;k_{\gamma}^{(j)}\rangle$.

The wavevectors $k_{\gamma}^{(j)}$ and $k_{\gamma\mu}^{(j)}$ belong to the same set γ and are related through

$$\hat{\mathbf{z}}k_{\gamma\mu}^{(j)} = \hat{\mathbf{z}}k_{\gamma}^{(j)} + \hat{\mathbf{z}}g_{\mu}, \tag{53}$$

and $\mathrm{Re}\left[k_{\gamma}^{(j)}\right]$ lies inside the first Brillouin zone.

4.5.2 EQUIVALENT SOLUTIONS AND BOUNDARY CONDITIONS:

In this second part of the Appendix (4.5) we analyse the *superlattice state function* and the *boundary condition matrix* in the light of the above discussion about *equivalent solutions.*

4.5.2.1. Superlattice Wavefunction and Equivalent States:

As above, let $j = 1, 2$ be a label to identify either one of the two constituent semiconductors forming the superlattice. The set of Bloch states $\{|\mathbf{k}_{\|} E; k_{\lambda}^{(j)}\rangle\}$ in solid j is a solution of the bulk Schrödinger equation:

$$\hat{H}^{(j)} |\mathbf{k}_{\|} E; k_{\lambda}^{(j)}\rangle = E(\mathbf{k}_{\|}, k_{\lambda}^{(j)}) |\mathbf{k}_{\|} E; k_{\lambda}^{(j)}\rangle, \tag{1}$$

where $\hat{H}^{(j)}$ refer to the bulk Hamiltonian in solid j, and $[\lambda = 1, \ldots, 2N]$.

Let the superlattice state at fixed parallel wavevector $\mathbf{k}_{\|}$ and energy E in solid j be $|\mathbf{k}_{\|} E; \mathbf{q}; j\rangle$, where $\mathbf{q}$ is a quantum number that labels the superlattice states. The label $\mathbf{q}$ is referred to as the *superlattice wavevector.* Let the $\hat{\mathbf{z}}$ be the direction normal to the superlattice interfaces.

We now expand the superlattice state $|\mathbf{k}_{\|} E; \mathbf{q}; j\rangle$ on the set of Bloch solutions $\{|\mathbf{k}_{\|} E; k_{\lambda}^{(j)}\rangle\}$ in each solid j:

$$|\mathbf{k}_{\|} E; \mathbf{q}; j\rangle = \sum_{\lambda=1}^{2N} |\mathbf{k}_{\|} E; k_{\lambda}^{(j)}\rangle f^{(j)}(k_{\lambda}^{(j)}, \mathbf{q}; \mathbf{k}_{\|}), \tag{2}$$

where the amplitudes $f^{(j)}(k_{\lambda}^{(j)}, \mathbf{q}; \mathbf{k}_{\|})$ indicate the admixture of the bulk Bloch state $|\mathbf{k}_{\|} E; k_{\lambda}^{(j)}\rangle$ in the superlattice state $|\mathbf{k}_{\|} E; \mathbf{q}; j\rangle$.

• k · p Approach:

As seen in the previous section, the Bloch solutions in solid j, $\{|\mathbf{k}_{\|} E; k_{\lambda}^{(j)}\rangle\}$, are described in a zone-center expansion set $\{|m\rangle\}$ which is associated with a reference

solid,

$$\langle \mathbf{x}|\mathbf{k}_{\|}E;k_{\lambda}^{(j)}\rangle \equiv \exp(i\mathbf{k}_{\|}\cdot\mathbf{x}_{\|})\exp(ik_{\lambda}^{(j)}z)u(\mathbf{k}_{\|},k_{\lambda}^{(j)};\mathbf{x}), \tag{3.a}$$

$$\langle \mathbf{x}|\mathbf{k}_{\|}E;k_{\lambda}^{(j)}\rangle = \exp(i\mathbf{k}_{\|}\cdot\mathbf{x}_{\|})\exp(ik_{\lambda}^{(j)}z)\sum_{m=1}^{N}\langle \mathbf{x}|m\rangle C^{(j)}(m,k_{\lambda}^{(j)};\mathbf{k}_{\|}E). \tag{3.b}$$

As before, the index m will refer to a $\mathbf{k}_0 = \mathbf{0}$ basis function in the reference solid.

• Local Pseudopotentials Approach:

Is is also possible to carry out this expansion of the set of Bloch solutions $\{|\mathbf{k}_{\|}E;k_{\lambda}^{(j)}\rangle\}$, on a set of plane waves $\{|\mathbf{g}\rangle\}$ associated with the reciprocal lattice vectors,

$$\langle \mathbf{x}|\mathbf{k}_{\|}E;k_{\lambda}^{(j)}\rangle = \exp(i\mathbf{k}_{\|}\cdot\mathbf{x}_{\|})\exp(ik_{\lambda}^{(j)}z)\sum_{\mathbf{g}}\langle \mathbf{x}|\mathbf{g}\rangle C^{(j)}(\mathbf{g},k_{\lambda}^{(j)};\mathbf{k}_{\|}E). \tag{4}$$

The relation between the sets of coefficients $C^{(j)}(m,k_{\lambda}^{(j)};\mathbf{k}_{\|}E)$ and $C^{(j)}(\mathbf{g},k_{\lambda}^{(j)};\mathbf{k}_{\|}E)$ is obtained through the matrix $U(\mathbf{g},m)$

$$C^{(j)}(\mathbf{g},k_{\lambda}^{(j)};\mathbf{k}_{\|}E) = \sum_{m}U(\mathbf{g},m)C^{(j)}(m,k_{\lambda}^{(j)};\mathbf{k}_{\|}E). \tag{5}$$

We now break the total $2N$ solutions $k_{\lambda}^{(j)}$ into $2M < 2N$ sets $k_{\gamma\mu}^{(j)}$ of *non-equivalent solutions.* We *relabel the solutions* $k_{\lambda}^{(j)}$ *into sets of non-equivalent Bloch states.* Let us make the change of label for the solutions $k_{\lambda}^{(j)}$ in solid $j = 1, 2$

$$k_{\lambda}^{(j)}\rightarrow k_{\gamma\mu}^{(j)}, \tag{6.a}$$

for the wavevector,

$$|\mathbf{k}_{\|}E;k_{\lambda}^{(j)}\rangle\rightarrow|\mathbf{k}_{\|}E;k_{\gamma\mu}^{(j)}\rangle, \tag{6.b}$$

for the associated Bloch states, and

$$f^{(j)}(k_{\chi}^{(j)}, \mathbf{q}; \mathbf{k}_{\|}) \rightarrow f^{(j)}(k_{\gamma\mu}^{(j)}, \mathbf{q}; \mathbf{k}_{\|}), \tag{6.c}$$

for the amplitudes.

As above, γ labels the sets of non-equivalent Bloch states and μ labels the equivalent partners within the set γ, and $[\gamma = 1, \ldots, 2M]$.

We now rewrite the expansion of the superlattice state function as

$$|\mathbf{k}_{\|} E; \mathbf{q}; j\rangle = \sum_{\gamma=1}^{2M} \sum_{\mu} |\mathbf{k}_{\|} E; k_{\gamma\mu}^{(j)}\rangle f^{(j)}(k_{\gamma\mu}^{(j)}, \mathbf{q}; \mathbf{k}_{\|}). \tag{7}$$

The summation $\sum_{\gamma=1}^{2M}$ is over the $2M$ sets of non-equivalent solutions. The summation $\sum_{\mu}$ is over the partner solutions within the set γ.

The relation between the equivalent partners μ of a set γ is

$$|\mathbf{k}_{\|} E; k_{\gamma\mu}^{(j)}\rangle = \exp\left[i\varphi^{(j)}(\gamma, \mu)\right] |\mathbf{k}_{\|} E; k_{\gamma}^{(j)}\rangle, \tag{8}$$

where the state $|\mathbf{k}_{\|} E; k_{\gamma}^{(j)}\rangle$ belongs to the eigenvalue $k_{\gamma}^{(j)}$ and the state $|\mathbf{k}_{\|} E; k_{\gamma\mu}^{(j)}\rangle$ belongs to the eigenvalue $k_{\gamma\mu}^{(j)}$. The phase $\exp\left[i\varphi^{(j)}(\gamma, \mu)\right]$ relates a Bloch solution outside the first Brillouin, $|\mathbf{k}_{\|} E; k_{\gamma\mu}^{(j)}\rangle$, to a solution inside the first Brillouin zone $|\mathbf{k}_{\|} E; k_{\gamma}^{(j)}\rangle$. As above, we adopt the convention that $\mathrm{Re}\left[k_{\gamma}^{(j)}\right]$ lies inside the first Brillouin zone.

We can now write

$$|\mathbf{k}_{\|} E; \mathbf{q}; j\rangle = \sum_{\gamma=1}^{2M} \sum_{\mu} |\mathbf{k}_{\|} E; k_{\gamma\mu}^{(j)}\rangle f^{(j)}(k_{\gamma\mu}^{(j)}, \mathbf{q}; \mathbf{k}_{\|}), \tag{9.a}$$

or, using

$$|\mathbf{k}_{\|} E; k_{\gamma\mu}^{(j)}\rangle = \exp\left[i\varphi^{(j)}(\gamma, \mu)\right] |\mathbf{k}_{\|} E; k_{\gamma}^{(j)}\rangle, \tag{9.b}$$

we have

$$|\mathbf{k}_{\|}E;\mathbf{q};j\rangle = \sum_{\gamma=1}^{2M}\sum_{\mu}\exp\left[i\varphi^{(j)}(\gamma,\mu)\right]|\mathbf{k}_{\|}E;k_{\gamma}^{(j)}\rangle f^{(j)}(k_{\gamma\mu}^{(j)},\mathbf{q};\mathbf{k}_{\|}), \qquad (10.a)$$

or, regrouping,

$$|\mathbf{k}_{\|}E;\mathbf{q};j\rangle = \sum_{\gamma=1}^{2M}|\mathbf{k}_{\|}E;k_{\gamma}^{(j)}\rangle\left[\sum_{\mu}\exp\left[i\varphi^{(j)}(\gamma,\mu)\right]f^{(j)}(k_{\gamma\mu}^{(j)},\mathbf{q};\mathbf{k}_{\|})\right], \qquad (10.b)$$

and finally,

$$|\mathbf{k}_{\|}E;\mathbf{q};j\rangle = \sum_{\gamma=1}^{2M}|\mathbf{k}_{\|}E;k_{\gamma}^{(j)}\rangle f^{(j)}(k_{\gamma}^{(j)},\mathbf{q};\mathbf{k}_{\|}), \qquad (11.a)$$

where we have defined,

$$f^{(j)}(k_{\gamma}^{(j)},\mathbf{q};\mathbf{k}_{\|}) \equiv \sum_{\mu}\exp\left[i\varphi^{(j)}(\gamma,\mu)\right]f^{(j)}(k_{\gamma\mu}^{(j)},\mathbf{q};\mathbf{k}_{\|}). \qquad (11.b)$$

Since *only the non-equivalent solutions correspond to physically distinct situations we only should regard the sum*

$$f^{(j)}(k_{\gamma}^{(j)},\mathbf{q};\mathbf{k}_{\|}) \equiv \sum_{\mu}\exp\left[i\varphi^{(j)}(\gamma,\mu)\right]f^{(j)}(k_{\gamma\mu}^{(j)},\mathbf{q};\mathbf{k}_{\|}), \qquad (12)$$

as physically meaningful. Then, within the local pseudopotential formalism, we know that *there are only* $2M$ *physically significant amplitudes,* $f^{(j)}(k_{\gamma}^{(j)},\mathbf{q};\mathbf{k}_{\|})$, *where* M *is the number of distinct* $\mathbf{g}_{\|}$ *included in the expansion of the Bloch state.* The amplitudes $f^{(j)}(k_{\gamma}^{(j)},\mathbf{q};\mathbf{k}_{\|})$, $[\gamma = 1,\ldots,2M]$ are the quantities of interest.

• k · p Approach: Multi-component Envelope Function

Then the superlattice state in solid j can be expressed as a linear combination of zone-center basis functions $\{|m\rangle\}$ of a reference solid. By using explicitly a

x-representation, we can expand on the set of $2M$ non-equivalent solutions,

$$\langle \mathbf{x}|\mathbf{k}_{\|}E;\mathbf{q};j\rangle = \sum_{\gamma=1}^{2M} \langle \mathbf{x}|\mathbf{k}_{\|}E;k_{\gamma}^{(j)}\rangle f^{(j)}(k_{\gamma}^{(j)},\mathbf{q};\mathbf{k}_{\|}), \tag{13.a}$$

$$= \sum_{\gamma=1}^{2M}\left[\exp(i\mathbf{k}_{\|}\cdot\mathbf{x}_{\|})\exp(ik_{\gamma}^{(j)}z)\sum_{m=1}^{N}\langle \mathbf{x}|m\rangle C^{(j)}(m,k_{\gamma}^{(j)};\mathbf{k}_{\|}E)\right] f^{(j)}(k_{\gamma}^{(j)},\mathbf{q};\mathbf{k}_{\|}),$$

$$= \sum_{m=1}^{N}\langle \mathbf{x}|m\rangle\left[\exp(i\mathbf{k}_{\|}\cdot\mathbf{x}_{\|})\sum_{\gamma=1}^{2M}\exp(ik_{\gamma}^{(j)}z)C^{(j)}(m,k_{\gamma}^{(j)};\mathbf{k}_{\|}E)f^{(j)}(k_{\gamma}^{(j)},\mathbf{q};\mathbf{k}_{\|})\right],$$

and finally,

$$\langle \mathbf{x}|\mathbf{k}_{\|}E;\mathbf{q};j\rangle \equiv \sum_{m=1}^{N}\langle \mathbf{x}|m\rangle F^{(j)}(m;\mathbf{k}_{\|}\mathbf{q};\mathbf{x}). \tag{13.b}$$

The functions $F^{(j)}(m;\mathbf{k}_{\|}\mathbf{q};\mathbf{x})$ are referred to as multi-component envelope functions and are defined to be the expression in [...] of Eq.(13):

$$F^{(j)}(m;\mathbf{k}_{\|}\mathbf{q};\mathbf{x}) \equiv \exp(i\mathbf{k}_{\|}\cdot\mathbf{x}_{\|})\cdot$$

$$\sum_{\gamma=1}^{2M}\left[\exp(ik_{\gamma}^{(j)}z)C^{(j)}(m,k_{\gamma}^{(j)};\mathbf{k}_{\|}E)\right] f^{(j)}(k_{\gamma}^{(j)},\mathbf{q};\mathbf{k}_{\|}), \tag{14}$$

in terms of the basis states at $\mathbf{k}_0 = \mathbf{0}$ in the reference solid, $\{|m\rangle\}$, and

$$f^{(j)}(k_{\gamma}^{(j)},\mathbf{q};\mathbf{k}_{\|}) \equiv \sum_{\mu}\exp\left[i\varphi^{(j)}(\gamma,\mu)\right] f^{(j)}(k_{\gamma\mu}^{(j)},\mathbf{q};\mathbf{k}_{\|}). \tag{15}$$

• Pseudopotential Approach: Multi-component Envelope Function

In the local pseudopotential formalism, the superlattice state in solid j can be expressed as a linear combination of plane waves $\{|\mathbf{g}\rangle\}$. By using explicitly a **x**-representation, we can expand on the set of $2M$ non-equivalent solutions,

$$\langle \mathbf{x}|\mathbf{k}_{\|}E;\mathbf{q};j\rangle = \sum_{\gamma=1}^{2M} \langle \mathbf{x}|\mathbf{k}_{\|}E;k_{\gamma}^{(j)}\rangle f^{(j)}(k_{\gamma}^{(j)},\mathbf{q};\mathbf{k}_{\|}), \tag{16.a}$$

$$= \sum_{\gamma=1}^{2M} \left[\exp(i\mathbf{k}_{\|} \cdot \mathbf{x}_{\|}) \exp(ik_{\gamma}^{(j)} z) \sum_{\mathbf{g}} \langle \mathbf{x}|\mathbf{g}\rangle C^{(j)}(\mathbf{g}, k_{\gamma}^{(j)}; \mathbf{k}_{\|} E) \right] f^{(j)}(k_{\gamma}^{(j)}, \mathbf{q}; \mathbf{k}_{\|}),$$

$$= \sum_{\mathbf{g}} \langle \mathbf{x}|\mathbf{g}\rangle \left[\exp(i\mathbf{k}_{\|} \cdot \mathbf{x}_{\|}) \sum_{\gamma=1}^{2M} \exp(ik_{\gamma}^{(j)} z) C^{(j)}(\mathbf{g}, k_{\gamma}^{(j)}; \mathbf{k}_{\|} E) f^{(j)}(k_{\gamma}^{(j)}, \mathbf{q}; \mathbf{k}_{\|}) \right],$$

and finally,

$$\langle \mathbf{x}|\mathbf{k}_{\|} E; \mathbf{q}; j\rangle \equiv \sum_{\mathbf{g}} \langle \mathbf{x}|\mathbf{g}\rangle F^{(j)}(\mathbf{g}; \mathbf{k}_{\|}\mathbf{q}; \mathbf{x}). \tag{16.b}$$

The sets of coefficients $C^{(j)}(m, k_{\gamma}^{(j)}; \mathbf{k}_{\|} E)$ and $C^{(j)}(\mathbf{g}, k_{\gamma}^{(j)}; \mathbf{k}_{\|} E)$ are related through the matrix $U(\mathbf{g}, m)$

$$C^{(j)}(\mathbf{g}, k_{\gamma}^{(j)}; \mathbf{k}_{\|} E) = \sum_{m} U(\mathbf{g}, m) C^{(j)}(m, k_{\gamma}^{(j)}; \mathbf{k}_{\|} E). \tag{17}$$

The functions $F^{(j)}(\mathbf{g}; \mathbf{k}_{\|}\mathbf{q}; \mathbf{x})$ are referred to as multi-component envelope functions and are defined to be the expression in [...] of Eq.(16):

$$F^{(j)}(\mathbf{g}; \mathbf{k}_{\|}\mathbf{q}; \mathbf{x}) \equiv \exp(i\mathbf{k}_{\|} \cdot \mathbf{x}_{\|}) \cdot$$

$$\sum_{\gamma=1}^{2M} \left[\exp(ik_{\gamma}^{(j)} z) C^{(j)}(\mathbf{g}, k_{\gamma}^{(j)}; \mathbf{k}_{\|} E) \right] f^{(j)}(k_{\gamma}^{(j)}, \mathbf{q}; \mathbf{k}_{\|}), \tag{18}$$

in terms of the plane waves basis $\{|\mathbf{g}\rangle\}$, and

$$f^{(j)}(k_{\gamma}^{(j)}, \mathbf{q}; \mathbf{k}_{\|}) \equiv \sum_{\mu} \exp\left[i\varphi^{(j)}(\gamma, \mu) \right] f^{(j)}(k_{\gamma\mu}^{(j)}, \mathbf{q}; \mathbf{k}_{\|}). \tag{19}$$

4.5.2.2 Boundary Conditions and Reduced Transfer Matrix:

In this section, we indicate how to obtain the *reduced transfer matrix* in terms of non-equivalent solutions $k_\gamma^{(j)}$ inside the first Brillouin zone. The phase $\exp\left[i\varphi^{(j)}(\gamma,\mu)\right]$ relates a Bloch solution outside the first Brillouin, $|\mathbf{k}_\parallel E; k_{\gamma\mu}^{(j)}\rangle$, to a solution inside the first Brillouin zone $|\mathbf{k}_\parallel E; k_\gamma^{(j)}\rangle$. We use the local pseudopotential approach to derive the *boundary conditions matrix* and the *transfer matrix*.

• **Local Pseudopotential Approach: Boundary Conditions**

Let us expand the superlattice state function in solid $j = 1, 2$ in terms of N plane waves, $\{|\mathbf{g}\rangle\}$,

$$\langle \mathbf{x}|\mathbf{k}_\parallel E; \mathbf{q}; j\rangle = \sum_{\lambda=1}^{2N} \langle \mathbf{x}|\mathbf{k}_\parallel E; k_\lambda^{(j)}\rangle f^{(j)}(k_\lambda^{(j)}, \mathbf{q}; \mathbf{k}_\parallel), \tag{20}$$

$$= \sum_{\lambda=1}^{2N} \left[\exp(i\mathbf{k}_\parallel \cdot \mathbf{x}_\parallel)\exp(ik_\lambda^{(j)} z)\sum_{\mathbf{g}} \exp(i\mathbf{g}\cdot\mathbf{x}) C^{(j)}(\mathbf{g}, k_\lambda^{(j)}; \mathbf{k}_\parallel E)\right] f^{(j)}(k_\lambda^{(j)}, \mathbf{q}; \mathbf{k}_\parallel),$$

$$= \sum_{\mathbf{g}} \exp(i\mathbf{g}\cdot\mathbf{x})\left[\exp(i\mathbf{k}_\parallel \cdot \mathbf{x}_\parallel)\sum_{\lambda=1}^{2N} \exp(ik_\lambda^{(j)} z) C^{(j)}(\mathbf{g}, k_\lambda^{(j)}; \mathbf{k}_\parallel E) f^{(j)}(k_\lambda^{(j)}, \mathbf{q}; \mathbf{k}_\parallel)\right],$$

where we have written the plane wave as

$$\langle \mathbf{x}|\mathbf{g}\rangle \equiv \exp(i\mathbf{g}\cdot\mathbf{x}). \tag{21}$$

The superlattice primitive cell is shown in Figure (1). The interface plane has been taken to be at $z_0 = 0$ for convenience.

• The solid (1) extends from $z_0 = -b$ to the *left* of the interface plane up to $z_0 = 0$. The solid (2) extends from $z_0 = 0$ up to $z_0 = a$ to the *right* of the interface plane.

Let $\mathbf{R}_0$ be the superlattice lattice translation vector. We apply the following set of boundary conditions on the superlattice wavefunction on both sides of the interface:

(i) Continuity of the superlattice wavefunction at the interface plane $z_0 = 0$

$$\left[\langle \mathbf{x}|\mathbf{k}_{\|}E;\mathbf{q};1\rangle\right]_{z=0} = \left[\langle \mathbf{x}|\mathbf{k}_{\|}E;\mathbf{q};2\rangle\right]_{z=0}. \tag{22.a}$$

(ii) Continuity of the normal derivative of superlattice wavefunction at the interface plane $z_0 = 0$

$$\left[\hat{\mathbf{z}}\cdot\nabla\langle \mathbf{x}|\mathbf{k}_{\|}E;\mathbf{q};1\rangle\right]_{z=0} = \left[\hat{\mathbf{z}}\cdot\nabla\langle \mathbf{x}|\mathbf{k}_{\|}E;\mathbf{q};2\rangle\right]_{z=0}. \tag{22.b}$$

(iii) Bloch theorem for the superlattice wavefunction,

$$\exp(i\mathbf{q}\cdot\mathbf{R}_0)\left[\langle \mathbf{x}|\mathbf{k}_{\|}E;\mathbf{q};1\rangle\right]_{z=-b} = \left[\langle \mathbf{x}|\mathbf{k}_{\|}E;\mathbf{q};2\rangle\right]_{z=a}. \tag{22.c}$$

(iv) Bloch theorem for the normal derivative of superlattice wavefunction,

$$\exp(i\mathbf{q}\cdot\mathbf{R}_0)\left[\hat{\mathbf{z}}\cdot\nabla\langle \mathbf{x}|\mathbf{k}_{\|}E;\mathbf{q};1\rangle\right]_{z=-b} = \left[\hat{\mathbf{z}}\cdot\nabla\langle \mathbf{x}|\mathbf{k}_{\|}E;\mathbf{q};2\rangle\right]_{z=a}. \tag{22.d}$$

We expand the superlattice state function and equate the coefficients corresponding to the same plane wave $\mathbf{g}$. We now express the above set of boundary conditions in an *eigenvalue system* for the $4N$ unknown coefficients $f^{(j)}(k_{\lambda}^{(j)},\mathbf{q};\mathbf{k}_{\|})$, where $j = 1, 2$. By using the definition of the envelope function,

$$F^{(j)}(\mathbf{g};\mathbf{k}_{\|}\mathbf{q};\mathbf{x}) \equiv \exp(i\mathbf{k}_{\|}\cdot\mathbf{x}_{\|})\cdot$$

$$\sum_{\lambda=1}^{2N}\left[\exp(ik_{\lambda}^{(j)}z)C^{(j)}(\mathbf{g},k_{\lambda}^{(j)};\mathbf{k}_{\|}E)\right]f^{(j)}(k_{\lambda}^{(j)},\mathbf{q};\mathbf{k}_{\|}), \tag{23}$$

we obtain the following relations for $\mathbf{g} = 1, 2, \ldots, N$, after cancelling a common factor $\exp\left[i(\mathbf{k}_{\|}+\mathbf{g}_{\|})\cdot\mathbf{x}_{\|}\right]$

$$\sum_{\lambda=1}^{2N}\left[C^{(1)}(\mathbf{g},k_{\lambda}^{(1)};\mathbf{k}_{\|}E)\right]f^{(1)}(k_{\lambda}^{(1)},\mathbf{q};\mathbf{k}_{\|}) =$$

$$\sum_{\lambda=1}^{2N}\left[C^{(2)}(\mathbf{g},k_\lambda^{(2)};\mathbf{k}_\parallel E)\right]f^{(2)}(k_\lambda^{(2)},\mathbf{q};\mathbf{k}_\parallel) \tag{24.a}$$

$$\sum_{\lambda=1}^{2N}\left[\left(k_\lambda^{(1)}+g_z\right)C^{(1)}(\mathbf{g},k_\lambda^{(1)};\mathbf{k}_\parallel E)\right]f^{(1)}(k_\lambda^{(1)},\mathbf{q};\mathbf{k}_\parallel)=$$

$$\sum_{\lambda=1}^{2N}\left[\left(k_\lambda^{(2)}+g_z\right)C^{(2)}(\mathbf{g},k_\lambda^{(2)};\mathbf{k}_\parallel E)\right]f^{(2)}(k_\lambda^{(2)},\mathbf{q};\mathbf{k}_\parallel) \tag{24.b}$$

$$\exp(i\mathbf{q}\cdot\mathbf{R}_0)\cdot$$

$$\exp(-ig_z b)\sum_{\lambda=1}^{2N}\left[C^{(1)}(\mathbf{g},k_\lambda^{(1)};\mathbf{k}_\parallel E)\exp(-ik_\lambda^{(1)}b)\right]f^{(1)}(k_\lambda^{(1)},\mathbf{q};\mathbf{k}_\parallel)=$$

$$\exp(ig_z a)\sum_{\lambda=1}^{2N}\left[C^{(2)}(\mathbf{g},k_\lambda^{(2)};\mathbf{k}_\parallel E)\exp(ik_\lambda^{(2)}a)\right]f^{(2)}(k_\lambda^{(2)},\mathbf{q};\mathbf{k}_\parallel) \tag{24.c}$$

$$\exp(i\mathbf{q}\cdot\mathbf{R}_0)\cdot$$

$$\exp(-ig_z b)\sum_{\lambda=1}^{2N}\left[\left(k_\lambda^{(1)}+g_z\right)C^{(1)}(\mathbf{g},k_\lambda^{(1)};\mathbf{k}_\parallel E)\exp(-ik_\lambda^{(1)}b)\right]\cdot$$

$$f^{(1)}(k_\lambda^{(1)},\mathbf{q};\mathbf{k}_\parallel)=$$

$$\exp(ig_z a)\sum_{\lambda=1}^{2N}\left[\left(k_\lambda^{(2)}+g_z\right)C^{(2)}(\mathbf{g},k_\lambda^{(2)};\mathbf{k}_\parallel E)\exp(ik_\lambda^{(2)}a)\right]\cdot$$

$$f^{(2)}(k_\lambda^{(2)},\mathbf{q};\mathbf{k}_\parallel) \tag{24.d}$$

We now break the total $2N$ solutions $k_\lambda^{(j)}$ into $2M < 2N$ sets $k_{\gamma\mu}^{(j)}$ of *non-equivalent solutions.* We *relabel the solutions* $k_\lambda^{(j)}$ *into sets of non-equivalent*

Bloch states. Let us make the change of label for the solutions $k_{\lambda}^{(j)}$ in solid $j = 1, 2$

$$k_{\lambda}^{(j)} \rightarrow k_{\gamma\mu}^{(j)}, \tag{25.a}$$

for the wavevector, and,

$$f^{(j)}(k_{\lambda}^{(j)}, \mathbf{q}; \mathbf{k}_{\|}) \rightarrow f^{(j)}(k_{\gamma\mu}^{(j)}, \mathbf{q}; \mathbf{k}_{\|}), \tag{25.b}$$

for the amplitudes.

- The set of boundary conditions now becomes,

$$\sum_{\gamma\mu=1}^{2N} \left[C^{(1)}(\mathbf{g}, k_{\gamma\mu}^{(1)}; \mathbf{k}_{\|} E) \right] f^{(1)}(k_{\gamma\mu}^{(1)}, \mathbf{q}; \mathbf{k}_{\|}) =$$

$$\sum_{\gamma\mu=1}^{2N} \left[C^{(2)}(\mathbf{g}, k_{\gamma\mu}^{(2)}; \mathbf{k}_{\|} E) \right] f^{(2)}(k_{\gamma\mu}^{(2)}, \mathbf{q}; \mathbf{k}_{\|}) \tag{26.a}$$

$$\sum_{\gamma\mu=1}^{2N} \left[(k_{\gamma\mu}^{(1)} + g_z) C^{(1)}(\mathbf{g}, k_{\gamma\mu}^{(1)}; \mathbf{k}_{\|} E) \right] f^{(1)}(k_{\gamma\mu}^{(1)}, \mathbf{q}; \mathbf{k}_{\|}) =$$

$$\sum_{\gamma\mu=1}^{2N} \left[(k_{\gamma\mu}^{(2)} + g_z) C^{(2)}(\mathbf{g}, k_{\gamma\mu}^{(2)}; \mathbf{k}_{\|} E) \right] f^{(2)}(k_{\gamma\mu}^{(2)}, \mathbf{q}; \mathbf{k}_{\|}) \tag{26.b}$$

$$\exp(i\mathbf{q} \cdot \mathbf{R}_0) \cdot$$

$$\exp(-ig_z b) \sum_{\gamma\mu=1}^{2N} \left[C^{(1)}(\mathbf{g}, k_{\gamma\mu}^{(1)}; \mathbf{k}_{\|} E) \exp(-ik_{\gamma\mu}^{(1)} b) \right] f^{(1)}(k_{\gamma\mu}^{(1)}, \mathbf{q}; \mathbf{k}_{\|}) =$$

$$\exp(ig_z a) \sum_{\gamma\mu=1}^{2N} \left[C^{(2)}(\mathbf{g}, k_{\gamma\mu}^{(2)}; \mathbf{k}_{\|} E) \exp(ik_{\gamma\mu}^{(2)} a) \right] f^{(2)}(k_{\gamma\mu}^{(2)}, \mathbf{q}; \mathbf{k}_{\|}) \tag{26.c}$$

$$\exp(i\mathbf{q}\cdot\mathbf{R}_0)\cdot$$

$$\exp(-ig_z b)\sum_{\gamma\mu=1}^{2N}\left[(k_{\gamma\mu}^{(1)}+g_z)C^{(1)}(\mathbf{g},k_{\gamma\mu}^{(1)};\mathbf{k}_\parallel E)\exp(-ik_{\gamma\mu}^{(1)}b)\right]\cdot$$

$$f^{(1)}(k_{\gamma\mu}^{(1)},\mathbf{q};\mathbf{k}_\parallel)=$$

$$\exp(ig_z a)\sum_{\gamma\mu=1}^{2N}\left[(k_{\gamma\mu}^{(2)}+g_z)C^{(2)}(\mathbf{g},k_{\gamma\mu}^{(2)};\mathbf{k}_\parallel E)\exp(ik_{\gamma\mu}^{(2)}a)\right]\cdot$$

$$f^{(2)}(k_{\gamma\mu}^{(2)},\mathbf{q};\mathbf{k}_\parallel) \qquad (26.d)$$

Matrix Formulation:

Let us express the above set of $4N$ equations given for the $4N$ unknown coefficients $f^{(j)}(k_{\gamma\mu}^{(j)},\mathbf{q};\mathbf{k}_\parallel)$ in a matrix form. To do so, let us define the $[2N]$ - dimensional column vector $\mathbf{f}^{(j)}(\mathbf{q})$ composed of the expansion coefficients $f^{(j)}(k_{\gamma\mu}^{(j)},\mathbf{q};\mathbf{k}_\parallel)$ of the envelope function $F^{(j)}(\mathbf{g};\mathbf{k}_\parallel\mathbf{q};\mathbf{x})$.

Also let us define the $[2N\cdot 2N]$ diagonal matrix $\mathbf{D}(k_{\gamma\mu}^{(j)})$ whose matrix elements are the complex-$\mathbf{k}$ values $k_{\gamma\mu}^{(j)}$ in solid j.

We define the $[2N\cdot 2N]$ diagonal matrix $\mathbf{D}(\mathbf{q})$ whose matrix elements are the complex-$\mathbf{q}$ values of the superlattice wavevector.

We also define the z-dependent *boundary condition matrix* $[2N\cdot 2N]$ matrix $\mathbf{M}(\mathbf{k}_\parallel E;j;z)$ whose first $[N\cdot 2N]$ elements are the first set of the above equations, and whose second $[N\cdot 2N]$ elements are the second set of the above equations. The matrix $\mathbf{M}(\mathbf{k}_\parallel E;j;z)$ has matrix elements $\mathbf{M}(\mathbf{g},k_{\gamma\mu}^{(j)};\mathbf{k}_\parallel E;j;z)$ in the $\{|\mathbf{g}\rangle\}$-representation.

We can thus write, symbolically,

$$\mathbf{M}(\mathbf{k}_\parallel E;j;z)\equiv\mathbf{M}(\mathbf{g},k_{\gamma\mu}^{(j)};\mathbf{k}_\parallel E;j;z)$$

$$\equiv \begin{bmatrix} \exp(ig_z z) & 0 \\ 0 & \exp(ig_z z) \end{bmatrix} \cdot \begin{bmatrix} C^{(j)}(\mathbf{g}, k^{(j)}_{\gamma\mu}; \mathbf{k}_\parallel E) \\ (k^{(j)}_{\gamma\mu} + g_z) C^{(j)}(\mathbf{g}, k^{(j)}_{\gamma\mu}; \mathbf{k}_\parallel E) \end{bmatrix} \tag{27}$$

Thus the set of boundary equations can be written as

$$\mathbf{M}(\mathbf{k}_\parallel E; 1; 0) \cdot \mathbf{f}^{(1)}(\mathbf{q}) = \mathbf{M}(\mathbf{k}_\parallel E; 2; 0) \cdot \mathbf{f}^{(2)}(\mathbf{q}), \tag{28.a}$$

for the first set of equations, and,

$$\exp\left[i\mathbf{D}(\mathbf{q}) \cdot \mathbf{R}_0\right] \cdot \mathbf{M}(\mathbf{k}_\parallel E; 1; -b) \cdot \exp\left[-i\mathbf{D}(k^{(1)}_{\gamma\mu})b\right] \cdot \mathbf{f}^{(1)}(\mathbf{q}) =$$

$$\mathbf{M}(\mathbf{k}_\parallel E; 2; a) \cdot \exp\left[i\mathbf{D}(k^{(2)}_{\gamma\mu})a\right] \cdot \mathbf{f}^{(2)}(\mathbf{q}), \tag{28.b}$$

for the second set of equations.

The above set of equations constitues a set of two $[2N \cdot 2N]$ matrix equations to be solved for the two $[2N]$ -dimensional column vectors $\mathbf{f}^{(j)}(\mathbf{q})$ in solids $j = 1, 2$.

It is now a simple matter to express the above set as an eigensystem for the column vector $\mathbf{f}^{(1)}(\mathbf{q})$. Inverting Eq.(28.a) we find

$$\mathbf{f}^{(2)}(\mathbf{q}) = \left[\mathbf{M}(\mathbf{k}_\parallel E; 2; 0)\right]^{-1} \cdot \mathbf{M}(\mathbf{k}_\parallel E; 1; 0) \cdot \mathbf{f}^{(1)}(\mathbf{q}), \tag{29}$$

or, by defining the *transfer matrix* $\mathbf{T}(\mathbf{k}_\parallel E; z, z')$ as

$$\mathbf{T}(\mathbf{k}_\parallel E; z, z') \equiv \left[\mathbf{M}(\mathbf{k}_\parallel E; 2; z)\right]^{-1} \cdot \mathbf{M}(\mathbf{k}_\parallel E; 1; z'), \tag{30.a}$$

or, explicitly,

$$\mathbf{T}(k^{(2)}_{\gamma\mu}, k^{(1)}_{\gamma'\mu'}; \mathbf{k}_\parallel E; z, z') \equiv \sum_{\mathbf{g}} \left[\mathbf{M}(\mathbf{g}, k^{(2)}_{\gamma\mu}; \mathbf{k}_\parallel E; 2; z)\right]^{-1} \cdot \mathbf{M}(\mathbf{g}, k^{(1)}_{\gamma'\mu'}; \mathbf{k}_\parallel E; 1; z'), \tag{30.b}$$

we can write,

$$\mathbf{f}^{(2)}(\mathbf{q}) = \mathbf{T}(\mathbf{k}_\parallel E; 0, 0) \cdot \mathbf{f}^{(1)}(\mathbf{q}), \tag{32.a}$$

or more explicitly,

$$f^{(2)}(k^{(2)}_{\gamma\mu}, \mathbf{q}; \mathbf{k}_{\|}) = \sum_{\gamma'\mu'} \mathbf{T}(k^{(2)}_{\gamma\mu}, k^{(1)}_{\gamma'\mu'}; \mathbf{k}_{\|}E; 0, 0) \cdot f^{(1)}(k^{(1)}_{\gamma'\mu'}, \mathbf{q}; \mathbf{k}_{\|}). \qquad (32.b)$$

The physical meaning of the transfer matrix $\mathbf{T}(\mathbf{k}_{\|}E)$ is clear: *The transfer matrix indicates the mixing between the different Bloch states* $\{|\mathbf{k}_{\|}E; k^{(j)}_{\gamma\mu}\rangle\}$ *across the interface plane.*

Then Eq.(28.b) becomes,

$$\exp\left[i\mathbf{D}(\mathbf{q}) \cdot \mathbf{R}_0\right] \cdot \mathbf{M}(\mathbf{k}_{\|}E; 1; -b) \cdot \exp\left[-i\mathbf{D}(k^{(1)}_{\gamma\mu})b\right] \cdot \mathbf{f}^{(1)}(\mathbf{q}) =$$

$$\mathbf{M}(\mathbf{k}_{\|}E; 2; a) \cdot \exp\left[i\mathbf{D}(k^{(2)}_{\gamma\mu})a\right] \cdot \mathbf{T}(\mathbf{k}_{\|}E; 0, 0) \cdot \mathbf{f}^{(1)}(\mathbf{q}). \qquad (33)$$

By rearranging,

$$\exp\left[i\mathbf{D}(\mathbf{q}) \cdot \mathbf{R}_0\right] \cdot \mathbf{f}^{(1)}(\mathbf{q}) =$$

$$\exp\left[i\mathbf{D}(k^{(1)}_{\gamma\mu})b\right] \cdot \left[\mathbf{T}(\mathbf{k}_{\|}E; a, -b)\right]^{-1} \cdot \exp\left[i\mathbf{D}(k^{(2)}_{\gamma\mu})a\right] \cdot \mathbf{T}(\mathbf{k}_{\|}E; 0, 0) \cdot$$

$$\mathbf{f}^{(1)}(\mathbf{q}). \qquad (34)$$

Equation (34) constitutes an eigensystem for the column vector $\mathbf{f}^{(1)}(\mathbf{q})$. Diagonalization of the matrix,

$$\exp\left[i\mathbf{D}(k^{(1)}_{\gamma\mu})b\right] \cdot \left[\mathbf{T}(\mathbf{k}_{\|}E; a, -b)\right]^{-1} \cdot \exp\left[i\mathbf{D}(k^{(2)}_{\gamma\mu})a\right] \cdot \mathbf{T}(\mathbf{k}_{\|}E; 0, 0), \qquad (35)$$

yields the complex-**q** band structure of the superlattice through the matrix of Bloch factors,

$$\exp\left[i\mathbf{D}(\mathbf{q}) \cdot \mathbf{R}_0\right]. \qquad (36)$$

Once the set of coefficients $\mathbf{f}^{(1)}(\mathbf{q})$ is known in solid (1), the set of coefficients $\mathbf{f}^{(2)}(\mathbf{q})$ in solid (2), can be calculated with the use of the transfer matrix, $\mathbf{T}(\mathbf{k}_{\|}E; 0, 0)$,

$$\mathbf{f}^{(2)}(\mathbf{q}) = \mathbf{T}(\mathbf{k}_{\|}E; 0, 0) \cdot \mathbf{f}^{(1)}(\mathbf{q}). \qquad (37)$$

Reduced Transfer Matrix:

As pointed out above the *physically meaningful quantities are the expansion coefficients*

$$f^{(j)}(k_{\gamma}^{(j)}, \mathbf{q}; \mathbf{k}_{\|}) \equiv \sum_{\mu} \exp\left[i\varphi^{(j)}(\gamma, \mu)\right] f^{(j)}(k_{\gamma\mu}^{(j)}, \mathbf{q}; \mathbf{k}_{\|}), \tag{38}$$

where $\mathrm{Re}[k_{\gamma}^{(j)}]$ is in the first Brillouin zone and the sum $\sum_{\mu}$ is over the *equivalent partners belonging to the set* γ.

Equivalent Solutions: M-Matrix:

• To rewrite the above system of equations for the coefficients $f^{(j)}(k_{\gamma}^{(j)}, \mathbf{q}; \mathbf{k}_{\|})$, we must study the behavior of the *boundary conditions matrices* $\mathbf{M}(\mathbf{k}_{\|}E; j; z)$.

From the above discussion on the pseudopotential formalism, we know that if the wavevectors $k_{\gamma\mu}^{(j)}$ and $k_{\gamma\mu'}^{(j)}$ belong to the same set γ and are related through

$$\hat{\mathbf{z}}k_{\gamma\mu'}^{(j)} = \hat{\mathbf{z}}k_{\gamma\mu}^{(j)} + \hat{\mathbf{z}}g_{\mu\mu'}, \tag{39}$$

then

$$|\mathbf{k}_{\|}E; k_{\gamma\mu'}^{(j)}\rangle = \exp\left[i\varphi^{(j)}(\gamma, \mu\mu')\right] |\mathbf{k}_{\|}E; k_{\gamma\mu}^{(j)}\rangle, \tag{40}$$

where the state $|\mathbf{k}_{\|}E; k_{\gamma\mu}^{(j)}\rangle$ belongs to the eigenvalue $k_{\gamma\mu}^{(j)}$ and the state $|\mathbf{k}_{\|}E; k_{\gamma\mu'}^{(j)}\rangle$ belongs to the eigenvalue $k_{\gamma\mu'}^{(j)}$. As shown above, this is a direct consequence of the fact that,

$$C^{(j)}(\mathbf{g}, k_{\gamma\mu}^{(j)} + g_{\mu\mu'}; \mathbf{k}_{\|}E) = C^{(j)}(\mathbf{g} + \hat{\mathbf{z}}g_{\mu\mu'}, k_{\gamma\mu}^{(j)}; \mathbf{k}_{\|}E) \exp\left[i\varphi^{(j)}(\gamma, \mu\mu')\right]. \tag{41}$$

• We now examine the effect of shifting the solution by a reciprocal lattice vector $\hat{\mathbf{z}}g_{\mu\mu'}$ on the boundary conditions matrices $\mathbf{M}(\mathbf{k}_{\|}E; j; z)$. For simplicity, let us consider, the top half of the boundary condition matrices. With the above

definition, we have that

$$\mathbf{M}(\mathbf{k}_{\|}E;j;z) \equiv \mathbf{M}(\mathbf{g},k_{\gamma\mu}^{(j)};\mathbf{k}_{\|}E;j;z) \equiv \exp(ig_z z)C^{(j)}(\mathbf{g},k_{\gamma\mu}^{(j)};\mathbf{k}_{\|}E). \tag{42}$$

Let the wavevectors $k_{\gamma\mu}^{(j)}$ and $k_{\gamma\mu'}^{(j)}$, in solid j, belong to the same set γ and are related through

$$\hat{\mathbf{z}}k_{\gamma\mu'}^{(j)} = \hat{\mathbf{z}}k_{\gamma\mu}^{(j)} + \hat{\mathbf{z}}g_{\mu\mu'}. \tag{43}$$

Let us look at the quantity,

$$\mathbf{M}(\mathbf{g},k_{\gamma\mu'}^{(j)};\mathbf{k}_{\|}E;j;z)\exp(ik_{\gamma\mu'}^{(j)}z).$$

By definition,

$$\mathbf{M}(\mathbf{g},k_{\gamma\mu'}^{(j)};\mathbf{k}_{\|}E;j;z)\exp(ik_{\gamma\mu'}^{(j)}z) \equiv \exp(ig_z z)C^{(j)}(\mathbf{g},k_{\gamma\mu'}^{(j)};\mathbf{k}_{\|}E)\exp(ik_{\gamma\mu'}^{(j)}z),$$

$$\equiv \exp(ig_z z)C^{(j)}(\mathbf{g},k_{\gamma\mu}^{(j)}+g_{\mu\mu'};\mathbf{k}_{\|}E)\exp\left[i(k_{\gamma\mu}^{(j)}+g_{\mu\mu'})z\right],$$

$$\equiv \exp\left[i(g_z+g_{\mu\mu'})z\right]C^{(j)}(\mathbf{g}+\hat{\mathbf{z}}g_{\mu\mu'},k_{\gamma\mu}^{(j)};\mathbf{k}_{\|}E)\exp\left[i\varphi^{(j)}(\gamma,\mu\mu')\right].\exp(ik_{\gamma\mu}^{(j)}z),$$

and finally by making the substitution,

$$g_z \rightarrow g_z + g_{\mu\mu'},$$

we obtain

$$\mathbf{M}(\mathbf{g},k_{\gamma\mu'}^{(j)};\mathbf{k}_{\|}E;j;z)\exp(ik_{\gamma\mu'}^{(j)}z) = \exp\left[i\varphi^{(j)}(\gamma,\mu\mu')\right]\exp(ik_{\gamma\mu}^{(j)}z)\cdot$$

$$\mathbf{M}(\mathbf{g}+\hat{\mathbf{z}}g_{\mu\mu'},k_{\gamma\mu}^{(j)};\mathbf{k}_{\|}E;j;z), \tag{44}$$

We can rewrite the above expression as,

$$\mathbf{M}(\mathbf{g},k_{\gamma\mu'}^{(j)};\mathbf{k}_{\|}E;j;z) = \exp\left[i\varphi^{(j)}(\gamma,\mu\mu')\right]\exp\left[i(k_{\gamma\mu}^{(j)}-k_{\gamma\mu'}^{(j)})z\right]\cdot$$

$$\mathbf{M}(\mathbf{g} + \hat{\mathbf{z}} g_{\mu\mu'}, k^{(j)}_{\gamma\mu}; \mathbf{k}_{\|} E; j; z), \tag{45}$$

which is equivalent to

$$\mathbf{M}(\mathbf{g}, k^{(j)}_{\gamma\mu'}; \mathbf{k}_{\|} E; j; z) \equiv \exp\left[i\varphi^{(j)}(\gamma, \mu\mu')\right] \exp(-ig_{\mu\mu'} z) \cdot$$

$$\mathbf{M}(\mathbf{g} + \hat{\mathbf{z}} g_{\mu\mu'}, k^{(j)}_{\gamma\mu}; \mathbf{k}_{\|} E; j; z), \tag{46}$$

whenever

$$\hat{\mathbf{z}} k^{(j)}_{\gamma\mu'} = \hat{\mathbf{z}} k^{(j)}_{\gamma\mu} + \hat{\mathbf{z}} g_{\mu\mu'}. \tag{47}$$

A similar relation holds for the inverse of the matrix $\mathbf{M}(\mathbf{k}_{\|} E; j; z)$.

Equivalent Solutions: Transfer Matrix:

Let us now examine the effect of shifting the solutions by a reciprocal lattice vector on the transfer matrices, $\mathbf{T}(\mathbf{k}_{\|} E; z, z')$ as

$$\mathbf{T}(\mathbf{k}_{\|} E; z, z') \equiv \left[\mathbf{M}(\mathbf{k}_{\|} E; 2; z)\right]^{-1} \cdot \mathbf{M}(\mathbf{k}_{\|} E; 1; z'), \tag{48}$$

or, explicitly,

$$\mathbf{T}(k^{(2)}_{\gamma\mu}, k^{(1)}_{\gamma'\mu'}; \mathbf{k}_{\|} E; z, z') \equiv \sum_{\mathbf{g}} \left[\mathbf{M}(\mathbf{g}, k^{(2)}_{\gamma\mu}; \mathbf{k}_{\|} E; 2; z)\right]^{-1} \cdot \mathbf{M}(\mathbf{g}, k^{(1)}_{\gamma'\mu'}; \mathbf{k}_{\|} E; 1; z'), \tag{49}$$

o Let us shift $k^{(1)}_{\gamma'\mu'}$ belonging to the set γ' by a reciprocal lattice vector $g^{(1)}_{\mu'\beta}$,

$$\hat{\mathbf{z}} k^{(1)}_{\gamma'\beta} \equiv \hat{\mathbf{z}} k^{(1)}_{\gamma'\mu'} + \hat{\mathbf{z}} g^{(1)}_{\mu'\beta}. \tag{50}$$

Then, we have,

$$\mathbf{M}(\mathbf{g}, k^{(1)}_{\gamma'\beta}; \mathbf{k}_{\|} E; 1; z) \equiv \exp\left[i\varphi^{(1)}(\gamma', \mu'\beta)\right] \exp(-ig^{(1)}_{\mu'\beta} z) \cdot$$

$$\mathbf{M}(\mathbf{g} + \hat{\mathbf{z}} g^{(1)}_{\mu'\beta}, k^{(1)}_{\gamma'\mu'}; \mathbf{k}_{\|} E; 1; z).$$

o Let us shift $k^{(2)}_{\gamma\mu}$ belonging to the set γ by a reciprocal lattice vector $g^{(2)}_{\mu\alpha}$,

$$\hat{\mathbf{z}}k^{(2)}_{\gamma\alpha} \equiv \hat{\mathbf{z}}k^{(2)}_{\gamma\mu} + \hat{\mathbf{z}}g^{(2)}_{\mu\alpha}. \tag{51}$$

Then, we have,

$$\mathbf{M}(\mathbf{g}, k^{(2)}_{\gamma\alpha}; \mathbf{k}_{\|}E; 2; z) \equiv \exp\left[i\varphi^{(2)}(\gamma, \mu\alpha)\right] \exp(-ig^{(2)}_{\mu\alpha}z) \cdot$$

$$\mathbf{M}(\mathbf{g} + \hat{\mathbf{z}}g^{(2)}_{\mu\alpha}, k^{(2)}_{\gamma\mu}; \mathbf{k}_{\|}E; 2; z).$$

Let us now express the quantity

$$\exp(-ik^{(2)}_{\gamma\alpha}z) \cdot \mathbf{T}(k^{(2)}_{\gamma\alpha}, k^{(1)}_{\gamma'\beta}; \mathbf{k}_{\|}E; z, z') \cdot \exp(ik^{(1)}_{\gamma'\beta}z'), \tag{52}$$

that relates the states $k^{(2)}_{\gamma\alpha}$ and $k^{(1)}_{\gamma'\beta}$, in terms of the quantity

$$\exp(-ik^{(2)}_{\gamma\mu}z) \cdot \mathbf{T}(k^{(2)}_{\gamma\mu}, k^{(1)}_{\gamma'\mu'}; \mathbf{k}_{\|}E; z, z') \cdot \exp(ik^{(1)}_{\gamma'\mu'}z'), \tag{53}$$

that relates the states $k^{(2)}_{\gamma\mu}$ and $k^{(1)}_{\gamma'\mu'}$.

We have

$$\exp(-ik^{(2)}_{\gamma\alpha}z) \cdot \mathbf{T}(k^{(2)}_{\gamma\alpha}, k^{(1)}_{\gamma'\beta}; \mathbf{k}_{\|}E; z, z') \cdot \exp(ik^{(1)}_{\gamma'\beta}z') \equiv$$

$$\exp\left[-i\left(k^{(2)}_{\gamma\mu} + g^{(2)}_{\gamma\alpha}\right)z\right] \cdot$$

$$\sum_{\mathbf{g}}\left[\mathbf{M}(\mathbf{g}, k^{(2)}_{\gamma\alpha}; \mathbf{k}_{\|}E; 2; z)\right]^{-1} \cdot \mathbf{M}(\mathbf{g}, k^{(1)}_{\gamma'\beta}; \mathbf{k}_{\|}E; 1; z') \cdot$$

$$\exp\left[i\left(k^{(1)}_{\gamma'\mu'} + g^{(1)}_{\gamma'\beta}\right)z'\right], \tag{54.a}$$

or, by using the shifting properties of the matrices $\mathbf{M}(\mathbf{g}, k^{(2)}_{\gamma\alpha}; \mathbf{k}_{\|}E; 2; z)$, and $\mathbf{M}(\mathbf{g}, k^{(1)}_{\gamma'\beta}; \mathbf{k}_{\|}E; 1; z')$, we have,

$$\exp(-ik^{(2)}_{\gamma\alpha}z) \cdot \mathbf{T}(k^{(2)}_{\gamma\alpha}, k^{(1)}_{\gamma'\beta}; \mathbf{k}_{\|}E; z, z') \cdot \exp(ik^{(1)}_{\gamma'\beta}z') \equiv$$

$$\exp(-ik^{(2)}_{\gamma\mu}z)\cdot$$

$$\exp\left[i\left(\varphi^{(1)}(\gamma',\mu'\beta)-\varphi^{(2)}(\gamma,\mu\alpha)\right)\right]\cdot$$

$$\exp\left[i\left(g^{(1)}_{\mu'\beta}z'-g^{(2)}_{\mu\alpha}z\right)\right]\cdot\exp\left[-i\left(g^{(1)}_{\mu'\beta}z'-g^{(2)}_{\mu\alpha}z\right)\right]\cdot$$

$$\sum_{\mathbf{g}}\left[\mathbf{M}(\mathbf{g}+\hat{\mathbf{z}}g^{(2)}_{\mu\alpha},k^{(2)}_{\gamma\mu};\mathbf{k}_{\|}E;2;z)\right]^{-1}\cdot\mathbf{M}(\mathbf{g}+\hat{\mathbf{z}}g^{(1)}_{\mu'\beta},k^{(1)}_{\gamma'\mu'};\mathbf{k}_{\|}E;1;z')\cdot$$

$$\exp(ik^{(1)}_{\gamma'\mu'}z'). \tag{54.b}$$

We must take the case whereby,

$$g^{(1)}_{\mu'\beta}\equiv g^{(2)}_{\mu\alpha}$$

in order for the definition

$$\mathbf{T}(k^{(2)}_{\gamma\mu},k^{(1)}_{\gamma'\mu'};\mathbf{k}_{\|}E;z,z')\equiv\sum_{\mathbf{g}}\left[\mathbf{M}(\mathbf{g},k^{(2)}_{\gamma\mu};\mathbf{k}_{\|}E;2;z)\right]^{-1}\cdot\mathbf{M}(\mathbf{g},k^{(1)}_{\gamma'\mu'};\mathbf{k}_{\|}E;1;z'), \tag{55}$$

to be valid. That is *the two wavevectors must be shifted by the same reciprocal lattice vector.*

Let us consider the following case whereby *one solution is brought within the first Brillouin zone but not necessarily the other.*

Let $g_{\mu'}$ be the reciprocal lattice vector that brings $k^{(1)}_{\gamma'\mu'}$ back into the first Brillouin zone. Then we have,

$$\hat{\mathbf{z}}k^{(1)}_{\gamma'}=\hat{\mathbf{z}}k^{(1)}_{\gamma'\mu'}+\hat{\mathbf{z}}g_{\mu'}, \tag{56}$$

and

$$\hat{\mathbf{z}}k^{(2)}_{\gamma\mu'}=\hat{\mathbf{z}}k^{(2)}_{\gamma\mu}+\hat{\mathbf{z}}g_{\mu'}, \tag{57}$$

where $Re\left[k^{(1)}_{\gamma'}\right]$ *lies inside the first Brillouin zone, but* $Re\left[k^{(2)}_{\gamma\mu'}\right]$ *does not necessarily.*

We then have, by summing over the partners μ' corresponding to the solutions $k^{(1)}_{\gamma'\mu'}$,

$$\exp(-ik^{(2)}_{\gamma\mu'}z)\cdot\mathbf{T}(k^{(2)}_{\gamma\mu'},k^{(1)}_{\gamma'};\mathbf{k}_{\|}E;z,z')\cdot\exp(ik^{(1)}_{\gamma'}z')\equiv$$

$$\sum_{\mu'}\exp(-ik^{(2)}_{\gamma\mu}z)\cdot\exp\left[i\left(\varphi^{(1)}(\gamma',\mu')-\varphi^{(2)}(\gamma,\mu\mu')\right)\right]\cdot$$

$$\sum_{\mathbf{g}}\left[\mathbf{M}(\mathbf{g}+\hat{\mathbf{z}}g_{\mu'},k^{(2)}_{\gamma\mu};\mathbf{k}_{\|}E;2;z)\right]^{-1}\cdot\mathbf{M}(\mathbf{g}+\hat{\mathbf{z}}g_{\mu'},k^{(1)}_{\gamma'\mu'};\mathbf{k}_{\|}E;1;z')\cdot$$

$$\exp(ik^{(1)}_{\gamma'\mu'}z'), \tag{58}$$

or, equivalently,

$$\exp(-ik^{(2)}_{\gamma\mu'}z)\cdot\mathbf{T}(k^{(2)}_{\gamma\mu'},k^{(1)}_{\gamma'};\mathbf{k}_{\|}E;z,z')\cdot\exp(ik^{(1)}_{\gamma'}z')\equiv$$

$$\sum_{\mu'}\exp(-ik^{(2)}_{\gamma\mu}z)\cdot\exp\left[-i\varphi^{(2)}(\gamma,\mu\mu')\right]\cdot$$

$$\mathbf{T}(k^{(2)}_{\gamma\mu},k^{(1)}_{\gamma'\mu'};\mathbf{k}_{\|}E;z,z')\cdot$$

$$\exp\left[i\varphi^{(1)}(\gamma',\mu')\right]\cdot\exp(ik^{(1)}_{\gamma'\mu'}z'), \tag{59}$$

where the *non-reduced transfer matrix* is

$$\mathbf{T}(k^{(2)}_{\gamma\mu},k^{(1)}_{\gamma'\mu'};\mathbf{k}_{\|}E;z,z')\equiv\sum_{\mathbf{g}}\left[\mathbf{M}(\mathbf{g},k^{(2)}_{\gamma\mu};\mathbf{k}_{\|}E;2;z)\right]^{-1}\cdot\mathbf{M}(\mathbf{g},k^{(1)}_{\gamma'\mu'};\mathbf{k}_{\|}E;1;z'), \tag{60}$$

and couples all the partners $k^{(1)}_{\gamma'\mu'}$ and $k^{(2)}_{\gamma\mu}$ of the non-equivalent sets γ and γ'.

The phase factor

$$\exp\left[i\varphi^{(1)}(\gamma',\mu')\right]$$

relates the solutions $k_{\gamma'}^{(1)}$ and $k_{\gamma'\mu'}^{(1)}$, and the phase factor

$$\exp\left[i\varphi^{(2)}(\gamma, \mu\mu')\right]$$

relates the solutions $k_{\gamma\mu'}^{(2)}$ and $k_{\gamma\mu}^{(2)}$.

We now define the *semi-reduced transfer matrix* by,

$$\mathbf{T}(k_{\gamma\mu'}^{(2)}, k_{\gamma'}^{(1)}; \mathbf{k}_\parallel E; z, z') \equiv \sum_{\mathbf{g}} \left[\mathbf{M}(\mathbf{g}, k_{\gamma\mu'}^{(2)}; \mathbf{k}_\parallel E; 2; z)\right]^{-1} \cdot \mathbf{M}(\mathbf{g}, k_{\gamma'}^{(1)}; \mathbf{k}_\parallel E; 1; z'), \tag{61}$$

where $k_{\gamma'}^{(1)}$ lies within the first Brillouin zone but $k_{\gamma\mu'}^{(2)}$ does not.

In the above expression *the wavevector $k_{\gamma'}^{(1)}$ has been brought inside the first Brillouin zone by $g_{\mu'}$, but not the wavevector $k_{\gamma\mu'}^{(2)}$*. We must now bring the wavevector $k_{\gamma\mu'}^{(2)}$ back inside the first Brillouin zone. Let g_μ the reciprocal lattice vector that brings the wavevector $k_{\gamma\mu'}^{(2)}$ back inside the first Brillouin zone,

$$\hat{\mathbf{z}} k_\gamma^{(2)} = \hat{\mathbf{z}} k_{\gamma\mu'}^{(2)} + \hat{\mathbf{z}} g_{\mu'}, \tag{62}$$

where now $\mathrm{Re}\left[k_\gamma^{(2)}\right]$ lies inside the first Brillouin zone.

Let us write

$$\varphi^{(2)}(\gamma, \mu\mu') = \varphi^{(2)}(\gamma, \mu) - \varphi^{(2)}(\gamma, \mu'), \tag{63}$$

where

- $\varphi^{(2)}(\gamma, \mu)$ is the phase that brings $k_{\gamma\mu}^{(2)}$ into $k_\gamma^{(2)}$, and
- $\varphi^{(2)}(\gamma, \mu')$ is the phase that brings $k_{\gamma\mu'}^{(2)}$ into $k_\gamma^{(2)}$.

We then have

$$\exp\left[-i(k_\gamma^{(2)} - g_{\mu'})z\right] \cdot \mathbf{T}(k_{\gamma\mu'}^{(2)}, k_{\gamma'}^{(1)}; \mathbf{k}_\parallel E; z, z') \cdot \exp(ik_{\gamma'}^{(1)} z') \equiv$$

$$\sum_{\mu'} \exp(-ik_{\gamma\mu}^{(2)} z) \cdot \exp\left[-i\varphi^{(2)}(\gamma, \mu)\right] \cdot \exp\left[i\varphi^{(2)}(\gamma, \mu')\right] \cdot$$

$$\mathbf{T}(k^{(2)}_{\gamma\mu}, k^{(1)}_{\gamma'\mu'}; \mathbf{k}_{\|} E; z, z') \cdot$$

$$\exp\left[i\varphi^{(1)}(\gamma', \mu')\right] \cdot \exp(ik^{(1)}_{\gamma'\mu'} z'), \tag{64}$$

or,

$$\exp(-ik^{(2)}_{\gamma} z) \cdot$$

$$\left[\exp(-ig_{\mu'} z) \exp\left[-i\varphi^{(2)}(\gamma, \mu')\right] \mathbf{T}(k^{(2)}_{\gamma\mu'}, k^{(1)}_{\gamma'}; \mathbf{k}_{\|} E; z, z')\right]$$

$$\exp(ik^{(1)}_{\gamma'} z') \equiv$$

$$\sum_{\mu'} \exp(-ik^{(2)}_{\gamma\mu} z) \cdot \exp\left[-i\varphi^{(2)}(\gamma, \mu)\right] \cdot$$

$$\mathbf{T}(k^{(2)}_{\gamma\mu}, k^{(1)}_{\gamma'\mu'}; \mathbf{k}_{\|} E; z, z') \cdot$$

$$\exp\left[i\varphi^{(1)}(\gamma', \mu')\right] \cdot \exp(ik^{(1)}_{\gamma'\mu'} z'), \tag{65}$$

• Finally, by summing over the partners μ' corresponding to the set of eigenvalues $k^{(2)}_{\gamma\mu'}$, we obtain,

$$\exp(-ik^{(2)}_{\gamma} z) \cdot$$

$$\left[\sum_{\mu'} \exp(-ig_{\mu'} z) \exp\left[i\varphi^{(2)}(\gamma, \mu')\right] \mathbf{T}(k^{(2)}_{\gamma\mu'}, k^{(1)}_{\gamma'}; \mathbf{k}_{\|} E; z, z')\right]$$

$$\exp(ik^{(1)}_{\gamma'} z') \equiv$$

$$\sum_{\mu\mu'} \exp(-ik^{(2)}_{\gamma\mu} z) \cdot \exp\left[-i\varphi^{(2)}(\gamma, \mu)\right] \cdot$$

$$\mathbf{T}(k^{(2)}_{\gamma\mu}, k^{(1)}_{\gamma'\mu'}; \mathbf{k}_{\|} E; z, z') \cdot$$

$$\exp\left[i\varphi^{(1)}(\gamma', \mu')\right] \cdot \exp(ik^{(1)}_{\gamma'\mu'} z'). \tag{66}$$

Reduced Eigensystem and Transfer matrix:

We now define the *reduced transfer matrix* as the sum over all the partners μ and μ',

$$\Omega(k_{\gamma}^{(2)}, k_{\gamma'}^{(1)}; \mathbf{k}_{\|} E; z, z') \equiv$$

$$\sum_{\mu'} \exp(-ig_{\mu'} z) \exp\left[i\varphi^{(2)}(\gamma, \mu')\right] \mathbf{T}(k_{\gamma\mu'}^{(2)}, k_{\gamma'}^{(1)}; \mathbf{k}_{\|} E; z, z'), \tag{67}$$

where the *semi-reduced transfer matrix* is defined by,

$$\mathbf{T}(k_{\gamma\mu'}^{(2)}, k_{\gamma'}^{(1)}; \mathbf{k}_{\|} E; z, z') \equiv$$

$$\sum_{\mathbf{g}} \left[\mathbf{M}(\mathbf{g}, k_{\gamma\mu'}^{(2)}; \mathbf{k}_{\|} E; 2; z)\right]^{-1} \cdot \mathbf{M}(\mathbf{g}, k_{\gamma'}^{(1)}; \mathbf{k}_{\|} E; 1; z'),$$

where $k_{\gamma'}^{(1)}$ lies within the first Brillouin zone but $k_{\gamma\mu'}^{(2)}$ does not.

Then we arrive at the final relation, *involving only solutions* $k_{\gamma'}^{(1)}$ *and* $k_{\gamma}^{(2)}$ *lying within the first Brillouin zone,*

$$\exp(-ik_{\gamma}^{(2)} z) \cdot \Omega(k_{\gamma}^{(2)}, k_{\gamma'}^{(1)}; \mathbf{k}_{\|} E; z, z') \cdot \exp(ik_{\gamma'}^{(1)} z') \equiv$$

$$\sum_{\mu\mu'} \exp(-ik_{\gamma\mu}^{(2)} z) \cdot \exp\left[-i\varphi^{(2)}(\gamma, \mu)\right] \cdot$$

$$\mathbf{T}(k_{\gamma\mu}^{(2)}, k_{\gamma'\mu'}^{(1)}; \mathbf{k}_{\|} E; z, z') \cdot$$

$$\exp\left[i\varphi^{(1)}(\gamma', \mu')\right] \cdot \exp(ik_{\gamma'\mu'}^{(1)} z'), \tag{68}$$

where the *non-reduced transfer matrix* is

$$\mathbf{T}(k_{\gamma\mu}^{(2)}, k_{\gamma'\mu'}^{(1)}; \mathbf{k}_{\|} E; z, z') \equiv \sum_{\mathbf{g}} \left[\mathbf{M}(\mathbf{g}, k_{\gamma\mu}^{(2)}; \mathbf{k}_{\|} E; 2; z)\right]^{-1} \cdot \mathbf{M}(\mathbf{g}, k_{\gamma'\mu'}^{(1)}; \mathbf{k}_{\|} E; 1; z'), \tag{69}$$

and couples all the partners $k_{\gamma'\mu'}^{(1)}$ and $k_{\gamma\mu}^{(2)}$ of the non-equivalent sets γ and γ'.

The reduced transfer matrix

$$\Omega(k_{\gamma}^{(2)}, k_{\gamma'}^{(1)}; \mathbf{k}_{\|} E; z, z')$$

relates the states $k_{\gamma}^{(2)}$ and $k_{\gamma'}^{(1)}$ where *both* $Re\left[k_{\gamma'}^{(1)}\right]$ *and* $Re\left[k_{\gamma}^{(2)}\right]$ *lie inside the first Brillouin zone.*

Reduced Eigensystem and Transfer matrix:

We now obtain the *reduced eigensystem for the non-equivalent solutions,*

$$f^{(j)}(k_\gamma^{(j)}, \mathbf{q}; \mathbf{k}_\parallel) \equiv \sum_\mu \exp\left[i\varphi^{(j)}(\gamma, \mu)\right] f^{(j)}(k_{\gamma\mu}^{(j)}, \mathbf{q}; \mathbf{k}_\parallel), \tag{70}$$

where $\mathrm{Re}\left[k_\gamma^{(j)}\right]$ is in the first Brillouin zone and the sum $\sum_\mu$ is over the *equivalent partners belonging to the set* γ.

First Equation:

Let us now consider the first equation involving $\mathbf{T}(\mathbf{k}_\parallel E; 0, 0)$,

$$\mathbf{f}^{(2)}(\mathbf{q}) = \mathbf{T}(\mathbf{k}_\parallel E; 0, 0) \cdot \mathbf{f}^{(1)}(\mathbf{q}), \tag{71.a}$$

or more explicitly,

$$f^{(2)}(k_{\gamma\mu}^{(2)}, \mathbf{q}; \mathbf{k}_\parallel) = \sum_{\gamma'\mu'} \mathbf{T}(k_{\gamma\mu}^{(2)}, k_{\gamma'\mu'}^{(1)}; \mathbf{k}_\parallel E; 0, 0) \cdot f^{(1)}(k_{\gamma'\mu'}^{(1)}, \mathbf{q}; \mathbf{k}_\parallel). \tag{71.b}$$

We want to transform this equation in an equation for the amplitudes

$$f^{(1)}(k_{\gamma'}^{(1)}, \mathbf{q}; \mathbf{k}_\parallel) \equiv \sum_{\mu'} \exp\left[i\varphi^{(1)}(\gamma', \mu')\right] \cdot f^{(1)}(k_{\gamma'\mu'}^{(1)}, \mathbf{q}; \mathbf{k}_\parallel), \tag{72.a}$$

and,

$$f^{(2)}(k_\gamma^{(2)}, \mathbf{q}; \mathbf{k}_\parallel) \equiv \sum_\mu \exp\left[i\varphi^{(2)}(\gamma, \mu)\right] \cdot f^{(2)}(k_{\gamma\mu}^{(2)}, \mathbf{q}; \mathbf{k}_\parallel), \tag{72.b}$$

where $\mathrm{Re}\left[k_\gamma^{(j)}\right]$ lies inside the first Brillouin zone for $j = 1, 2$.

Let us insert

$$\sum_\mu \exp\left[i\varphi^{(2)}(\gamma, \mu)\right]$$

on both sides of the equality,

$$\sum_{\mu} \exp\left[i\varphi^{(2)}(\gamma,\mu)\right] f^{(2)}(k^{(2)}_{\gamma\mu}, \mathbf{q}; \mathbf{k}_{\|}) =$$

$$\sum_{\mu} \exp\left[i\varphi^{(2)}(\gamma,\mu)\right] \sum_{\gamma'\mu'} \mathbf{T}(k^{(2)}_{\gamma\mu}, k^{(1)}_{\gamma'\mu'}; \mathbf{k}_{\|}E; 0, 0) \cdot f^{(1)}(k^{(1)}_{\gamma'\mu'}, \mathbf{q}; \mathbf{k}_{\|}). \tag{73}$$

Let us insert a factor

$$\exp\left[i\varphi^{(1)}(\gamma',\mu')\right] \exp\left[-i\varphi^{(1)}(\gamma',\mu')\right] \equiv 1, \tag{74}$$

on the right side of the equation to obtain,

$$\sum_{\mu} \exp\left[i\varphi^{(2)}(\gamma,\mu)\right] f^{(2)}(k^{(2)}_{\gamma\mu}, \mathbf{q}; \mathbf{k}_{\|}) =$$

$$\sum_{\gamma'\mu'} \cdot \left[\sum_{\mu} \exp\left[i\varphi^{(2)}(\gamma,\mu)\right] \mathbf{T}(k^{(2)}_{\gamma\mu}, k^{(1)}_{\gamma'\mu'}; \mathbf{k}_{\|}E; 0, 0) \exp\left[-i\varphi^{(1)}(\gamma',\mu')\right]\right] \cdot$$

$$\left[\sum_{\mu'} \exp\left[i\varphi^{(1)}(\gamma',\mu')\right] \cdot f^{(1)}(k^{(1)}_{\gamma'\mu'}, \mathbf{q}; \mathbf{k}_{\|})\right]. \tag{75}$$

Let us now define

$$f^{(1)}(k^{(1)}_{\gamma'}, \mathbf{q}; \mathbf{k}_{\|}) \equiv \sum_{\mu'} \exp\left[i\varphi^{(1)}(\gamma',\mu')\right] \cdot f^{(1)}(k^{(1)}_{\gamma'\mu'}, \mathbf{q}; \mathbf{k}_{\|}), \tag{76.a}$$

and,

$$f^{(2)}(k^{(2)}_{\gamma}, \mathbf{q}; \mathbf{k}_{\|}) \equiv \sum_{\mu} \exp\left[i\varphi^{(2)}(\gamma,\mu)\right] \cdot f^{(2)}(k^{(2)}_{\gamma\mu}, \mathbf{q}; \mathbf{k}_{\|}), \tag{76.b}$$

where $\mathrm{Re}\left[k^{(j)}_{\gamma}\right]$ lies inside the first Brillouin zone for $j = 1, 2$.

In this case the *reduced transfer matrix* is simply given by

$$\Omega(k^{(2)}_{\gamma}, k^{(1)}_{\gamma'}; \mathbf{k}_{\|}E; 0, 0) \equiv$$

$$= \sum_{\mu\mu'} \exp\left[-i\varphi^{(2)}(\gamma,\mu)\right] \cdot \mathbf{T}(k^{(2)}_{\gamma\mu}, k^{(1)}_{\gamma'\mu'}; \mathbf{k}_{\|}E; 0, 0) \cdot \exp\left[i\varphi^{(1)}(\gamma',\mu')\right] \qquad (77)$$

We then obtain,

$$f^{(2)}(k^{(2)}_{\gamma}, \mathbf{q}; \mathbf{k}_{\|}) = \sum_{\gamma'} \Omega(k^{(2)}_{\gamma}, k^{(1)}_{\gamma'}; \mathbf{k}_{\|}E; 0, 0) \cdot f^{(1)}(k^{(1)}_{\gamma'}, \mathbf{q}; \mathbf{k}_{\|}). \qquad (78)$$

Second Equation:

We now look at the equation involving the transfer matrix $\mathbf{T}(\mathbf{k}_{\|}E; a, -b)$,

$$\exp[i\mathbf{D}(\mathbf{q}) \cdot \mathbf{R}_0] \cdot$$

$$\exp\left[-i\mathbf{D}(k^{(2)}_{\gamma\mu})a\right] \cdot \left[\mathbf{T}(\mathbf{k}_{\|}E; a, -b)\right]^{-1} \cdot \exp\left[-i\mathbf{D}(k^{(1)}_{\gamma\mu})b\right] \cdot$$

$$\mathbf{f}^{(1)}(\mathbf{q}) = \mathbf{f}^{(2)}(\mathbf{q}), \qquad (79)$$

or, more explicitly,

$$\exp[i\mathbf{D}(\mathbf{q}) \cdot \mathbf{R}_0] \cdot$$

$$\sum_{\gamma'\mu'} \exp(-ik^{(2)}_{\gamma\mu}a) \cdot \left[\mathbf{T}(k^{(2)}_{\gamma\mu}, k^{(1)}_{\gamma'\mu'}; \mathbf{k}_{\|}E; a, -b)\right]^{-1} \cdot \exp(-ik^{(1)}_{\gamma'\mu'}b) \cdot$$

$$f^{(1)}(k^{(1)}_{\gamma'\mu'}, \mathbf{q}; \mathbf{k}_{\|}) = f^{(2)}(k^{(2)}_{\gamma\mu}, \mathbf{q}; \mathbf{k}_{\|}). \qquad (80)$$

Again, we want to solve for the amplitudes

$$f^{(1)}(k^{(1)}_{\gamma'}, \mathbf{q}; \mathbf{k}_{\|}) \equiv \sum_{\mu'} \exp\left[i\varphi^{(1)}(\gamma',\mu')\right] \cdot f^{(1)}(k^{(1)}_{\gamma'\mu'}, \mathbf{q}; \mathbf{k}_{\|}), \qquad (81.a)$$

and,

$$f^{(2)}(k^{(2)}_{\gamma}, \mathbf{q}; \mathbf{k}_{\|}) \equiv \sum_{\mu} \exp\left[i\varphi^{(2)}(\gamma,\mu)\right] \cdot f^{(2)}(k^{(2)}_{\gamma\mu}, \mathbf{q}; \mathbf{k}_{\|}), \qquad (81.b)$$

where $\mathrm{Re}\left[k^{(j)}_{\gamma}\right]$ lies inside the first Brillouin zone for $j = 1, 2$.

Let us insert

$$\sum_{\mu} \exp\left[i\varphi^{(2)}(\gamma, \mu)\right]$$

on both sides of the equality to get,

$$\exp\left[i\mathbf{D}(\mathbf{q}) \cdot \mathbf{R}_0\right] \cdot \sum_{\mu} \exp\left[i\varphi^{(2)}(\gamma, \mu)\right]$$

$$\sum_{\gamma'\mu'} \exp(-ik^{(2)}_{\gamma\mu} a) \cdot \left[\mathbf{T}(k^{(2)}_{\gamma\mu}, k^{(1)}_{\gamma'\mu'}; \mathbf{k}_{\|} E; a, -b)\right]^{-1} \cdot \exp(-ik^{(1)}_{\gamma'\mu'} b) \cdot$$

$$f^{(1)}(k^{(1)}_{\gamma'\mu'}, \mathbf{q}; \mathbf{k}_{\|}) =$$

$$\sum_{\mu} \exp\left[i\varphi^{(2)}(\gamma, \mu)\right] f^{(2)}(k^{(2)}_{\gamma\mu}, \mathbf{q}; \mathbf{k}_{\|}). \tag{82}$$

In that case the *reduced transfer matrix* is

$$\Omega(k^{(2)}_{\gamma}, k^{(1)}_{\gamma'}; \mathbf{k}_{\|} E; a, -b) \equiv$$

$$= \sum_{\mu} \exp\left[-i\varphi^{(2)}(\gamma, \mu)\right] \cdot \exp(-ig_{\mu} a) \cdot \mathbf{T}(k^{(2)}_{\gamma\mu}, k^{(1)}_{\gamma'}; \mathbf{k}_{\|} E; a, -b), \tag{83}$$

where the *semi-reduced transfer matrix* is defined as above,

$$\mathbf{T}(k^{(2)}_{\gamma\mu}, k^{(1)}_{\gamma'}; \mathbf{k}_{\|} E; a, -b) \equiv \sum_{\mathbf{g}} \left[\mathbf{M}(\mathbf{g}, k^{(2)}_{\gamma\mu}; \mathbf{k}_{\|} E; 2; a)\right]^{-1} \cdot \mathbf{M}(\mathbf{g}, k^{(1)}_{\gamma'}; \mathbf{k}_{\|} E; 1; -b),$$

where $k^{(1)}_{\gamma'}$ lies within the first Brillouin zone but $k^{(2)}_{\gamma\mu}$ does not.

We then obtain the following equations

$$\exp\left[i\mathbf{D}(\mathbf{q}) \cdot \mathbf{R}_0\right] \cdot \sum_{\gamma'} \exp(-ik^{(2)}_{\gamma} a) \cdot \left[\Omega(k^{(2)}_{\gamma}, k^{(1)}_{\gamma'}; \mathbf{k}_{\|} E; a, -b)\right]^{-1} \cdot$$

$$\exp(-ik^{(1)}_{\gamma'} b) \cdot f^{(1)}(k^{(1)}_{\gamma'}, \mathbf{q}; \mathbf{k}_{\|}) = f^{(2)}(k^{(2)}_{\gamma}, \mathbf{q}; \mathbf{k}_{\|}). \tag{84}$$

Reduced Eigensystem:

By combining the two sets of equations, we obtain the *reduced eigensystem*

$$f^{(2)}(k_\gamma^{(2)}, \mathbf{q}; \mathbf{k}_\parallel) = \sum_{\gamma'} \Omega(k_\gamma^{(2)}, k_{\gamma'}^{(1)}; \mathbf{k}_\parallel E; 0, 0) \cdot f^{(1)}(k_{\gamma'}^{(1)}, \mathbf{q}; \mathbf{k}_\parallel). \tag{85.a}$$

and,

$$f^{(2)}(k_\gamma^{(2)}, \mathbf{q}; \mathbf{k}_\parallel) = \exp\left[i\mathbf{D}(\mathbf{q}) \cdot \mathbf{R}_0\right] \cdot$$

$$\sum_{\gamma'} \exp(-ik_\gamma^{(2)} a) \cdot \left[\Omega(k_\gamma^{(2)}, k_{\gamma'}^{(1)}; \mathbf{k}_\parallel E; a, -b)\right]^{-1} \cdot$$

$$\exp(-ik_{\gamma'}^{(1)} b) \cdot f^{(1)}(k_{\gamma'}^{(1)}, \mathbf{q}; \mathbf{k}_\parallel). \tag{85.b}$$

for the expansion amplitudes

$$f^{(1)}(k_{\gamma'}^{(1)}, \mathbf{q}; \mathbf{k}_\parallel) \equiv \sum_{\mu'} \exp\left[i\varphi^{(1)}(\gamma', \mu')\right] \cdot f^{(1)}(k_{\gamma'\mu'}^{(1)}, \mathbf{q}; \mathbf{k}_\parallel), \tag{86.a}$$

and,

$$f^{(2)}(k_\gamma^{(2)}, \mathbf{q}; \mathbf{k}_\parallel) \equiv \sum_{\mu} \exp\left[i\varphi^{(2)}(\gamma, \mu)\right] \cdot f^{(2)}(k_{\gamma\mu}^{(2)}, \mathbf{q}; \mathbf{k}_\parallel), \tag{86.b}$$

where $\mathrm{Re}\left[k_\gamma^{(j)}\right]$ lies inside the first Brillouin zone for $j = 1, 2$.

References:

1. M. Lax, *Symmetry Principles in Solid-State and Molecular Physics*, (Wiley-Interscience Publication, New York ,1974) p. 210.

APPENDIX 4.6

k · p Formalism for Equivalent States:

In this appendix, we indicate how to obtain the *reduced transfer matrix*,

$$\Omega(k_\gamma^{(2)}, k_{\gamma'}^{(1)}; \mathbf{k}_\parallel E; z, z'),$$

for *non-equivalent* Bloch solutions $\{|\mathbf{k}_\parallel E; k_\gamma^{(j)}\rangle\}$ where the wavevector $k_\gamma^{(j)}$ is in the first Brillouin zone of the solid $j = 1, 2$.

• To do so, we must include the contribution from *equivalent* Bloch states, *i.e.*, Bloch states whose wavevectors $k_{\gamma\mu}^{(j)}$ are apart from a reciprocal lattice vector in the $\hat{\mathbf{z}}$ direction. This is most easily done by considering the *pseudopotential formalism*.

Here again, we adopt the convention that the eigenvalue $k_\gamma^{(j)}$ *has its real part within the first Brillouin zone*, in solid $j = 1, 2$. That is, $\mathrm{Re}[k_\gamma^{(j)}]$ lies inside the first Brillouin zone. We label the equivalent partner solutions of $k_\gamma^{(j)}$ by $k_{\gamma\mu}^{(j)}$. Then we have

$$|\mathbf{k}_\parallel E; k_{\gamma\mu}^{(j)}\rangle = \exp\left[i\varphi^{(j)}(\gamma, \mu)\right]|\mathbf{k}_\parallel E; k_\gamma^{(j)}\rangle, \tag{1}$$

where the state $|\mathbf{k}_\parallel E; k_\gamma^{(j)}\rangle$ belongs to the eigenvalue $k_\gamma^{(j)}$ within the first Brillouin zone and the state $|\mathbf{k}_\parallel E; k_{\gamma\mu}^{(j)}\rangle$ belongs to the eigenvalue $k_{\gamma\mu}^{(j)}$. The phase $\exp\left[i\varphi^{(j)}(\gamma, \mu)\right]$ relates a Bloch solution outside the first Brillouin, $|\mathbf{k}_\parallel E; k_{\gamma\mu}^{(j)}\rangle$, to a solution inside the first Brillouin zone $|\mathbf{k}_\parallel E; k_\gamma^{(j)}\rangle$. The wavevectors $k_\gamma^{(j)}$ and $k_{\gamma\mu}^{(j)}$ belong to the same set γ and are related through

$$\hat{\mathbf{z}}k_{\gamma\mu}^{(j)} = \hat{\mathbf{z}}k_\gamma^{(j)} + \hat{\mathbf{z}}g_\mu, \tag{2}$$

and $\mathrm{Re}[k_\gamma^{(j)}]$ lies inside the first Brillouin zone.

4.6.1 Pseudopotentials and k · p Approaches:

The set of $\mathbf{k}_0 = \mathbf{0}$ states, $\{|m\rangle\}$ is related to the set of plane waves $\{|\mathbf{g}\rangle\}$, where $\mathbf{g}$ is a reciprocal lattice vector, by

$$|m\rangle = \sum_{\mathbf{g}} |\mathbf{g}\rangle U(\mathbf{g}, m). \tag{3}$$

In the $\mathbf{x}$-representation, we have explicitly

$$\langle \mathbf{x}|m\rangle \equiv u_m(\mathbf{x}), \tag{4.a}$$

for the $\mathbf{k}_0 = \mathbf{0}$ basis functions, and

$$\langle \mathbf{x}|\mathbf{g}\rangle \equiv \exp(i\mathbf{g}\cdot\mathbf{x}), \tag{4.b}$$

for the plane waves.

The matrix $\mathbf{U}$ is the *eigenvector matrix that diagonalizes the pseudopotential Hamiltonian of the reference solid,*

$$\hat{H}^{(0)}(\mathbf{g}\mathbf{g}';\mathbf{k}) = \frac{\hbar^2}{2m}[\mathbf{k}+\mathbf{g}]^2\delta^3(\mathbf{g}-\mathbf{g}') + V^{(0)}(\mathbf{g}\mathbf{g}'), \tag{5}$$

at $\mathbf{k} = \mathbf{0}$. The off-diagonal matrix elements $V(\mathbf{g}\mathbf{g}')$ are the *pseudopotentials form factors.*

For a complete set $\{|m\rangle\}$ we have the *closure relation*

$$\sum_m |m\rangle\langle m| = \mathbf{1}, \tag{6.a}$$

which, in the $\{|\mathbf{g}\rangle\}$, translates into

$$\sum_m U(\mathbf{g}, m)\cdot\left[U(\mathbf{g}', m)\right]^\dagger = \delta^3(\mathbf{g}-\mathbf{g}'). \tag{6.b}$$

With this transformation, we can expand the Bloch solutions $\{|\mathbf{k}_{\|}E; k_{\gamma\mu}^{(j)}\rangle\}$ as

$$|\mathbf{k}_{\|}E; k_{\gamma\mu}^{(j)}\rangle = \exp(i\mathbf{k}_{\|}\cdot\mathbf{x}_{\|})\exp(ik_{\gamma\mu}^{(j)}z)\left[\sum_{m=1}^{N}\langle\mathbf{x}|m\rangle C^{(j)}(m, k_{\gamma\mu}^{(j)}; \mathbf{k}_{\|}E)\right], \quad (7)$$

where the index m in the set of coefficients $C^{(j)}(m, k_{\gamma\mu}^{(j)}; \mathbf{k}_{\|}E)$ refer to the $\mathbf{k}_0 = \mathbf{0}$ basis functions $\langle\mathbf{x}|m\rangle$ of the reference solid as described in Appendix (4.4) and are associated with the solution $k_{\gamma\mu}^{(j)}$ in solid $j = 1, 2$.

In the $\mathbf{k}\cdot\mathbf{p}$ formalism, the expansion set consists of the $\mathbf{k}_0 = \mathbf{0}$ basis functions, $\{|m\rangle\}$, of the reference solid. Therefore, we can write,

$$|\mathbf{k}_{\|}E; k_{\gamma\mu}^{(j)}\rangle = \exp(i\mathbf{k}_{\|}\cdot\mathbf{x}_{\|})\exp(ik_{\gamma\mu}^{(j)}z)\left[\sum_{m=1}^{N}\langle\mathbf{x}|m\rangle C^{(j)}(m, k_{\gamma\mu}^{(j)}; \mathbf{k}_{\|}E)\right]. \quad (8)$$

In the local pseudopotential formalism, the expansion set consists of the plane waves $\{|\mathbf{g}\rangle\}$. Thus,

$$|\mathbf{k}_{\|}E; k_{\gamma\mu}^{(j)}\rangle = \exp(i\mathbf{k}_{\|}\cdot\mathbf{x}_{\|})\exp(ik_{\gamma\mu}^{(j)}z)\sum_{\mathbf{g}}|\mathbf{g}\rangle C^{(j)}(\mathbf{g}, k_{\gamma\mu}^{(j)}; \mathbf{k}_{\|}E), \quad (9)$$

where the expansion coefficients $C^{(j)}(\mathbf{g}, k_{\gamma\mu}^{(j)}; \mathbf{k}_{\|}E)$ in the plane wave basis, $\{|\mathbf{g}\rangle\}$, are related to the coefficients $C^{(j)}(m, k_{\gamma\mu}^{(j)}; \mathbf{k}_{\|}E)$ in the $\mathbf{k}_0 = \mathbf{0}$ basis, $\{|m\rangle\}$, through,

$$C^{(j)}(\mathbf{g}, k_{\gamma\mu}^{(j)}; \mathbf{k}_{\|}E) \equiv \sum_{n=1}^{N} U(\mathbf{g}, m)\cdot C^{(j)}(m, k_{\gamma\mu}^{(j)}; \mathbf{k}_{\|}E), \quad (9.b)$$

Thus *the matrix* **U** *allows us to transform from the* $\mathbf{k}_0 = \mathbf{0}$ *basis to the plane wave basis.*

4.6.2 Reduced Transfer Matrix:

We now wish to express the transfer matrix using the pseudopotential formulation. The *non-reduced transfer matrix* is defined to be

$$\mathbf{T}(k^{(2)}_{\gamma\mu}, k^{(1)}_{\gamma'\mu'}; \mathbf{k}_{\|}E; z, z') \equiv \sum_{\mathbf{g}} \left[\mathbf{M}(\mathbf{g}, k^{(2)}_{\gamma\mu}; \mathbf{k}_{\|}E; 2; z)\right]^{-1} \cdot \mathbf{M}(\mathbf{g}, k^{(1)}_{\gamma'\mu'}; \mathbf{k}_{\|}E; 1; z'), \tag{10}$$

and couples all the partners $k^{(1)}_{\gamma'\mu'}$ and $k^{(2)}_{\gamma\mu}$ of the non-equivalent sets γ and γ'.

The *reduced transfer matrix*

$$\Omega(k^{(2)}_{\gamma}, k^{(1)}_{\gamma'}; \mathbf{k}_{\|}E; z, z')$$

relates the states $k^{(2)}_{\gamma}$ and $k^{(1)}_{\gamma'}$ where *both* $Re\left[k^{(1)}_{\gamma'}\right]$ *and* $Re\left[k^{(2)}_{\gamma}\right]$ *lie inside the first Brillouin zone.*

- We now indicate how to obtain the *reduced transfer matrix*

$$\Omega(k^{(2)}_{\gamma}, k^{(1)}_{\gamma'}; \mathbf{k}_{\|}E; z, z')$$

explicitly.

Suppose that two Bloch states have their wavevectors $k^{(j)}_{\gamma\mu}$ and $k^{(j)}_{\gamma}$ separated by a reciprocal lattice vector in the $\hat{\mathbf{z}}$ direction, say $\hat{\mathbf{z}}g_{\mu}$, where μ labels the reciprocal lattice vector,

$$\hat{\mathbf{z}}k^{(j)}_{\gamma\mu} = \hat{\mathbf{z}}k^{(j)}_{\gamma} + \hat{\mathbf{z}}g_{\mu}, \tag{11}$$

and $\mathrm{Re}\left[k^{(j)}_{\gamma}\right]$ lies inside the first Brillouin zone.

The relation between the equivalent partners of a set γ is

$$|\mathbf{k}_{\|}E; k^{(j)}_{\gamma\mu}\rangle = \exp\left[i\varphi^{(j)}(\gamma, \mu)\right]|\mathbf{k}_{\|}E; k^{(j)}_{\gamma}\rangle, \tag{12}$$

where the state $|\mathbf{k}_{\|}E; k^{(j)}_{\gamma}\rangle$ belongs to the eigenvalue $k^{(j)}_{\gamma}$ and the state $|\mathbf{k}_{\|}E; k^{(j)}_{\gamma\mu}\rangle$ belongs to the eigenvalue $k^{(j)}_{\gamma\mu}$. The phase $\exp\left[i\varphi^{(j)}(\gamma, \mu)\right]$ relates a Bloch solution

outside the first Brillouin, $|\mathbf{k}_{\|}E;k_{\gamma\mu}^{(j)}\rangle$, to a solution inside the first Brillouin zone $|\mathbf{k}_{\|}E;k_{\gamma}^{(j)}\rangle$. As above, we adopt the convention that $\mathrm{Re}\left[k_{\gamma}^{(j)}\right]$ lies inside the first Brillouin zone. We must *sum over the equivalent solutions* to obtain the transfer matrix.

Let $\mathbf{M}(\mathbf{g},k_{\gamma\mu}^{(j)};\mathbf{k}_{\|}E;j)$ be the boundary condition matrix in the plane wave basis, $\{|\mathbf{g}\rangle\}$,

We can thus write, symbolically,

$$\mathbf{M}(\mathbf{k}_{\|}E;j)\equiv\mathbf{M}(\mathbf{g},k_{\gamma\mu}^{(j)};\mathbf{k}_{\|}E;j;z)$$

$$\equiv\begin{bmatrix}\exp(ig_z z) & 0\\ 0 & \exp(ig_z z)\end{bmatrix}\cdot\begin{bmatrix}C^{(j)}(\mathbf{g},k_{\gamma\mu}^{(j)};\mathbf{k}_{\|}E)\\ (k_{\gamma\mu}^{(j)}+g_z)C^{(j)}(\mathbf{g},k_{\gamma\mu}^{(j)};\mathbf{k}_{\|}E)\end{bmatrix},\qquad(13.a)$$

or,

$$\mathbf{M}(\mathbf{k}_{\|}E;j)\equiv\mathbf{M}(\mathbf{g},k_{\gamma\mu}^{(j)};\mathbf{k}_{\|}E;j;z)$$

$$\equiv\exp\left[i\mathbf{D}(g_z z)\right]\cdot\mathbf{M}(\mathbf{g},k_{\gamma\mu}^{(j)};\mathbf{k}_{\|}E;j),\qquad(13.b)$$

where we have defined the z-dependent diagonal matrix,

$$\exp\left[i\mathbf{D}(g_z z)\right]\equiv\begin{bmatrix}\exp(ig_z z) & 0\\ 0 & \exp(ig_z z)\end{bmatrix},\qquad(13.c)$$

and the z-independent matrix,

$$\mathbf{M}(\mathbf{g},k_{\gamma\mu}^{(j)};\mathbf{k}_{\|}E;j)\equiv\begin{bmatrix}C^{(j)}(\mathbf{g},k_{\gamma\mu}^{(j)};\mathbf{k}_{\|}E)\\ (k_{\gamma\mu}^{(j)}+g_z)C^{(j)}(\mathbf{g},k_{\gamma\mu}^{(j)};\mathbf{k}_{\|}E)\end{bmatrix},\qquad(13.d)$$

and where the columns label all the solutions $k_{\gamma\mu}^{(j)}$ and the rows label the plane waves $|\mathbf{g}\rangle$.

The *transfer matrix* that couples *non-equivalent states* is defined to be,

$$\Omega(k_{\gamma}^{(2)},k_{\gamma'}^{(1)};\mathbf{k}_{\|}E;z,z')\equiv\sum_{\mu\mu'}\mathbf{T}(k_{\gamma\mu}^{(2)},k_{\gamma'\mu'}^{(1)};\mathbf{k}_{\|}E;z,z'),\qquad(14.a)$$

$$\equiv \sum_{\mu\mu'} \sum_{\mathbf{g}}$$

$$\left[\mathbf{M}(\mathbf{g}, k_{\gamma\mu}^{(2)}; \mathbf{k}_{\|} E; 2; z)\right]^{-1} \cdot \mathbf{M}(\mathbf{g}, k_{\gamma'\mu'}^{(1)}; \mathbf{k}_{\|} E; 1; z'), \tag{14.b}$$

or, using,

$$\mathbf{M}(\mathbf{g}, k_{\gamma\mu}^{(j)}; \mathbf{k}_{\|} E; j; z) \equiv \exp\left[i\mathbf{D}(g_z z)\right] \cdot \mathbf{M}(\mathbf{g}, k_{\gamma\mu}^{(j)}; \mathbf{k}_{\|} E; j), \tag{15}$$

we have,

$$\Omega(k_{\gamma}^{(2)}, k_{\gamma'}^{(1)}; \mathbf{k}_{\|} E; z, z') \equiv \sum_{\mu\mu'} \sum_{\mathbf{g}}$$

$$\left[\mathbf{M}(\mathbf{g}, k_{\gamma\mu}^{(2)}; \mathbf{k}_{\|} E; 2)\right]^{-1} \exp\left[-i\mathbf{D}(g_z z)\right] \cdot$$

$$\exp\left[i\mathbf{D}(g_z z')\right] \mathbf{M}(\mathbf{g}, k_{\gamma'\mu'}^{(1)}; \mathbf{k}_{\|} E; 1), \tag{16.a}$$

or,

$$\Omega(k_{\gamma}^{(2)}, k_{\gamma'}^{(1)}; \mathbf{k}_{\|} E; z, z') \equiv \sum_{\mu\mu'} \sum_{\mathbf{g}}$$

$$\left[\mathbf{M}(\mathbf{g} + \hat{\mathbf{z}} g_{\mu}, k_{\gamma}^{(2)}; \mathbf{k}_{\|} E; 2)\right]^{-1} \cdot \exp\left[-i\mathbf{D}(g_z z)\right] \cdot$$

$$\exp\left[i\mathbf{D}(g_z z')\right] \cdot \mathbf{M}(\mathbf{g} + \hat{\mathbf{z}} g_{\mu'}, k_{\gamma'}^{(1)}; \mathbf{k}_{\|} E; 1), \tag{16.b}$$

where *both* $Re\left[k_{\gamma'}^{(1)}\right]$ *and* $Re\left[k_{\gamma}^{(2)}\right]$ *lie inside the first Brillouin zone.*

Let us now insert a closure relation,

$$\sum_{m} |m\rangle\langle m| \equiv \sum_{m} U(\mathbf{g}, m)\left[U(\mathbf{g}', m)\right]^{\dagger} = \delta^3(\mathbf{g} - \mathbf{g}'). \tag{17}$$

Then

$$\Omega(k_{\gamma}^{(2)}, k_{\gamma'}^{(1)}; \mathbf{k}_{\|} E; z, z') \equiv \sum_{\mu\mu'} \sum_{\mathbf{g}} \left[\mathbf{M}(\mathbf{g} + \hat{\mathbf{z}} g_{\mu}, k_{\gamma}^{(2)}; \mathbf{k}_{\|} E; 2)\right]^{-1} \cdot$$

$$\exp\left[i\mathbf{D}\left(g_z(z' - z)\right)\right] \cdot$$

$$\sum_m U(\mathbf{g}, m) \cdot \left[U(\mathbf{g}', m)\right]^\dagger \cdot$$

$$\exp\left[i\mathbf{D}\big(g_z(z' - z)\big)\right] \cdot$$

$$\mathbf{M}(\mathbf{g} + \hat{\mathbf{z}} g_{\mu'}, k_{\gamma'}^{(1)}; \mathbf{k}_\parallel E; 1), \tag{18}$$

or,

$$\Omega(k_\gamma^{(2)}, k_{\gamma'}^{(1)}; \mathbf{k}_\parallel E; z, z') \equiv \sum_{\mu\mu'} \sum_{\mathbf{g}} \sum_{\mathbf{g}'} \left[\mathbf{M}(\mathbf{g} + \hat{\mathbf{z}} g_\mu, k_\gamma^{(2)}; \mathbf{k}_\parallel E; 2)\right]^{-1} \cdot$$

$$\sum_m U(\mathbf{g}, m) \cdot \left[U(\mathbf{g}', m)\right]^\dagger \cdot$$

$$\exp\left[i\mathbf{D}\big(g_z'(z' - z)\big)\right] \cdot$$

$$\mathbf{M}(\mathbf{g}' + \hat{\mathbf{z}} g_{\mu'}, k_{\gamma'}^{(1)}; \mathbf{k}_\parallel E; 1), \tag{19}$$

by using the fact that

$$\sum_{\mathbf{g}'} \mathbf{M}(\mathbf{g}', k_{\gamma'}^{(1)}; \mathbf{k}_\parallel E; 1) \delta^3(\mathbf{g} - \mathbf{g}') = \mathbf{M}(\mathbf{g}, k_{\gamma'}^{(1)}; \mathbf{k}_\parallel E; 1). \tag{20}$$

We can now change the labels

$$\mathbf{g} \rightarrow \mathbf{g} + \hat{\mathbf{z}} g_\mu$$

and

$$\mathbf{g}' \rightarrow \mathbf{g}' + \hat{\mathbf{z}} g_{\mu'}$$

to get

$$\Omega(k_\gamma^{(2)}, k_{\gamma'}^{(1)}; \mathbf{k}_\parallel E; z, z') \equiv \sum_{\mu\mu'} \sum_{\mathbf{g}} \sum_{\mathbf{g}'} \left[\mathbf{M}(\mathbf{g}, k_\gamma^{(2)}; \mathbf{k}_\parallel E; 2)\right]^{-1} \cdot$$

$$\sum_m U(\mathbf{g} - \hat{\mathbf{z}} g_\mu, m) \cdot \left[U(\mathbf{g}' - \hat{\mathbf{z}} g_{\mu'}, m)\right]^\dagger \cdot$$

$$\exp\left[iD\left((g_z' - g_{\mu'})(z' - z)\right)\right] \cdot$$

$$\mathbf{M}(\mathbf{g}', k_{\gamma'}^{(1)}; \mathbf{k}_{\|} E; 1). \tag{21}$$

At this point we can insert another closure relation,

$$\sum_m |m\rangle\langle m| \equiv \sum_m U(\mathbf{g}, m)\left[U(\mathbf{g}', m)\right]^{\dagger} = \delta^3(\mathbf{g} - \mathbf{g}'). \tag{22}$$

to get

$$\Omega(k_{\gamma}^{(2)}, k_{\gamma'}^{(1)}; \mathbf{k}_{\|} E; z, z') \equiv \sum_{\mu\mu'} \sum_{\mathbf{g}} \sum_{\mathbf{g}'} \sum_{\mathbf{g}''} \left[\mathbf{M}(\mathbf{g}, k_{\gamma}^{(2)}; \mathbf{k}_{\|} E; 2)\right]^{-1} \cdot$$

$$\sum_{m'} U(\mathbf{g}, m') \cdot \left[U(\mathbf{g}', m')\right]^{\dagger} \cdot$$

$$\sum_m U(\mathbf{g}' - \hat{\mathbf{z}} g_{\mu}, m) \cdot \left[U(\mathbf{g}'' - \hat{\mathbf{z}} g_{\mu'}, m)\right]^{\dagger} \cdot$$

$$\exp\left[iD\left((g_z'' - g_{\mu'})(z' - z)\right)\right] \cdot$$

$$\mathbf{M}(\mathbf{g}'', k_{\gamma'}^{(1)}; \mathbf{k}_{\|} E; 1). \tag{23}$$

By inserting another closure relation,

$$\sum_m |m\rangle\langle m| \equiv \sum_m U(\mathbf{g}, m)\left[U(\mathbf{g}', m)\right]^{\dagger} = \delta^3(\mathbf{g} - \mathbf{g}'), \tag{24}$$

we finally obtain,

$$\Omega(k_{\gamma}^{(2)}, k_{\gamma'}^{(1)}; \mathbf{k}_{\|} E; z, z') \equiv \sum_{\mu\mu'} \sum_{\mathbf{g}} \sum_{\mathbf{g}'} \sum_{\mathbf{g}''} \sum_{\mathbf{g}'''} \left[\mathbf{M}(\mathbf{g}, k_{\gamma}^{(2)}; \mathbf{k}_{\|} E; 2)\right]^{-1} \cdot$$

$$\sum_{m'} U(\mathbf{g}, m') \cdot \left[U(\mathbf{g}', m')\right]^{\dagger} \cdot$$

$$\sum_m U(\mathbf{g}' - \hat{\mathbf{z}} g_{\mu}, m) \cdot \left[U(\mathbf{g}'' - \hat{\mathbf{z}} g_{\mu'}, m)\right]^{\dagger} \cdot$$

$$\exp\left[iD\left((g_z'' - g_{\mu'})(z' - z)\right)\right] \cdot$$

$$\sum_{m''} U(\mathbf{g}'', m'') \cdot \left[U(\mathbf{g}''', m'')\right]^{\dagger} \cdot$$

$$\mathbf{M}(\mathbf{g}''', k_{\gamma'}^{(1)}; \mathbf{k}_{\parallel} E; 1). \tag{25}$$

We can now regroup to obtain,

$$\Omega(k_{\gamma}^{(2)}, k_{\gamma'}^{(1)}; \mathbf{k}_{\parallel} E; z, z') \equiv \sum_{\mu\mu'} \sum_{m} \sum_{m'} \sum_{m''}$$

$$\sum_{\mathbf{g}} \left[\mathbf{M}(\mathbf{g}, k_{\gamma}^{(2)}; \mathbf{k}_{\parallel} E; 2)\right]^{-1} \cdot U(\mathbf{g}, m') \cdot$$

$$\sum_{\mathbf{g}'} \left[U(\mathbf{g}', m')\right]^{\dagger} \cdot U(\mathbf{g}' - \hat{\mathbf{z}} g_{\mu}, m) \cdot$$

$$\sum_{\mathbf{g}''} \left[U(\mathbf{g}'' - \hat{\mathbf{z}} g_{\mu'}, m)\right]^{\dagger} \cdot \exp\left[iD\left((g_z'' - g_{\mu'})(z' - z)\right)\right] \cdot U(\mathbf{g}'', m'') \cdot$$

$$\sum_{\mathbf{g}'''} \left[U(\mathbf{g}''', m'')\right]^{\dagger} \cdot \mathbf{M}(\mathbf{g}''', k_{\gamma'}^{(1)}; \mathbf{k}_{\parallel} E; 1), \tag{26}$$

Let us now contract the matrices and write, in the $\{|m\rangle\}$ representation,

$$\left[\mathbf{M}(m', k_{\gamma}^{(2)}; \mathbf{k}_{\parallel} E; 2)\right]^{-1} \equiv \sum_{\mathbf{g}} \left[\mathbf{M}(\mathbf{g}, k_{\gamma}^{(2)}; \mathbf{k}_{\parallel} E; 2)\right]^{-1} \cdot U(\mathbf{g}, m'), \tag{27.a}$$

$$O(m', m; \hat{\mathbf{z}} g_{\mu}; 0, 0) \equiv \sum_{\mathbf{g}'} \left[U(\mathbf{g}', m')\right]^{\dagger} \cdot U(\mathbf{g}' - \hat{\mathbf{z}} g_{\mu}, m), \tag{27.b}$$

$$O(m, m''; \hat{\mathbf{z}} g_{\mu'}; z, z') \equiv \sum_{\mathbf{g}''} \left[U(\mathbf{g}'' - \hat{\mathbf{z}} g_{\mu'}, m)\right]^{\dagger} \cdot$$

$$\exp\left[iD\left((g_z'' - g_{\mu'})(z' - z)\right)\right] \cdot U(\mathbf{g}'', m''), \tag{27.c}$$

$$\mathbf{M}(m'', k_{\gamma'}^{(1)}; \mathbf{k}_{\|} E; 1) \equiv \sum_{\mathbf{g}'''} \left[U(\mathbf{g}''', m'')\right]^{\dagger} \cdot \mathbf{M}(\mathbf{g}''', k_{\gamma'}^{(1)}; \mathbf{k}_{\|} E; 1). \qquad (27.d)$$

We can finally write the *reduced transfer matrix*

$$\Omega(k_{\gamma}^{(2)}, k_{\gamma'}^{(1)}; \mathbf{k}_{\|} E; z, z') \equiv \sum_{\mu\mu'} \sum_{m} \sum_{m'} \sum_{m''} \cdot$$

$$\left[\mathbf{M}(m', k_{\gamma}^{(2)}; \mathbf{k}_{\|} E; 2)\right]^{-1} \cdot O(m', m; \hat{\mathbf{z}} g_{\mu}; 0, 0) \cdot$$

$$O(m, m''; \hat{\mathbf{z}} g_{\mu'}; z, z') \cdot \mathbf{M}(m'', k_{\gamma'}^{(1)}; \mathbf{k}_{\|} E; 1), \qquad (28)$$

where $\mathrm{Re}\left[k_{\gamma}^{(j)}\right]$ lie inside the first Brillouin zone.

4.6.3 Reduced Transfer Matrix: $\mathbf{k}\cdot\mathbf{p}$

In this section, we express the *z-dependent transfer matrix in the* $\mathbf{k}\cdot\mathbf{p}$ *formalism.* As seen above, in the pseudopotential formalism, we can write,

$$\mathbf{M}(\mathbf{k}_{\|}E;j) \equiv \mathbf{M}(\mathbf{g}, k_{\gamma\mu}^{(j)};\mathbf{k}_{\|}E;j;z)$$

$$\equiv \begin{bmatrix} \exp(ig_z z) & 0 \\ 0 & \exp(ig_z z) \end{bmatrix} \cdot \begin{bmatrix} C^{(j)}(\mathbf{g}, k_{\gamma\mu}^{(j)};\mathbf{k}_{\|}E) \\ (k_{\gamma\mu}^{(j)} + g_z)C^{(j)}(\mathbf{g}, k_{\gamma\mu}^{(j)};\mathbf{k}_{\|}E) \end{bmatrix}, \tag{29.a}$$

or,

$$\mathbf{M}(\mathbf{k}_{\|}E;j) \equiv \mathbf{M}(\mathbf{g}, k_{\gamma\mu}^{(j)};\mathbf{k}_{\|}E;j;z)$$

$$\equiv \exp[i\mathbf{D}(g_z z)] \cdot \mathbf{M}(\mathbf{g}, k_{\gamma\mu}^{(j)};\mathbf{k}_{\|}E;j), \tag{29.b}$$

where we have defined the z-dependent diagonal matrix,

$$\exp[i\mathbf{D}(g_z z)] \equiv \begin{bmatrix} \exp(ig_z z) & 0 \\ 0 & \exp(ig_z z) \end{bmatrix}, \tag{29.c}$$

and the z-independent matrix,

$$\mathbf{M}(\mathbf{g}, k_{\gamma\mu}^{(j)};\mathbf{k}_{\|}E;j) \equiv \begin{bmatrix} C^{(j)}(\mathbf{g}, k_{\gamma\mu}^{(j)};\mathbf{k}_{\|}E) \\ (k_{\gamma\mu}^{(j)} + g_z)C^{(j)}(\mathbf{g}, k_{\gamma\mu}^{(j)};\mathbf{k}_{\|}E) \end{bmatrix}, \tag{29.d}$$

and where the columns label all the solutions $k_{\gamma\mu}^{(j)}$ and the rows label the plane waves $|\mathbf{g}\rangle$.

Now the *non-reduced transfer matrix* is

$$\mathbf{T}(k_{\gamma\mu}^{(2)}, k_{\gamma'\mu'}^{(1)};\mathbf{k}_{\|}E;z,z') \equiv \sum_{\mathbf{g}} \left[\mathbf{M}(\mathbf{g}, k_{\gamma\mu}^{(2)};\mathbf{k}_{\|}E;2;z)\right]^{-1} \cdot \mathbf{M}(\mathbf{g}, k_{\gamma'\mu'}^{(1)};\mathbf{k}_{\|}E;1;z'), \tag{30}$$

or,

$$\mathbf{T}(k_{\gamma\mu}^{(2)}, k_{\gamma'\mu'}^{(1)};\mathbf{k}_{\|}E;z,z') \equiv \sum_{\mathbf{g}} \left[\mathbf{M}(\mathbf{g}, k_{\gamma\mu}^{(2)};\mathbf{k}_{\|}E;2)\right]^{-1} \exp[-i\mathbf{D}(g_z z)] \cdot$$

$$\exp\left[i\mathbf{D}(g_z z')\right]\mathbf{M}(\mathbf{g}, k^{(1)}_{\gamma'\mu'}; \mathbf{k}_\parallel E; 1), \tag{31}$$

by using the matrix product,

$$\mathbf{M}(\mathbf{k}_\parallel E; j) \equiv \mathbf{M}(\mathbf{g}, k^{(j)}_{\gamma\mu}; \mathbf{k}_\parallel E; j; z)$$

$$\equiv \exp\left[i\mathbf{D}(g_z z)\right] \cdot \mathbf{M}(\mathbf{g}, k^{(j)}_{\gamma\mu}; \mathbf{k}_\parallel E; j). \tag{32}$$

By inserting two closure relations,

$$\sum_m |m\rangle\langle m| \equiv \sum_m U(\mathbf{g}, m)\left[U(\mathbf{g}', m)\right]^\dagger = \delta^3(\mathbf{g} - \mathbf{g}'), \tag{33}$$

we have

$$\mathbf{T}(k^{(2)}_{\gamma\mu}, k^{(1)}_{\gamma'\mu'}; \mathbf{k}_\parallel E; z, z') \equiv$$

$$\sum_{\mathbf{g}} \sum_{\mathbf{g}'} \sum_{\mathbf{g}''} \left[\mathbf{M}(\mathbf{g}, k^{(2)}_{\gamma\mu}; \mathbf{k}_\parallel E; 2)\right]^{-1} \cdot$$

$$\sum_m U(\mathbf{g}, m) \cdot \left[U(\mathbf{g}', m)\right]^\dagger \cdot$$

$$\exp\left[i\mathbf{D}\left(g_z(z - z')\right)\right] \cdot$$

$$\sum_{m'} U(\mathbf{g}', m') \cdot \left[U(\mathbf{g}'', m')\right]^\dagger \cdot$$

$$\mathbf{M}(\mathbf{g}'', k^{(1)}_{\gamma'\mu'}; \mathbf{k}_\parallel E; 1). \tag{34}$$

As before we define the following matrices, in the $\{|m\rangle\}$ representation,

$$\left[\mathbf{M}(m, k^{(2)}_{\gamma\mu}; \mathbf{k}_\parallel E; 2)\right]^{-1} \equiv \sum_{\mathbf{g}} \left[\mathbf{M}(\mathbf{g}, k^{(2)}_{\gamma\mu}; \mathbf{k}_\parallel E; 2)\right]^{-1} \cdot U(\mathbf{g}, m), \tag{35.a}$$

$$O(m, m'; z - z') \equiv \sum_{\mathbf{g}'} \left[U(\mathbf{g}', m)\right]^\dagger \cdot U(\mathbf{g}', m') \exp\left[i\mathbf{D}\left(g_z'(z - z')\right)\right], \tag{35.b}$$

$$\mathbf{M}(m', k^{(1)}_{\gamma'\mu'}; \mathbf{k}_{\|}E; 1) \equiv \sum_{\mathbf{g}''} \left[U(\mathbf{g}'', m')\right]^{\dagger} \cdot \mathbf{M}(\mathbf{g}'', k^{(1)}_{\gamma'\mu'}; \mathbf{k}_{\|}E; 1). \tag{35.c}$$

We then obtain the transfer matrix in the $\{|m\rangle\}$ representation,

$$\mathbf{T}(k^{(2)}_{\gamma\mu}, k^{(1)}_{\gamma'\mu'}; \mathbf{k}_{\|}E; z, z') \equiv$$

$$\sum_{m} \sum_{m'} \left[\mathbf{M}(m, k^{(2)}_{\gamma\mu}; \mathbf{k}_{\|}E; 2)\right]^{-1} \cdot$$

$$O(m, m'; z - z') \cdot$$

$$\mathbf{M}(m', k^{(1)}_{\gamma'\mu'}; \mathbf{k}_{\|}E; 1). \tag{36}$$

The matrix

$$O(m, m'; z - z')$$

is the *overlap matrix* between two basis functions $\langle \mathbf{x}|m\rangle$ separated by $z - z'$. Thus when $z - z'$, is a bulk lattice translation vector $\mathbf{R}$, we have,

$$O(m, m'; \mathbf{R}) \equiv 1, \tag{37.a}$$

due to the periodicity of the basis functions $\langle \mathbf{x}|m\rangle$,

$$u_m(\mathbf{x} + \mathbf{R}) = u_m(\mathbf{x}). \tag{37.b}$$

APPENDIX 4.7

Symmetry properties of Transfer matrix:

In this appendix, we enumerate the *symmetry properties of the reduced transfer matrix*,

$$\Omega(k_\gamma^{(2)}, k_{\gamma'}^{(1)}; \mathbf{k}_\parallel E),$$

where $\mathrm{Re}[k_\gamma^{(j)}]$ lie inside the first Brillouin zone. We consider two symmetries:

- Symmetry under *time-reversal*,

$$k_\gamma^{(j)} \rightarrow -k_\gamma^{(j)^*}. \tag{1.a}$$

- Symmetry under *inversion*,

$$k_\gamma^{(j)} \rightarrow -k_\gamma^{(j)}. \tag{1.b}$$

4.7.1 Symmetry under Time-Reversal:

- We repeat here the argument of Appendix (4.4) for *time-reversed Bloch states*. Let us consider the case of $\mathbf{k}_\parallel = \mathbf{0}$. The Bloch state $\langle \mathbf{x}|\mathbf{k}_\parallel E; k_\lambda\rangle$ can be expanded in terms of the $\mathbf{k}_0 = \mathbf{0}$ basis functions,

$$\psi(k_\lambda; \mathbf{x}) = \exp(ik_\lambda z) \sum_{m=1}^{N} u_m(\mathbf{x}) C(m, k_\lambda), \tag{2}$$

where we have written $\psi(k_\lambda; \mathbf{x})$ for $\langle \mathbf{x}|\mathbf{k}_\parallel E; k_\lambda\rangle$ at $\mathbf{k}_\parallel = \mathbf{0}$ for simplicity.

- According to Appendix A, the *degenerate time-reversed* state is simply the *complex conjugate in the absence of spin-orbit*. Then we can write the time-reversed partner of $\psi(k_\lambda; \mathbf{x})$ as

$$\psi^*(k_\lambda; \mathbf{x}) = \exp(-ik_\lambda^* z) \sum_{m=1}^{N} u_m^*(\mathbf{x}) C^*(m, k_\lambda), \tag{3.a}$$

or,

$$\psi^*(k_\lambda;\mathbf{x}) = \exp\left[i(-k_\lambda^*)z\right] \sum_{m=1}^{N} u_m^*(\mathbf{x})C^*(m,k_\lambda). \tag{3.b}$$

Thus the time-reversed partner of a Bloch state with wavevector k_λ is a Bloch state with wavevector $-k_\lambda^*$, to within a phase factor, $\exp(i\varphi)$.

We can then relate the time-reversed pair of Bloch states as,

$$\psi^*(k_\lambda;\mathbf{x}) \equiv \exp(-i\varphi)\psi(-k_\lambda^*;\mathbf{x}), \tag{4.a}$$

or,

$$\psi(k_\lambda;\mathbf{x}) \equiv \exp(i\varphi)\psi^*(-k_\lambda^*;\mathbf{x}), \tag{4.b}$$

to within a constant phase factor, $\exp(-i\varphi)$ By comparing Eq.(19) and Eq.(20), we have

$$\sum_{m=1}^{N} u_m(\mathbf{x})C(m,k_\lambda) = \exp(i\varphi) \sum_{m=1}^{N} u_m^*(\mathbf{x})C^*(m,-k_\lambda^*). \tag{5}$$

• According to the *phase convention* we have that $\mathbf{k}_0 = \mathbf{0}$ basis functions have no definite parity and are taken to be *real.* Then we have,

$$u_m^*(\mathbf{x}) = u_m(\mathbf{x}). \tag{6.a}$$

$$C(m,k_\lambda) = \exp(i\varphi)C^*(m,-k_\lambda^*). \tag{6.b}$$

To determine the phase factor $\exp(i\varphi)$, we adopted the following phase convention on the expansion coefficients, *the maximum component of the coefficient* $C(m,k_\lambda)$ *is taken to be real and positive.* Since the maximum component of $C(m,k_\lambda)$ and $C^*(m,-k_\lambda^*)$ occurs for the same index m, then we have that

$$C(m,k_\lambda) = C^*(m,-k_\lambda^*), \tag{7}$$

which fixes the phase factor to be

$$\exp(i\varphi) \equiv 1. \tag{8}$$

• In the kp formulation, the transfer matrix can be written as,

$$\Omega(k_\gamma^{(2)}, k_{\gamma'}^{(1)}; \mathbf{k}_\parallel E) \equiv \sum_m \left[\mathbf{M}(m, k_\gamma^{(2)}; \mathbf{k}_\parallel E; 2)\right]^{-1} \cdot \mathbf{M}(m, k_{\gamma'}^{(1)}; \mathbf{k}_\parallel E; 1). \tag{9}$$

Under time-reversal, we have,

$$k_\gamma^{(2)} \rightarrow -k_\gamma^{(2)^*}, \tag{10.a}$$

$$k_{\gamma'}^{(1)} \rightarrow -k_{\gamma'}^{(1)^*}, \tag{10.b}$$

and, from the relation

$$C(m, k_\lambda) = C^*(m, -k_\lambda^*), \tag{11}$$

we have

$$\mathbf{M}(m, k_\gamma^{(2)}; \mathbf{k}_\parallel E; 2) = \mathbf{M}^*(m, -k_\gamma^{(2)^*}; \mathbf{k}_\parallel E; 2), \tag{12.a}$$

$$\mathbf{M}(m, k_{\gamma'}^{(1)}; \mathbf{k}_\parallel E; 1) = \mathbf{M}^*(m, -k_{\gamma'}^{(1)^*}; \mathbf{k}_\parallel E; 1). \tag{12.b}$$

• Then, we can write the transfer matrix for the *time-reversed states*,

$$\Omega(-k_\gamma^{(2)^*}, -k_{\gamma'}^{(1)^*}; \mathbf{k}_\parallel E) \equiv \sum_m \left[\mathbf{M}(m, -k_\gamma^{(2)^*}; \mathbf{k}_\parallel E; 2)\right]^{-1} \cdot \mathbf{M}(m, -k_{\gamma'}^{(1)^*}; \mathbf{k}_\parallel E; 1), \tag{13.a}$$

$$= \sum_m \left[\mathbf{M}^*(m, k_\gamma^{(2)}; \mathbf{k}_\parallel E; 2)\right]^{-1} \cdot \mathbf{M}^*(m, k_{\gamma'}^{(1)}; \mathbf{k}_\parallel E; 1), \tag{13.b}$$

$$= \left[\sum_m \left[\mathbf{M}(m, k_\gamma^{(2)}; \mathbf{k}_\parallel E; 2)\right]^{-1} \cdot \mathbf{M}(m, k_{\gamma'}^{(1)}; \mathbf{k}_\parallel E; 1)\right]^*, \tag{13.c}$$

$$\equiv \left[\Omega(k_\gamma^{(2)}, k_{\gamma'}^{(1)}; \mathbf{k}_\parallel E)\right]^*. \tag{13.d}$$

• The symmetry of the transfer matrix under *time-reversal* is therefore,

$$\Omega(-k_\gamma^{(2)^*}, -k_{\gamma'}^{(1)^*}; \mathbf{k}_\parallel E) = \left[\Omega(k_\gamma^{(2)}, k_{\gamma'}^{(1)}; \mathbf{k}_\parallel E)\right]^*. \tag{14}$$

4.7.2 Symmetry under Inversion:

- The symmetry of the transfer matrix under *inversion* is

$$\Omega(-k_{\gamma}^{(2)}, -k_{\gamma'}^{(1)}; \mathbf{k}_{\parallel} E) = \pm\Omega(k_{\gamma}^{(2)}, k_{\gamma'}^{(1)}; \mathbf{k}_{\parallel} E) \tag{15}$$

GENERAL APPENDICES

PROPERTIES OF COMPLEX-k ENERGY BAND STRUCTURES

ENERGY BAND OFFSETS

Appendix 5.1

Properties of Complex-k Band Structures

The purpose of this appendix is to list some of the properties associated with crystal Hamiltonian when the wavevector $\mathbf{k}$ is complex. That is , we study symmetries of the function $E_n(\mathbf{k})$ for complex values of $\mathbf{k}$. This appendix is more a *collection* of the symmetries of the function $E_n(\mathbf{k})$ for complex $\mathbf{k}$, than *derivations* of them. Derivations can be found in the work of Blount[1] and Heine[2].

As seen previously, it is useful to define a Hamiltonian $\hat{H}(\mathbf{k})$ acting on the cell-periodic part of the Bloch solutions. Given that the set of Bloch states $\{|n\mathbf{k}\rangle\}$ are solutions to the Schrödinger equation for the bulk solid:

$$\hat{H}|n\mathbf{k}\rangle = E_n(\mathbf{k})|n\mathbf{k}\rangle. \tag{A.1}$$

The Hamiltonian is

$$\hat{H} = \frac{1}{2m}\mathbf{p}^2 + V(\mathbf{x}), \tag{A.2}$$

where $V(\mathbf{x}+\mathbf{R}) = V(\mathbf{x})$ is the crystal potential which has the symmetry of the crystal space group. The momentum operator is $\mathbf{p} \equiv -i\hbar\nabla$. The energy eigenvalues, $E_n(\mathbf{k})$, for the band structure of bulk solid. The Bloch states are of the form,

$$\langle \mathbf{x}|n\mathbf{k}\rangle = \exp(i\mathbf{k}\cdot\mathbf{x})u_n(\mathbf{k};\mathbf{x}), \tag{A.3}$$

where $u_n(\mathbf{k};\mathbf{x})$ is the cell-periodic part of the Bloch function:

$$u_n(\mathbf{k};\mathbf{x}+\mathbf{R}) = u_n(\mathbf{k};\mathbf{x}), \tag{A.4}$$

where $\mathbf{R}$ is a Bravais lattice vector generating the $\mathbf{x}$-space lattice. The index n is the band index and $\hbar\mathbf{k}$ is the crystal momentum. We now wish to obtain the eigenvalue equation for the cell-periodic part of the Bloch function, $u_n(\mathbf{k};\mathbf{x})$, by direct substitution of the form Eq.(A.3) into the Schrödinger equation Eq.(A.1):

$$\left[\frac{1}{2m}\mathbf{p}^2 + V(\mathbf{x})\right] \exp(i\mathbf{k}\cdot\mathbf{x}) u_n(\mathbf{k};\mathbf{x}) = E_n(\mathbf{k}) u_n(\mathbf{k};\mathbf{x}). \qquad (A.5)$$

By commuting the plane wave $\exp(i\mathbf{k}\cdot\mathbf{x})$ across the Hamiltonian, we arrive at:

$$\hat{H}(\mathbf{k}) u_n(\mathbf{k};\mathbf{x}) = E_n(\mathbf{k}) u_n(\mathbf{k};\mathbf{x}), \qquad (A.6)$$

where the Hamiltonian $\hat{H}(\mathbf{k})$ is defined to be :

$$\hat{H}(\mathbf{k}) \equiv \frac{1}{2m}(\mathbf{p} + \hbar\mathbf{k})^2 + V(\mathbf{x}), \qquad (A.7.a)$$

or,

$$\hat{H}(\mathbf{k}) \equiv \frac{1}{2m}\mathbf{p}^2 + \frac{\hbar}{m}\mathbf{k}\cdot\mathbf{p} + \frac{\hbar^2}{2m}\mathbf{k}^2 + V(\mathbf{x}), \qquad (A.7.b)$$

The form of the Hamiltonian $\hat{H}(\mathbf{k})$ corresponds to a *gauge transformation*,

$$\hat{H}(\mathbf{k}) \equiv \hat{H}(\mathbf{p}+\mathbf{k};\mathbf{x}) \equiv \exp(-i\mathbf{k}\cdot\mathbf{x}) \cdot \hat{H}(\mathbf{p};\mathbf{x}) \cdot \exp(i\mathbf{k}\cdot\mathbf{x}). \qquad (A.8)$$

If we now allow the wavevector $\mathbf{k}$ in Eq.(A.8) to take complex values, then the operator $\hat{H}(\mathbf{k})$ is no longer hermitian, but enjoys the property that

$$\hat{H}^{\dagger}(\mathbf{k}) = \hat{H}(\mathbf{k}^*). \qquad (A.9)$$

Since $\hat{H}(\mathbf{k})$ is non-hermitian, the eigenvectors of $\hat{H}(\mathbf{k})$ are not orthogonal. Also, $\hat{H}(\mathbf{k})$ can be diagonal only when the eigenvalues are distinct.

We consider the two eigenvalue problem associated with the operator $\hat{H}(\mathbf{k})$: the *direct problem*,

$$\hat{H}(\mathbf{k}) u_n(\mathbf{k};\mathbf{x}) = E_n(\mathbf{k}) u_n(\mathbf{k};\mathbf{x}), \qquad (A.10.a)$$

satisfied by the set of functions $u_n(\mathbf{k};\mathbf{x})$, and the *adjoint problem*,

$$v_n(\mathbf{k};\mathbf{x})\hat{H}^{\dagger}(\mathbf{k}) = E_n(\mathbf{k})v_n(\mathbf{k};\mathbf{x}), \qquad (A.10.b)$$

satified by the set of functions $v_n(\mathbf{k};\mathbf{x})$. Since $\hat{H}(\mathbf{k})$ is not hermitian, the set of eigensolutions of the adjoint problem, $v_n(\mathbf{k};\mathbf{x})$, is not equal to the hermitian conjugate $u_n^{\dagger}(\mathbf{k};\mathbf{x})$ of the eigensolutions of the direct problem, $u_n(\mathbf{k};\mathbf{x})$. Thus, instead of the orthogonality relation

$$\langle n\mathbf{k}|n'\mathbf{k}'\rangle = \delta(n,n')\delta^3(\mathbf{k}-\mathbf{k}'), \qquad (A.11.a)$$

or,

$$\int d^3\mathbf{x}\, u_n^*(\mathbf{k};\mathbf{x})u_{n'}(\mathbf{k}';\mathbf{x})\exp\left[i(\mathbf{k}'-\mathbf{k})\cdot\mathbf{x}\right] = \delta(n,n')\delta^3(\mathbf{k}-\mathbf{k}'), \qquad (A.11.b)$$

is replaced by the orthogonality relation,

$$\langle n\mathbf{k}|n'\mathbf{k}'\rangle = \delta(n,n')\delta^3(\mathbf{k}-\mathbf{k}'), \qquad (A.12.a)$$

or,

$$\int d^3\mathbf{x}\, u_n^*(\mathbf{k}^*;\mathbf{x})u_{n'}(\mathbf{k}';\mathbf{x})\exp\left[i(\mathbf{k}'-\mathbf{k}^*)\cdot\mathbf{x}\right] = \delta(n,n')\delta^3(\mathbf{k}-\mathbf{k}'). \qquad (A.12.b)$$

In Eqs(A.12) we used the fact that

$$v_n(\mathbf{k}^*;\mathbf{x}) = u_n^{\dagger}(\mathbf{k};\mathbf{x}), \qquad (A.13)$$

from

$$\hat{H}^{\dagger}(\mathbf{k}) = \hat{H}(\mathbf{k}^*). \qquad (A.14)$$

That is, if the direct problem involves Bloch states with wavevector $\mathbf{k}$, then the adjoint problem involves Bloch states with wavevector $\mathbf{k}^*$.

The relation

$$\hat{H}^{\dagger}(\mathbf{k}) = \hat{H}(\mathbf{k}^{*}), \tag{A.15.a}$$

on the operator $\hat{H}(\mathbf{k})$ implies

$$E_n^{*}(\mathbf{k}) = E_n(\mathbf{k}^{*}), \tag{A.15.b}$$

on the set of eigenvalues $E_n(\mathbf{k})$. It also implies that for *real* $\mathbf{k}$, we have hermicity of $\hat{H}(\mathbf{k})$, *i.e.*,

$$\hat{H}^{\dagger}(\mathbf{k}) = \hat{H}(\mathbf{k}) \qquad \text{for} \mathbf{k}^{*} = \mathbf{k}, \tag{A.16}$$

and the eigenvalues $E_n(\mathbf{k})$ are *real*.

We now study further symmetries of the function $E_n(\mathbf{k})$. In a crystal, the group of the Hamiltonian is the *space group of the crystal structure* plus the *operation of time reversal*. We define the time-reversal operator[3] as

$$\hat{K} \equiv -i\sigma_2\hat{K}_0, \tag{A.17}$$

where σ_2 is the Pauli spin matrix,

$$\sigma_2 \equiv \begin{bmatrix} 0 & -i \\ i & 0 \end{bmatrix}, \tag{A.18.a}$$

and $\hat{K}_0$ is, in the Schrödinger representation, the operation of taking the complex conjugate,

$$\hat{K}_0\Psi(\mathbf{x}) \equiv \Psi^{*}(\mathbf{x}). \tag{A.18.b}$$

The complex conjugation operator is *antilinear*

$$\hat{K}_0[a_1\Psi_1(\mathbf{x}) + a_2\Psi_2(\mathbf{x})] = a_1^{*}\hat{K}_0\Psi_1(\mathbf{x}) + a_2^{*}\hat{K}_0\Psi_2(\mathbf{x}), \tag{A.18.b}$$

and *antiunitary*

$$\langle\hat{K}_0\Psi|\hat{K}_0\Phi\rangle = \langle\Phi|\Psi\rangle. \tag{A.18.b}$$

The time-reversal operator reverses the momentum $\mathbf{p}$,

$$\hat{K}\,\mathbf{p}\hat{K}^{-1} = -\mathbf{p}, \qquad (A.19.a)$$

and the spin $\mathbf{s}$,

$$\hat{K}\,\mathbf{s}\hat{K}^{-1} = -\mathbf{s}, \qquad (A.19.b)$$

but not the position $\mathbf{x}$,

$$\hat{K}\,\mathbf{x}\hat{K}^{-1} = \mathbf{x}. \qquad (A.19.c)$$

Without spin-orbit interactions, the time-reversal operator $\hat{K}$ is equivalent to the complex conjugation operator $\hat{K}_0$,

$$\hat{K} \equiv \hat{K}_0 \qquad \text{no spin-orbit interaction} (A.20)$$

Kramer's theorem[3] states that, *in the absence of a magnetic field, if Ψ is a one-electron eigenstate of the Hamiltonian $\hat{H}$, then the time-reversed function $\hat{K}\Psi$ is also an eigenstate of $\hat{H}$ with the same energy eigenvalue.* Furthermore, *the time-reversed solution $\hat{K}\Psi$ is orthogonal to Ψ.* That is, if

$$\hat{H}\Psi = E\Psi, \qquad (A.21.a)$$

then we apply the time-reversal operator,

$$\hat{K}\hat{H}\Psi = E\hat{K}\Psi, \qquad (A.21.b)$$

$$\hat{H}\left[\hat{K}\Psi\right] = E\left[\hat{K}\Psi\right], \qquad (A.21.c)$$

since $\hat{H}$ commutes with $\hat{K}$,

$$\left[\hat{K}, \hat{H}\right] = 0. \qquad (A.22)$$

Then, *for real Hamiltonian $\hat{H}$ and in the absence of spin-orbit interaction*, we have that if Ψ is a solution of the Schrödinger equation

$$\hat{H}\Psi = E\Psi, \tag{A.23.a}$$

then the complex conjugate Ψ^* is also a solution belonging to the same eigenvalue E,

$$\hat{H}\Psi^* = E\Psi^*. \tag{A.23.b}$$

For complex-$\mathbf{k}$, we see that if Ψ is a solution of $\hat{H}$ belonging to the complex eigenvalue E,

$$\hat{H}\Psi = E\Psi, \tag{A.24.a}$$

then Ψ^* is a solution of $\hat{H}^\dagger$ belonging to the eigenvalue E^*,

$$\hat{H}^\dagger\Psi^* = E^*\Psi^*. \tag{A.24.b}$$

Given a Bloch state of the form,

$$\langle \mathbf{x}|n\mathbf{k}\rangle = \exp(i\mathbf{k}\cdot\mathbf{x})u_n(\mathbf{k};\mathbf{x}), \tag{A.25}$$

we apply the conjugation operator $\hat{K}_0$ to get

$$\hat{K}_0\langle \mathbf{x}|n\mathbf{k}\rangle = \exp\left[i(-\mathbf{k}^*)\cdot\mathbf{x}\right]u_n^*(\mathbf{k};\mathbf{x}). \tag{A.26.a}$$

But we can write, to within a phase factor $\exp(i\varphi)$, that

$$u_n^*(\mathbf{k};\mathbf{x}) = \exp(i\varphi)u_n(-\mathbf{k}^*;\mathbf{x}). \tag{A.26.b}$$

We then have the relation between a Bloch state and its time-reversed partner,

$$\hat{K}_0\langle \mathbf{x}|n\mathbf{k}\rangle \equiv \exp(i\varphi)\langle \mathbf{x}|n - \mathbf{k}^*\rangle. \tag{A.26.b}$$

We see that *a Bloch state with wavevector* $-\mathbf{k}^*$ *is the time-reversed partner of the Bloch state with wavevector* $\mathbf{k}$, *to within a phase factor* $\exp(i\varphi)$. We can thus write,

$$\hat{K}\,|n\mathbf{k}\rangle = \exp(i\varphi)|n - \mathbf{k}^*\rangle. \tag{A.27}$$

When spin-orbit interactions are present, the time-reversal operator reverses the spin component,

$$\hat{K}\,|n\mathbf{k};\uparrow\rangle = \exp(i\varphi)|n - \mathbf{k}^*;\downarrow\rangle, \tag{A.28.a}$$

$$\hat{K}\,|n\mathbf{k};\downarrow\rangle = \exp(i\varphi)|n - \mathbf{k}^*;\uparrow\rangle. \tag{A.28.b}$$

Thus the eigenvalues $E_n(-\mathbf{k}^*)$ associated with the time-reversed Bloch state $|n - \mathbf{k}^*\rangle$ of wavevector $-\mathbf{k}^*$, are *complex conjugate* to the eigenvalues $E_n(\mathbf{k})$ associated with the Bloch state $|n\mathbf{k}\rangle$ of wavevector $\mathbf{k}$,

$$E_n(-\mathbf{k}^*) = E_n^*(\mathbf{k}). \tag{A.29}$$

Combining Eqs.(A.27) and (A.15.b) we have,

$$E_n(-\mathbf{k}^*) = E_n^*(\mathbf{k}) = E_n(\mathbf{k}^*). \tag{A.30}$$

For real eigenvalues $E_n(\mathbf{k})$ we have,

$$E_n(-\mathbf{k}^*) = E_n(\mathbf{k}) = E_n(\mathbf{k}^*). \tag{A.31}$$

References

1. E. I. Blount, *Solid State Physics, Volume 13*, edited by F.Seitz and D. Turnbull, (Academic, New York, 1962) p. 305.
1. V. Heine, *Proc. Phys. Soc. London* **89**, 443 (1963).
3. C. Kittel, *Quantum Theory of Solids* , (John Wiley, New York, 1963) p. 182.

Appendix 5.2

Energy Band Offsets at Semiconductor Interfaces, Quantum Well Structures and Semiconductor Superlattices

The purpose of this appendix is to give a general idea of the *energy band offsets* at semiconductor interfaces. Also, this appendix introduces the concepts and the terminology pertaining to the study of semiconductor surfaces and interfaces. We also give general descriptions of what is meant by *quantum well structures* and *semiconductor superlattices.*

An interface made up from two semiconductors of different nature is called a *heterojunction.* When two dissimilar, but otherwise lattice-matched, semiconductors are brought into contact at an interface, their respective *valence and conduction band edges do not line up.* Therefore, we must find a relative energy scale between the two semiconductors forming the heterojunction. The difference in energy band gaps between the two semiconductors, ΔE_g , is split into a *conduction band offset,* ΔE_c , and a *valence band offset,* ΔE_v . Naturally, the following sum rule

$$\Delta E_g = \Delta E_v + \Delta E_c \,, \qquad (B.1)$$

must be verified. The question of determining the energy band offsets is by no means a trivial one. We have not addressed this question here, and we regard the quantities ΔE_v and ΔE_c as *inputs* of the calculations presented in this work rather than *outputs.* Let us just mention that, according to a rule developped by Anderson[1], the conduction band offset ΔE_c can be related in a simple way to the

electron affinities χ of the two semiconductors forming the heterojunction,

$$\Delta E_c = \chi^{(1)} - \chi^{(2)}, \qquad (B.2.a)$$

and therefore,

$$\Delta E_v = \Delta E_g - \Delta E_c\,, \qquad (B.2.b)$$

$$\Delta E_v = \Delta E_g - \left[\chi^{(1)} - \chi^{(2)}\right]. \qquad (B.2.c)$$

The electron affinity $\chi^{(j)}$ in semiconductor j is defined as the energy required to take an electron from the conduction band edge $E_c^{(j)}$ to the vacuum level, *i.e.*,

$$\chi^{(j)} \equiv E_{\text{vacuum}} - E_c^{(j)}. \qquad (B.3)$$

Before describing an *energy band diagram* of an idealized semiconductor heterojunction, we pause to make the distinction between *direct* and *indirect* semiconductors.

• A semiconductor is said to be *direct* if the maximum of the valence band and the minimum of the conduction band both occur at the same **k** point in the Brillouin zone.

• A semiconductor is said to be *indirect* if the maximum of the valence band and the minimum of the conduction band occur at different **k** points in the Brillouin zone.

To be specific, let us consider a heterojunction made up of GaAs and $Ga_{1-x}Al_xAs$. GaAs is a direct semiconductor and $Ga_{1-x}Al_xAs$ is also a direct semiconductor[2] for alloy compositions in the range $x < 0.45$. For alloy compositions x exceeding this value, the minimum of the conduction band is at the X-point,

$$\mathbf{k}(X) = \left[\frac{2\pi}{a}\right](1, 0, 0), \qquad (B.4.a)$$

whereas the maximum of the valence band is at the Γ-point,

$$\mathbf{k}(\Gamma) = \left[\frac{2\pi}{a}\right](0, 0, 0), \tag{B.4.b}$$

where a is the length of the conventional cubic unit cell.

An *energy band diagram* of a heterojunction is a *plot of the band edge energy at some fixed* $\mathbf{k}$*-point (usually* $\mathbf{k}_0 = \mathbf{0}$*) as a function of the position normal to the interface plane.* The energy band diagram for the band edge at the Γ-point of a GaAs-$Ga_{1-x}Al_xAs$ heterojunction is shown in Figure (1) along with the definitions of the various energies mentioned above. The $\hat{\mathbf{z}}$ direction is perpendicular to the interface plane. The energy $E_F(\mathbf{x})$ is the Fermi level. At equilibrium, $E_F(\mathbf{x})$ is constant throughout the system, *i.e.*,

$$\hat{\mathbf{z}} \cdot \nabla E_F(\mathbf{x}) \equiv 0. \tag{B.5}$$

Figure (1) corresponds to a composition x of $Ga_{1-x}Al_xAs$ such that the alloy is *direct.* In this case the energy band edge at $\mathbf{k}(\Gamma) \equiv \mathbf{0}$, is plotted as a function of position along $\hat{\mathbf{z}}$. Let us just mention that, in the case of indirect semiconductors, care must be exercised to as which band edge to depict in the energy band diagram.

Useful as it might be, let us mention that this picture is oversimplified: In a real heterojunction system, there occur *repartitions of the charges at the interface that create local electric fields causing the energy band edges to bend near the interface.* Throughout this study, we have neglected the energy band bendings and considered only geometrically abrupt interfaces.

We now introduce the concepts of *semiconductor quantum well structures* and *semiconductor superlattices.* The energy band edge discontinuities, that arise when the heterojunction is formed, constitute potential energy barriers for the electronic states within these structures. Having defined a heterojunction,

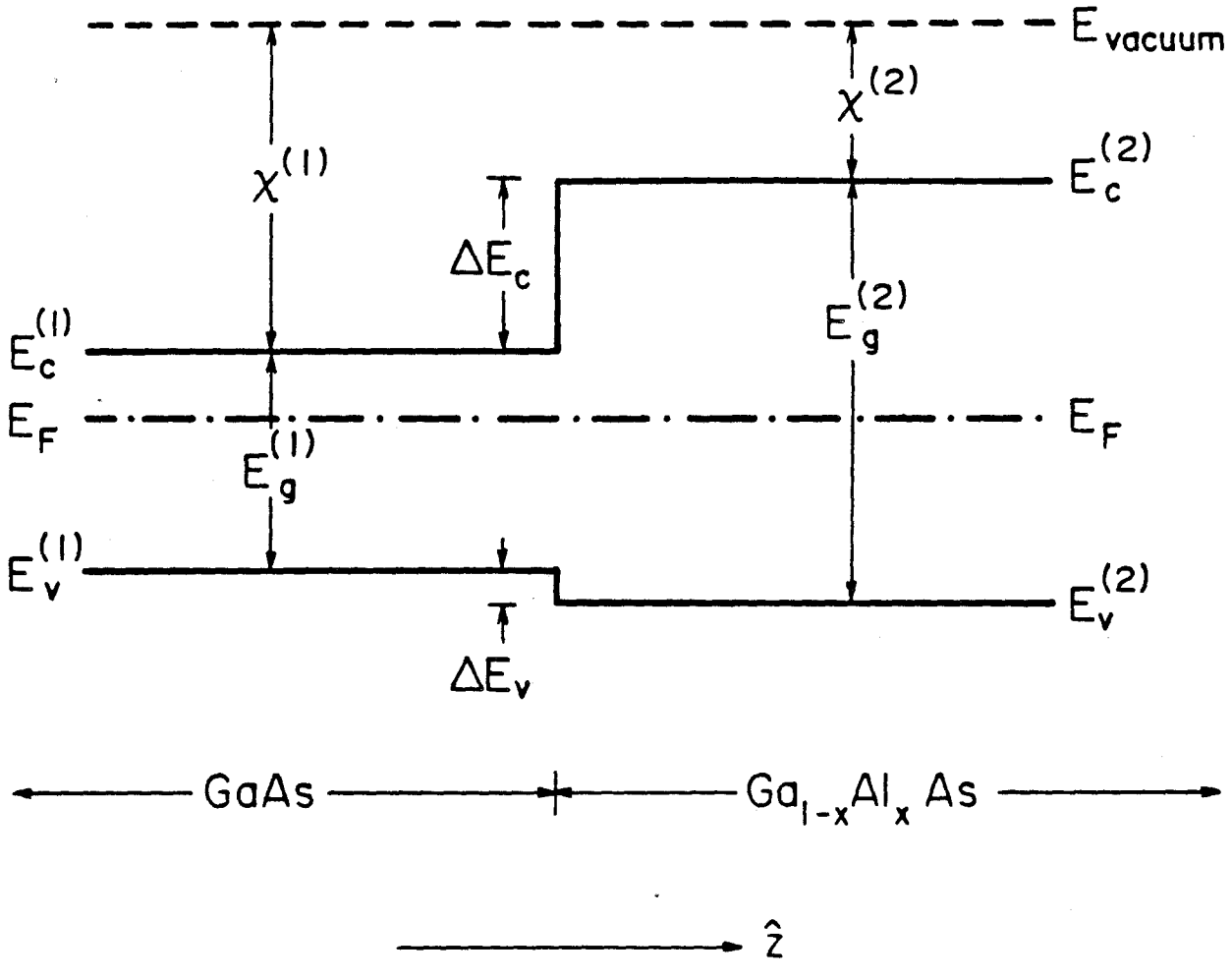

Figure 1. Energy band diagram of an ideal GaAs-$Ga_{1-x}Al_xAs$ heterojunction. The quantities ΔE_c and ΔE_v refer to the *conduction band offset* and to the *valence band offset*, respectively. The electron affinity $\chi^{(j)}$ in semiconductor j is defined as the energy required to take an electron from the conduction band edge $E_c^{(j)}$ to the vacuum level. The energy E_F is the Fermi level.

it is possible to envision more complicated structures. In the case where two heterojunctions are formed back to back, the energy band diagram of the structure resembles either that of a *one-dimensional quantum well*, (if a small band gap semiconductor is centered between two large band gap semiconductors), or that of a one-dimensional *barrier* (if a large band gap semiconductor is centered between two small band gap semiconductors). In the case where the semiconductors are grown in an alternating way, we obtain a periodic set of heterojunctions. An energy band diagram of such a structure resembles that of a periodic series of quantum wells separated by barriers. We call such a structure a *semiconductor superlattice.*

References

1. R. L. Anderson, *Solid State Electronics* **5**, 341 (1962).

2. H. C. Casey and M. B. Panish, *Heterostructure Lasers* (Academic Press, New York, 1978), Part A, Chapter 4.

3. J. C. Slater and G. F. Koster, *Phys. Rev.* **94**, 1498 (1954).